

11-12-2021

## Multifaceted Approach to Understanding *Acinetobacter baumannii* Biofilm Formation and Drug Resistance

Jessie L. Allen  
*University of South Florida*

Follow this and additional works at: <https://digitalcommons.usf.edu/etd>



Part of the [Microbiology Commons](#)

---

### Scholar Commons Citation

Allen, Jessie L., "Multifaceted Approach to Understanding *Acinetobacter baumannii* Biofilm Formation and Drug Resistance" (2021). *USF Tampa Graduate Theses and Dissertations*.  
<https://digitalcommons.usf.edu/etd/9063>

This Dissertation is brought to you for free and open access by the USF Graduate Theses and Dissertations at Digital Commons @ University of South Florida. It has been accepted for inclusion in USF Tampa Graduate Theses and Dissertations by an authorized administrator of Digital Commons @ University of South Florida. For more information, please contact [digitalcommons@usf.edu](mailto:digitalcommons@usf.edu).

Multifaceted Approach to Understanding *Acinetobacter baumannii* Biofilm Formation  
and Drug Resistance

by

Jessie L. Allen

A dissertation submitted in partial fulfillment  
of the requirements for the degree of  
Doctor of Philosophy  
Department of Cell Biology, Microbiology, and Molecular Biology  
College of Arts and Sciences  
University of South Florida

Major Professor: Lindsey N. Shaw, Ph.D.  
Yu Chen, Ph.D.  
Sophie Darch, Ph.D.  
James Riordan, Ph.D.  
Prahathees Eswara, Ph.D.

Date of Approval:  
November 11, 2021

Keywords: universal stress protein, antimicrobial peptides, high-throughput, ESKAPE

Copyright © 2021, Jessie L. Allen

## **Dedication**

This work is dedicated to my husband Lucas Allen who has been my rock throughout this entire process. Thank you for leaving your friends and family to come with me to Florida. Thank you for cooking me meals, keeping up with chores, and taking care of our baby boy on countless occasions when I was working late. Thank you for continuing to give me confidence when I was having a hard time. Thank you for welcoming me home with a huge hug and a smile on your face regardless of how your day went. Thank you for putting us first and believing in me. I could not have done it without you. I love you so much.

## **Acknowledgments**

First, I would like to thank my mentor Dr. Lindsey Shaw for pushing me to achieve more than I thought possible. It was a comfort to know that no matter what, you had my back. We always joke about how PIs are also therapists, but it is true! Thank you for embracing my squirrelness, corralling my wild ideas, lifting me up when I was certain I couldn't make it, and helping to mold my scientific mind. Thank you for supporting me beyond what is required of a PI. It was pretty awesome to have a mentor that was willing to fly to the middle of Kansas for a wedding in the hottest month of the year and to attend our baby shower. Lucas and I are very grateful. It was a pleasure working with you and being a member of your lab.

Next, I would like to thank all of the current and previous lab members that made ISA6014 a home. To the members that came before me, thank you for taking the time to teach me how to be a successful scientist through editing my work, forcing me to take time for social events, demonstrating techniques, or talking through concepts. Your mentorship inspired me to do my best to keep the comradery in the lab and make sure all lab members felt supported. To all past and current lab members, thank you for making the Shaw lab a fun place to be. The struggle was real, but the memories made are well worth it. Thank you to those who shared protocols, collaborated on projects, and let me dive into your brainstorming sessions. To the current members, I hope you continue to work hard and keep treating each other like family.

In a similar vein, I want to express how thankful I am for all of the work my undergraduate volunteers contributed to the projects within this document as well as the various other projects. Thank you for helping me juggle multiple projects at once and for putting in the time even when the work got a bit tedious. You guys are rockstars and I can't wait see where you end up. Your countless hours assisting in drug screening or biofilm processing did not go unnoticed! Your input made a big difference and I only hope that the experience you gained helped to prepare you for your future positions.

I would also like to thank my original mentor Dr. Stella Lee who took the time to teach me the basics of bench work and adequately prepared me for my graduate school experience. Thank you for also giving me independence and teaching/mentoring experience that translated to leadership skills. I will never forget the fun times too: our trips to call hall to get ice cream on my moped and doing Etina's makeup for her dance recital.

I am also thankful for the faculty within the CMMB department that I was lucky enough to work with as a teaching assistant. Last, but certainly not least, I thank my committee members for their guidance and support over the years. The conversations and difficult questions greatly contributed to my success, and I am forever grateful.

## Table of Contents

List of Tables.....	v
List of Figures.....	vi
Abstract.....	ix
Chapter 1: Introduction.....	1
Bacterial Biofilms.....	1
What is a biofilm?.....	1
Biofilm Forming Bacteria and Associated Disease Manifestations.....	1
Impact of Bacterial Biofilms in the Clinic and the Environment.....	4
Biofilm Formation, Effectors and Regulation.....	5
<i>Acinetobacter baumannii</i> .....	7
Background.....	7
Disease Manifestations.....	9
Antibiotic and Antiseptic Resistance.....	11
Treatment Options.....	13
Contributors of Virulence in <i>A. baumannii</i> .....	15
Regulators of Virulence.....	15
Virulence Factors.....	16
Capsule and Immune Evasion.....	18
Desiccation Tolerance.....	18
<i>Acinetobacter baumannii</i> Biofilms.....	19
Types of Biofilms.....	19
Regulators and Known Effectors of Biofilm Formation.....	19
Antimicrobial Peptides.....	21
Origins and Properties.....	21
Methods for Discovery.....	23
AMPs in Plants.....	26
AMPs as Antibiotics.....	26
AMP Mechanisms of Action.....	28
Project Aim.....	29
Chapter 2: Identification and Characterization of Factors Required for Biofilm Formation in <i>Acinetobacter baumannii</i> .....	30
Introduction.....	30
Materials and Methods.....	35
Strains and Growth Conditions.....	35
Screening Transposon Library Mutants for Biofilm Production.....	35
Secondary Screening of Mutant Strains.....	36
Complement Strain Generation.....	36

Real-Time Biofilm Analysis. ....	37
eDNA Quantification. ....	37
Extracellular Matrix Component Inhibition Assays. ....	38
Extracellular Matrix Component Disruption Assays. ....	38
Results .....	39
An Unbiased Global Screen to Identify Novel Components Influencing Biofilm Formation in <i>A. baumannii</i> . ....	39
Ontological Assessment of Factors Identified as Influencing Biofilm Formation. ....	42
Real-Time Profiling of Biofilm Formation. ....	45
Characterization of eDNA Abundance in Mutant Strains. ....	49
Exploring the Impact of Protease on Biofilm Initiation of Mutant Strains. ....	52
Investigating the Dispersive Effects of Proteinase K on Established Biofilms. ....	55
Dissecting the Contribution of Polysaccharide to Differential Biofilm Formation. ....	57
Evaluation of Polysaccharide Content in Established Biofilms via Dispersal Experiments. ....	58
Discussion .....	60
 Chapter 3: Characterization of Universal Stress Protein G in the Oxidative Stress and Cell Envelope Stress Response of <i>Acinetobacter</i> <i>baumannii</i> .....	75
Introduction. ....	75
Materials and Methods .....	80
Bacterial Strains and Growth Conditions. ....	80
Growth Curve Analysis. ....	80
Construction of a <i>uspG</i> Complementing Strain. ....	81
Western Blot Analysis. ....	82
RNA Sequencing. ....	82
RNA Sequencing Bioinformatics. ....	83
Minimum Inhibitory Concentration Determination. ....	84
Motility Assessment. ....	85
Survival in Whole Human Blood. ....	85
Results .....	86
Bioinformatic Considerations of Usps in <i>A. baumannii</i> 5075. ....	86
Universal Stress Protein G Disruption Results in a Growth Defect. ....	91
UspG Baseline Protein Expression Increases Over Time and Remains Stable. ....	92
RNA-sequencing Analysis Reveals Vast Changes in <i>uspG::tn</i> . ....	93
Shifts in the Expression of Energy and Translation Involved Genes Result in Susceptibility of the <i>uspG::tn</i> Mutant to Aminoglycosides. ....	117

Increased Susceptibility to Biocides and CCCP Indicates Significant Changes in <i>uspG</i> ::tn Cell Envelope Structure.....	120
Ethanol Susceptibility is Enhanced Due to Downregulation of Ethanol Metabolic Enzymes. ....	122
Motility is Hindered in <i>uspG</i> ::tn Likely Due to Shifts in Pili Expression.....	124
Oxidative Stress Tolerance is Hindered in <i>uspG</i> ::tn. ....	127
Inhibition of UspG Leads to the Inability to Resist DNA Damaging Agents.....	128
UspG Plays an Essential Role During Survival within Whole Human Blood.....	129
Discussion .....	131
 Chapter 4: The Discovery of Plant Derived Antimicrobial Peptides Using the “PepSAVI-MS” Pipeline.....	140
Introduction.....	140
Materials and Methods .....	145
Plant Species.....	145
Bacterial Strains and Growth Conditions. ....	146
Antimicrobial Activity Screening using Resazurin. ....	147
Antimicrobial Activity Screening using Optical Density. ....	148
Validation of CyO <sub>2</sub> Activity from <i>Viola odorata</i> . ....	149
Minimum Bactericidal Concentration to Determine Activity of CC-AMP1. ....	149
Results .....	150
Optimization of Resazurin Assay to Assess Antimicrobial Peptide Activity by Quantifying Respiration. ....	150
The PepSAVI-MS Approach to Antimicrobial Peptide Discovery.....	152
Assessing the Activity of <i>Viola odorata</i> (VO) to Validate the PepSAVI-MS Approach Reveals Novel Antimicrobial Activity. ....	153
Bioassay Screening of Fractionated Ethnobotanical Plant Species Against the ESKAPE Pathogens. ....	155
Fast-Tracking Screening Procedure via Assessing Single Fraction Isolates Against the ESKAPE Pathogens.....	162
Overcoming Colorimetric Interferences via Turbidity-Based Assessment.....	164
<i>Amaranthus tricolor</i> (ATr) has Limited Activity Against ESKAPE Pathogens but Shows Enhanced Activity Against <i>Escherichia coli</i> . ....	169
Transcriptome Mining Reveals Potential Antimicrobial Peptide Candidates Effective Against Select ESKAPE Pathogens. ....	172
<i>Capsicum chinense x frutescens</i> (CC) a Hybrid Ghost Pepper Plant Displays Gram-Negative Specific Activity. ....	175
Discussion .....	180

Chapter 5: Concluding Remarks and Future Directions .....	187
Final Discussion .....	187
Chapter 2 .....	187
Chapter 3 .....	190
Chapter 4 .....	191
Future Directions .....	192
Chapter 2 .....	192
Chapter 3 .....	194
Chapter 4 .....	198
References .....	200
Appendices .....	240
Appendix I: Supplemental Figures for Chapter 2 .....	241
Appendix II: Supplemental Tables for Chapter 2 .....	248

## List of Tables

Table 1. Lead Transposon Mutant Strains Confirmed to Significantly Alter Biofilm Formation .....	41
Table 2. Lead Mutant Strains Selected for ECM Profiling .....	45
Table 3. Bacterial Strains and Plasmids.....	80
Table 4. Usp Paralogs in AB5075 .....	86
Table 5. Ontological Grouping of Genes with Decreased Expression in the <i>uspG::tn</i> Mutant Strain.....	94
Table 6. Ontological Grouping of Genes with Increased Expression in the <i>uspG::tn</i> Mutant Strain.....	112
Table 7. Plant Genre for Plant Peptide Library Creation and Testing.....	146
Table 8. Bacterial Strains Used in This Study .....	147

## List of Figures

Figure 1. Stages of Biofilm Formation .....	6
Figure 2. Mutants Identified as Demonstrating Altered Biofilm Biomass Following Secondary Screen .....	40
Figure 3. Ontological Grouping of Mutants Identified as Having Differential Biofilm Forming Capacities .....	43
Figure 4. Real-Time Profiling of Biofilm Formation Mirrors that Obtained via CV Staining.....	47
Figure 5. Probing the Contribution of eDNA to Mutant Biofilm Formation .....	51
Figure 6. ECM Profiling Reveals Differential Contribution of Protein to Biofilm Initiation .....	53
Figure 7. The Importance of Proteins to Mature Biofilm ECM Differs Between Lead Strains .....	56
Figure 8. ECM Profiling of Lead Mutants Indicate the Importance of Polysaccharides During Biofilm Development.....	57
Figure 9. The ECM of Mature Biofilms are Less Dependent on Polysaccharides for Integrity .....	59
Figure 10. Universal Stress Proteins of AB5075 Show Little Sequence Similarity.....	87
Figure 11. Rendering of Predicted ABUW_1763 Protein Structure .....	89
Figure 12. Top 11 Species with Usp Proteins Sharing Similarity to ABUW_1763 .....	90
Figure 13. <i>uspG</i> ::tn Strain Exhibits a Growth Deficit When Compared to Wildtype .....	91

Figure 14. UspG Expression is Stable Over Time .....	92
Figure 15. Disruption of <i>uspG</i> Leads to Vast Changes in Transcriptome.....	93
Figure 16. Translational Machinery Shows Altered Transcription in the <i>uspG::tn</i> Strain .....	118
Figure 17. Aminoglycoside Sensitivity Exhibited by <i>uspG::tn</i> Strain.....	120
Figure 18. Cell Envelope Altered in <i>uspG::tn</i> Strain Based on Sensitivity to Biocides and CCCP.....	122
Figure 19. Ethanol Sensitivity Exhibited by <i>uspG::tn</i> Strain.....	123
Figure 20. Motility Defect Observed in <i>uspG</i> - (M) Strain.....	125
Figure 21. <i>uspG::tn</i> Strain Demonstrates Deficiency in Motility Following 2 Weeks of Incubation at 27°C.....	126
Figure 22. Various Genes Involved in ROS Mediation are Downregulated in <i>uspG::tn</i> Strain .....	127
Figure 23. <i>uspG::tn</i> Strain is More Sensitive to H <sub>2</sub> O <sub>2</sub> Exposure .....	128
Figure 24. <i>uspG::tn</i> Strain is More Sensitive to DNA Damaging Agents .....	129
Figure 25. UspG Plays Critical Role in Human Blood Survival.....	130
Figure 26. Workflow for PepSAVI-MS Pipeline and Project Goals .....	144
Figure 27. False-Positive Activity Arises with Overexposure of Resazurin.....	151
Figure 28. Determination of Differences in ESKAPE OD <sub>600</sub> vs CFU/mL.....	152
Figure 29. Bioactivity of <i>Viola odorata</i> Fraction Library .....	154
Figure 30. Bioactivity of <i>Linum spp.</i> Fraction Library.....	156
Figure 31. Bioactivity of <i>Solanum spp.</i> Fraction Library .....	158
Figure 32. Bioactivity of <i>Silybum spp.</i> Fraction Library.....	159
Figure 33. Bioactivity of <i>Silybum spp.</i> 3x Fraction Library.....	161
Figure 34. Bioactivity of Single Fraction Libraries .....	163

Figure 35. Growth of <i>E. faecium</i> Reveals 5 Hours to be Optimal Assay Point .....	166
Figure 36. Growth of <i>S. aureus</i> Reveals 4 Hours to be Optimal Assay Point .....	167
Figure 37. Growth of <i>K. pneumonia</i> Reveals 4 Hours to be Optimal Assay Point.....	167
Figure 38. Growth of <i>A. baumannii</i> Reveals 5 Hours to be Optimal Assay Point .....	168
Figure 39. Growth of <i>P. aeruginosa</i> Reveals 7 Hours to be Optimal Assay Point .....	168
Figure 40. Growth of <i>E. cloacae</i> Reveals 4 Hours to be Optimal Assay Point .....	169
Figure 41. Bioactivity of <i>Amaranthus tricolor</i> Fraction Library .....	170
Figure 42. Bioactivity of <i>Amaranthus tricolor</i> Concentrated Fraction Against ESKAPE and <i>E. coli</i> .....	171
Figure 43. Bioactivity of <i>Amaranthus tricolor</i> Partially Purified Lipopeptide Atr-LTP1 Against ESKAPE .....	173
Figure 44. Bioactivity of <i>Amaranthus tricolor</i> Purified Lipopeptide ATr-LTP1 Against <i>K. pneumonia</i> .....	174
Figure 45. Bioactivity of <i>Amaranthus tricolor</i> ATr-Def1 Against ESKAPE .....	175
Figure 46. Bioactivity of <i>Capsicum chinense x frutescens</i> CC-AMP1 Against APE .....	177
Figure 47. Bioactivity of <i>Capsicum chinense x frutescens</i> CC-AMP1 Peptide Against ESKAP .....	178
Figure 48. Bactericidal Activity of CC-AMP1 Against <i>A. baumannii</i> .....	179

## **Abstract**

*Acinetobacter baumannii* is a multi-drug resistant nosocomial pathogen known for causing wound related- and respiratory-infections. It is currently on the WHO's list of critical pathogens due to its broadly drug resistant nature and the constant appearance of pan-resistant isolates. A majority of the infections caused by this organism are biofilm associated, however there is limited existing knowledge regarding the mechanisms used to engage in this multicellular lifestyle. As such, we set out to explore the factors influencing this behavior using an 10,000+ isolate transposon mutant library of *A. baumannii* strain AB5075. Of the strains tested, 6.45% demonstrated some level of change to their biofilm forming capacity (either increased or decreased). The screen, coupled with more in-depth (extracellular matrix) ECM analyses and real-time biofilm tracking, allowed us to further characterize 16 of the most influential strains. During this investigation, the most significant biofilm phenotype was observed for a tn mutant of a universal stress protein, which demonstrated an 8-fold increase in biofilm formation compared to the wildtype strain. This led us to investigate the function of this protein. Through this, we have named the protein UspG based on structure prediction tools and demonstrate its essentiality in the survival of AB5075 in whole human blood; likely mediated at least in part by aiding in protection against oxidative stress. In addition, we reveal its importance during exponential growth through expression monitoring and RNA sequencing analysis. These studies reveal that UspG broadly influences cellular behavior, and specifically the processes of virulence, metabolism, and cell envelope

homeostasis. Collectively, these studies provide a deeper understanding of pathways important in the formation and maintenance of biofilms in *A. baumannii*. Further examination of the factors highlighted herein will provide promising insight into potential targets for therapeutic intervention in the clinical setting.

Towards the latter point, the rising rates of multi-drug resistant bacterial infections demonstrate a pressing need for the development of new antibacterial agents with novel mechanisms of action. Medicinal plants are a viable source for antimicrobial peptides and therefore we have worked with collaborators on development of the PepSAVI-MS pipeline for bioactive peptide discovery. This platform uses mass spectrometry coupled with statistics to create a highly versatile approach to isolating bioactive peptides from complex multi-cellular systems. Our primary focus in this regard is ribosomally synthesized post-translationally modified peptides (RiPPs), which have been largely overlooked in standard AMP fractionation techniques. We have validated this approach through the screening of *Viola odorata* fractions and thereafter assessing the bioactivity of purified AMPs of interest, including cycloviolacin O2, against the ESKAPE pathogens. Herein we report the bioactivity of several additional ethnobotanical species, many of which possess profound and broad-spectrum activity against an array of multi-drug resistant bacterial pathogens. With the evident promise of our preliminary analyses based on bioactivity alone, we are confident that this pipeline will reveal novel antimicrobial peptides with potential as future therapeutics.

## **Chapter 1: Introduction**

### **Bacterial Biofilms**

**What is a biofilm?** Bacterial biofilms are a collection of cells encompassed by a protective matrix largely composed of macromolecules such as proteins, eDNA and polysaccharides. The formation of a biofilms is ubiquitous in nature. They serve as a means of protection and allow for survival from harsh surrounding environments and external threats. Biofilms can exist on a variety of abiotic or biotic surfaces or as free-floating aggregates. In addition, bacteria can form mono-culture biofilms, however, many times multi-species biofilms are formed. These can include bacteria exclusively or bacteria and fungal mixtures. Based on reports of fossilized formations within rock and from deep sea hydrothermal vents, it is estimated that biofilms have been forming for billions of years[1]. The first description of a live biofilm was recorded as early as 1683 when Antoni van Leeuwenhoek observed a scraping from his teeth using his famous primitive microscope[2]. Since then, biofilms have been attributed to a variety of diseases and will be discussed in depth in the following sections.

**Biofilm Forming Bacteria and Associated Disease Manifestations.** It has been estimated that 80% of bacterial infections are biofilm associated[3]. In addition, there are currently no FDA approved antibiotic or chemical treatments with the ability to eradicate

biofilms. This is further exacerbated by the fact that biofilms can be up to 1000x more resistant to antibiotic intervention than their planktonic counterparts. Of equal concern, is the lack of standardized practices for the study of biofilms in the laboratory setting[3], which leads to variations in experimental results, yielding studies that cannot be directly related and thus slows progress in the field.

Bacteria within biofilms are protected from the external environment, which leaves them adept at evading parts of the immune system; however, there are disadvantages to this state that the bacteria must overcome. For example, nutrients are not as readily available, and resources become scarce quickly. This leads to metabolically distinct populations within the biofilm based on location. Levels of oxygen within the biofilms are limited within the center which forces bacteria to adapt[2]. Some bacteria are dormant, while others become persisters, and yet others demonstrate a stationary phase-type lifestyle. Thus, inevitabilities such as nutrient limitation greatly influence cellular behavior. Bacteria are able to overcome some of these limitations by forming structures that allow channels of water and nutrients to access more of the biofilm population and provide routes for waste elimination to avoid toxicity. In addition, cells have mechanisms to communicate and signals to dictate when the biofilm should disperse and relocate.

There are, however, other advantages to bacteria living in a biofilm state within, say, the human body. One such advantage to cells becoming metabolically inactive and dormant is the subsequent downregulation of a variety of systems that antibiotics rely on to properly function and eliminate target bacteria[2]. Therefore, they are much more tolerant

to antibiotic treatment. Biofilms within the body induce the innate and adaptive immune responses depending on their growth phase, however, bacterial clearance is usually unsuccessful, and instead results in host tissue damage as a byproduct of the immune response[3, 4].

Biofilm associated disease manifestations of the body include: otitis media, infective endocarditis, atherosclerosis, salivary duct stones, recalcitrant typhoid fever, inflammatory bowel disease, colorectal cancer, wound infections, bacterial vaginosis, chronic endometritis, pharyngitis, laryngitis, pertussis, cystic fibrosis, chronic bacterial prostatitis, gingivitis and urinary tract infections [2]. In addition, biofilms can be formed on a variety of indwelling medical devices and can often result in bloodstream infections that are then considered biofilm associated[5]. The same is true for ventilator associated pneumonia. Some examples of medical devices on which biofilms are known to grow include central venous catheters and their needleless connectors, contact lenses, endotracheal tubes, intrauterine devices, medical heart valves, pacemakers, peritoneal dialysis catheters, prosthetic joints, tympanostomy tubes, urinary catheters, and voice prostheses[5, 6]. The kind of bacteria typically associated with indwelling devices is dependent upon the location of the device. In some instances, they are able to form single organism biofilms, however, multi-species biofilms are also common. *Staphylococcus aureus* may be the most commonly isolated bacteria from biofilms with typical isolations from central venous catheters, prosthetic heart valves, diabetic foot infections, artificial hip prosthetics, and intrauterine devices[5]. *Klebsiella pneumoniae* and *Escherichia coli* are commonly isolated from central venous catheters as well as urinary catheters, while

*Pseudomonas aeruginosa* is commonly found on artificial hip prosthetics[5]. Both Gram-negative and Gram-positive bacteria are able to form the same type of biofilm associated infections, many times, together[7]. Examples include biofilms of the oral cavity, otitis media, diabetic foot infections and cystic fibrosis[8].

The most well studied co-culture biofilm is demonstrated by cystic fibrosis patients that go through cycles of colonization with *S. aureus* and *P. aeruginosa*. Typically, children are predominantly colonized with *S. aureus* and as they age *P. aeruginosa* becomes the primary organism, however, they continue to coexist. The secretion and sensing of bacterial byproducts and signaling molecules by each organism can result in exacerbated disease symptoms for the host[9, 10]. Specifically, *P. aeruginosa* produces a variety of anti-staphylococcal virulence factors such as proteases and toxins that can target *S. aureus*, but also host cells[11].

**Impact of Bacterial Biofilms in the Clinic and the Environment.** Bacterial biofilms not only influence and lead to chronic, persistent infections, but they present problems in other areas. For example, biofilms formed by bacteria such as *Listeria monocytogenes* and *Salmonella spp.* can cause food poisoning and are commonly found in food processing plants with below-average sanitation practices[12, 13]. Bacteria such as *Escherichia coli* are very prominent biofilm formers in humans, but also cause food borne illness due to growth on produce such as lettuce[14]. Instances such as this not only pose a threat to human health, but cause significant economic costs due to necessary recalls and associated food spoilage[13]. Another example of a strong biofilm forming organism

is *Vibrio cholera*, which exists as a biofilm within its natural environment, water, but readily colonizes the gut of humans upon ingestion[15]. Biofilms are also associated with man-made structures where they can cause the disruption of waterways or pipes, which is referred to as biofouling.

Biofilms are not all bad, however, as some populations are able to fix nitrogen and bioremediate wastewater. Further, biofilms have recently been used for biomass production from N<sub>2</sub> through microbial electrosynthesis which could be the next approach in creating sustainable biofuels[16, 17].

**Biofilm Formation, Effectors and Regulation.** Typically, biofilm formation has been described as a cycle that includes four to five steps and will be described in the form of a summary of these references and in **Figure 1**[18-20]. For surface associated biofilm formation, the first step includes the reversible attachment of planktonically growing bacteria to a surface. This is accompanied by the downregulation of motility genes and the upregulation of adhesins. The next step is the irreversible attachment of the bacterial community which starts to accumulate in the form of a microcolony. Bacteria are actively growing during this stage, and cell-cell adhesion starts to occur with production of extracellular matrix (ECM) components also accumulating. The ECM continues to form and mature during the third step, referred to as maturation I. During this step, the cells are still growing, and the biofilm structure starts to take form as microcolonies merge to form a macrocolony. The fourth step is maturation II, or full maturation, which is the most resistant to chemical or immune cell exposure. A biofilm structure can be flat or form a

mushroom like configuration containing fluid filled channels that transport nutrients to various locations within the biofilm. Finally, once a certain threshold is met and resources are exhausted, signaling triggers the dispersal of the biofilm where cells re-enter a planktonic state and disseminate to other parts of the body. This is step five and initiates the cycle to start again and form a biofilm at a different location.

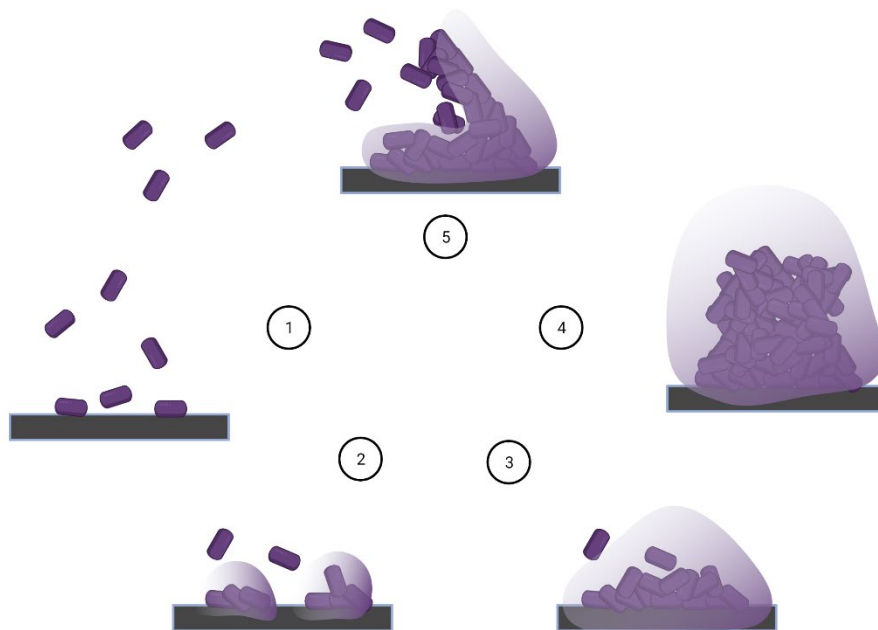


**Figure 1. Stages of Biofilm Formation.** 1) Bacteria in a planktonic state reversibly attach to a surface and start to accumulate. 2) Cells adhering near each other start to form microcolonies and ECM is starting to form. 3) Microcolonies start to merge into macrocolonies and ECM continues to grow. 4) Mature biofilm is formed where cell growth is minimal and ECM is established. 5) Dispersal is initiated and cells re-enter a planktonic state to find new location to restart biofilm cycle. Created using Biorender.com.

Surface composition can greatly influence the speed and efficiency of attachment for biofilms. In general, bacterial cell surfaces are negatively charged and therefore the attachment to positively charged surfaces is more likely[6]. However, factors such as adhesins are important and can promote binding to biotic surfaces that may have similar charges[6]. There are differences between Gram-positive and Gram-negative bacteria

when it comes to surface charge although they are both negatively charged overall. For example, wall teichoic acids contribute to charge in Gram-positive organisms while lipopolysaccharide (LPS) is this component in Gram-negative organisms[6]. In addition to charge, hydrophobic surfaces are typically better for the attachment of bacteria to surfaces as compared to hydrophilic surfaces[21, 22].

The regulation of biofilms is unique to each bacterium, however there are some universal triggers to initiate the process. One regulator of biofilm formation is the secondary messenger cyclic di-GMP, produced by diguanylate cyclase enzymes. This molecule is accumulated in biofilms and promotes several biofilm effectors such as adhesins and capsule production[23]. Other initiators include two component systems, small RNAs, secreted signaling molecules, and quorum sensing systems[24].

### ***Acinetobacter baumannii***

**Background.** *Acinetobacter baumannii* is a Gram-negative, coccobacilli bacterium that is ubiquitous in nature. It has been recovered from sources such as water, soil, animals, and humans[25]. *A. baumannii* is considered the most pathogenic of the *Acinetobacter* genus and similarly most commonly causes infections in humans[26]. *A. baumannii* has high similarity to *A. calcoaceticus* and until recently their distinction was very difficult. Therefore, reporting on and studies of these pathogens likely overlapped, thus literature reflects a combination of these species[26]. The same is true for two other species that are known to cause both community acquired and nosocomial infections: *A. pittii* and *A. nosocomialis*[27]. These species are often collectively referred to as *A. baumannii*[28].

Further, many times *Acinetobacter* genomic species 3 and 13TU are also referred to as *A. baumannii* complex or simply *A. baumannii*. There are over 50 species within the *Acinetobacter* genus, however, it was estimated by the CDC in 2004 that 80% of infections are caused by *A. baumannii* specifically.

*A. baumannii* has a particularly dire association with war, as it was one of the most common Gram-negative organisms isolated from traumatic injuries of wounded soldiers in Vietnam[25], and was commonly isolated from wounded soldiers during the Iraq and Afghanistan War[29]. Indeed, the species is sometimes referred to as “Iraqibacter” due to this association. Although it is tempting to presume that the correlation of infections and wartime stems from the exposure of wounded soldiers to environmental isolates of *A. baumannii*, this is highly unlikely. Instead, it is the unique ability of *A. baumannii* to exist for extended periods of time on a variety of surfaces that results in the transfer of infecting *A. baumannii* strains from hospital to hospital and patient to patient[29]. Specifically, *A. baumannii* isolates are able to persist for days on inanimate surfaces such as medical equipment, in sinks, on pillows and mattresses, on stainless steel trolleys, bedrails, and tables[25]. The hypothesis that persistence and transmission of *A. baumannii* in hospitals leads to higher infection rates of soldiers during wartime instead of the presumed environmental soil exposure hypothesis was validated by a study of soil samples within a region of war that yielded only one *A. baumannii* isolate, clonally distinct from those found in soldiers[30]. Further supporting this notion was the isolation of *A. baumannii* from every health care facility on the evacuation route from both Afghanistan and Iraq[30].

Outside of human-to-human transmission, an additional source of *A. baumannii* isolation is food, which may serve as an additional source for exposure of hospital patients. Specifically, *A. baumannii* can be found on a variety of vegetables including apples, potatoes, lettuce, sweet corn and mushrooms, among others[31]. In addition, transmission to humans via body lice has also been reported[32]. With standard medical equipment, food, and insect vectors all serving as sources for *A. baumannii* exposure, it is easy to visualize how quickly this organism can spread within health care facilities. This also highlights how important it is to maintain a hygienic environment if transmission control is to be effective.

*A. baumannii* is considered an opportunistic pathogen that is extremely adept at colonization. This species is regularly isolated from hospitalized patient urine samples and respiratory secretions without being associated with disease[25]. Within the body, it is able to colonize a variety of locations including the digestive tract[33]. Although *Acinetobacter* species such as *A. Iwoffii* are commonly found on the skin of healthy individuals as normal flora, it is rare to find *A. baumannii* on the skin[34] particularly outside of urban areas[35]. Therefore, the most likely mode of colonization is ingestion or inhalation with patients who are immunocompromised at much higher risk for infection.

**Disease Manifestations.** According to the CDC, patients at most risk for *A. baumannii* infection are those within healthcare facilities with ventilators, catheters, open surgical wounds, patients of the intensive care unit (ICU) or those who have extended hospital stays. Further there has been a correlation between infection and organ type. Infections

tend to manifest in areas where organs are liquid filled such as the respiratory tract, the peritoneum, or the urinary tract. In the United States between 2009-2010 it was estimated that *A. baumannii* was the cause of 1.8% of all healthcare associated infections (HAIs) with an average of 45,000 per year becoming infected[36, 37]. Globally it was estimated that 1 million infections were caused by *A. baumannii* annually[37]. By 2013 the estimation of multidrug resistant infections reached 7,300 per year in the US, which resulted in 500 deaths. In a report published in 2020 discussing the infections of 2017, *Acinetobacter* species were ranked as the 14<sup>th</sup> most reported pathogen within long term acute care facilities and hospital ICUs[38]. Carbapenem and multi-drug resistant isolates accounted for a large majority of strains identified within long-term healthcare facilities, particularly those causing ventilator associated pneumonia (VAP) and blood stream infections[38].

Types of infection caused by *A. baumannii* include pneumonia, bacteremia, urinary tract infections, wound infections, exudates and abscess formation, meningitis, endocarditis, osteomyelitis, and endophthalmitis. The highest number of infections seems to occur between the months of July-October[25, 39]. Although the reasoning behind this is unclear there has been an association with heat and high humidity (tropical environments)[40] which could result in higher chances for colonization. This is based on evidence that *A. baumannii* can be transmissible through the air and lead to colonization[41]. The highest number of infections are nosocomial, but community acquired infections do occur[40]. Most *A. baumannii* infections occur within the ICU of hospitals with up to 54% mortality reported[25]. One example comes from the study of

bacteremia caused by *A. baumannii* which showed a mortality rate of 42.2% in the ICU while bacteremia caused by other organisms had a mortality rate of 34.4%[42]. This suggests that morbidity due to blood stream infections is slightly elevated for *A. baumannii*. However, an additional study of pneumonia infections concluded that *A. baumannii* infection outcomes were similar to that of the same infection type caused by other organisms[43]. More studies with higher patient pools are needed to accurately associate morbidity due to *A. baumannii* infection types compared to other organisms in addition to the reasoning behind the differences. However, the increasing use of collaborative reporting and advancements in bioinformatic analyses will undoubtedly lead to more accurate infection surveillance very soon.

**Antibiotic and Antiseptic Resistance.** *A. baumannii* has the ability to resist a variety of antimicrobial treatments including but not limited to fluoroquinolones, aminoglycosides, tetracyclines, beta-lactams, glycolcyclines, and polymyxin antibiotics. The strains of most concern, however, are those considered resistant to the newest class of beta-lactam, carbapenems. Carbapenem resistance is defined as a strain with the ability to resist exposure to one or more of the carbapenem antibiotics such as imipenem, doripenem, or meropenem. According to one study, it was estimated that carbapenem resistant *A. baumannii* infects 22,950 people annually in the United States with 75,000 estimated infections globally[37]. This estimated resistance in turn contributes to almost 5,000 excess deaths per year at an excess cost of \$389,000,000 in the United States[37]. This valuation is slightly off of the CDC estimation of 8,500 infections, 700 deaths and \$281,000,000 in costs annually due to carbapenem resistant *A. baumannii* infections[44].

Regardless of the source of reporting, it is clear that this organism causes detrimental impacts on both human health and the economy that need to be addressed.

The last line of treatment for carbapenem-resistant strains is the use of colistin, a membrane disrupting antibiotic, however, *A. baumannii* has a variety of ways to resist this antibiotic. Colistin acts by targeting and binding the lipid A anchor of LPS or lipooligosaccharides (LOS) and the outer membrane phospholipids which leads to membrane disruption and ultimately cell death. *A. baumannii* is able to resist colistin treatment through the modification of lipid A by the addition of galactosamine[45] or phosphoethanolamine[46, 47]. Bacterial strains can accomplish this through forming mutations in the *pmrAB* two-component system, which leads to the overexpression of *pmrC*, encoding a lipid A modifying enzyme[48]. Alternatively, mutations in the *lpxACD* operon can result in the deletion of LOS[49], therefore, colistin binding is prevented altogether.

Another means of resistance to a variety of antibiotics comes in the form of efflux pumps. These allow the bacterium to resist antibiotic exposure by expelling the drug and preventing its accumulation within the cell, thus resulting in an increased minimum inhibitory concentration (MIC). *A. baumannii* produces a multitude of efflux pumps some of which are yet to be characterized. In particular, *A. baumannii* possesses pumps of the major facilitator superfamily (MFS), small multidrug resistance (SMR) family, multidrug and toxic compound extrusion (MATE) family, proteobacterial antimicrobial compound efflux (PACE) family, and most importantly, the resistance-nodulation cell division (RND)

family[50]. RND family pumps are known for their ability to expel a variety of antibiotics as well as antiseptics, biocides, detergents, and dyes[50]. One of the best studied examples is the RND efflux pump in *A. baumannii* is encoded by *adeABC*, which is under the control of a two-component system AdeRS. This pump is responsible for expelling a variety of antibiotics including aminoglycosides, fluoroquinolones, and tigecycline while concurrently contributing to better fitness *in vivo*[51]. In addition, the AdeAB and Acel efflux pumps of *A. baumannii* are responsible for the expulsion of chlorohexidine, a commonly used antiseptic that targets bacterial membranes[52] thus, in part, contributing to the persistence of this organism on hospital surfaces. Resistance to other antiseptics such as ethanol and hydrogen peroxide have also been reported. Additional mechanisms of resistance by *A. baumannii* include the production of beta-lactamases, cephalosporinases, carbapenemases, antibiotic modifying enzymes, shifts in membrane permeability, and alterations of antibiotic target sites[50].

**Treatment Options.** Colistin is primarily used when dealing with pan-resistant isolates, or for the treatment of severe infections, such as meningitis, and has shown to be very effective[53, 54]. The combination of colistin and sulbactam has also been used for the treatment of VAP[55]. The use of colistin and similar polymyxins is effective, however, many patients present with negative side effects such as nephrotoxicity following treatment and resistance does occur. Difficult to treat *A. baumannii* strains causing intraabdominal infections are commonly successfully treated with the glycylycline tigecycline, however, more studies are necessary before it is universally recommended[56]. The safest options to treat *A. baumannii* infections with minimal

patient side effects include the use of beta-lactams or fluoroquinolones. However, a multitude of resistance mechanisms exist and therefore *A. baumannii* strains must be tested to ensure susceptibility to the antibiotic of choice prior to treatment of the patient.

There have been attempts made to develop vaccines targeting *A. baumannii*, however these efforts have remained unsuccessful thus far. This is in part due to the high amount of genetic diversity seen for *A. baumannii* strains. For example, within the species, nearly 40 serotypes have been identified. Therefore, vaccines are not likely to be a functional option for treatment of *A. baumannii* infections now or in the foreseeable future. There is however hope, as two novel antibacterial agents are showing promising anti-*A. baumannii* activity. First, cefiderocol, a catechol-substituted siderophore cephalosporin was recently approved (2019) by the FDA to treat complicated urinary tract infections caused by Gram-negative bacteria and is now being evaluated for its ability to treat VAP and sepsis with promising results[56]. Second, is the FDA approved synthetic fluorocycline, eravacycline, recommended for the treatment of complicated intraabdominal infections. It is similar to tigecycline, but more potent against *A. baumannii*[56]. These drugs will serve as reliable first-line treatments of *A. baumannii* infections allowing for more limited use of toxic salvage therapies such as colistin.

The CDC has been surveilling carbapenem resistant infections in the United States through the Emerging Infections Program. Recently, in 2021, they have extended this surveillance to track the occurrence of carbapenem resistant *A. baumannii* from normally sterile sites, such as urine specimens, lower respiratory tracts, and wounds. This effort is

tracking the presence of these pathogens in nine states within the US and will give better insights into the best way to treat resistant infections. However, the overall consensus is that by tailoring an antibiotic regimen to a particular clinical isolate through laboratory testing prior to antibiotic treatment, resistance can be mitigated, and overall better patient outcomes will result.

### **Contributors of Virulence in *A. baumannii***

**Regulators of Virulence.** One of the global virulence regulators in *A. baumannii* has been identified as the two-component system GacSA, which regulates motility, pili synthesis, biofilm formation, amino acid metabolism and survival within the host[57]. Another regulator of virulence is the transcriptional regulator Fur (ferric uptake regulator), which controls systems for iron acquisition, an essentiality for survival *in vivo*. Another similar regulator of virulence controlling metal homeostasis is Zur, which controls two distinct zinc acquisition systems within *A. baumannii*[58]. An additional, rather unique regulator of virulence is BlsA, which responds to light and temperature to influence virulence through iron metabolism via direct interactions with Fur[59]. Photoregulation is a unique feature in *A. baumannii* virulence that is not yet fully understood. However, it is tempting to speculate that this regulator, BlsA, contributes to the shifts in cell behavior outside of the host that require persistence on surfaces, and within the host, where light is absent, but iron scavenging and virulence factor production are necessary.

**Virulence Factors.** The most well studied virulence factor produced by *A. baumannii* is OmpA, an outer membrane protein that facilitates the adherence to host cells, mediates their invasion and promotes cell death. *A. baumannii* also produces a variety of porins (Omp22, Omp33, Omp36, CarO) similar to OmpA that induce host cell death. Other membrane associated factors are also essential and contribute to virulence in *A. baumannii*. For example, type two secretion systems (T2SS) secrete factors that are required for virulence such as the lipoyl synthases LipA [60] and LipH as well as proteases such as CpaA [61]. Phospholipase C as well as LPS and penicillin binding proteins also serve as virulence factors by contributing to resistance to serum and promoting survival in vivo [62].

Although *Acinetobacter* translates to non-motile rod, it is now known that *A. baumannii* is capable of two forms of motility- twitching motility and surface associated motility. Specifically, *A. baumannii* demonstrates twitching motility through the use of type IV pili, allowing the organism to travel on wet surfaces in a flagella-independent manner. Surface associated motility is in part controlled by quorum sensing, however, a mechanism for this is unclear [63]. These forms of motility are considered virulence effectors as they contribute to survival within the host and certain components such as PilA serve to assist in immune evasion [62].

Another mechanism of virulence is the ability of *A. baumannii* to scavenge metals from the host such as zinc, iron, copper, and manganese. These metals are necessary to serve as structural cofactors for a variety of proteins and essential systems and are therefore

important for the survival of *A. baumannii*. Zinc acquisition is accomplished via the expression of the ZnuABC system, which is regulated by the Zur transcription factor and allows for resistance to calprotectin zinc sequestration by the host when levels of zinc are low[64]. Another Zur regulated system induced following zinc starvation is the metallochaperone ZigA, which sequesters zinc from histidine-zinc complexes with the help of HutH[65].

Copper resistance is also a major contributor of virulence in *A. baumannii*. This is achieved through the production of a variety of proteins that function to regulate copper transport, oxidation, sequestration, and homeostasis. Copper is used by the immune system as a means for bacterial clearance due to its toxicity and therefore these resistance mechanisms are vital to ensure survival *in vivo*[66]. The regulation of iron is equally important, and homeostasis is regulated in some part by Fur. *A. baumannii* also possesses a variety of heme oxygenase enzymes which remove iron from heme. Other uptake systems for iron are present in *A. baumannii* as well as the production of siderophores that chelate iron[67]. Iron uptake can also be regulated by a membrane porin, OmpW that also contributes to antibiotic resistance through colistin binding[68].

*A. baumannii* also produces a variety of putative efflux pumps, fimbriae systems, pili components and membrane proteins that are yet to be characterized, but likely contribute to virulence. In addition, this species has a variety of stress response proteins that protect the cell from external threats such as DNA damage, exposure to reactive oxygen species (ROS) and nutrient starvation.

**Capsule and Immune Evasion.** A significant way that *A. baumannii* can avoid detection by the immune system is through the production of glycoconjugates: bacterial carbohydrates that act as a line of defense against host cells and the environment. One such glycoconjugate is a capsule consisting of polysaccharides. Specifically, capsule formation can protect against complement mediated killing[69]. Immune evasion also comes in the form of glycosylation of type IV pili to render them undetectable by host cell antibodies[70]. Capsules also play a role in the formation of biofilms which protect *A. baumannii* and allow them to persist within the infected host.

**Desiccation Tolerance.** One of the reasons *A. baumannii* is able to thrive within the hospital environment is its ability to survive for extended periods of time without water or nutrients[71]. Its ability to persist on objects such as medical equipment and bed rails for longer than a week allows for a variety of opportunities for secondary infections and patient exposure[72, 73]. Depending on the strain, *A. baumannii* isolates such as AB5075 can survive desiccation for over 90 days[74]. Based on this study, desiccation tolerance was attributed to the function of BfmR, a response regulator that controls the production of oxidative stress response genes as well as other factors following nutrient starvation or high osmolarity. In general, tolerance is thought to be due to the expression of capsular polysaccharides, which can assist in retaining water for extended periods of time[70]. In addition, changes in the cell envelope that induce a thicker cell wall, a shift from rod shape to cocci shape cells and higher electron density occur following desiccation[75].

## ***Acinetobacter baumannii* Biofilms**

**Types of Biofilms.** *Acinetobacter baumannii* is able to form biofilms as free-floating aggregates, at the surface-liquid interface of cultures or at the air-liquid interface in the form of a pellicle. Surface associated biofilms are able to form on a variety of surfaces typically found within a clinical setting such as glass, rubber, porcelain, polypropylene, stainless steel, and polycarbonate[21]. Of these, polycarbonate and stainless steel promote the most biomass accumulation. Polycarbonate is hydrophobic, which is a characteristic that is common for the promotion of bacterial attachment. Biofilms can also form under static conditions or within flow cell systems such as bioreactors where nutrients are continually replenished and the biofilm is under sheer stress[76]. Flow cell systems attempt to mimic the environment that would be experienced within the body and therefore serve as a good model for biofilm characterization *in vitro*. Importantly, the system of study dictates the biofilm structure and cell behavior which is very different when parameters such as media, temperature, length of incubation, and stasis are changed[44]. Therefore, it is important to continue to investigate multiple forms of biofilms produced by *A. baumannii*. Thus, we will understand the major regulators controlling biofilms residing within the hospital on surfaces as well as those causing persistent infections *in vivo* that are increasingly difficult to treat.

**Regulators and Known Effectors of Biofilm Formation.** BfmRS is one of the best characterized regulators of biofilm formation in *A. baumannii*, particularly due to its control of the *csu*-operon-encoded usher pili system essential for the formation of biofilms on

abiotic surfaces[77]. In addition, GacSA has been shown to regulate this operon and indirectly influence biofilm formation[57].

Other than the expression of the *csu* operon, other factors exist that contribute to biofilm formation. For example, Bap encodes a very large biofilm associated protein that assists in maintaining a stable mature biofilm structure[78]. Further, a type I secretion system exists to export Bap, and thus assists in maintaining biofilm stability[79]. In addition, the production of an autotransporter adhesion (Ata) assists in adherence of biofilms to membranes of the host[80]. Another essential component of a successful biofilm is the production of poly- $\beta$ -1,6-*N*-acetylglucosamine (PNAG) encoded by the *pgaABCD* locus[81]. The production of capsule in the form of polysaccharides has also been attributed to better biofilm formation[69]. In addition, O-linked glycosylation is important for virulence as well as biofilm formation[82].

Pili systems are also known to be upregulated during biofilm formation, specifically *filF*, *fimA*, and *papC* transcripts are universally upregulated regardless of the time of incubation or differing growth conditions of *A. baumannii*[44]. In addition, RND efflux pumps and iron acquisition systems are upregulated in *A. baumannii* biofilms, which links antibiotic resistance to biofilm formation[44]. This connection has been explored for a variety of antibiotics. More recently, connections have been drawn between the presence of biofilm associated genes such as pili and the presence of a CRISPER/cas system, however the details behind their involvement remains unclear[83].

## Antimicrobial Peptides

**Origins and Properties.** Antimicrobial peptides (AMPs) are produced by every domain of life. The first AMP was isolated from a soil bacterium, *Bacillus brevis* in 1939 following experiments that showed protection of mice against pneumococcal infection[84, 85]. The peptide was later identified as a mixture collectively named gramicidin. Since then, a variety of peptides have been identified in plants, animals, protozoa, fungi, and insects. In addition, many have been synthetically derived.

Humans produce AMPs as a first line of defense against invading pathogens. The most important and best studied human AMP is the cathelicidin LL-37 that functions to kill invading bacteria, but also modulates the immune system and ensures it does not overreact to the exposure of bacterial components such as LPS[86]. LL-37 can protect against infection in a variety of areas, including the pulmonary and digestive systems, the genitourinary system, salivary glands, skin, and ocular surfaces[86].

AMPs are characteristically small, typically cationic, and amphipathic. According to the peptide database, ADP3, ([aps.unmc.edu/classification](http://aps.unmc.edu/classification)) however, they can be classified as either cationic, neutral, or anionic. Further they can be hydrophobic, amphipathic, or hydrophilic. Peptides within this database are considered to be AMPs if they consist of between 2-100 amino acids. AMPs made up of greater than 100 amino acids are instead considered antimicrobial proteins which includes lysozyme or histones, for example. In addition, if the AMP composition consists of at least 25% of a single amino acid (X), they

are termed X-rich peptides. For example, proline-rich or glycine-rich peptides have been discovered to have antimicrobial properties[87-89]. They can be classified based on their biological function, for example some are antibacterial or antifungal, while others are chemotactic, insecticidal or mediate wound healing. Another form of classification is termed the universal classification system (UC) which separates AMPs into four classes: class I (UCLL) are linear one-chain peptides or two linear peptides not connected covalently; class II (UCSS) are sidechain-sidechain linked peptides; class III (UCSB) are polypeptide chains with a sidechain to backbone connection; and class IV (UCBB) are circular polypeptides with a peptide bond between both termini[90]. Examples of class II include disulfide containing defensins or ether-bond containing lanthibiotics, while class III include bacterial lasso peptides and fuscaricidins[90]. Finally, class IV peptides include cyclotides from plants or theta-defensins from animals[90]. An additional layer of classification is the distinction between peptides based on the presence or absence of beta sheets or alpha helices in their secondary structure. For example, AMPs within the alpha family contain helical structures, while those within the beta family are composed of beta-strands and those within the alpha-beta family have both. The final family within this classification is the non-alpha-beta family, with AMPs that do not possess helices or beta-strands.

These numerous forms of classification allow for quick insights into the characteristics of a particular peptide. This is necessary to readily distinguish between each AMP as the number of sequences within the databases rapidly rises. As of October 20, 2021, there are 3,273 AMPs within APD3, 2,756 of which are considered antibacterial

(aps.unmc.edu). There are a variety of other AMP databases, however, ADP3 is the largest that is specific to AMPs. For example, there is a biofilm AMP database, but only 221 peptides are present (baamps.it). This is likely due to the juvenescence of this niche field. Databases such as these are a great resource to promote the understanding of AMPs and to collectively compare newly identified peptides to those reported within the databases.

**Methods for Discovery.** Natural products drug discovery has had many successes over the years, however, approaches to identify new environmental compounds is not always as easy as screening large synthetic small molecule libraries. For example, fractionation and purification are considered far more laborious than the high-throughput screening of combinatorial libraries[91, 92]. However, new advancements in biotechnologies have resulted in a better understanding of genomics, natural product biosynthesis, synthetic biology, transcriptomics, and post-translational modifications. These advancements have propelled us towards what we hope to call the New Golden Age of natural products drug discovery[91]. For example, platforms have emerged that are aimed at targeting druggable proteins and peptides and predicting ligands through chemoproteomics resulting in target specific identification from a variety of natural product sources[93].

A number of approaches have been considered the gold standards for AMP discovery, such as bioassay guided fractionation. This includes the isolation of peptides through solvent extraction followed by fractionation using chromatography. These crude fractions are then tested for bioactivity and bioactive fractions are then reassessed to identify the

component within contributing to activity. Bioactive components are then isolated, purified, and retested, while their structure is simultaneously elucidated. Unfortunately, this requires multiple rounds of fractionation and subsequent bioactivity screening before a single peptide can be isolated. A disadvantage to this approach is the inability to isolate active peptides from a crude fraction of peptides. There are multiple reasons for this, including the degradation of bioactive components during purification due to its instability, the existence of bioactive peptides at too low of a concentration, thus preventing isolation, or the interdependence of multiple peptides within a fraction working synergistically to exhibit bioactivity[94]. Further to this, there is a disappointingly high rate of reisolating peptides that have previously been discovered using such approaches.

A way in which to avoid this repetition is through the use of dereplication or the pre-analysis of partially purified (fractionated) samples using NMR or mass spectrometry. The efficiency of this step is also growing as dereplication databases such as the Dictionary of Natural Products for spectral alignments is expanding. Resources such as the Global Natural Product Social molecular networking platform (GNPS) is also growing rapidly and allows for the annotation of bioactive products. Certain groups have proposed the use of a workflow termed bioactive molecular networking which integrates bioactivity scoring and MS/MS data to assist in bioassay guided fractionation processes[94]. This approach is similar to the novel pipeline that was created by our collaborators at the University of North Carolina, Chapel Hill -the statistically guided bioactive peptides prioritized via mass spectrometry (PepSAVI-MS) approach. This allows for bioactivity to be attributed to peptides through simultaneous mass spectrometric analysis with bioassay guided

statistics to identify peptides with bioactivity[95]. This pipeline aims to identify cationic peptides of medicinal plants, but it has proven as successful in identifying novel AMPs from other sources as well.

When considering experimental design for assessing bioactivity there are additional challenges. The cationic nature of AMPs can cause off-target binding to certain assay materials that make screening a extensively thought out process. Peptides can bind to components within the media being tested, other experimental materials, compound vials, or even transport material, such as pipette tips. Therefore, testing must account for the physiochemistry of the AMPs to be tested. Common laboratory consumables are composed of polypropylene, polystyrene, or borosilicate glass, each of which elicit some level of AMP binding[96, 97]. Experimental design, however, can limit this interaction, leading to more representative results. Another feature of AMPs that is their tendency to be unstable. To overcome this limitation, AMPs should be tested within the same day, freeze-thaw cycles should be minimized, and AMP concentrations should be increased to account for loss due to binding. In addition, selecting a media that allows for the AMP being tested to remain soluble within the testing range is essential.

The advantageous approach of testing the bioactivity of AMPs within the same day to ensure peptide stability can be achieved by tracking bacterial respiration instead of implementing traditional overnight MIC assays. Fluorescent dyes have been used for this purpose, however, the nontoxic dye, resazurin is superior to most for a multitude of reasons.

**AMPs in Plants.** Plant derived natural products have been used since ancient times to cure common ailments such as inflammation, sickness, and nausea. Documentation of plant based medicinal systems can be found in the histories of almost every human civilization[92]. Today, it is estimated that more than 70% of the global population rely on the use of medicinal plants and herbs for their health due to the inability to afford western medicines[92]. However, there are some disadvantages to the use of herbs and plants in this regard, including the observation that certain components of plants are toxic, and that manufacturing of herbal supplements is not regulated by the FDA. It is important to consider that natural does not equal safe.

Distinct from humans, plants do not possess a form of adaptive immunity, and therefore rely on factors such as AMPs for protection against bacteria and fungi[98]. A general characteristic of plant derived AMPs that makes them unique is their high cysteine content, which results in multiple disulfide bonds[99]. The best studied groups of plant AMPs are thionins, defensins, and cyclotides, however there are many other classes. In addition, each portion of a plant is known to contain AMPs. Previous research has shown that plant based peptides can even work synergistically to combat bacterial biofilms, the most concerning form of infection[100].

**AMPs as Antibiotics.** Natural products have long been a successful source for medicinal discovery over synthetic compounds. In fact, a majority of FDA approved drugs are natural products, or synthetic derivatives of natural products[92]. Peptides serve as

advantageous options for therapeutic treatments due to their reduced immunogenicity, better tissue penetration, and relatively low manufacturing costs compared to antibody or protein therapies. In addition, advances in biotechnology have allowed for better systems for AMP production. For example, the recombinant expression of AMPs in plants for molecular farming has been proposed as a sustainable approach to upscaling AMP production[101].

Although AMPs are not always bioactive, they are universally produced leaving vast opportunities for discovery. In addition, their scaffolds can serve as inspiration for semi- or wholly synthetic derivatives with improved bioactivity. For example, peptide length and composition can be altered to enhance target specificity. Other methods to enhance pharmacokinetic properties can be achieved through peptide modification or encapsulation.

To date there are 3,273 AMPs within the antimicrobial peptide database, however, only a few AMPs have FDA approval for use in humans: gramicidin, daptomycin, colistin, vancomycin, oritavancin, dalbavacin, nisin, polymyxin, bacitracin and telavancin. One of the main features of these AMPs is their stability- their long half-lives give them greater therapeutic potential. The first, Gramicidin, was isolated from *Bacillus brevis* as a mixture of pore forming peptides in 1939[84, 85]. Original testing was unsuccessful as the peptide was toxic within the peritoneum of mice[102]. However, topical applications led to FDA approval in 1955, and gramicidin was introduced as a component of Neosporin. This topical antibiotic is used for everyday applications, such as skinned knees and minor cuts.

Bacitracin is also only approved for topical use, however, several of the other AMPs with FDA approval such as polymyxin B, colistin and daptomycin are bioavailable and approved for use via injection[103]. Thus, peptides such as colistin that are bioavailable and very effective are held in reserve as antibiotics and are considered very valuable. There are also a variety of AMPs undergoing clinical trials, and with the biotechnological advances discussed in earlier sections, we expect to see more enter the market each year.

**AMP Mechanisms of Action.** The most common mechanism of action for antibacterial AMPs relies on their cationic nature. Specifically, they target bacterial cell membranes and cause disintegration of the lipid bilayer which results in lysis[104]. These are referred to as membrane-active AMPs. The ability to integrate into membranes is based on their amphipathic nature, which means they possess a cationic portion as well as a hydrophobic portion. This feature ensures cationic interaction with the negatively charged membranes, and the integration into these membranes via their hydrophobic portion. There are a variety of mechanisms in which this can occur depending on the properties of the AMP. For example, some peptides aggregate and bind to the surface of cells as a cluster, which results in a large gapping of the membrane and subsequent pore formation. This mechanism mimics surfactants and is referred to as the carpet method[105]. Another mechanism of pore formation comes when a disordered peptide contacts a lipid membrane and then becomes ordered, which alters its secondary structure in a way that ultimately leads to membrane penetration[105].

More recent reports, however, have shown that some AMPs can target intracellular functions, such as protein synthesis, without any membrane damage. These are referred to as cell penetrating peptides. In addition, others such as buforin II have demonstrated the ability to bind DNA and RNA intracellularly without membrane disruption, instead functioning via diffusion into cells[106].

### **Project Aim**

This work will cover three distinct (but important) topics associated with both the virulence of *A. baumannii*, and antimicrobial therapies for other major human pathogens. Chapters 2-3 aim to further our understanding of biofilm formation and virulence in a highly pathogenic and clinically relevant *A. baumannii* strain, AB5075. Chapter 2 will address the biofilm population as well as describe our approach for the identification and characterization of factors important for *A. baumannii* biofilm formation. Within Chapter 3, UspG (a newly identified negative effector of biofilm formation) will be characterized for its roles in *A. baumannii* virulence and stress adaptation. Finally, Chapter 4 aims to describe how we use natural products discovery to combat antimicrobial resistance. Our successes in plant-derived AMP discovery will be outlined with focus on the evolution of our collaborator's novel pipeline and demonstratable antibacterial activity against a panel of multi-drug resistant bacteria.

## **Chapter 2: Identification and Characterization of Factors Required for Biofilm**

### **Formation in *Acinetobacter baumannii***

#### **Introduction**

*Acinetobacter baumannii* is a dangerous pathogen often referred to as “Iraqibacter” due to its emergence in wounded soldiers during the Iraq war[27]. It is commonly known for causing myriad diseases, such as ventilator associated pneumonia, wound infections, diabetic foot infections, peritonitis, and urinary tract infections, as well as meningitis and bacteremia[107-109]. In 2019, the CDC released a list of multi-drug resistant microorganisms and presented carbapenemase producing *A. baumannii* as a highest priority pathogen for drug resistance. Additionally, a substantial number of *A. baumannii* clinical isolates are also extended spectrum beta-lactamase (ESBL) producers, rendering even the most recent generations of beta-lactam antibiotics ineffective[110, 111]. Unfortunately, most strains of *A. baumannii* are resistant to common clinical antibiotic classes, such as aminoglycosides, fluoroquinolones, and tetracyclines, among others[112]. The resistance capacity of this organism is further exacerbated when growing in a biofilm as tolerance to environmental stressors and antimicrobial agents becomes significantly increased when in this state[70]. This problem is magnified when one considers that a majority of the infections caused by *A. baumannii* are likely mediated through biofilm formation[70].

Bacterial biofilms cause up to 80% of chronic infections[113], and are defined as dense, aggregated communities with a population(s) of bacteria encased within a protective layer (extracellular matrix, ECM). They can form by attachment to host tissues or abiotic surfaces, can exist as free-floating aggregates, or form pellicles at air liquid interfaces. This serves as a line of defense against external stress, the immune system, and antibiotics, among other factors. *A. baumannii* has the unique ability to form various types of biofilms dependent on the environment in which it is grown. For example, unlike other *Acinetobacter* species, *A. baumannii* strains can form biofilms at air-liquid interface and can survive for days in a desiccated environment, making a hospital setting ideal for it to thrive[114-116].

A number of factors have already been identified as being essential for biofilm formation in *A. baumannii* thus far. It has been demonstrated that nutrient availability, pili, flagella, outer membrane proteins, adhesins, quorum sensing systems, metals and secreted macromolecules all play a role in biofilm formation[117]. One of the better studied factors influencing biofilm formation in *A. baumannii* is the membrane embedded biofilm associated protein (Bap), a giant protein (469kDa) that is highly conserved in *A. baumannii* strains and shares similarity to Bap produced by *Staphylococcus aureus*[78, 118]. This protein is highly abundant within *A. baumannii* biofilms [119], and is predicted to play a role in cell-cell adhesion to support mature biofilm structure[78, 118]. In order to stabilize biofilms, Bap monomers self-assemble into amyloid like formations important for altering the hydrophobicity of cell surfaces, so as to attach to biotic (human cells) and abiotic surfaces[120, 121]. In terms of Bap expression and regulation, little is known,

however, low iron concentrations increase Bap production during biofilm formation[122]. *A. baumannii* has also been known to produce Bap like proteins (Blp1 and Blp2) that influence biofilm formation and architecture, sharing Ig-like domains, N-terminal motifs, and expression profile similarities[123, 124].

In addition to Bap, OmpA, an outer membrane protein, is believed to possess a biofilm associated role *in vivo* through attachment to epithelial cells, and also *in vitro* through attachment to polystyrene[125, 126]. Studies have suggested that *ompA* is present in both strong biofilm forming strains and non-biofilm forming strains, indicating that its role in virulence through host cell cytotoxicity following adherence may be its primary function[122]. Another surface associated factor essential for biofilm formation *in vitro* and *in vivo* is the *Acinetobacter* trimeric autotransporter adhesin (Ata). This adhesin has the ability to bind to various host extracellular matrix and basal membrane components, such as collagen and laminin, in addition to plastic [80, 127]. As collagen I is the most abundant ECM component in the lung, it is predicted that this trimeric autotransporter can take advantage of exposed collagen to initiate and maintain a biofilm in this niche during infection[80]. That being said, there is evidence to suggest that *ata* is only present in certain clonal lineages of *A. baumannii* (78%), such as ATCC 17978, and thus its role is clearly not conserved across all strains [128, 129]. In addition to these factors, the well-studied usher pili system made up of the Csu proteins A/B,A-E is very important for attachment to abiotic surfaces[130], and is considered key to biofilm formation.

When considering polysaccharides, the production of Poly- $\beta$ -1-6-*N*-Acetylglucosamine (PNAG) is critical for biofilm formation in *A. baumannii*[81]. The *pgaABCD* locus encodes genes for the production of PNAG, which is a major component of biofilm ECM in many species of bacteria and is universally conserved among *A. baumannii* isolates[81, 131, 132]. In general, polysaccharides act to assist in biofilm adhesion, providing protection from the host, and maintaining structural integrity of the biofilm. In *A. baumannii* it seems that PNAG production occurs in biofilms at the liquid-surface interface when under shear force (S1 strain)[81], while it is produced within pellicles formed at the air-liquid interface under static conditions (ATCC 17978 strain)[133]. In addition, the process of O-linked glycosylation, which is a part of capsule production, has been shown to be important in surface-liquid biofilms, as defects are observed in biofilms formed without a functioning PglC protein, which typically initiates glycosyltransferase activity[134]. Furthermore, O-linked protein glycosylation of biofilm associated polysaccharides through the O-Oligosaccharyltransferase (O-OTase) PglL has been shown to be important for proper biofilm formation in this organism[82]. It is also known that eDNA is required for ECM formation, however there is little to no evidence regarding the mechanics of this process. One suggestion is that eDNA is transported from the cell through membrane vesicles, however this contention still requires validation[135].

In terms of regulating the biofilm process, much less information is available, however, a few global transcriptional regulators have been identified. First, the two-component system BfmRS has been shown to regulate the *csu* operon and the K-locus for capsule production[136-138], both of which are required for biofilm formation. Similarly, the TCS

GacAS influences biofilm formation via regulation of the *csu* operon, as well as *ompA* [57]. This TCS has also been found to be highly expressed within pellicles indicating involvement in various types of biofilms formed by *A. baumannii*[133]. Quorum-sensing has also been implicated in influencing biofilm formation in *A. baumannii*, as deletions in the autoinducer synthase *abaI* lead to impaired biofilm forming capabilities[139-141]. Importantly, inhibition of the quorum-sensing receptor, AbaR, by non-native *N*-acyl homoserine lactones has been shown to reduce biofilm formation in *A. baumannii*[142].

Although a number of studies have explored the contribution of various factors to *A. baumannii* biofilm formation, there is still a paucity of information on this important topic (given the relevance this lifestyle plays in disease causation for this organism). As such, herein we sought to uncover in a global, unbiased manner, factors contributing to biofilm formation at the surface liquid interface in the highly virulent *A. baumannii* strain AB5075[143]. To do so, we make use of an ordered transposon mutant library to screen for biofilm impaired or biofilm enhanced phenotypes compared to the wildtype strain. In so doing, we identified a wealth of novel factors that influence biofilm formation, including those important for transcriptional regulation, transport, stress response and metabolism. Mutants for these genes were comprehensively characterized, quantifying biofilm biomass, eDNA production, ECM composition and adhesion capabilities. As such, this work shines new light on the process of biofilm formation in *A. baumannii*, providing new avenues for further investigation, and the potential to serve as future targets for antimicrobial therapeutic intervention.

## Materials and Methods

**Strains and Growth Conditions.** Transposon mutant strains used in this study were obtained from the University of Washington transposon mutant library of *A. baumannii* AB5075-UW[144]. All strains were stored at -80°C in Lysogeny Broth (LB) with 25% glycerol. Mutants containing the T26 transposon were grown on LB agar (LBA) supplemented with 12.5 µg/mL tetracycline or LB containing 5 µg/mL tetracycline. Mutants containing the T101 transposon were grown in LBA and LB containing 160 µg/mL hygromycin B.

**Screening Transposon Library Mutants for Biofilm Production.** For screening purposes, 96 well plate glycerol stocks of the *A. baumannii* transposon library were defrosted, and 20 µL was removed and added to 180 µL tryptic soy broth (TSB) in tissue culture treated 96 well plates (Falcon). Plates were then sealed with parafilm and masking tape and incubated for 24 hours under static conditions at 37°C. After this time, OD<sub>600</sub> values were recorded and wells were gently aspirated, prior to fixing with 100% ethanol. Once dry, cells were stained for 15 minutes using 0.3% crystal violet (CV) and then rinsed three times in PBS, before being allowed to air dry. CV was eluted by a 10 min incubation with 100% ethanol and their OD<sub>550</sub> was recorded using a Synergy 2 plate reader (BioTek). All liquid handling processes were performed using of a viaflo 96-well pipetting robot (INTEGRA Biosciences Corp.). For every assay plate, data was subjected to normal distribution statistics to establish a list of leads due to the absence of a wildtype control within the transposon mutant library plates. The CV values for each assay plate was

averaged, with maximum and minimum values determined. Thereafter a Z-score was calculated for each strain by subtracting the raw CV value for each well from the mean of the assay plate. This value was divided by the standard deviation of each sample plate to obtain a Z-score. To generate a prioritized list of mutants within a given plate, a cutoff was established as  $\pm 12.5^{\text{th}}$  percentile from the mean for each assay plate.

**Secondary Screening of Mutant Strains.** Each mutant identified in the primary screen was rescreened alongside the wild-type strain in technical sextuplicate, using methods outlined above, to ensure retention of phenotype. Mutants were narrowed by quantifying fold change from the parental strain, and only those whose biofilm was altered  $\pm 2$ -fold were considered for further study.

**Complement Strain Generation.** All cloning strains, plasmids and primers are listed in **Supplemental Tables A1 and A2**. Flanking primers were designed for target genes to include the native promotor as well as 100-200 nt of DNA 3' of translational stop codons. Each fragment was amplified by PCR and products were cloned into pMQ557. Strains were confirmed by PCR and Sanger sequencing (GeneWiz) prior to transformation into the relevant mutant strain. Mutant strains containing complementation plasmid were again confirmed by PCR and Sanger sequencing (GeneWiz). Assays were performed using Hygromycin B at a concentration of 160  $\mu\text{g}/\text{mL}$  to maintain the plasmid. Empty vector controls for each mutant strain and the wildtype strain were included for complementation assays.

**Real-Time Biofilm Analysis.** An xCELLigence Real Time Cell Analysis (RTCA) instrument was used to evaluate biofilms, according to manufacture protocols (ACEA Biosciences Inc.). Each strain was grown overnight with shaking at 37°C in TSB supplemented with antibiotics relevant to the transposon marker being used. Prior to each assay, cells were standardized to an OD<sub>600</sub> of 0.5 in PBS. Antibiotic free TSB (180µL) was used to blank the system before 20µL of each strain was added to each well leading to a final OD<sub>600</sub> of 0.05 (~5x10<sup>7</sup> CFU). Plates were incubated statically in the RTCA device at 37°C, and electrode output readings were taken every 5 minutes for up to 72 hours. Each strain was seeded in biological triplicate and technical duplicate for n=6 for each strain. Units are expressed as cell-sensor impedance (CI), which is automatically calculated at each time-point as  $(X_n - X_b)/5$  with  $X_n$  indicating the impedance at said time-point and  $X_b$  representing the background impedance recorded prior to the addition of cells into the assay plate.

**eDNA Quantification.** Extracellular DNA was evaluated for planktonic and biofilm populations of each strain using the Quant-iT™ PicoGreen® biofilm kit (Invitrogen). Biofilms were prepared as detailed above, and a standard curve was generated using λ DNA according to the manufacturer's protocols. Planktonic cells were carefully removed from wells before biofilms were disrupted and resuspended in 100µL TE buffer. Each sample was then transferred to a black walled 96 well plate before 100µL of TE + PicoGreen® reagent was added to each well. Plates were incubated for 4 minutes in the dark before reads were taken using a Synergy 2 plate reader (BioTek). Measurements were recorded at an excitation of 480nm and 520nm emission. Controls of TE alone and

TE + PicoGreen® were included in each assay. Background was subtracted prior to calculation of eDNA concentration. A standard curve was generated using manufacturer provided DNA and a slope equation ( $Y=mX+B$ ) was used to determine eDNA concentrations present in samples. Each strain was tested in biological triplicate and technical duplicate giving  $n=6$  for each mutant.

**Extracellular Matrix Component Inhibition Assays.** Assays were performed similar to Sager et. al. with the following modifications[145]. In brief, overnight cultures were standardized to an  $OD_{600}$  of 0.5 in PBS before 96-well tissue culture treated plates were seeded with 180 $\mu$ L TSB with or without proteinase K (25 $\mu$ g/mL) or sodium periodate (2.5mM). Wells were then inoculated with 20 $\mu$ L of each standardized strain giving a final sample volume of 200 $\mu$ L. Proteinase K was solvated in 20mM Tris-HCl (pH 7.5) and 100mM NaCl, while sodium periodate was solvated in deionized water. Plates were incubated for 24 hours at 37°C under static conditions. After this time, plates were analyzed using the CV procedure described above. For each strain, no-treatment wells were averaged and used to calculate fold change from treatment groups. All data is presented based on testing each mutant in biological triplicate.

**Extracellular Matrix Component Disruption Assays.** Biofilms were seeded as described above and allowed to form for 24 hours. After this time, they were treated with either 25 $\mu$ g/mL proteinase K, 2.5mM sodium periodate, or solvent, and were then allowed to incubate for an additional 24 hours prior to processing. Processing and analysis were performed using methods described in the previous section.

## Results

**An Unbiased Global Screen to Identify Novel Components Influencing Biofilm Formation in *A. baumannii*.** Although a number of genes have previously been shown to influence biofilm formation in *A. baumannii* [117, 146], to our knowledge there has not, to date, been a large scale, unbiased approach to identifying them. Accordingly, we made use of the ordered transposon library previously reported in strain AB5075 [144] by randomly selecting twenty-eight 96-well plates from this collection (~25%) and assessing the biofilm formation capacity of mutants contained within. Each plate was used to generate biofilms in a replica 96-well plate format, before being subjected to crystal violet (CV) staining after 24 hours of incubation. Because transposon mutant library plates do not contain a wildtype strain, each plate was subjected to normal distribution statistics to establish a list of leads. The CV values for each assay plate were averaged with the maximum and minimum values determined. Thereafter each well of the plate was given a Z-score that allowed a cutoff to be established by identifying strains that ranked furthest from the mean (**Supplemental Tables A3 and A4 Supplemental Figures A1 and A2**). For ease of processing, the cutoff used was  $\pm 12.5^{\text{th}}$  percentile from the mean of each plate. From this initial screen, we identified 171 (6.46%) isolates demonstrating differential biofilm biomass from the total of 2,648 screened (40 total wells were empty in the 28 plates screened) (**Supplemental Figures A1 and A2**). Of these, 79 showed significantly increased biofilm formation and 92 demonstrated a decrease in biofilm formation.

Following the initial screen, our 171 strains were validated using CV staining in sextuplet in direct comparison to the wildtype to establish a rigorous, quantitative cutoff. Using a baseline of  $\pm 2$ -fold alteration, along with statistical significance (**Figure 2**), we found 30 mutants demonstrating an increase in biofilm biomass, and 19 mutants with a decrease in biofilm biomass, when compared to the parental strain (**Table 1**). Of note, a presiding characteristic that eliminated mutants with decreased biofilm capacities at this stage was the presence of a growth defect (data not shown).

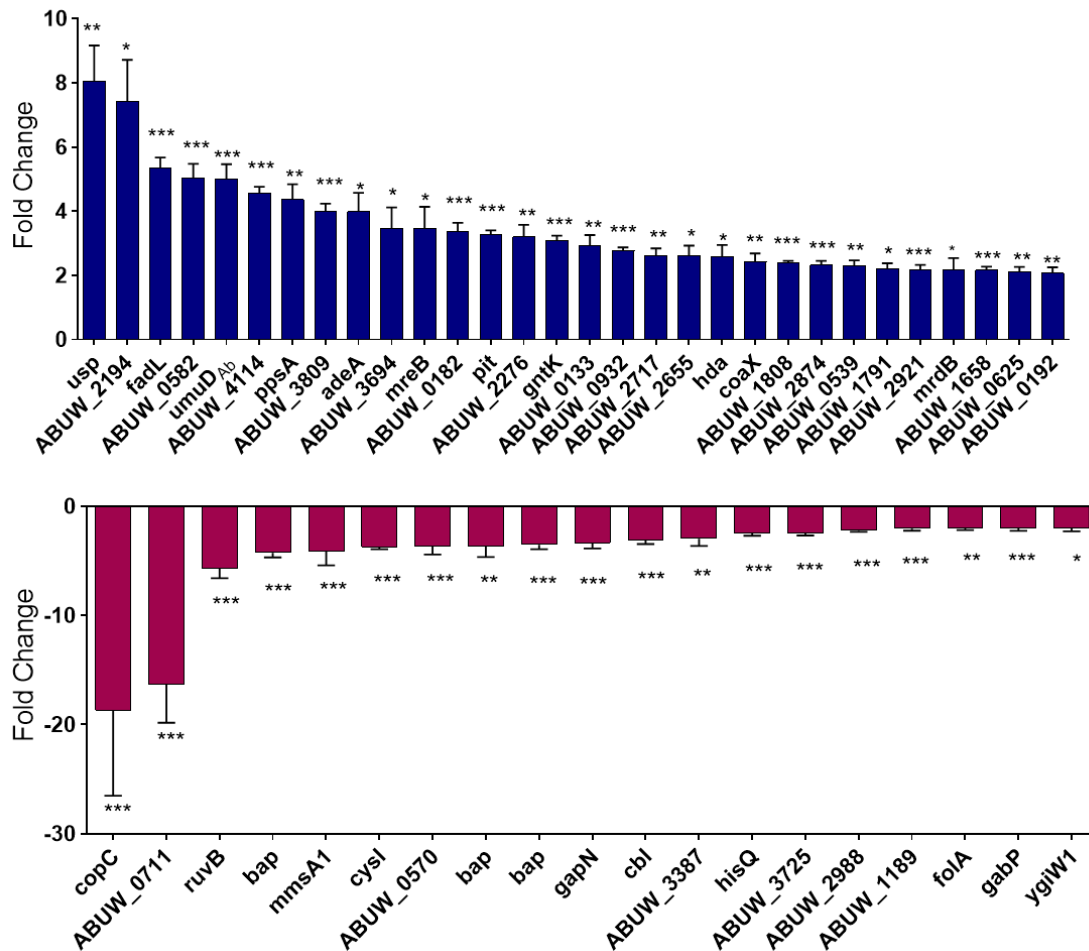


**Figure 2. Mutants Identified as Demonstrating Altered Biofilm Biomass Following Secondary Screening.** Shown is the crystal violet analysis of biofilms for mutant strains identified in the secondary screen as having significantly altered biomass as compared to the wild-type strain. Data is derived from 6 replicates per strain after 24h growth. Error bars are shown  $\pm$ SEM. Statistical significance was assessed using Student's t-test. P-value: \* =0.01 ; \*\* =0.001 ; \*\*\* = 0.0001.

**Table 1. Lead Transposon Mutant Strains Confirmed to Significantly Alter Biofilm Formation.**

ID	Gene	Description	CV Fold
<b>ABUW_1763</b>	<i>usp</i>	UspA domain protein	8.05
<b>ABUW_2194</b>	-	Acyl-CoA dehydrogenase, middle domain protein	7.43
<b>ABUW_3242</b>	<i>fadL</i>	FilD	5.34
<b>ABUW_0582</b>	-	Phage-related capsid scaffolding protein (GPO-like)	5.04
<b>ABUW_2431</b>	<i>umuD</i>	DNA polymerase V component	5.00
<b>ABUW_4114</b>	-	TraH family protein	4.56
<b>ABUW_1555</b>	<i>ppsA</i>	Phosphoenolpyruvate synthase	4.37
<b>ABUW_3809</b>	-	Transcriptional regulator, GntR	4.00
<b>ABUW_1974</b>	<i>adeA</i>	Multidrug efflux protein AdeA	3.98
<b>ABUW_3694</b>	-	Protein YegH	3.47
<b>ABUW_0715</b>	<i>mreB</i>	Rod shape-determining protein MreB	3.46
<b>ABUW_0182</b>	-	Two-component system hybrid histidine kinase/response regulator	3.38
<b>ABUW_2925</b>	<i>pit</i>	Phosphate transporter	3.27
<b>ABUW_2276</b>	-	Transcriptional regulator, ArsR family	3.20
<b>ABUW_3391</b>	<i>gntK</i>	Shikimate kinase	3.09
<b>ABUW_0133</b>	-	Ribosomal protein S30EA/sigma 54 modulation protein	2.94
<b>ABUW_0932</b>	-	Non-ribosomal peptide synthetase	2.77
<b>ABUW_2717</b>	-	3-oxoacyl-(acyl carrier protein) synthase	2.62
<b>ABUW_2655</b>	-	Hypothetical protein	2.60
<b>ABUW_0983</b>	<i>hda</i>	DnaA family protein	2.59
<b>ABUW_3133</b>	<i>coax</i>	Pantothenate kinase, type III	2.43
<b>ABUW_1808</b>	-	Hypothetical protein	2.39
<b>ABUW_2874</b>	-	Hypothetical protein	2.33
<b>ABUW_0539</b>	-	Hypothetical protein	2.29
<b>ABUW_1791</b>	-	Hypothetical protein	2.20
<b>ABUW_2921</b>	-	Formylglycine-generating sulfatase enzyme domain-containing protein	2.18
<b>ABUW_1244</b>	<i>mrdB</i>	Rod shape-determining protein RodA (EsvE3)	2.17
<b>ABUW_1658</b>	-	Hypothetical protein	2.16
<b>ABUW_0625</b>	-	Sporulation related domain-containing protein	2.11
<b>ABUW_0192</b>	-	Hypothetical protein	2.07
<b>ABUW_1352</b>	<i>ygiW1</i>	Bacterial OB fold domain-containing protein YgiW	-2.03
<b>ABUW_0201</b>	<i>gabP</i>	GABA permease	-2.04
<b>ABUW_3421</b>	<i>folA</i>	Dihydrofolate reductase	-2.04
<b>ABUW_1189</b>	-	ErfK/YbiS/YcfS/YnhG family	-2.05
<b>ABUW_2988</b>	-	Transcriptional regulator, LysR family	-2.24

**Table 1. Lead Transposon Mutant Strains Confirmed to Significantly Alter Biofilm Formation. (Continued)**

<b>ABUW_3725</b>	-	Transporter, drug/metabolite exporter family	-2.44
<b>ABUW_1340</b>	<i>hisQ</i>	Histidine transport system permease protein HisQ	-2.48
<b>ABUW_3387</b>	-	Leucine carboxyl methyltransferase	-2.99
<b>ABUW_1016</b>	<i>cbl</i>	Transcriptional regulator, LysR family	-3.11
<b>ABUW_3390</b>	<i>gapN</i>	Aldehyde dehydrogenase	-3.37
<b>ABUW_0885</b>	-	Biofilm associated protein	-3.53
<b>ABUW_0885</b>	-	Biofilm associated protein	-3.64
<b>ABUW_0570</b>	-	Phage-related baseplate assembly protein (GPJ-like)	-3.66
<b>ABUW_0643</b>	<i>cysI</i>	Sulfite reductase	-3.73
<b>ABUW_3783</b>	<i>mmsA1</i>	Methylmalonate-semialdehyde dehydrogenase	-4.15
<b>ABUW_0885</b>	-	Biofilm associated protein	-4.27
<b>ABUW_0999</b>	<i>ruvB</i>	Holliday junction DNA helicase RuvB	-5.70
<b>ABUW_3326</b>	<i>copC</i>	Copper resistance protein CopC	-16.28
<b>ABUW_0711</b>	-	Intracellular protease, Pfpl family	-18.70

Each biofilm was tested in technical sextuplicate for biofilm formation. CV Fold refers to the calculated fold change in biomass of the indicated mutant strain compared to wildtype AB5075. Positive fold changes were calculated by dividing the average CV of the mutant / the average CV of AB5075. Negative fold changes were calculated by dividing the average CV of AB5075 / the average CV of the mutant then multiplying by -1. CV: crystal violet staining.

### **Ontological Assessment of Factors Identified as Influencing Biofilm Formation. We**

next took the 49 genes from our secondary screen and organized them ontologically, based on predicted or known function (**Figure 3**). Importantly, when reviewing this list, we identified three different mutants in ABUW\_0885 (*bap::tn*) as having a marked decrease in overall biofilm production ( $\geq 3.5$  fold). Bap plays an important role in *A. baumannii* biofilm formation by assisting in cell-cell and cell-host adherence and maintaining mature biofilm structure on biotic and abiotic surfaces[118-121]. The substantial defects in biofilm formation observed for all three *tn* mutants thus serves as proof of principle for the efficacy of this study. Beyond this, the majority of strains fell into the categories of general metabolism or hypothetical proteins. Specifically, 13 of the 49 strains contribute to some form of metabolism within the cell, with seven found to exhibit

a stronger biofilm while six showed a biofilm defect. The metabolic pathways associated with each group were broad with no clear correlation, however this is potentially due to the nature of our randomized screen. Of interest, all six genes within the hypothetical protein category demonstrated increased biofilm formation, highlighting various potential new targets influencing biofilm formation. Each of these uncharacterized genes encode proteins ranging from 38 to 356 amino acids in length. Otherwise, nothing is known about these proteins in terms of function or homology, with no clear domains detectable from multiple different bioinformatic interrogations[147].

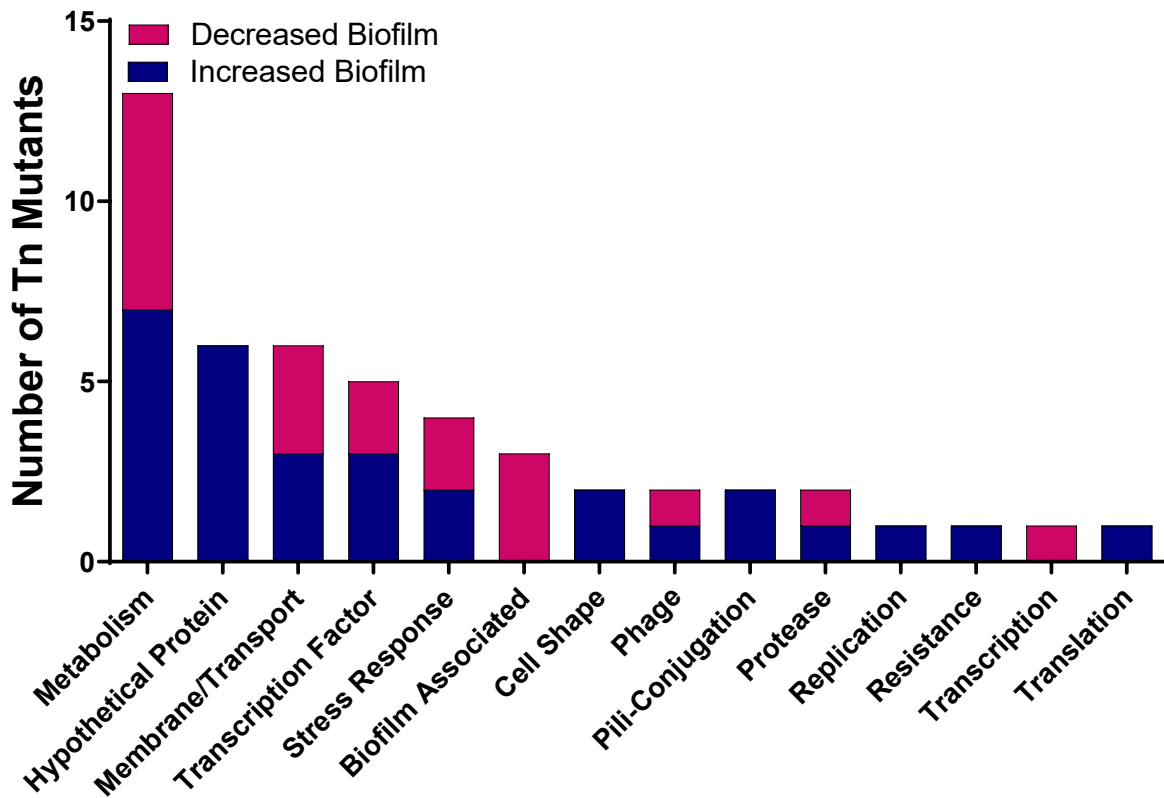


**Figure 3. Ontological Grouping of Mutants Identified as Having Differential Biofilm Forming Capacities.** Mutants altered in their ability to form a biofilm from our secondary screen were categorized ontologically based on known or predicted function.

Another abundant ontological grouping, transcription factors, contained five strains, three of which demonstrated increased biofilm formation. Of these, one was a hybrid two-component system component of unknown function, ABUW\_0182. The other two mutants belong to the ArsR (ABUW\_2276) and GntR (ABUW\_3809) transcription factor families. Both of the regulatory factors within the decreased biofilm group were members of the LysR family (ABUW\_1016 & ABUW\_2988), the most abundant class in *A. baumannii*[148]. The first of these, ABUW\_1016, is annotated as *cbl*, and would appear to be a homolog of CysB, which is involved in sulfur metabolism in *Escherichia coli*[149]; whilst the second is uncharacterized in terms of function, but demonstrates homology with the OxyR transcriptional regulator of *P. aeruginosa* (HHPred search [147]).

Further to this, we identified two mutants with enhanced biofilm formation that are predicted to engage in the general stress response, ABUW\_1763 (*usp::tn*) and ABUW\_2431 (*umuD<sub>Ab</sub>::tn*)[150, 151]. We also identified disruption of an uncharacterized membrane gene/protein as producing a defect in biofilm formation. Interestingly, bioinformatic analysis of this gene product reveals a peptidoglycan binding domain and an ErfK domain, the latter of which is a conserved lipo-protein anchoring transpeptidase domain. Several other membrane/transporter mutants were identified, two of which had reduced biofilm forming abilities (ABUW\_1340, ABUW\_3725), while the other three had an increased ability to form a biofilm (ABUW\_2874, ABUW\_2925, ABUW\_3694). ABUW\_1340 encodes HisQ, a histidine transport system permease protein, while ABUW\_3725 is an uncharacterized member of the drug/metabolite exporter family. As for the mutants with increased biofilm forming capacities, ABUW\_2925 (*pit*) is involved in the

transport of phosphate while ABUW\_3964 is not yet characterized, but putatively has a role in ion transport based on the presence of a TlyC domain. ABUW\_2874, also uncharacterized, is a hypothetical membrane protein of unknown function.

Of interest, two mutants found to have enhanced biofilms had disruptions in genes associated with cell shape determination. Specifically, ABUW\_0715 encodes the rod-shaped determining factor MreB whilst ABUW\_1244 encodes the rod shape determining factor MrdB. Two phage related genes were also identified, with ABUW\_0582 disruption leading to an increased biofilm phenotype and ABUW\_0570 presenting a decrease. ABUW\_0582 encodes a GPO-like phage related capsid scaffold protein, whilst ABUW\_0570 encodes a GPJ-like phage related base plate assembly protein.

**Real-Time Profiling of Biofilm Formation.** To explore our findings more fully, we next sought to understand the specific mechanisms behind altered biofilm formation using an array of analyses. To facilitate and streamline this, we elected to proceed with only those factors/strains that were the most underexplored and/or had the most striking phenotypic changes. As such, we narrowed the list to 16 mutants: 8 with increased biofilm forming capacities, and 8 with diminished formation (**Supplemental Figure A3, Table 2**).

**Table 2. Lead Mutant Strains Selected for ECM Profiling.**

<b>Gene No.</b>	<b>Description</b>	<b>Ontology Group</b>	<b>Fold CV</b>
<b>ABUW_1763</b>	<i>usp</i> , uspA domain containing protein	Stress Response	8.05
<b>ABUW_2431</b>	<i>umuD</i> , DNA polymerase V	Stress Response	5
<b>ABUW_4114</b>	<i>traH</i> , TraH domain containing protein	Pili-Conjugation	4.56
<b>ABUW_3809</b>	Transcriptional regulator GntR	Transcriptional R	4
<b>ABUW_3391</b>	<i>gntK</i> , shikimate kinase	Metabolism	3.09
<b>ABUW_0133</b>	Ribosomal S30EA/sigma 54 modulator	Translation	2.94

**Table 2. Lead Mutant Strains Selected for ECM Profiling. (Continued)**

<b>ABUW_2655</b>	Hypothetical protein	Uncharacterized	2.6
<b>ABUW_0983</b>	<i>hda</i> , DnaA	DNA replication	2.59
<b>ABUW_3421</b>	<i>folA</i> , dihydrofolate reductase	Metabolism	-2.04
<b>ABUW_0201</b>	<i>gabP</i> , GABA permease	Transport	-2.04
<b>ABUW_1189</b>	<i>IdtJ</i> , ErfK/YbiS/YcfS/YnhG family	Membrane	-2.05
<b>ABUW_3390</b>	<i>gapN</i> , aldehyde dehydrogenase	Metabolism	-3.37
<b>ABUW_0570</b>	Phage base plate assembly protein	Phage	-3.66
<b>ABUW_3783</b>	<i>mmsA1</i> , methylmalonate-semialdehyde dehydrogenase	Metabolism	-4.15
<b>ABUW_0885</b>	<i>bap</i> , biofilm associated protein	Biofilm Associated	-4.27
<b>ABUW_0999</b>	<i>ruvB</i> , holiday junction DNA helicase	DNA binding	-5.7

Each biofilm was grown in technical sextuplicate and Fold CV was calculated the same as shown in Table 1. Transcriptional R: Transcriptional regulator

First, to confirm the integrity of our screen, one strain was selected for complementation analysis to confirm that alterations in biofilm forming capacities observed were the result of the expected transposon disruption (**Supplemental Figure A4**). The expected result was observed, and complementation restored phenotypes to that of the parent strain. Following this, we next chose to measure the attachment and adherence of strains in real-time using an xCELLigence RTCA instrument (ACEA Biosciences). This technology works by monitoring electrical flow across a series of gold-plated networks at the bottom of modified 96-well plates. Any shift in overall charge caused by disruption of the signal (i.e. attachment to the bottom of the well) is measured and calculated in the context of control readings to establish a Cell Index (CI)[152]. For this assay, each mutant was tested in biological triplicate and technical duplicate (n=6), with reads taken automatically every 5 minutes for a 72-hour period (**Supplemental Figure A5 and A6**). Four of the strains demonstrating the most unique phenotypes are represented in **Figure 4**.

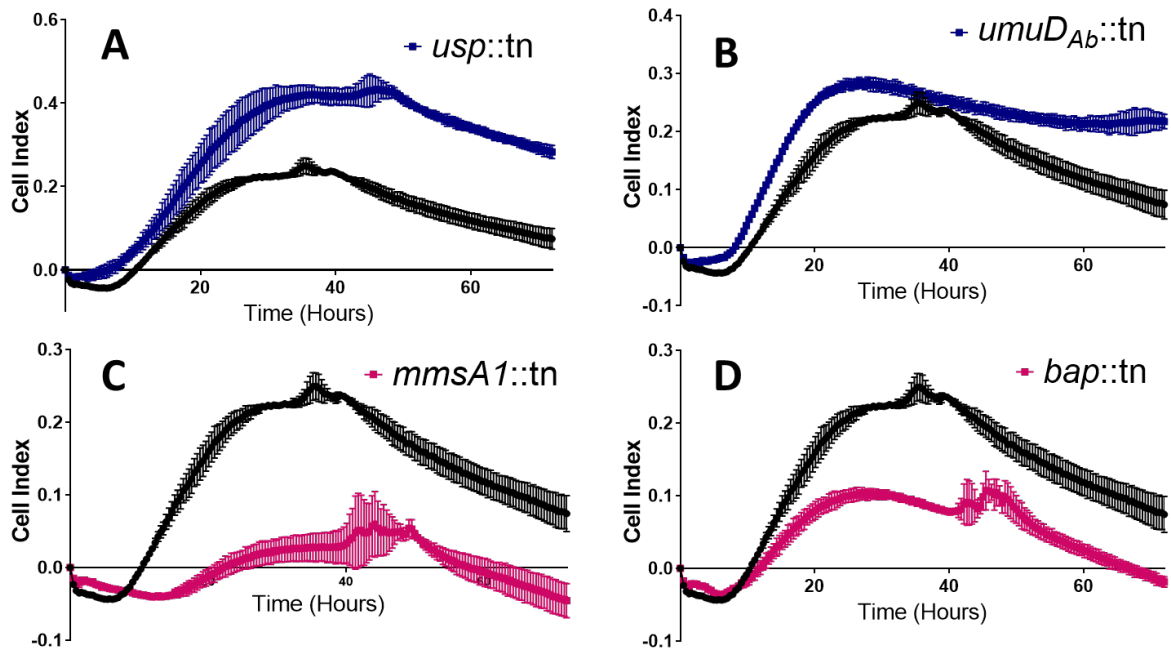


**Figure 4. Real-Time Profiling of Biofilm Formation Mirrors that Obtained via CV Staining.** Each mutant was seeded into the wells of gold-plated 96-well plates in biological triplicate and technical duplicate at an OD<sub>600</sub> of 0.05. Reads were taken every five minutes over a 72h growth period. Blue indicates strains with increased biofilm formation during CV staining, whilst pink indicates strains that had a defect in biofilm formation. Wildtype is shown in black in each case. Error bars are shown  $\pm$ SEM.

When reviewing this data, we noted that all strains experienced a decrease in impedance during the first 6h with the RTCA instrument, which is common for bacterial biofilms grown within this system; it is believed to indicate the initial attachment phase of biofilm formation [153-155]. For wildtype, this decline reached a CI of -0.04 before demonstrating a continual increase that registered positive values at 10.5h and plateaued at around 26h; remaining relatively stable through 40h. At this point the wildtype strain demonstrated a continual decline through the remainder of the assay. It is suggested that this decline indicates detachment of the biofilm in this system[154, 156].

Looking at the mutant strains, the first observation is that the RTCA assays were consistent with the end-point crystal violet studies, with the vast majority of mutants demonstrating identical results. There were exceptions to this, however, as ABUW\_4114 (*traH::tn*), ABUW\_0983 (*hda::tn*), and ABUW\_3391(*gntK::tn*) were categorized as enhanced biofilm formers using CV assays, but at intervals demonstrated a lower CI compared to the parent (**Supplemental Figure A5**). With that said, however, all four of these mutants did complete the RTCA experiments with a greater CI than the wild-type, thus explaining why our end-point CV assays ultimately assigned them as having enhanced biofilm formation. Conversely, ABUW\_0999 (*ruvB::tn*) demonstrated a biofilm deficiency during end-point CV studies, but had a higher impedance value compared to the parental strain through the first 20h of growth (**Supplemental Figure A6A**). Akin to that for the four previously listed mutants, however, the final CI values for this strain were ultimately lower than the parent, again explaining why this was ascribed as a reduced biofilm forming strain in our end-point assays.

Reviewing individual mutant data, we note that each demonstrated a unique phenotype as compared to the parent strain. For example, ABUW\_1763 (*usp::tn*) displayed a less severe decrease in impedance during the initial hours of assessment, and rapidly exceeded the CI of the parent strain thereafter, with a maximum value of 0.43 reached (compared to the wild-type at 0.25, **Figure 4A**). The profound ability of this mutant to form a biofilm is particularly interesting as this mutant demonstrates impaired cellular density during planktonic growth (**Supplemental Figure A7A**). Another mutant of interest was ABUW\_2431 (*umuD<sub>Ab</sub>::tn*), which mirrored the wildtype during early growth, albeit at a

slightly higher CI, however, thereafter it demonstrated relative stasis whilst the parental strain exhibited decline indicating there is some defect in the transition to detachment phase for this mutant (**Figure 4B**).

When looking at mutants with impaired biofilm formation, ABUW\_3783 (*mmsA1::tn*) had the most severe defect in impedance, with a maximum CI value  $\leq 0.06$  (**Figure 4C**). When reviewing the RCTA data for this strain, it appears that this mutant is defective in the initial attachment phase of biofilm formation as it is unable to generate a positive CI until at least 24h of growth. Indeed, even after this time, it barely registers on the Cell Index, indicating strongly impaired ability for biofilm formation, which is in agreement with our CV studies. Another similarly impaired biofilm forming mutant was ABUW\_0885 (*bap::tn*), although it was able to register a positive CI at a timeframe similar to that of the wildtype (**Figure 4D**). After this time, however, the mutant reached its maximum CI more quickly than WT and thereafter declined more rapidly, reaching a negative CI around 67h. This supports previous literature on the biofilm associated protein (Bap), which is known to play a role in stabilizing the structure of mature biofilms instead of being involved in the initial attachment phase [78, 118]. Collectively, our real-time cell analysis studies provide a useful companion to the end-point CV assays, generating unique insight into the biofilm formation process during attachment, development, and dispersal phases.

**Characterization of eDNA Abundance in Mutant Strains.** We next set out to investigate the composition of the extracellular matrix (ECM) for the wild-type and mutant

strains. First, eDNA was quantified as it is known to be a major component of *A. baumannii* biofilms[135]. Thus, biofilms were allowed to establish in 96 well plates under static conditions at 37°C for 24 hours, before planktonic populations were removed, and biofilm cells were assessed for eDNA production. Upon analysis (**Figure 5**) we noted that, for at least a subset of mutants, there was a clear correlation with decreased biofilm formation and significantly reduced eDNA production. The most substantial difference was observed for ABUW\_3783 (*mmsA1::tn*) which contained ~18-fold less eDNA within its ECM than wildtype. Another mutant with substantially less eDNA was ABUW\_0885 (*bap::tn*) with 3.85-fold less eDNA within its ECM. This is of particular interest, and perhaps provides insight into how Bap mediates stabilization of structure for mature biofilms. Beyond the *bap* mutant, ABUW\_0201 (*gabP::tn*) and ABUW\_0999 (*ruvB::tn*) possessed 7.89-fold and 2.59-fold less eDNA respectively in their biofilms, again likely explaining why deficiencies were observed for these strains. Additional to these strains, some of our mutants with enhanced biofilms also had increases in eDNA production, including ABUW\_0983 (*hda::tn*) and ABUW\_0133. It is clear, however, that these are only modest changes, and thus, although they perhaps contribute to the phenotypes observed, they clearly are not a definitive explanation.

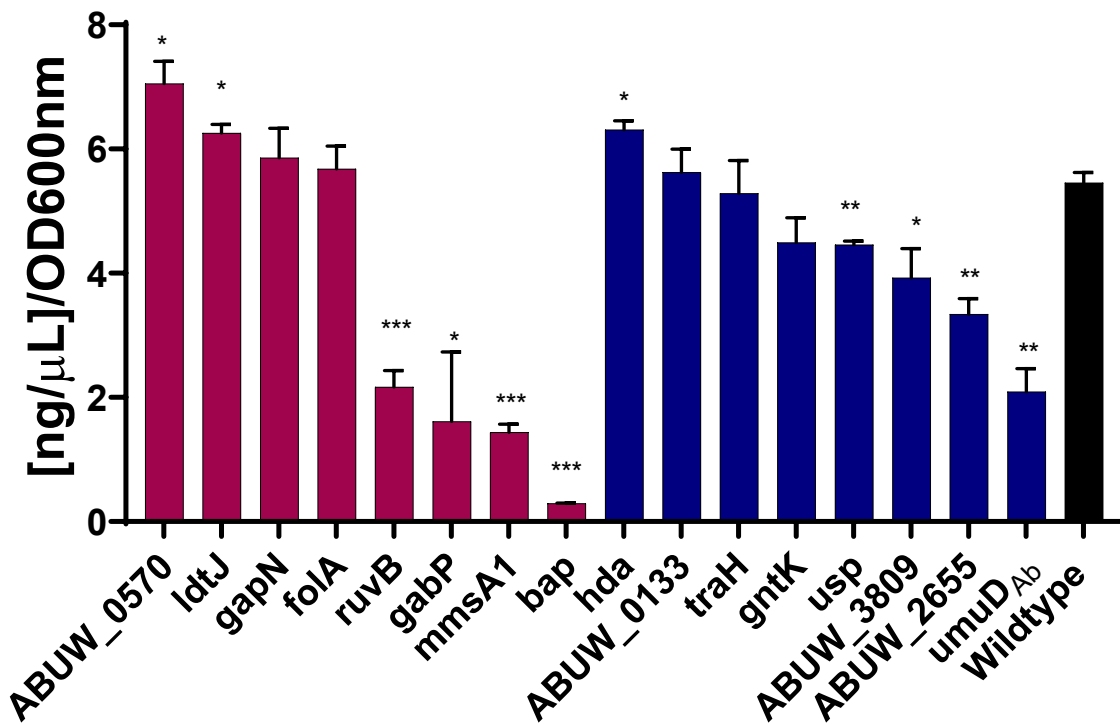


**Figure 5. Probing the Contribution of eDNA to Mutant Biofilm Formation.** Biofilms for each strain were seeded in biological triplicate and technical duplicate at an OD<sub>600</sub> of 0.05 prior to incubation for 24h. Blue indicates a strain that had increased biofilm formation during CV staining, whilst pink indicates strains that had a defect in biofilm formation. eDNA concentrations were calculated using a standard curve prior to normalization based on cell density. Error bars are shown  $\pm$ SEM. Significance was calculated using Student's *t*-test. \*,  $p < 0.05$ ; \*\*,  $p < 0.01$ ; \*\*\*,  $p < 0.001$ .

Beyond this we were able to discern no other correlation between biofilm phenotype observed during CV screening, and the amount of eDNA produced by each mutant. Indeed, for some mutants, findings that are in opposition to that expected were seen. For example, four of the eight mutants demonstrating a biofilm deficiency had greater levels of eDNA in their biofilms when compared to wildtype. Specifically, ABUW\_0570 showed the highest amount of eDNA in its biofilm ECM of all strains tested. ABUW\_1189 (*ldtJ::tn*), ABUW\_3390 (*gapN::tn*) and ABUW\_3421 (*foIA::tn*) also displayed higher levels of eDNA

within their biofilms, although these were relatively modest increases. Additionally, seven of the strains that were biofilm proficient had less eDNA within their biofilms compared to wildtype. Of those, ABUW\_2431 (*umuD<sub>Ab</sub>::tn*) produced a biofilm containing the least amount of eDNA (~3-fold less). Collectively, this data provides insight, and in some cases, obvious explanation for our CV and RTCA findings. For others, however, this is not the case, and thus a consideration of additional ECM components is required.

**Exploring the Impact of Protease on Biofilm Initiation of Mutant Strains.** To consider other components of the ECM produced by our mutant strains, we next tested the impact of proteinase K to determine which strains produce protein-mediated biofilms (**Figure 6**). Our first approach was to explore the impact of proteolysis on initial biofilm development; thus biofilms were allowed to establish as detailed above but in the presence of 25µg/mL proteinase K. Upon analysis of the wild-type biofilm we noted that it was impaired by 1.4-fold, indicating that, at least to some degree, proteins play a role in AB5075 biofilm initiation. Beyond this, of our 16 strains, nine were negatively impacted by preincubation with protease, whilst seven actually demonstrated increased biofilm formation.

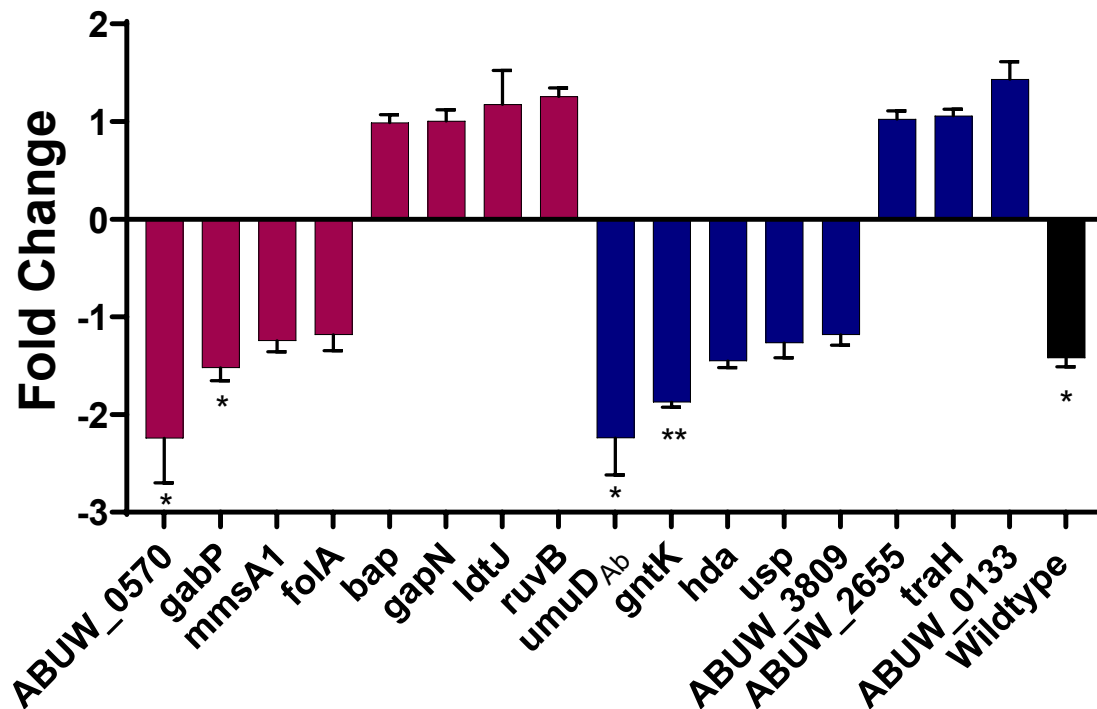


**Figure 6. ECM Profiling Reveals Differential Contribution of Protein to Biofilm Initiation.** Biofilms were seeded in biological triplicate at an OD<sub>600</sub> of 0.05 prior to incubation for 24h with or without 25 µg/mL Proteinase K. Blue indicates a strain that had increased biofilm formation during CV staining, whilst pink indicates strains that had a defect in biofilm formation. Fold change was calculated by comparing an individual strain's treated biofilm to non-treated. Error bars are shown ±SEM. Significance was calculated using Student's *t*-test. \*,  $p < 0.05$ ; \*\*,  $p < 0.01$ .

The two most profoundly affected strains by protease addition were ABUW\_0570 and ABUW\_2431(*umuD<sub>Ab</sub>::tn*). Interestingly, the former displayed a diminished biofilm forming capacity in CV and RTCA assays, whilst the latter had an enhanced capacity. Given that protease addition made the biofilm of ABUW\_0570 worse, this suggests that either: the already diminished ECM protein levels in this strain were further reduced by protease addition (reducing biofilm biomass), or that the biofilm formed by this strain is due to the loss of other ECM components, and that presence of ECM proteins in this strain facilitated

some level of biofilm formation, albeit to a reduced level. Regardless of outcome, it is clear that the presence of ECM proteins is important to the biofilm forming capacity of the ABUW\_0570 mutant. In line with this, three other biofilm impaired strains (ABUW\_0201 *gabP*::tn, ABUW\_3783 *mmsA1*::tn, and ABUW\_3421 *foIA*::tn) also demonstrated diminished biofilms when challenged with proteinase K.

With respect to the biofilm proficient ABUW\_2431(*umuD<sub>Ab</sub>*::tn) strain, it is apparent that biofilm initiation in this mutant is dependent on ECM proteins based on the reduced biofilms produced by this mutant under proteinase K challenge. Similarly, four additional strains (ABUW\_3391, *gntK*::tn; ABUW\_0983, *had*::tn; ABUW\_1763, *usp*::tn; and ABUW\_3809) had reduced biofilm forming capacities in the presence of proteinase K, but enhanced biofilm in CV and RTCA assays. Although not to the same level as the *umuD<sub>Ab</sub>* mutant, it seems likely that they too derive their enhanced biofilm forming abilities, at least in part, due to ECM proteins. In the case of the enhanced biofilm forming mutants ABUW\_2655, ABUW\_4114 (*traH*::tn), and ABUW\_0133, none were impacted by protease K addition, with all displaying modest increases in formation compared to no treatment controls; indicating their enhanced biofilm forming capacity is not protein driven. Finally, four biofilm deficient mutants (ABUW\_0999, *ruvB*::tn; ABUW\_0885, *bap*::tn; ABUW\_3390, *gapN*::tn; and ABUW\_1189, *ldtJ*::tn) actually had enhanced biofilm formation in the presence of proteinase K, suggesting proteinaceous inhibition of their respective biofilms.

**Investigating the Dispersive Effects of Proteinase K on Established Biofilms.** While observing the inhibitory effects of proteolysis in the context of biofilm development delivered useful insight, we also found it important to explore the effects of proteinase K on established biofilms. Thus, we measured biofilm strength/dispersal by allowing biofilms of our strains to form for 24 hours without treatment (**Figure 7**). After this time, undisturbed biofilms were treated with 25µg/mL of proteinase K for an additional 24 hours. Here, the wildtype strain showed a small reduction in biofilm mass, with a 1.31-fold decrease in biofilm observed following treatment of the established biofilm. In line with this, four of our 16 strains (ABUW\_0570; ABUW\_1189, *ldtJ*::tn; ABUW\_3783, *mmsA1*::tn; and ABUW\_0885, *bap*::tn) followed the same trend as the parent, indicating limited impact of ECM proteins on their biofilm strength/dispersal.

An additional eight strains had significantly diminished biofilm biomass as compared to the parental strain, with three previously demonstrating impaired biofilm formation using CV/RTCA tests (ABUW\_0999, *ruvB*::tn; ABUW\_3390, *gapN*::tn; and ABUW\_0201, *gabP*::tn), whilst the other five displayed enhanced biofilm biomass (ABUW\_4114, *traH*::tn; ABUW\_0133; ABUW\_3809; ABUW\_3391, *gntK*::tn; and ABUW\_2431, *umuD<sub>Ab</sub>*::tn). For the former three strains, this is similar to the scenario outlined above; namely, that either diminished ECM protein levels in these strains are further reduced by proteinase K in a mature biofilm, or that the weakened biofilms formed by these strains is due to the loss of other ECM components, and that presence of ECM proteins in this strain facilitated some level of biofilm formation, albeit at a reduced level. Regardless, ECM proteins would appear to be important to the strength of biofilm forming capacity in

these mutants. Similarly, for the latter five mutants, ECM proteins are clearly important to the strength of biofilms formed by these strains. The five other remaining strains all displayed resistance to proteinase K, with no biofilm dispersal observed, and in fact a modest increase in their CV levels was noted. Thus, in each case, it is clear that ECM proteins play no role in their altered biofilm formation from CV/RTCA tests.

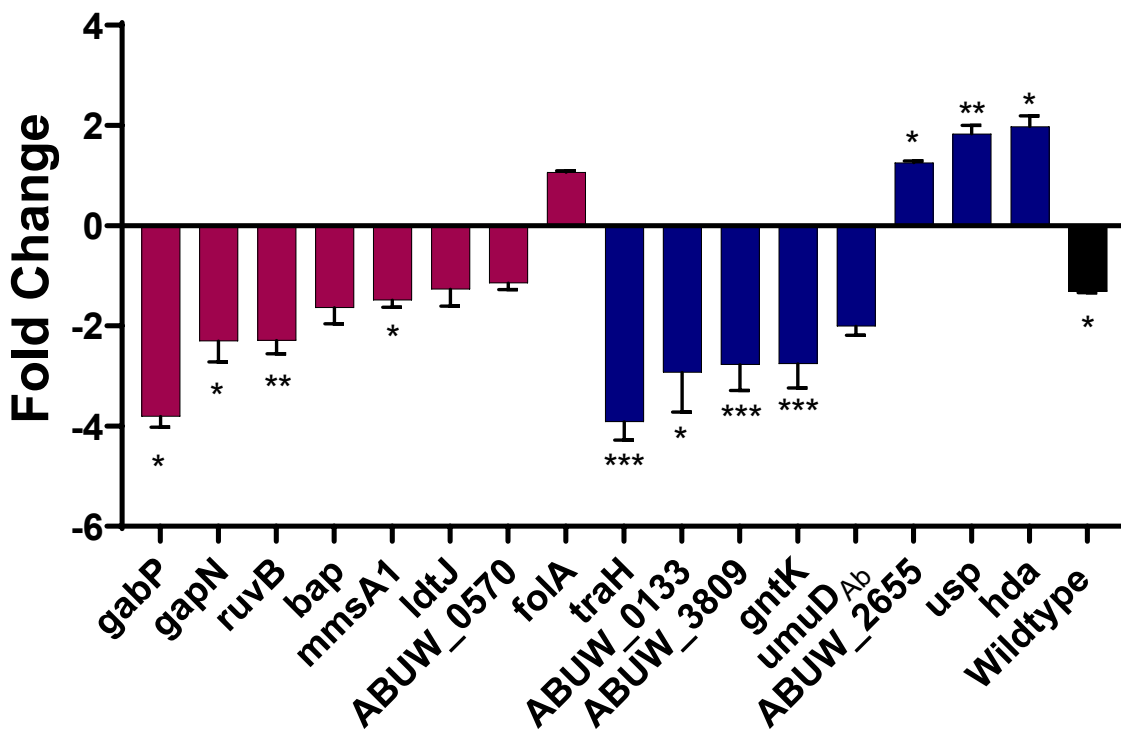


**Figure 7. The Importance of Proteins to Mature Biofilm ECM Differs Between Lead Strains.** Biofilms were seeded in biological triplicate at an OD<sub>600</sub> of 0.05 prior to incubation for 24h. After this time strains were treated with 25 µg/mL Proteinase K (or not) and incubated for an additional 24h. Blue indicates a strain that had increased biofilm formation during CV staining, whilst pink indicates strains that had a defect in biofilm formation. Fold change was calculated by comparing an individual strain's treated biofilm to non-treated. Error bars represent ±SEM. Significance was calculated using Student's *t*-test. \*,  $p < 0.05$ ; \*\*,  $p < 0.01$ ; \*\*\*,  $p < 0.001$ .

## Dissecting the Contribution of Polysaccharide to Differential Biofilm Formation.

The final step in considering alterations in ECM components of our selected mutants was to explore the contribution of polysaccharide to our observed phenotypes. To do this we treated biofilms of our various strains with sodium periodate, which targets the 1-6  $\beta$  linkage of extracellular polysaccharides such as N-acetylglucosamine[157]. Biofilms were seeded as with our other experiments, with or without 2.5mM of sodium periodate, followed by incubation for 24 hours (**Figure 8**).

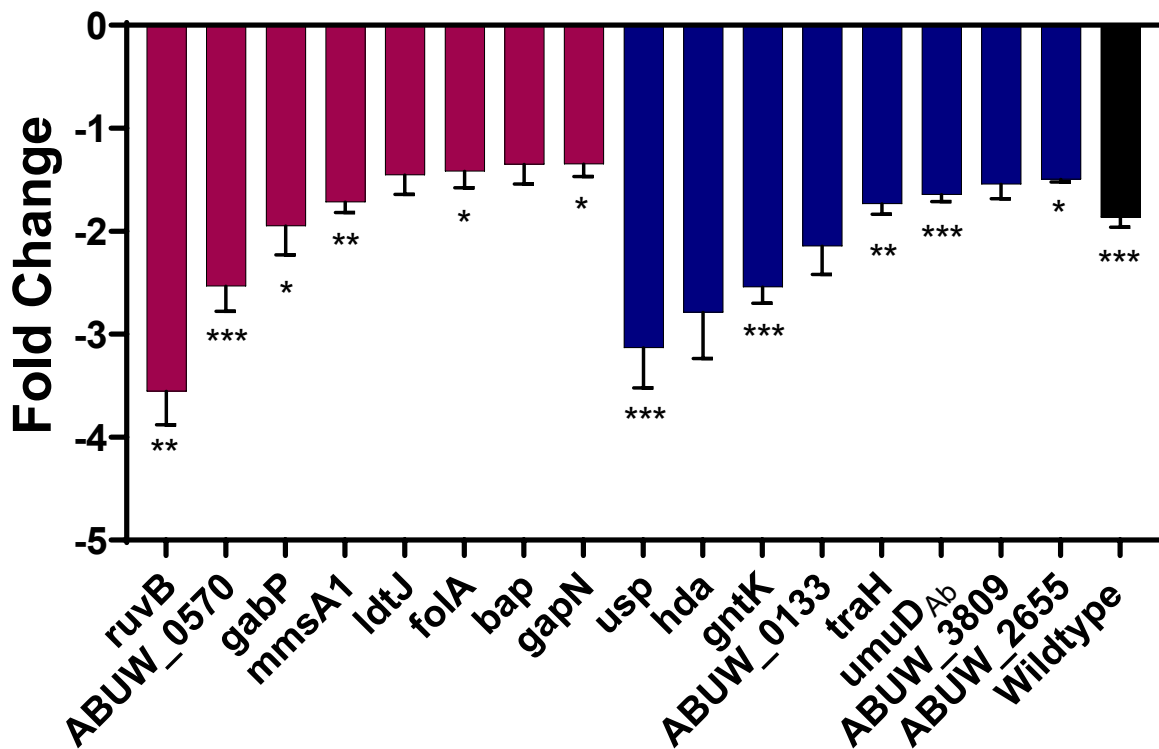


**Figure 8. ECM Profiling of Lead Mutants Indicate the Importance of Polysaccharides During Biofilm Development.** Biofilms were seeded in biological triplicate at an OD<sub>600</sub> of 0.05 prior to incubation for 24h with or without 2.5 mM Sodium Periodate. Blue indicates a strain that had increased biofilm formation during CV staining, whilst pink indicates strains that had a defect in biofilm formation. Fold change was calculated by comparing an individual strain's treated biofilm to non-treated. Error bars represent  $\pm$ SEM. Significance was calculated using Student's *t*-test. \*,  $p < 0.05$ ; \*\*,  $p < 0.01$ ; \*\*\*,  $p < 0.001$ .

Upon analysis we observed that biofilms produced by all strains were negatively impacted by the presence of sodium periodate, but to varying degrees. Of the 16 strains, 10 of them followed the same trend as the parental strain, whilst the remaining six all had significantly enhanced declines in biofilm biomass beyond the wildtype strain. Of these latter strains, two (ABUW\_0999, *ruvB::tn*; and ABUW\_0570) already demonstrated reduced biofilm formation in CV/RTCA tests, whilst the remaining four (ABUW\_1763, *usp::tn*; ABUW\_0983, *hda::tn*; ABUW\_3391, *gntK::tn*; and ABUW\_0133) had enhanced biofilm formation. For these latter strains, it is clear that polysaccharide plays an important role in the altered biofilm formation phenotype of these mutants. For the former, however, the suggestion is that either polysaccharide is the driving force behind their impaired biofilm formation, which the addition of sodium periodate only magnifies, or that loss of other ECM components is the explanation of their impaired biofilm biomass, and that polysaccharide was enabling, albeit in a limited way, some level of biofilm formation. Regardless of the explanation, it is clear that polysaccharides are important to the biofilm forming capacities of these strains.

**Evaluation of Polysaccharide Content in Established Biofilms via Dispersal Experiments.** As with proteinase K, the effect of sodium periodate on dispersing established biofilms was also assessed. To our surprise, 12 of the 16 strains followed the wild-type phenotype of a modest increase in biofilm biomass (**Figure 9**). The remaining four strains did have a decrease in biofilm formation in these tests, with two (ABUW\_1189, *ldtJ::tn*; and ABUW\_3421, *foiA::tn*) previously demonstrating impaired biofilm formation in CV/RTCA assays, and two (ABUW\_4114, *traH::tn* and ABUW\_3809) proving

increased. The explanation for these findings is likely the same as in the previous test, that for the latter two, polysaccharide plays a major role in the enhanced biofilm strength at later stages of growth, whilst for the former two polysaccharide is an important component of their diminished biofilms, but perhaps not the driving force behind the phenotypes observed in the original screen.

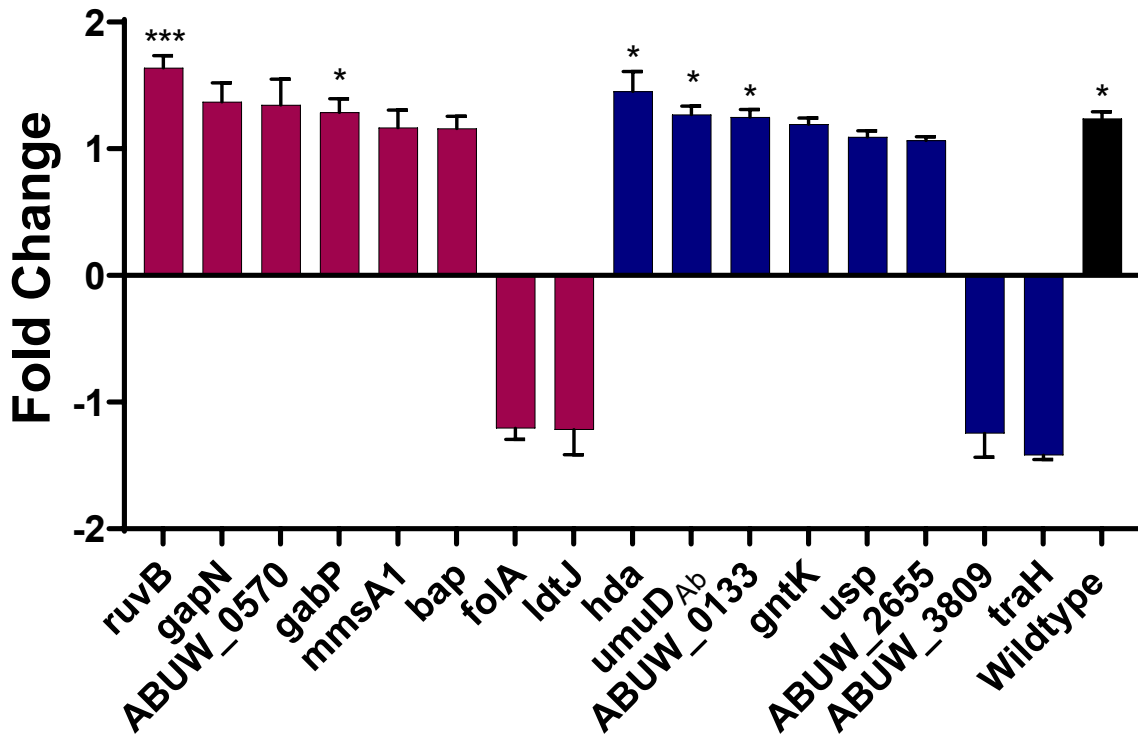


**Figure 9. The ECM of Mature Biofilms is Less Dependent on Polysaccharides for Integrity.** Biofilms were seeded in biological triplicate at an OD<sub>600</sub> of 0.05 prior to incubation for 24h. After this time strains were treated with 2.5 mM Sodium Periodate (or not) and incubated for an additional 24h. Blue indicates a strain that had increased biofilm formation during CV staining, whilst pink indicates strains that had a defect in biofilm formation. Fold change was calculated by comparing an individual strain's treated biofilm to non-treated. Error bars represent  $\pm$ SEM. Significance was calculated using Student's *t*-test. \*,  $p < 0.05$ ; \*\*\*,  $p < 0.001$ .

## Discussion

*A. baumannii* is known for its multi-drug resistant capacity and its ability to survive in a hospital setting. In addition, the ability to form biofilms allows for this organism to cause serious complications during infection. Herein, we have taken a non-biased, global approach to identify factors important for biofilm formation in *A. baumannii* AB5075. Through the screening of >2,500 Tn mutant strains we have identified 171 factors contributing to biofilm formation, with 49 of them influencing biofilm formation greater than 2-fold. Herein, we have investigated 16 of those targets in depth, uncovering unique phenotypes that provide insight into the intricacies of biofilm formation in *A. baumannii*. Through biofilm mass assessment and analysis of the ECM, our work has uncovered specific characteristics for the 16 mutants as summarized in **Table 2** and discussed in depth below.

During our investigation, we identified a mutation in ABUW\_0885 (*bap::tn*) as being impaired for biofilm formation. Importantly, this is a well-known membrane associated factor that has been widely documented for its role in biofilm formation in *A. baumannii*. Importantly, multiple *bap::tn* mutants were uncovered in our screen, each demonstrating a defect in biofilm forming capabilities (**Table 1**), thus validating the approach and data associated. Of these individual mutants, one was chosen to investigate more fully, producing a biofilm with 4.15-fold less biomass. In addition, RTCA analysis showed a severe attachment defect that was consistent throughout the 72-hour assay. This is in

line with previous studies identifying Bap as one of the major contributors to mature biofilm stability and structure[78, 118, 119]. In addition, the idea that Bap influences biofilm maturation and not the initial stages of biofilm formation are validated by RTCA where the trends of wildtype and the mutant were virtually identical for the first 10-15 hours of the assay.

Another mutant demonstrating a defect in biofilm formation was ABUW\_0201 (*gabP::tn*), a membrane transporter/permease responsible for the uptake of GABA (gamma-aminobutryic acid). This mutant was able to form a biofilm with 2.04-fold less biomass than the parent strain. Of note, GABA exposure has varying effects on biofilm formation, inducing formation in some species[158], but inhibiting formation in others[159]. It is likely that the *A. baumannii* version of this permease does in fact play a positive role in biofilm formation as the expression of *gabP* was increased 9.74-fold in four-day old static biofilms as compared to planktonic growing cells in a study by another group[160]. Of interest, in the same study, genes involved in GABA catabolism were expressed at lower levels in biofilms, while genes associated with GABA metabolism were increased in expression. This indicates that GABA is utilized in biofilms and is likely not broken down, but instead is transformed into other metabolites during biofilm formation. Indeed, in other organisms such as *Bacillus subtilis*, this permease is able to uptake GABA and proline, both of which are utilized in nitrogen metabolism[161]. Therefore, in *A. baumannii* it is not unreasonable to suggest that GabP may be importing other substrates important in biofilm formation and that the mutant may have an altered ability to metabolize nitrogen. In fact, nitrogen metabolism has been linked to various aspects of biofilm formation, including the

production of ECM components[162]. Based on our findings, it is clear that GabP is influencing critical components of the biofilm such as protein production and eDNA secretion, however, without further experimentation we cannot be certain of the specific mechanism behind this phenomenon.

We also observed a defect in biofilm formation for an ABUW\_1189 (*ldtJ::tn*) mutant, which specifies a periplasmic protein of the ErfK/YbiS/YcfS/YnhG (YkuD) family[163]. ABUW\_1189 was initially annotated as YkuD[163], but more recently as LdtJ in *A. baumannii*[164]. The STRING database along with Uniprot, identified a signal peptide, coiled coil region, peptidoglycan binding domain, and YkuD domain within this protein [165]. The YkuD family of proteins are known for their L-D transpeptidase (LDT) activity and are involved in peptidoglycan cross-linking within the cell envelope. In *E. coli*, YnhG (LdtE) specifically induces *meso*-DAP to *meso*-DAP crosslinking (3→3) instead of the penicillin binding protein controlled *meso*-DAP to D-alanine crosslinking (3→4)[166]. The same is true for LdtJ of *A. baumannii* (homolog of LdtE) which is also responsible for peptidoglycan editing through LD-carboxypeptidase activity, incorporating D-amino acids into peptidoglycan stem peptides during stationary phase[164]. Further, it has been determined that peptidoglycan editing during stationary phase is dependent on RackK (racemase) via the secretion of D-lysine for incorporation during the editing process[167]. Of interest, *rackK* has been shown to be upregulated in biofilms of ATCC 17978 indicating that peptidoglycan editing is in fact occurring during biofilm formation in *A. baumannii*[140]. Since we also know that LdtJ is responsible for incorporating the amino acids necessary for peptidoglycan editing into the cell wall (D-Asn, D-Arg, D-Lys, and D-

Met) it is logical that LdtJ would have a role in the biofilm formation process in *A. baumannii*[164]. In our study, *ldtJ::tn* demonstrated a 2.05-fold decrease in biomass accumulation in CV assays which is likely due to the lack of peptidoglycan editing in the absence of the *ldtJ*. With an altered cell wall, it is conceivable that the components making up the extracellular matrix are also altered. This is shown in **Figure 6** where more eDNA is found within this mutant as compared to the wildtype strain, perhaps as a result of more transient autolysis occurring in the *ldtJ* mutant strain.

The next lead mutant analyzed, ABUW\_3390 (*gapN::tn*), demonstrated a 3.37-fold decrease in biofilm formation. GapN encodes an aldehyde dehydrogenase, specifically non-phosphorylating NADP<sup>+</sup> dependent glyceraldehyde-3-phosphate dehydrogenase (EC 1.2.1.9) (KEGG) that functions to irreversibly convert glyceraldehyde-3-phosphate to 3-phosphoglycerate without the need of inorganic phosphate while reducing NADP<sup>+</sup> to NADPH[168, 169]. This is different from the standard housekeeping gene, GAPDH, which can reversibly convert NAD<sup>+</sup> and NADP<sup>+</sup> to NADH and NADPH while oxidizing glyceraldehyde-3-phosphate into diphosphoglyceric acid[169]. GAPDH also differs from that of GAPN by the fact that GAPN is not associated with glycolysis flux, but instead allows for the production of NADPH that can be used by the cell when levels of inorganic phosphate are low[170]. In addition, GapN allows for the use of a modified version of the Entner-Doudoroff pathway and glycolysis to produce NADPH and NADH to be used in anabolic processes in the cell[171]. Although this gene has not been functionally characterized in *A. baumannii* specifically, our group has observed an increase in expression of this gene by almost 2-fold in the biofilm population of AB5075 as compared

to their planktonic counter parts (Tomlinson & Shaw, unpublished data). This is in line with the inability of this strain to form a biofilm to the degree of the wildtype strain (this study). In addition, GapN was shown to be more abundant in biofilms formed by *Clostridium acetobutylicum*[172], further supporting our finding. In all, to the best of our knowledge this is the first time GapN has been implicated as a positive regulator of biofilm formation in *A. baumannii* and highlights a unique mechanism of the Embden-Meyerhof-Parnas (EMP) pathway of carbon metabolism that is prevalent within biofilm populations.

Another biofilm deficient mutant, ABUW\_3783 (*mmsA1::tn*) is also connected to metabolism. MmsA1 is a CoA-acylating methylmalonate semialdehyde dehydrogenase that is associated with propanoyl-CoA production, which is linked to the citrate cycle as well as the synthesis of type II polyketide backbones and 12-16-membered macrolides (KEGG). In this study, we found that this mutant was able to form a biofilm with 4.27-fold less biomass than the parent strain. In addition, disruption of this gene led to the formation of a thick, hypermucoviscous pellicle type structure at the air-liquid interface (**Supplemental Figure A6**). This is also supported by the RTCA assay that showed a significant inability to adhere throughout the length of the experiment. Further, *mmsA1::tn* biofilms were found to contain lower eDNA concentrations within the ECM (3.85-fold). Hypermucoviscosity is typically associated with the overproduction of polysaccharides [18, 173], however, our mutant did not demonstrate large differences in the presence of sodium periodate. On the other hand, it is possible that the pellicle produced at the air-liquid interface contains high levels of polysaccharide that would not be detected using the methods employed as, upon aspiration, the gelatinous biofilm is removed as one

globular unit for this strain. It has been shown that pellicles of *A. baumannii* contain cellulose like polymers high in glucose units[174], which has been associated with a gelatinous phenotype[175] as seen with our mutant strain. In all, this mutant demonstrates the inability to form a surface-liquid biofilm and instead forms a gelatinous pellicle that contains low levels of eDNA within the ECM. This unique phenotype is likely due to the overproduction of polysaccharides due to methylmalonate semialdehyde being transformed into 3-aminoisobutyrate instead of propionyl-CoA. It is unclear how this shift leads to excess polysaccharide production, however, MmsA1 likely acts as a negative regulator of pellicle formation under normal conditions.

An ABUW\_3421 (*folA::tn*) mutant, which encodes a dihydrofolate reductase, also demonstrated a biofilm defective phenotype. FolA is responsible for reducing dihydrofolate to tetrahydrofolate which is an intermediate used in dTMP synthesis, purine synthesis, the production of folic acid and the initiation of protein synthesis[176]. In terms of biofilm formation, *folA::tn* had 2.04-fold less biomass than the wildtype strain, indicating FolA to play a positive role in biofilm formation. In support of this finding, others have shown that AB5075 biofilms formed for 6 days under flow conditions had a 2.94-fold increase in expression of *folA* as compared to wildtype[177]. FolA is involved in central systems in bacteria, which would lead one to believe that the mutant would have a growth defect; however, this is not the case (**Supplemental Figure A70**). Indeed, many other bacterial species are able to survive without a functional *folA* gene[176]. In terms of biofilm formation, folate metabolism has been connected to the well characterized biofilm associated pili system, the *csu* operon. Specifically, under folate stress induced via the

treatment of ATCC 17978 with subinhibitory concentrations of trimethoprim, which targets FoaA, inhibition of the *csu* operon was observed coupled with a decrease in the ability to form a biofilm[178]. It is not unreasonable to predict that a transposon insertion disrupting this gene could lead to a similar outcome as we see for our mutant strain.

The most substantially reduced biofilm forming capacity was found for a mutant of ABUW\_0999 (*ruvB::tn*), which encodes RuvB, a component of the RuvAB Holliday junction DNA helicase. The Holliday junction helicase is one of the core SOS genes in gamma proteobacteria[179]. In fact, a recent report identified extracellular DNA within bacterial biofilms of multiple species that was similar to the DNA Holliday junction intermediates produced by RuvB's protein partner RuvA[180]. This is in line with the decrease in eDNA (2.59-fold less) observed in the biofilm of this mutant and the overall reduced biofilm forming capacity of the ABUW\_0999 (*ruvB::tn*) strain (5.70-fold less). Further, work by others reveals that six day old biofilms of AB5075 under flow conditions show *ruvB* expression levels 1.49-fold higher than planktonic cells, which also validates our findings herein[177].

The final mutant demonstrating a biofilm deficient phenotype (3.66-fold less) was ABUW\_0570, which encodes a putative GPJ-like phage base-plate assembly protein. Within the genome of AB5075, ABUW\_0570 is part of an operon containing 14 genes associated with bacteriophage assembly, 10 of which overlap with the *Pseudomonas* phiCTX phage (PHASTER search[181]). Although the phage present in AB5075 is

uncharacterized, general characteristics associated with lysogenic phages have been connected to biofilms. Lysogenic phages have been shown to spontaneously enter a lytic cycle in both planktonic and biofilm populations. Within the biofilm, higher levels of phage are released thus inducing cell lysis, which leads to the release of cellular components that can be recycled or incorporated into the ECM of biofilm populations[182-184]. In addition, the spontaneous release of phage is predicted to be universal for all lysogenic phages[185]. One specific example from *Streptococcus pneumoniae* revealed that strains carrying lysogenic phages had an enhanced capacity to form biofilms through phage mediated cell lysis and release of eDNA[185]. As noted above, this mutant did produce more eDNA than wildtype, however, it was not greater than 1.5-fold. Thus, we can predict that the inability of the ABUW\_0570 strain to generate a substantial biofilm is perhaps due to the absence of intact phage and that the ECM phenotypes associated are likely due to a cellular response to the phage components attempting to assemble, albeit unsuccessfully.

In terms of potential negative regulators of biofilm formation, ABUW\_3809 was identified. ABUW\_3809 encodes an uncharacterized transcriptional regulator of the GntR family. The increase in biofilm formation observed for this mutant (4-fold) suggests that this is indeed a negative regulator of biofilm formation when intact. This is supported by two separate studies finding the gene adjacent to this regulator are upregulated in *A. baumannii* biofilms. Specifically, levels of ABUW\_3809 were not detected in RNA sequencing experiments, but *prpB* (located directly adjacent) transcription was 3.29 and 6.6-fold higher in six day and 18-hour *A. baumannii* biofilms respectively[140, 177]. It is

highly likely that ABUW\_3809 itself negatively regulates the expression of the biofilm associated PrpB during exponential growth, while during biofilm formation it is itself downregulated via an unknown mechanism.

Another seemingly negative regulator of biofilm was ABUW\_2431 (*umuD<sub>Ab</sub>*), which produced a biofilm with 5-fold more biomass than the parent strain and had consistently higher adherence via RTCA (**Figure 6B**). *UmuD<sub>Ab</sub>* encodes a LexA type repressor protein that is dependent on RecA and controls the response to DNA damage and mitomycin C treatment[179, 186]. *UmuD<sub>Ab</sub>* has been proven to be a direct regulator of the DNA damage response in *A. baumannii* ATCC 17978 and oversees the activity of at least eight different DNA damage response genes, four of which are present in AB5075[187]. Each of the genes present in AB5075 as well as ATCC 17978 were shown to be derepressed when *umuD<sub>Ab</sub>* was disrupted, including *ddrR*, a described co-regulator[179]. This signifies that in our *umuD<sub>Ab</sub>::tn* mutant *ddrR* would be derepressed and constitutively expressed without the need for inducing conditions. This is of note because DdrR has been shown to regulate the biofilm impacting efflux pump AdeFGH[188] as well as A1S\_1147, which is only expressed in biofilms[140] in a manner independent of *UmuD<sub>Ab</sub>*[189]. Therefore, our mutant's increased capacity to form biofilms is likely a result of the de-repression of *ddrR* which in turn activates biofilm associated genes under its control without the need for a DNA damage inducing stimulant. In addition, *umuD<sub>Ab</sub>* transcription was found to be expressed 1.4-fold less in AB5075 biofilms growth under flow for 6 days[177], further supporting the role of *UmuD<sub>Ab</sub>* as a negative regulator during biofilm formation.

ABUW\_0983 (*hda::tn*) disruption resulted in the ability of AB5075 to form a biofilm with 2.59-fold more biomass than the wildtype strain. Hda has been characterized in detail in *Escherichia coli* as a inactivator of DnaA, which helps to prevent the unnecessary re-initiation of replication, an activity known as regulatory inactivation of DnaA (RIDA)[190]. In *Acinetobacter species*, Hda is conserved, sharing ~30% sequence similarity to its *E. coli* counterpart, but is predicted to share functional similarity in engaging with DnaA[191]. In *E. coli*, the loss of *hda* leads to the over-initiation of replication resulting in replication fork stalling and slower growth (and sometimes death)[190]. It is known that replication fork stalling leads to higher levels of DNA within the cell that in turn are secreted out of the cell in the form of eDNA. In terms of biofilm formation, there is limited knowledge on the influence of over-initiation of replication on the formation of biofilms in Gram negative organisms specifically. However, a negative regulator of replication in *Bacillus subtilis*, YabA, has been shown to negatively regulate biofilms when in-tact. Specifically, without YabA, over-initiation of replication occurs and a more substantial biofilm is formed, which is in line with the results of our study[192]. YabA is not an analog of Hda and each protein differs mechanistically, however, the outcome of their inhibitory influence on DnaA and the outcome of over-initiation is the same. Therefore, the phenotypes observed in our analysis are likely due to an over-initiation of replication that influence biofilm formation via a mechanism in line with that in *B. subtilis*. In addition, the loss of *hda* has been shown to increase the production of ribonucleotide reductases[193], which results in stronger biofilms; while deleting the genes responsible for their synthesis reduces biofilm formation[194]. This connection reveals yet another potential mechanism by which this mutant is able to form a better biofilm than the parent strain.

ABUW\_0133::tn was another mutant demonstrating an enhanced capacity to form biofilms, demonstrating a 2.94-fold more biomass than AB5075. ABUW\_0133 is annotated as a putative sigma-54 modulator, however this appears to be a historical misnomer (BLAST analysis, this study). Instead, the protein has strong homology to the ribosome hibernation factor (RHF) family, derived from Pfam, InterPro, and HHPred bioinformatic searches[147, 195, 196]. Ribosome hibernation factors are known to inhibit translation by helping to stabilize and promote 70S dimerization under stressful conditions leading to an inactive 100S ribosome. In addition, they function in preventing ribosomal turnover[197] meaning cells lacking ABUW\_0133 would theoretically undergo higher levels of this process. There have been multiple studies suggesting that ribosomal turnover is higher in biofilms produced by *A. baumannii* suggesting biofilms form more readily in the absence of ABUW\_0133[140, 177, 198]. Specifically, without the normally triggered inhibition of ribosomal activity, higher levels of protein would accumulate and could result in higher levels of protein being secreted, becoming a part of the ECM. This idea is supported by the 2.93-fold decrease in biofilm biomass for this mutant following the addition of proteinase K to mature cultures. Furthermore, in a study conducted in *A. baumannii* strain ATCC 17978, ABUW\_0133 was expressed at lower levels within biofilms as compared to planktonic or stationary phase cells[140]. Additionally, a six-day old AB5075 biofilm produced under flow conditions showed 5.57-fold lower expression of ABUW\_0133 in biofilms as compared to planktonic growing cells[177]. Each example is in line with our study highlighting that ABUW\_0133 plays an inhibitory role in biofilm formation.

In this study we have identified numerous metabolically linked negative regulators of biofilm formation. One such example is ABUW\_3391 (*gntK*), which encodes a gluconate kinase enzyme (gluconokinase); disruption of which resulted in a 3.09-fold increase in biofilm biomass. GntK is responsible for converting D-gluconate into 6-phospho-D-gluconate[199]. 6-P-Gluconate is used as an intermediate for the Entner-Doudoroff pathway. Therefore, in the absence of *gntK*, the Entner-Doudoroff pathway cannot generate pyruvate from 2-hydro-3-dexoxygluconate. In, a study in *Streptococcus pneumoniae*, disrupting various components of the Entner-Doudoroff pathway led to increased polysaccharide production[200]. As polysaccharides are a major component of bacterial biofilms, this finding corroborates our data, which indicates a higher level of polysaccharides produced during biofilm formation by the *gntK::tn* mutant, as shown in **Figure 9**. Indeed, a strain of *A. baumannii* lacking *gntK* was shown to respond to the presence of glucose by overproducing lipopolysaccharide[201] - further suggesting a shift towards biofilm formation upon loss of GntK, as mutants lacking LPS form weaker biofilms[202-204].

The identification of ABUW\_4114 (*traH::tn*) strain in our screen was unique as this gene is encoded on a large plasmid (p1AB5075) yet has a profound influence on biofilm formation. Specifically, *traH::tn* was able to form a biofilm with 4.56-fold more biomass than AB5075. In terms of function, ABUW\_4114 encodes a putative TraH domain containing protein. This type of domain within proteins is predicted to be a part of a relaxosome accessory protein of an F-like Type IV secretion system associated with conjugation. It is known that plasmid transfer via conjugation is more efficient within

biofilms regardless of nutrient availability and it is suggested that conjugation could itself induce biofilm formation[205]. Therefore, it would be assumed that without a functional TraH domain containing protein, a less robust biofilm would be formed. This is contradictory to our endpoint CV assay that demonstrated an increase in biofilm biomass (**Figure 4**), however, the RTCA demonstrated a delayed induction of adherence for this mutant that was ultimately overcome at the end of the assay (**Supplemental Figure A4C**). In addition, mutations in other components of the F-type type IV pilus, such as *traD* and *traX* in *E. coli*, lead to a more robust biofilm being formed - as seen for our *A. baumannii traH::tn* mutant[206]. Further, it is known that in *E. coli* the pilus cannot fully assemble in the absence of *traH*, but there is still expression of the pilus tip, and other outer membrane proteins such as TraN, which is responsible for the aggregation of cells [207, 208]. The increased biofilm forming capacity of this mutant is thus likely due to two things: the accumulation of proteinaceous products that are not able to assemble, and closer contact/aggregation of cells due to a truncated pilus. The truncated pilus would also explain why we see a lag in adherence via RTCA as less cells are aggregating initially, due to an inability to actively search for each other. In addition, the accumulation of proteins produced by this operon line up nicely with the sensitivity of this mutant to proteinase K challenge after the biofilm is established (**Figure 8**).

Another candidate identified, ABUW\_2655 encodes a 195-residue protein of unknown function that, when disrupted, leads to an increase in biofilm formation of 2.60-fold. Although it is unclear how loss of ABUW\_2655 produces this phenotype, it has been

shown to be expressed at levels 2.07-fold lower in six-day old AB5075 biofilms as compared to planktonically growing cells[177], which is in line with this study.

Finally, the mutant identified as having the most profound effect on AB5075 biofilm formation herein was ABUW\_1763 (*usp::tn*), which demonstrated a 8.05-fold increase in biomass. This phenotype, along with the drastically higher CI values via RTCA (**Figure 4A**) support the idea that Usp is a profound negative regulator of biofilm formation in *A. baumannii* when intact. In line with this, various other studies have shown decreased expression of universal stress proteins in *A. baumannii* biofilms[140, 177]. Universal stress proteins are generally known to help circumvent various forms of stress encountered by bacteria, including but not limited to: protection from reactive oxygen species, acidity, and toxins. However, a direct mechanism of Usp's functioning on a biochemical level remains elusive. In *A. baumannii* a paralog of *usp::tn*, UspA, is generally known for playing a role in virulence and survival within the host[209]. In other organisms, there are unique roles that UspA plays some of which are biofilm associated. Specifically, UspA and UspA-like proteins seem to be positive regulators of anaerobic biofilm formation in *Pseudomonas aeruginosa*[210, 211] and *Porphyromonas gingivalis*[212, 213]. Therefore, it is clear that we have uncovered a unique functional role for Usp in biofilm formation that is specific to *A. baumannii*, which merits further investigation and will be explored in depth in the following chapter.

In summary, using a high-throughput screening approach we have identified factors that influence biofilm formation in *A. baumannii* AB5075. This screen is the first step in finding new candidates that are likely to play a role in the complex regulatory cascade known as biofilm formation. Future studies into the specific mechanisms at play within these mutants will be critical to our understanding of this process in this dangerous organism and may provide new and novel candidates that could be used for future anti-biofilm based therapeutic strategies.

## **Chapter 3: Characterization of Universal Stress Protein G in the Oxidative Stress and Cell Envelope Stress Response of *Acinetobacter baumannii***

### **Introduction**

Universal stress proteins are known for their role in protecting organisms from various forms of stress. They act as global regulators to allow organisms to respond to external threats. The first universal stress protein, UspA was discovered in *Escherichia coli* in 1992. It was described as a 13.5kDa cytoplasmic protein that accumulates following nutrient starvation, or exposure to toxic chemicals such as heavy metals, oxidants, acids and antibiotics[214]. Its induction was found to be independent of many stress-induced global regulators such as OmpR, PhoB or H-NS[214]. Since then, thousands of universal stress proteins have been documented within all three kingdoms of life, in such diverse organisms as fungi, archaea, protozoa, and plants[215]. In such organisms, they have been characterized as protecting against starvation of nutrients such as: carbon, nitrogen, phosphate, sulphate, amino acids[216-219]. In bacteria, this means that expression is often induced during stationary phase where nutrient limitation naturally occurs[220]. A role in protection against oxidative stress, acidity, heat exposure, osmotic stress, chemical stress, exposure to heavy metals and DNA damage has also been described[221-224]. Evidence has shown that some bacterial Usp proteins are also involved in regulating motility, adhesion, and biofilm formation[222, 225, 226]. Finally,

within organisms such as *A. baumannii*, they are important for survival and virulence *in vivo*[209, 221, 224].

Proteins containing the UspA (or Usp) family domain (Pfam PF00582) can be composed solely of a Usp domain, or such a domain can be one amongst many. Members of this family have a Usp domain with an average length of 136 amino acids. Based on the nearly 60,000 sequences available (59,455 to be exact), the average percent sequence identity of full alignments is only 17%, indicating a high level of diversity among members of the Usp domain family. Indeed, within the Pfam database there are thousands of examples of protein sequences containing Usp domains, with a variety of domain organizations. With that said, the most common arrangement is a lone USP domain, as >31,000 protein sequences within databases contain just this configuration, whilst a further 10,000 or so proteins contain two tandem Usp domains. Further, there are 272 additional groups with unique architectures each containing a Usp domain[227]. For example, there are over 1,000 sequences that contain a Usp domain followed by a protein kinase domain. In addition to the high prevalence of Usps in nature demonstrated by Pfam alone, there are many organisms that harbor multiple Usp proteins within their genome.

In the best studied organism, *E. coli*, there are five paralogs of UspA that exist: UspC, UspD, UspE, UspF, and UspG. UspE is unique such that the protein contains two adjacent Usp domains, one of which has similarity to UspG and UspF and the other resembles UspA, UspC, and UspD[228]. Other bacteria also often have a variety of Usp proteins, for example *Streptococcus coelicolor* encodes 12 *usp* genes, *Mycobacterium*

*tuberculosis* possesses eight or nine and *Micrococcus luteus* has three[216, 228, 229]. Conversely, some species, such as *Xanthomonas campestris* only encode one[216]. The best examples to date that explain the connection between paralogs within a single species have been performed in *E. coli*. Synthesis of UspA, UspC, UspD, UspE, and UspG is induced by glucose or phosphate starvation, exposure to dinitrophenol and heat, and extended growth in nutrient rich media[215]. The overlap in expression demonstrates a form of functional redundancy between them. However, when separated into classes, distinct functions can be assigned to each set of proteins and even individuals within a class. For example, one class consists of UspA, UspC, and UspD, another consists of UspF and UspG; whilst UspE is broken into two classes. There is overlap and specificity between classes in terms of function. For example, UspA and UspD are important for protection against superoxide and DNA-damaging agents, while UspC and UspE are essential for motility and UspG and UspF promote adhesion[222]. However, UspA, UspC, UspD, and UspE play a role in protection against UV-irradiation[228]. Therefore, each Usp can function within the same pathway, but their functions are not explicitly redundant: the deletion of one does not allow for another to compensate. Additionally, although there are conditions that lead to a similar induction of each Usp, the level of induction of each Usp can be specific to the stressor. For example, UspA is induced >3-fold when exposed to low level heat shock, while UspC, UspD, and UspE, although also induced, are at levels less than 3-fold[228].

There is also diversity in terms of regulators of specific Usps. In *E. coli*, UspA is negatively regulated by FadR[230] while UspA, UspC, UspD, and UspE are negatively regulated by

FtsK[231], and positively regulated by RecA[231] and ppGpp[232]. UspG of *E. coli* is regulated by the two component system NtrB/NtrC[233] and is likely a substrate of GroEL[234]. The response regulator of a two-component system, DevR, is also important for regulating some of the Usps of *Mycobacterium smegmatis*[235]. In *Burkholderia glumae*, RpoS and the quorum sensing transcriptional regulator QsmR are known to transcriptionally regulate the expression of its various *usp* genes[236]. Conversely, *uspA* induction is not dependent on RpoS in *E. coli*[214]. In *E. coli* all *usp* genes are predicted to be under the control of  $\sigma^{70}$  (RpoD), the housekeeping sigma factor, based on the -10 and -35 regions upstream of *uspA*[218]. However, uniquely, UspD within the same organism is under the regulation of RpoE ( $\sigma^E$ ), the extracytoplasmic stress sensing sigma factor[237]. In another species, *Listeria monocytogenes*, RpoB is predicted to regulate *usp* genes based on  $\sigma^B$  boxes upstream of these genes[221].

Following translation, another form of regulation is present for Usps. Post-translational modifications such as ATP binding and phosphorylation, dimerization and protein-protein interactions also mediate the functionality of Usps. For example, UspA of *E. coli* can be detected in three different isoforms, two of which are phosphorylated[238]. This phosphorylation is induced upon entry into stationary phase and is dependent on the phosphotyrosine protein TypA. UspF and UspG of *E. coli* undergo post-translational modification through ATP binding while UspG can also autophosphorylate[239, 240]. This is also shown in the UspFG homolog MJ0577 of *Methanococcus jannaschii*, which can form homodimers that tightly bind ATP[241]. There is also evidence that an additional factor is required to release ATP from MJ0577. In addition to phosphorylation or substrate

binding, evidence of the formation of homo and heterodimers exist. For example, UspA, UspC, and UspD of *E. coli* are shown to interact with themselves as well as with each member of their class[242]. The same was found for UspF and UspG[242]. Further, UspE was found only to interact with itself, an interaction that is dependent on the presence of both Usp domains[242]. Therefore, interactions between different Usps would result in a different cellular response compared to Usp homodimers *in vivo*. Evidence for interactions between Usps and other protein complexes also exists. For example, Rv2623 of *M. tuberculosis* interacts with an ATP-dependent ABC transporter of lipooligosaccharides[243] and UspC of *E. coli* interacts with the Usp domain of KdpD under osmotic stress[244].

Usp proteins have a unique ability to exist in a variety of forms to influence cellular processes and function as global regulators in bacteria and other organisms. They can form complexes with themselves, bind substrates, interact with other proteins, and change phosphorylation state depending on their environment. The complexity increases within organism such as *A. baumannii* that possess multiple Usps that are yet to be characterized fully. Thus far in *A. baumannii*, only one Usp has been characterized phenotypically. The homolog of ABUW\_0890 in ATCC17978 (A1S\_2692) has been shown to have a role in oxidative stress tolerance, survival in the presence of 2,4-DNP, growth under acidic conditions, and survival *in vivo*[209]. Herein we show that in the absence of *uspG*, a paralog of *uspA*, *A. baumannii* is impaired in growth, energy metabolism, lipid metabolism, membrane integrity and the expression/function of various transporters. We also show that, like many other Usp proteins, the *uspG::tn* strain

demonstrates increased sensitivity to DNA-damaging agents, H<sub>2</sub>O<sub>2</sub>, and a variety of different antibiotics.

## Materials and Methods

**Bacterial Strains and Growth Conditions.** Bacteria were maintained on agar plates for no longer than 48 hours prior to assay and were stored at 4°C. All plasmids and strains used within this chapter are listed in **Table 3**. Bacterial strains were grown with shaking at 250 rpm and 37°C. Unless otherwise specified strains were grown in Luria Broth (LB) or Luria Broth Agar (LBA). For experiments using strains containing the pMQ557 plasmid, cultures were supplemented with 160µg/mL of Hygromycin B. Transposon mutants were grown on LBA containing 12.5µg/mL of tetracycline or in LB containing 5µg/mL of tetracycline.

**Table 3. Bacterial Strains and Plasmids.**

Strain	Description	Source
<i>A. baumannii</i>		
<b>AB5075</b>	Wildtype Strain	[143]
<i>uspG</i> ::tn	AB5075 with tn insertion in ABUW_1763 ( <i>uspG</i> )	[144]
<b>WT EV</b>	AB5075 containing pMQ557 (JLA2887)	This study
<i>uspG</i> <sup>-</sup> (M)	<i>uspG</i> ::tn containing pMQ557 (JLA2878)	This study
<i>uspG</i> <sup>+</sup> (C)	<i>uspG</i> ::tn containing pMQ557:: <i>uspG</i> -His <sub>6</sub> (JLA2879)	This study
<b>Plasmids</b>		
<b>pMQ557</b>	Cloning vector for complementation	Gift, Dr. R. Shanks, University of Pittsburgh
<b>pLSJA1</b>	pMQ557:: <i>uspG</i>	This study

**Growth Curve Analysis.** Bacterial strains were grown at 37°C shaking at 250 rpm for 15 hours with antibiotic supplementation. Strains were then synchronized by adding 50µL of culture to 5mL of fresh media and incubating while shaking for 3 hours. Each sample was

then standardized to an optical density at 600nm (OD<sub>600</sub>) of 0.05 in fresh media containing antibiotic. A 96-well polystyrene plate was seeded with each strain in biological triplicate and technical duplicate. Each well contained 200µL total. Measurements were taken at OD<sub>600</sub> every 15 minutes for 18 hours with continuous double-orbital shaking in between (Citation 5, BioTek). The temperature was maintained at 37°C.

**Construction of a *uspG* Complementing Strain.** To generate the complementing strain of *uspG*, flanking primers were designed for the ABUW\_1763 gene that included the promoter as well as 100-200 nt of DNA 3' of the translational stop codon. The fragment was PCR amplified and cloned into pMQ557. Primers for this can be found in **Supplementary Table A1**. The plasmid containing *uspG* and the *uspG::tn* strain were verified using PCR and sanger sequencing (GeneWiz) prior to transformation. *uspG*<sup>+</sup> (C) was generated by transforming the pMQ557::*uspG* plasmid into *uspG::tn*. *uspG*<sup>-</sup> (M) was created by transformation with the empty plasmid (pMQ557). Finally, AB5075 underwent transformation with empty vector (pMQ557) to generate the AB5075 WT strain. Strains and plasmids are listed in **Table 3**. Each strain containing plasmid was then confirmed by PCR amplification followed by Sanger sequencing (GeneWiz). Prior to setting up overnight cultures for each assay, colony PCRs were performed to confirm the integrity of the transposons and plasmids within each strain. Assays were performed using Hygromycin B at a concentration of 160µg/mL to maintain the plasmid. Each complementation assay included *uspG*<sup>-</sup> (M), *uspG*<sup>+</sup> (C), and AB5075 (WT).

**Western Blot Analysis.** The *uspG::tn* complement strain was synchronized and standardized as detailed above in biological triplicate, before 5mL samples were collected hourly for 8 hours. An 18-hour and 24-hour timepoint were also collected. Samples were harvested at 4150 x *g* for 10 minutes before supernatant was removed and pellets were stored at -80°C prior to normalization. Cytosolic proteins were harvested by resuspending each pellet in 500µL of PBS containing protease inhibitor cocktail (Thermo Fisher Scientific) followed by the inclusion of glass beads. Samples were lysed mechanically by bead beating 3 times for 30 second intervals. Samples were then centrifuged for 5 minutes at 17000 x *g* and supernatant was transferred to a fresh tube. Samples were then normalized to 100µg/mL using the ProteinQuant 660nm Kit (Thermo Fisher Scientific) and a BSA standard curve. Samples were separated using SDS-PAGE on a gradient 4-20% SDS precast gel (BioRad). The samples were subject to 90V for 2 hours prior to blotting on polyvinylidene difluoride (PVDF) membranes using a semi-wet transfer at 20V for 45 minutes (BioRad). Immunoblotting was performed using anti-6xHis polyclonal rabbit primary antibody (Invitrogen) incubating overnight at 4°C in blocking buffer. The secondary antibody was HRP-conjugated mouse anti-rabbit IgG (Cell Signaling Technologies) incubated for 1 hour at 27°C. HRP activity was assessed using the SuperSignal West Pico Chemiluminescent substrate kit (Thermo Fisher Scientific) and was visualized using X-ray film.

**RNA Sequencing.** Collection of AB5075 wildtype and AB5075 *uspG::tn* mutant samples was performed using the synchronization and standardization methods described above. Samples were tested in biological triplicate. Once cells were standardized to OD<sub>600</sub> 0.05,

they were grown for 3 additional hours. Samples were then harvested, added to an equal volume of ice-cold phosphate buffered saline (PBS), and centrifuged at 4°C. An RNeasy Kit (Quiagen) was used to isolate total RNA from cell pellets as previously described[245]. A TURBO DNA-free kit (Ambion) was used for DNA removal. DNA removal was confirmed using 16s rRNA specific primers. An Agilent 2100 Bioanalyzer system and Agilent RNA 6000 nano kit were used to assess sample quality and ensure RNA integrity. Samples used in this study measured an RIN of  $\geq 9.9$ . Biological replicates for each strain were pooled and normalized prior to rRNA removal using a Ribo-Zero Kit for Gram Negative Bacteria (Illumina). This was followed by mRNA enrichment using the MICROBExpress Bacterial mRNA enrichment kit (Agilent) before removal efficiency of rRNA was checked using a bioanalyzer and nano kit. These samples were then used for RNA sequencing on an Illumina NextSeq sequencer. RNA sequencing and Library preparation were performed using the Truseq Stranded mRNA Kit (Illumina) method but omitting the mRNA enrichment step. Prior to sequencing the quality, concentration, and average fragment size were measured and assessed using an Agilent 2100 Bioanalyzer system and a corresponding RNA 6000 Nano kit. The library concentration for pooling barcoded samples was evaluated via qPCR with a KAPA Library Quantification kit (KAPA Biosystems) to ensure high sensitivity. The Illumina NextSeq was used to run samples with a 150-cycle NextSeq mid Output Kit v2.5.

**RNA Sequencing Bioinformatics.** Data sets were exported from BaseSpace (Illumina) to CLC Genomics Workbench 20 (Quiagen Bioinformatics) for analysis in the fastq format. Reads were imported and failed reads removed using the Illumina Paired Importer tool.

Quality score parameter options were set to Illumina Pipelines 1.8 and later. rRNA reads were filtered and removed by aligning to known rRNA sequences. Remaining reads were then aligned using the RNA-seq Analysis Tool (v0.1) under default parameters. Strand specificity was defined through alignment to *A. baumannii* AB5075 NCBI reference genome (CP008706.1). The Expression Browser tool (v1.1) was used to calculate gene expression with transcripts per million (TPM) as the output value. To determine differential expression values, the Differential Expression in Two Groups tool (v1.1) for whole transcriptome samples was used. Fold change values of the *uspG::tn* mutant to wildtype samples were reported. Library size normalization was taken into account using the trimmed mean of M values (TMM) generated using the Differential Expression in Two Groups tool. Genes were classified ontologically using the Kyoto Encyclopedia of Genes and Genome (KEGG) database[246-248] for the related AB57 strain.

**Minimum Inhibitory Concentration Determination.** MIC assays were performed according to CLSI guidelines[249] using either LB or Mueller Hinton II (Ca-MHB) media. MICs were performed in 96-well polystyrene plates with a final volume of 200 $\mu$ L/well. Overnight cultures were diluted to a final OD<sub>600</sub> of 0.05 in fresh media containing the stressors to be tested alongside the appropriate solvent only controls. Media only controls were also included in each assay plate. Samples were wrapped in parafilm to prevent evaporation and incubated for 18 hours, shaking at 37°C. The following day, assay plates were measured at OD<sub>600</sub> (Cytation 5 Plate Reader, BioTek) and percent inhibition was calculated for each compound comparing treated samples to solvent only controls for each strain. MICs were verified on at least two separate days. Percent inhibition was

calculated following the subtraction of background from each well (average of OD<sub>600</sub> of media only wells) using the following formula: %inhibition = (1 - (OD<sub>600</sub> treated/average OD<sub>600</sub> solvent only controls)) x 100. Fold change was then calculated for each stressor tested by dividing the MICs of AB5075 and *uspG::tn*.

**Motility Assessment.** Overnight cultures of *uspG*<sup>-</sup> (M), *uspG*<sup>+</sup> (C), and AB5075 (WT) were synchronized in the presence of 160µg/mL hygromycin to maintain the plasmid. Following three hours of growth, samples were standardized to an OD<sub>600</sub> of 0.1 in fresh LB. Each strain was grown in biological triplicate and plated onto LBA+hygromycin by adding 10µL to the center of each agar plate. Samples were wrapped in parafilm and tape to prevent evaporation and were placed (without inversion) at 37°C and 27°C for incubation in the dark. The diameter of each sample was measured and recorded. Plates were incubated at 37°C and 27°C for 48 hours prior to recording the first measurement. Samples at 27°C were allowed to incubate for an additional 15 days prior to recording the final measurement. The same approach was taken to assess *uspG::tn* and wildtype AB5075 strains. Plates were poured without antibiotic prior to incubation for 14 days in the dark.

**Survival in Whole Human Blood.** Bacterial strains were grown overnight, synchronized and standardized according to the methods above and the assay was performed as previously described[250] with modifications. Each strain was grown in biological triplicate and following 3 hours of synchronization, samples were centrifuged at 4150 x *g*. Supernatant was then removed and samples were resuspended in 1mL of PBS prior to

standardization to an OD<sub>600</sub> of 0.5. Cells were then diluted in 3mL of whole human blood (BioIVT) to an OD<sub>600</sub> of 0.05. PBS samples were also prepared at OD<sub>600</sub> 0.05 to serve as a control for timepoint 0. An additional control for 0 minutes was taken immediately after inoculation in blood. Timepoints were then taken following 30 minutes, 1 hour, 2 hours, 3 hours, 4 hours, 5 hours and 6 hours of incubation. CFU/mL were calculated for each strain at each timepoint by serial dilution in PBS and plating on LBA. Blood cultures were incubated between collections at 37°C, rotating.

## Results

**Bioinformatic Considerations of Usps in *A. baumannii* 5075.** In Chapter 2 we identified a variety of genes/proteins in *A. baumannii* as being important for biofilm formation. One of the most profoundly impaired mutants from these was for gene ABUW\_1763, which contains a Universal Stress Protein (Usp) domain. A search of the AB5075 genome for other universal stress proteins revealed six genes encoding proteins with the Usp domain: ABUW\_0890, ABUW\_1661, ABUW\_1763, ABUW\_2639, ABUW\_3660, and ABUW\_3666 (**Table 4**).

**Table 4. Usp Paralogs in AB5075**

Gene	Bp Length	AA Length	% Seq ID	GenBank
ABUW_0890	438bp	145aa	50.34%	AKA30650.1
ABUW_1661	444bp	147aa	45.58%	AKA31399.1
ABUW_1763	444bp	147aa	-	AKA31499.1
ABUW_2639	843bp	280aa	27.03%	AKA32361.1
ABUW_3660 <sup>a</sup>	351bp	116aa	0%	KGP64547.1
ABUW_3666 <sup>b</sup>	528bp	175aa	27.34%	KGP64480.1

Bp: base pair, AA: amino acid, %Seq ID: Percent identity to ABUW\_1763 based on NCBI Blastp alignment, GenBank: ID from NCBI database. <sup>a</sup>No longer annotated as such, non-redundant protein ID WP\_000034558.1, alternate annotations: A591\_A3583/ABUW\_RS17825. <sup>b</sup>No longer annotated as such, protein ID WP\_000451088.1 record removed, alternate annotations: A591\_A3588/ABUW\_RS17850

Sequences of each Usp protein were aligned using CLC Genomics Workbench as visualized in **Figure 10**. When observing this alignment we note that ABUW\_2639 is much longer than the other proteins, which is evident by the large gaps in alignment within **Figure 10**. Indeed, according to the UniProt database, ABUW\_2639 possess two Usp domains, and therefore resembles UspE of *E. coli*. However, UspE of *E. coli* has been shown to possess the ATP binding domain G-2X-G-9X-G-N[251] while ABUW\_2963 does not. Further, ABUW\_3360 is similarly unlikely to bind ATP, as the sequence do not possess the characteristic G-2X-G-9X-G-S/T nor G-2x-G-9x-G-N sequence[216]. The remaining four Usps, do in fact possess this sequence (highlighted in Figure 1, black box) and are therefore likely to bind ATP. In addition, although ABUW\_1763 and ABUW\_1661 are of the same number of amino acids, their sequences are very different, which indicates they are of different classes of Usp with distinct functions.



**Figure 10. Universal Stress Proteins of AB5075 Show Little Sequence Similarity.** Each protein sequence was downloaded from the NCBI database as a fasta file and input into CLC genomics workbench to create the alignment.

Performing bioinformatic analysis with each of the Usp proteins in *A. baumannii* we note that each of the six proteins are strictly cytoplasmic. According to the Protter protein

visualization database, none of the sequences possess transmembrane domains nor signal peptide sequences and are therefore located within the cell following translation[252]. In addition, a blastp search was conducted and found that the *A. baumannii* Usp showing the greatest similarity to ABUW\_1763 was ABUW\_0890, with 50.34% identity (**Table 4**). The homolog of ABUW\_0890 has been phenotypically characterized in *A. baumannii* ATCC 17978 (A1S\_2692) and has the highest level of similarity to Usp2 of *Staphylococcus aureus* at ~ 49%[209].

To gain structural insights, the ABUW\_1763 protein sequence was submitted to two separate protein folding predictive software platforms (I-TASSER [253] and Phyre2[254]). The outcome of these searches was in agreement: demonstrating ABUW\_1763 as having the highest level of structural similarity to UspA of *Lactobacillus plantarum* (PDB: 3S3T) and MJ0577 of *Methanocaldococcus jannaschii* (PDB: 1MJH). However, sequence similarity of ABUW\_1763 to *L. plantarum* was 21.3% while alignments indicated 29.8% similarity to the Usp of *M. jannaschii*. The predicted structure of ABUW\_1763 is characterized by the Usp domain which spans amino acids 3-145 of the 147 amino acid sequence, according to the UniProt database. Structurally, ABUW\_1763 possesses 4 alpha helices making up 48% of the sequence and 5 beta sheets that account for 19% of the sequence according to the Phyre2 database analysis. In addition, it is predicted that 10% of the structure is disordered. The largest area of disorder is predicted to be between residues 43 and 54 in addition to the terminal amino acids on either end of the protein, not predicted to be part of the Usp domain. According to the RCSB protein database (rcsb.org), each protein is predicted to bind ATP while UspA of *L. plantarum* is also likely

to bind glycerol, acetate, and calcium. ATP binding is highly likely since the sequence G(2X)G(9X)G(S/T), characteristics of ATP binding[216], is present within the sequence of ABUW\_1763 and was predicted with 0.93/1.0 confidence in the I-TASSER prediction data for ligand binding sites. Further, GSHG-9X-GSV specifically is present within the ABUW\_1763 sequence and mirrors that of *M. jannaschii*'s usp, which is a proven ATP binding protein[255]. The Phyre 2 generated structure of ABUW\_1763 and the predicted binding site for ATP are shown in **Figure 11**.

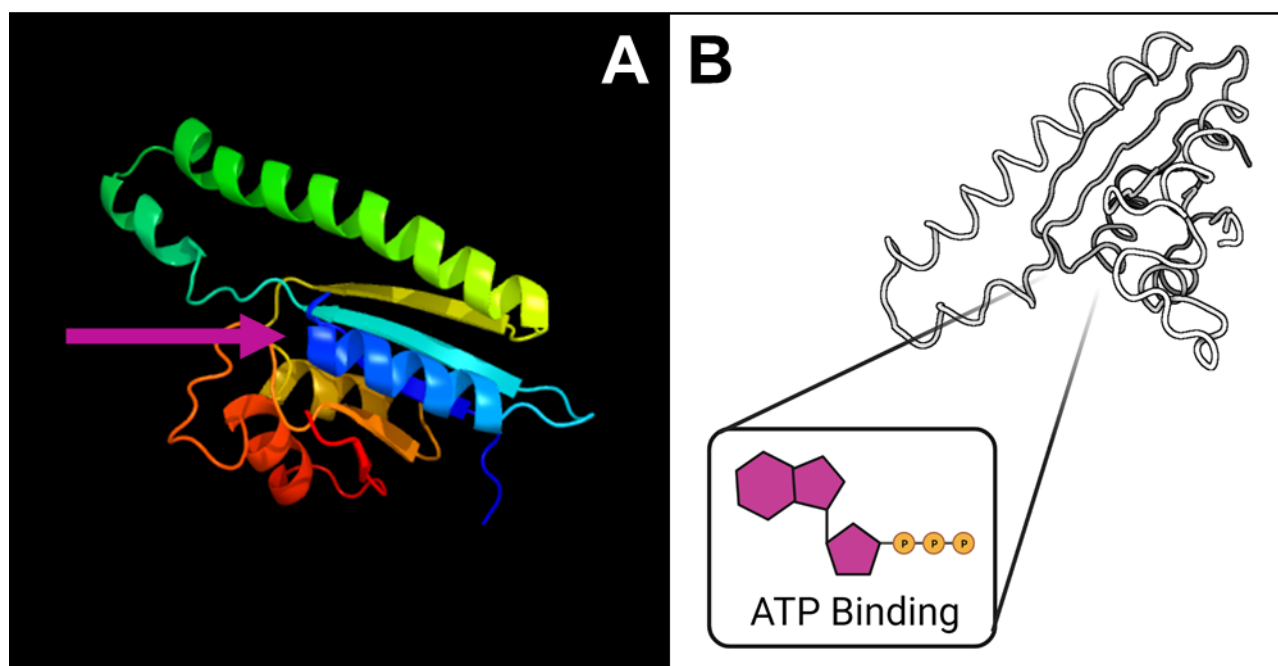


**Figure 11. Rendering of Predicted ABUW\_1763 Protein Structure.** (A) Predicted structure of ABUW\_1763 with 99% confidence generated using Phyre2 software modeled after 1mhj from *Methanocaldococcus jannaschii* with 95% coverage. N-terminus red to C-terminus blue in rainbow scheme. Pink arrow indicates predicted ATP binding region. (B) Structure indicates predicted pocket for ATP binding created using BioRender.com. UspA domain covers residues 3-145 of 147 amino acid sequence.

To identify Usp proteins of other organisms with similar sequence homology to ABUW\_1763, an additional NCBI blastp search was conducted. The ABUW\_1763 fasta

sequence aligned perfectly, with two partial sequences of Usp domain containing proteins of *E. coli* and *P. aeruginosa*. The alignment for these sequences and the next top 9 sequences showing the highest similarity are shown in **Figure 12**. The partial sequences could not be traced back to a specific class of Usp for each species and it is difficult to classify them simply based on sequence, however, based on the predicted ATP-binding activity that is typical for UspG class Usps, ABUW\_1763 will be referred to as UspG hereafter.

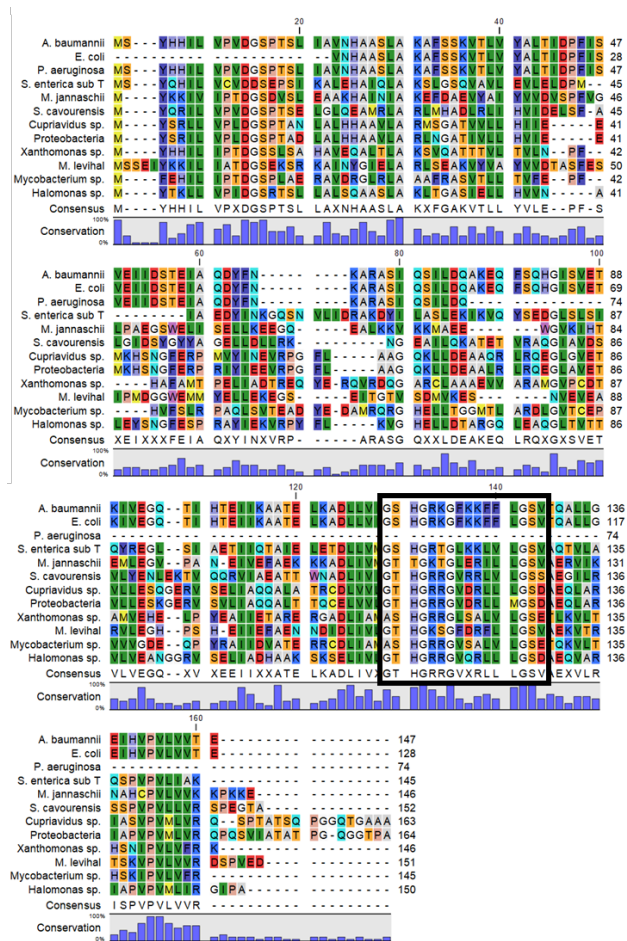


**Figure 12. Top 11 Species with Usp Proteins Sharing Similarity to ABUW\_1763.** An ncbi blastp search was conducted and the alignment was exported to CLC genomics workbench to generate the alignment presented. Black box outlines the sequence indicative of ATP binding capacity (G-2X-G-9X-G-S/T). ABUW\_1763 sequence is listed first.

**Universal Stress Protein G Disruption Results in a Growth Defect.** Based on previous connections between Usp function and growth, an analysis was performed to determine the impact of *uspG::tn* on *A. baumannii* growth. Cultures were synchronized to mid-exponential phase and were then standardized to an OD<sub>600</sub> of 0.05 in fresh media prior to measurement over time. It was found that *uspG*<sup>-</sup> (M) has a slight growth defect and an extended lag phase (**Figure 13**) that is partially complemented in the *uspG*<sup>+</sup> (C) strain. Growth defects have been observed in other *A. baumannii* strains lacking *usp* analogs[209, 256]. However, this seems to be unique to *A. baumannii*, as single *usp* mutants of other organisms in nutrient rich conditions grow indistinguishable from the WT strains[221, 257]. In addition, complementation of *uspA* in *A. baumannii* has only been demonstrated for a strain created to harbor two chromosomal copies of the gene and expression values of 20-fold that of the wildtype strain[209]. Therefore, it is perhaps unsurprising that our complement strain was unable to fully restore growth to wild-type levels.

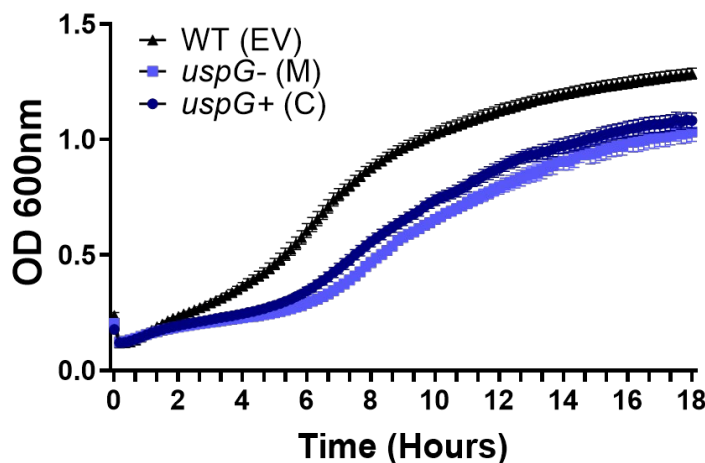


**Figure 13. *uspG::tn* Strain Exhibits a Growth Deficit When Compared to Wildtype AB5075.** Each strain was synchronized and standardized to an OD<sub>600</sub> of 0.05 prior to analysis. Measurements were taken every 15 minutes for 15 hours. Error bars represent ±SEM of three biological replicates.

**UspG Baseline Protein Expression Increases Over Time and Remains Stable.** Many UspG are expressed following the induction by stressors, but they are also known to accumulate as cells enter stationary phase as nutrients become limited[220]. In order to determine whether UspG of AB5075 is similarly accumulated during stationary phase, it was important to evaluate protein expression. To do this, our complement strain *uspG*<sup>+</sup> (C), which bears a C-terminally included his-tag was tested for expression. The strain was synchronized standardized before growth over 24 hours at 37°C shaking in LB. An empty vector control of AB5075 (WT) was used and was grown in concert with the *uspG*<sup>+</sup> (C) expression strain. As shown in **Figure 14**, UspG accumulates with expression seen from 2-24 hours. Expression could be detected following 2 hours of growth indicating UspG is present in exponential phase, which is unique for UspG and could indicate a novel role for UspG of AB5075. In line with Usp accumulation in other organisms during stationary phase, UspG is in high abundance at the later time points. This data also indicates that protein is likely stable over time. The highest level of expression seen after 24 hours of growth is, again, not surprising as *uspA* and *uspG* of *E. coli* are shown to be expressed under conditions of growth arrest[234, 238]. Further, the control samples (WT) were treated with the same conditions and no banding was observed (data not shown), verifying that the band seen within **Figure 13** is specific to His-tagged UspG.

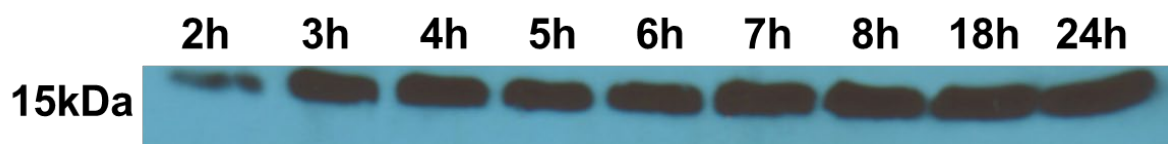


**Figure 14. UspG Expression is Stable Over Time.** Samples of *uspG*<sup>+</sup> (C) were taken at described timepoints and normalized to 100µg/mL prior to gel loading. Western blot exposed using histidine-6 antibody. Image represents results observed for three biological replicates.

**RNA-sequencing Analysis Reveals Vast Changes in *uspG::tn*.** With protein expression seen within exponentially growing cells in the absence of stress, it is clear that UspG is employed by the *A. baumannii* cell during standard growth. Given the importance of these enzymes in other organisms, we decided to explore UspG function using transcriptomic analyses. These were performed on 3-hour synchronized cultures of *uspG::tn* and the wildtype AB5075 strain. Upon analysis, a substantial number of genes were differentially expressed and therefore a cutoff of  $\geq 4$ -fold was established. Overall, 326 genes fell within this cutoff and were organized ontologically (**Figure 15**).

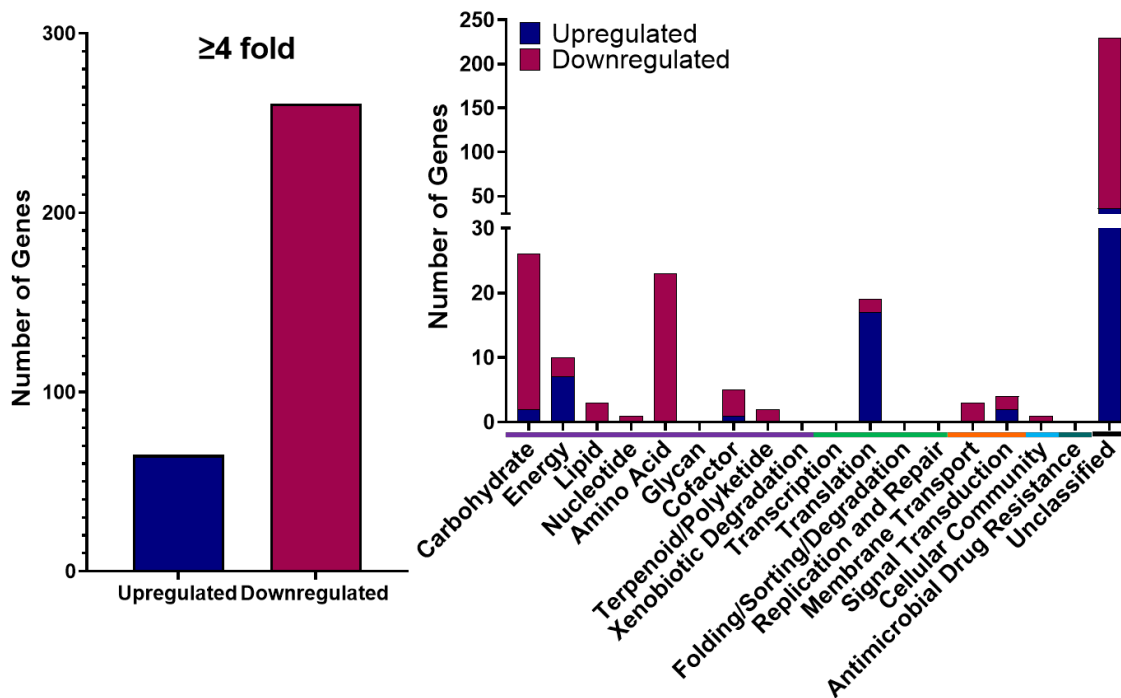


**Figure 15. Disruption of *uspG* Leads to Vast Changes in Transcriptome.** Overall number of genes changed (left). Genes with changes in expression greater than or less than 4-fold as compared to wildtype were grouped ontologically based on KEGG searches (right). Genes with higher expression within *uspG::tn* are shown in blue, genes with lower expression are shown in pink. Categories: metabolism (purple), genetic information and processing (green), environmental processing (orange), cellular processing (teal), human disease (dark green), and unclassified (black).

Specifically, 261 genes were downregulated by greater than 4-fold in the *uspG::tn* mutant strain compared to the wildtype AB5075 strain (**Table 5**). Conversely, 65 genes had increased expression greater than 4-fold in the mutant strain (**Table 6**). Ontological groupings were established using the KEGG orthology database, however AB5075 is not specifically represented within the system. To overcome this, gene identifiers were converted to homologous genes in the closely related AB57 *A. baumannii* strain prior to the search. Genes were then organized into six categories with relevant subcategories as shown in **Figure 15**: metabolism (carbohydrate, energy, lipid, nucleotide, amino acid, glycan, cofactor, terpenoid/polyketide, xenobiotic degradation), genetic information processing (transcription, translation, folding/sorting/degradation, replication/repair), environmental information processing (membrane transport, signal transduction), cellular processing (cellular community), human diseases (antimicrobial drug resistance), and unclassified. While a majority of the genes identified are considered unclassified based on the comparative cross-referencing of homologs of AB57 within KEGG, some correlations could be deduced based on genomic location or gene annotations and protein descriptions found utilizing the UniProt knowledgebase[258].

**Table 5. Ontological Grouping of Genes with Decreased Expression in the *uspG::tn* Mutant Strain**

ABUW_	Annotation	Description	Fold
<b>Metabolism</b>			
<b>Amino Acid Metabolism</b>			
ABUW_0066	<i>hpd hppD</i>	4-hydroxyphenylpyruvate dioxygenase (EC 1.13.11.27) (HppD 4-hydroxyphenylpyruvate dioxygenase)	-7.49
ABUW_0069	<i>maiA hmgC</i>	MaiA maleylacetoacetate isomerase (Maleylacetoacetate isomerase) (Maleylacetoacetate isomerase (MAAI)) (EC 5.2.1.2)	-4.18
ABUW_0077	<i>hutU</i>	Urocanate hydratase (Urocanase) (EC 4.2.1.49) (Imidazolonepropionate hydrolase)	-6.03
ABUW_0078	<i>hutH</i>	Histidine ammonia-lyase (Histidase) (EC 4.3.1.3)	-9.75

**Table 5. Ontological Grouping of Genes with Decreased Expression in the *uspG::tn* Mutant Strain (Continued)**

ABUW_0080	<i>hutI</i>	Imidazolonepropionase (EC 3.5.2.7) (Imidazolone-5-propionate hydrolase)	-8.93
ABUW_0081	<i>hutG</i>	Formimidoylglutamase (EC 3.5.3.8) (Formiminoglutamase) (Formiminoglutamate hydrolase)	-6.94
ABUW_1635	<i>ligE_2 ligE ligE_1</i>	Glutathione S-transferase (Glutathione S-transferase family protein) (Glutathione S-transferase, N-terminal domain protein)	-4.97
ABUW_1726		D-amino acid dehydrogenase 3 small subunit	-5.11
ABUW_2410	<i>yfcF</i>	Glutathione S-transferase (Glutathione S-transferase family protein) (Glutathione transferase) (Putative glutathione S-transferase) (EC 2.5.1.18)	-6.29
ABUW_2452	<i>clbF_14 ivd</i>	Acyl-CoA dehydrogenase (EC 1.3.8.1) (Colibactin biosynthesis dehydrogenase ClbF) (Isovaleryl-CoA dehydrogenase) (EC 1.3.8.4) (Isovaleryl-CoA dehydrogenase (IVD))	-10.98
ABUW_2453		Acetyl-CoA carboxylase (EC 2.1.3.1) (Methylcrotonoyl-CoA carboxylase) (Methylcrotonoyl-CoA carboxylase beta chain) (Methylcrotonoyl-CoA carboxylase carboxyl transferase subunit) (EC 6.4.1.4)	-25.05
ABUW_2454	<i>mgh</i>	3-methylglutaconyl-CoA hydratase (Enoyl-CoA hydratase) (EC 4.2.1.17) (Enoyl-CoA hydratase/isomerase family protein) (Methylglutaconyl-CoA hydratase) (EC 4.2.1.18)	-31.71
ABUW_2455	<i>accA1_2</i>	Acetyl-CoA carboxylase biotin carboxylase subunit (Acetyl/propionyl/methylcrotonyl-CoA carboxylase subunit alpha) (Acyl-CoA carboxylase alpha chain protein) (Methylcrotonoyl-CoA carboxylase subunit alpha) (Methylcrotonoyl-Coenzyme A carboxylase 1 (Alpha)) (Methylcrotonyl-CoA carboxylase biotin-containing subunit) (EC 6.4.1.4)	-36.01
ABUW_2526	<i>paaF paaK</i>	Phenylacetate-coenzyme A ligase (EC 6.2.1.30) (Phenylacetyl-CoA ligase)	-7
ABUW_2529	<i>paaG paaB</i>	2-(1,2-epoxy-1,2-dihydrophenyl)acetyl-CoA isomerase (EC 5.3.3.18) (Enoyl-CoA hydratase) (EC 4.2.1.17) (Enoyl-CoA hydratase, phenylacetic acid degradation) (PaaB phenylacetate degradation probable enoyl-CoA hydratase paaB) (Phenylacetate degradation enoyl-CoA hydratase PaaB)	-7.19

**Table 5. Ontological Grouping of Genes with Decreased Expression in the *uspG::tn* Mutant Strain (Continued)**

ABUW_2531	<i>paaK hmp_2</i>	Flavodoxin reductase (EC 1.17.1.-) (Phenylacetate-CoA oxygenase/reductase) (Phenylacetate-CoA oxygenase/reductase subunit PaaK) (Phenylacetate-CoA oxygenase/reductase, PaaK subunit) (Phenylacetic acid degradation protein) (Putative phenylacetic acid degradation NADH oxidoreductase paaE)	-7.87
ABUW_2532	<i>paaJ paaD</i>	Metal-sulfur cluster biosynthetic protein (PaaJ phenylacetate-CoA oxygenase, PaaJ subunit) (Phenylacetate-CoA oxygenase) (Phenylacetate-CoA oxygenase subunit PaaJ) (Phenylacetate-CoA oxygenase, PaaJ subunit) (Putative 1,2-phenylacetyl-CoA epoxidase, subunit D)	-8.44
ABUW_2533	<i>paaI2 paaC paaI</i>	Phenylacetate-CoA oxygenase (Phenylacetate-CoA oxygenase subunit PaaC) (Phenylacetate-CoA oxygenase subunit PaaI) (Phenylacetate-CoA oxygenase, PaaI subunit) (Phenylacetic acid degradation protein paaC) (Subunit of Phenylacetate-CoA oxygenase)	-7.55
ABUW_2534	<i>paaB paaH</i>	1,2-phenylacetyl-CoA epoxidase subunit B (EC 1.14.13.149) (1,2-phenylacetyl-CoA epoxidase, subunit B) (PaaB) (Phenylacetate-CoA oxygenase) (Phenylacetate-CoA oxygenase subunit PaaB) (Phenylacetate-CoA oxygenase, PaaH subunit) (Phenylacetic acid degradation protein paaB)	-6.57
ABUW_2535	<i>paaA paaG</i>	1,2-phenylacetyl-CoA epoxidase subunit A (1,2-phenylacetyl-CoA epoxidase, subunit A) (EC 1.14.13.149) (AAA family ATPase) (ATPase AAA) (Phenylacetate-CoA oxygenase) (Phenylacetate-CoA oxygenase subunit PaaA) (Phenylacetate-CoA oxygenase, PaaG subunit) (Phenylacetic acid degradation protein paaA)	-8.67
ABUW_2537	<i>sdaA</i>	L-serine dehydratase (EC 4.3.1.17)	-4.4
ABUW_3473	<i>yfcG_1 yfcG_2 yfcG_3</i>	Disulfide-bond oxidoreductase YfcG (EC 1.8.4.-) (Glutathione S-transferase) (EC 2.5.1.18) (Glutathione S-transferase family protein) (Glutathione S-transferase, N-terminal domain protein)	-6.13
ABUW_3782	<i>mmsB Hgd</i>	3-hydroxyisobutyrate dehydrogenase (HIBADH) (EC 1.1.1.31)	-170.82
<b>Carbohydrate Metabolism</b>			
ABUW_2099	<i>thIA_2 thIA_1</i>	Acetyl-CoA C-acetyltransferase family protein (Acetyl-CoA C-acyltransferase) (Acetyl-CoA acetyltransferase) (EC 2.3.1.16) (EC 2.3.1.9) (Acetyl-CoA acetyltransferase(Acetoacetyl-CoA thiolase)) (Thiolase family protein)	-26.47

**Table 5. Ontological Grouping of Genes with Decreased Expression in the *uspG::tn* Mutant Strain (Continued)**

ABUW_0175	<i>acsA_1 acsA_2 mbtA</i>	Acetyl-coenzyme A synthetase (AcCoA synthetase) (Acs) (EC 6.2.1.1) (Acetate--CoA ligase) (Acyl-activating enzyme)	-8.98
ABUW_1574	<i>acsA_2 acsA_1</i>	AMP-binding protein (Acetyl-CoA synthetase/AMP-(Fatty) acid ligase) (EC 6.2.1.1) (Acetyl-coenzyme A synthetase) (Acyl-CoA ligase) (Acyl-CoA synthetase)	-24.54
ABUW_1621	<i>ald1 acoD</i>	Acetaldehyde dehydrogenase 2(Acetaldehyde dehydrogenaseII) (ACDH-II) (Ald1) (Aldehyde dehydrogenase) (EC 1.2.1.3) (Aldehyde dehydrogenase family protein)	-21.75
ABUW_1624	<i>dhaT_1 dhaT_2 lap_2</i>	1,3-propanediol dehydrogenase (EC 1.1.1.202) (Alcohol dehydrogenase) (Alcohol dehydrogenase, iron-containing) (Iron-containing alcohol dehydrogenase) (Iron-containing alcohol dehydrogenase family protein) (L-threonine dehydrogenase) (Listeria adhesion protein Lap) (Putative alcohol dehydrogenase) (EC 1.1.1.1)	-10.71
ABUW_2092	<i>bdhA</i>	3-hydroxybutyrate dehydrogenase (BdhA) (D-beta-hydroxybutyrate dehydrogenase) (EC 1.1.1.30)	-10.26
ABUW_2096	<i>atoD scoA</i>	3-oxoadipate CoA-transferase (EC 2.8.3.6)	-33.66
ABUW_2097	<i>scoB atoA</i>	3-oxoadipate CoA-transferase (EC 2.8.3.6)	-26.44
ABUW_2126	<i>gutB</i>	(R,R)-butanediol dehydrogenase (EC 1.1.1.14) (EC 1.1.1.4) (2,3-butanediol dehydrogenase) (Butanediol dehydrogenase) (GutB Sorbitol dehydrogenase) (Zinc-binding alcohol dehydrogenase) (Zinc-binding dehydrogenase)	-87.11
ABUW_2127	<i>budC budC_1</i>	Diacetyl reductase [(S)-acetoin forming] (EC 1.1.1.304)	-70.07
ABUW_2129	<i>acoC</i>	Dihydrolipoamide acetyltransferase component of pyruvate dehydrogenase complex (EC 2.3.1.-)	-77.77
ABUW_2436	<i>katE</i>	Catalase (EC 1.11.1.6)	-6.76
ABUW_2456	<i>yngG_1</i>	Hydroxymethylglutaryl-CoA lyase (EC 4.1.3.4) (Hydroxymethylglutaryl-CoA lyase(HMG-CoA lyase))	-29.34
ABUW_2504	<i>srpA</i>	Catalase-related peroxidase (EC 1.11.1.-)	-7.2
ABUW_2528	<i>paaC paaH_2</i>	3-hydroxyacyl-CoA dehydrogenase (EC 1.1.1.35) (3-hydroxyacyl-CoA dehydrogenase PaaC) (3-hydroxybutyryl-CoA dehydrogenase) (EC 1.1.1.157) (PaaC)	-6.63
ABUW_2530	<i>caiD echA8_4</i>	2,3-dehydroadipyl-CoA hydratase (Enoyl-CoA hydratase, phenylacetic acid degradation) (EC 4.2.1.17) (Enoyl-CoA hydratase/isomerase family protein) (Phenylacetate degradation enoyl-CoA hydratase PaaA) (enoyl-CoA hydratase)	-6.92

**Table 5. Ontological Grouping of Genes with Decreased Expression in the *uspG::tn* Mutant Strain (Continued)**

ABUW_2603	<i>bccA accC_2</i>	BccA (EC 6.3.4.14) (Biotin carboxylase) (Carbamoyl-phosphate synthase)	-27.73
ABUW_2933	<i>mro</i>	Aldose 1-epimerase (EC 5.1.3.3)	-5.07
ABUW_3122	<i>otsB</i>	Trehalose 6-phosphate phosphatase (EC 3.1.3.12)	-20.34
ABUW_3779	<i>echA8_8</i>	Enoyl-CoA hydratase (EC 4.2.1.17) (Putative enoyl-CoA hydratase) (Short-chain enoyl-CoA hydratase)	-92.31
ABUW_3781	<i>acs</i>	AMP-binding protein (Acetyl-coenzyme A synthetase) (EC 6.2.1.1)	-205.98
ABUW_3783	<i>mmsA1</i> <i>mmsA</i> <i>mmsA3</i> <i>mmsA_2</i>	CoA-acylating methylmalonate-semialdehyde dehydrogenase (EC 1.2.1.27) (Methylmalonate-semialdehyde dehydrogenase) (Methylmalonate-semialdehyde dehydrogenase (Acylating)) (Methylmalonate-semialdehyde dehydrogenase (CoA acylating)) (MmsA methylmalonate-semialdehyde dehydrogenase (Acylating)) (NAD-dependent aldehyde dehydrogenase)	-118.41
ABUW_3806	<i>acnD</i>	Aconitate hydratase (EC 4.2.1.3)	-4.17
ABUW_3807	<i>prpC</i>	Citrate synthase	-4.96
<b>Cofactor Metabolism</b>			
ABUW_2438	<i>cinA1 cinA</i>	CinA family protein (CinA-like protein) (Competence damage-inducible protein A) (Competence-damaged family protein) (Competence-damaged protein) (Competence/damage-inducible protein CinA) (Damage-inducible protein CinA)	-30.29
ABUW_3312	<i>pntB</i>	NAD(P) transhydrogenase subunit beta (EC 7.1.1.1) (Nicotinamide nucleotide transhydrogenase subunit beta)	-4.69
ABUW_3313	<i>pntA pntA2</i>	Proton-translocating NAD(P)(+) transhydrogenase (EC 7.1.1.1)	-4.81
ABUW_3314	<i>pntAA pntA-1</i> <i>pntA1</i>	Proton-translocating NAD(P)(+) transhydrogenase (EC 7.1.1.1)	-5.34
<b>Energy Metabolism</b>			
ABUW_2389	<i>cydA_2 cioA</i> <i>cydA_1</i>	Bacterial Cytochrome Ubiquinol Oxidase family protein (Cyanide insensitive terminal oxidase) (Cytochrome D ubiquinol oxidase subunit I) (Cytochrome bd ubiquinol oxidase, subunit I) (Cytochrome bd-I ubiquinol oxidase subunit 1) (EC 1.10.3.10) (Cytochrome bd-type quinol oxidase subunit 1) (EC 1.10.3.-) (Cytochrome ubiquinol oxidase subunit I) (Putative Cytochrome bd2)	-6.84
ABUW_0259	<i>ychM_1</i>	Sulfate permease (Sulfate transporter)	-4.31
ABUW_2122	<i>fccB</i>	Oxidoreductase (EC 1.8.2.3) (TIGR01244 family phosphatase)	-5

**Table 5. Ontological Grouping of Genes with Decreased Expression in the *uspG::tn* Mutant Strain (Continued)**

<b>Lipid Metabolism</b>			
ABUW_0324	<i>lip</i>	Lactonizing lipase(Triacylglycerol lipase) (Lipase) (Triacylglycerol lipase) (EC 3.1.1.3)	-4.28
ABUW_0921	<i>glpQ</i>	Glycerophosphodiester phosphodiesterase (Glycerophosphoryl diester phosphodiesterase) (EC 3.1.4.46) (Glycerophosphoryl diester phosphodiesterase(Glycerophosphodiester phosphodiesterase))	-6.5
ABUW_1227		Acyl-coenzyme A dehydrogenase (EC 1.3.8.7) (EC 1.3.8.8)	-8.01
<b>Nucleotide Metabolism</b>			
ABUW_3217	<i>add2 add</i>	Adenosine deaminase (EC 3.5.4.4) (Adenosine aminohydrolase)	-6.87
<b>Terpenoid Metabolism</b>			
ABUW_0485	<i>fabG_1</i>	2,4-dienoyl-CoA reductase (Citronellol and citronellal dehydrogenase) (Dehydrogenase) (EC 1.1.1.-) (EC 1.1.1.100) (Oxidoreductase short-chain dehydrogenase/reductase family) (Peroxisomal trans-2-enoyl-CoA reductase)	-4.64
ABUW_0487		Acyl-CoA dehydrogenase (EC 1.3.8.1) (Acyl-CoA dehydrogenase family protein) (Acyl-CoA dehydrogenase, C-terminal domain protein) (Acyl-CoA dehydrogenase, N-terminal domain protein) (Citronellyl-CoA dehydrogenase)	-4.58
<b>Genetic Information and Processing</b>			
<b>Translation</b>			
ABUW_0231		N/A	-5.67
ABUW_0906		N/A	-10.66
<b>Environmental Information Processing</b>			
<b>Membrane Transport</b>			
ABUW_2331	<i>gltK_2 gltK gltK_1</i>	ABC transporter permease subunit (Amino ABC transporter, permease, 3-TM region, His/Glu/Gln/Arg/opine family domain protein) (Amino acid ABC transporter permease) (Binding-protein-dependent transport system inner membrane component family protein) (Glutamate Aspartate transport system permease protein GltK) (Glutamate/Aspartate transport system permease protein) (Glutamate/aspartate ABC transporter) (Glutamate/aspartate import permease protein GltK) (Glutamate/aspartate transport system permease protein GltK) (Glutamate/aspartate transporter permease GltK)	-7.88

**Table 5. Ontological Grouping of Genes with Decreased Expression in the *uspG::tn* Mutant Strain (Continued)**

ABUW_2332	<i>gltJ gltK_1 gltK_2</i>	ABC transporter permease subunit (Amino acid ABC transporter permease) (Amino acid transporter) (Binding-protein-dependent transport system inner membrane component family protein) (Glutamate Aspartate transport system permease protein GltJ) (Glutamate/aspartate transport system permease protein GltJ) (Glutamate/aspartate transport system permease protein GltK) (glutamate/aspartate transport system permease protein)	-9.1
ABUW_2333	<i>gltI pebA_1</i>	ABC transporter substrate-binding protein (Amino acid ABC transporter substrate-binding protein) (Bifunctional adhesin/ABC transporter aspartate/glutamate-binding protein) (Glutamate Aspartate periplasmic binding protein GltI) (Glutamate/aspartate import solute-binding protein) (Glutamate/aspartate periplasmic-binding protein) (Glutamate/aspartate transport protein (ABC superfamily, peri_bind)) (Glutamate/aspartate transport system substrate-binding protein) (Transporter substrate-binding domain-containing protein)	-6.62
<b>Signal Transduction</b>			
ABUW_0304	<i>pilA1 fimA_1</i>	PilA1 (Pilin) (Prepilin-type N-terminal cleavage/methylation domain-containing protein) (Prepilin-type cleavage/methylation domain-containing protein) (Type IV pilin PilA) (Type IV pilin structural subunit)	-7.58
ABUW_2098	<i>atoE</i>	Short chain fatty acid transporter family protein (Short-chain fatty acid transporter) (Short-chain fatty acid transporter (ScFAT family)) (Short-chain fatty acids transporter)	-18.56
<b>Cellular Processes</b>			
<b>Cellular Community</b>			
ABUW_3485		Integral membrane protein	-5.06
<b>Unclassified</b>			
ABUW_0022		Transporter	-4.56
ABUW_0053	<i>yjtA</i>	UPF0391 membrane protein A7M79_16605	-6.36
ABUW_0055		Glucose dehydrogenase (Glucose sorbosone dehydrogenase) (PQQ-dependent oxidoreductase, gdhB family) (PQQ-dependent sugar dehydrogenase)	-4.28
ABUW_0057	<i>yfdC</i>	Formate transporter (Formate/nitrate transporter) (Formate/nitrite transporter family) (Formate/nitrite transporter family protein) (Transport)	-7.11

**Table 5. Ontological Grouping of Genes with Decreased Expression in the *uspG::tn* Mutant Strain (Continued)**

ABUW_0068	<i>fosB</i>	Fosfomycin resistance protein FosB (Glyoxalase) (Glyoxalase family protein) (Glyoxalase/Bleomycin resistance /Dioxygenase superfamily protein) (Glyoxalase/Bleomycin resistance protein/Dioxygenase superfamily protein) (Glyoxalase/bleomycin resistance protein/dioxygenase) (Glyoxalase/bleomycin resistance/dioxygenase family protein) (Homogentisate 1,2-dioxygenase) (EC 1.13.11.5) (Metallothiol transferase FosB) (EC 2.5.1.-) (VOC family protein)	-6.76
ABUW_0079	<i>proY</i>	Amino acid permease (Gamma-aminobutyrate permease) (Proline-specific permease ProY)	-7.23
ABUW_0139		DUF2147 domain-containing protein (Signal peptide)	-4.3
ABUW_0166		Membrane protein (Omp25) (Outer membrane protein) (Putative porin)	-4.37
ABUW_0181		Uncharacterized protein	-6.48
ABUW_0183	<i>yjch yjch_1 yjch_2</i>	Acetate permease (DUF485 domain-containing protein) (Membrane protein) (inner membrane protein Yjch)	-5.29
ABUW_0184	<i>actP actP_1 actP_2</i>	Acetate permease (Acetate permease ActP) (Cation acetate symporter) (Cation/acetate symporter actP (Acetate transporter actP) (Acetatepermease)) (Na <sup>+</sup> /solute symporter) (Sodium/solute symporter)	-4.81
ABUW_0210		Aldehyde-activating protein (GFA family protein) (Gfa-like protein) (Glutathione-dependent formaldehyde-activating GFA) (Glutathione-dependent formaldehyde-activating enzyme family protein)	-5.44
ABUW_0233		Signal peptide	-4.98
ABUW_0339	<i>sodC sodCl</i>	Superoxide dismutase [Cu-Zn] (EC 1.15.1.1)	-5.44
ABUW_0359		Putative signal peptide-containing protein (Signal peptide protein) (Signal peptide-containing protein)	-9.86
ABUW_0360		Putative signal peptide protein (Putative signal peptide-containing protein) (Signal peptide protein)	-10.71
ABUW_0468		DUF2789 domain-containing protein (DUF2789 family protein) (Protein of uncharacterized function (DUF2789))	-4.88
ABUW_0628	<i>ahpC_1</i>	Alkyl hydroperoxide reductase C (Peroxioredoxin) (Thioredoxin peroxidase)	-7.99
ABUW_0646		Glyoxalase/Bleomycin resistance protein/Dioxygenase superfamily protein (PhnB protein) (VOC family protein)	-14.75

**Table 5. Ontological Grouping of Genes with Decreased Expression in the *uspG::tn* Mutant Strain (Continued)**

ABUW_0667		Activator of HSP90 ATPase (Activator of Hsp90 ATPase homolog 1-like family protein) (SRPBCC family protein) (Toxin)	-8
ABUW_0673		DUF1508 domain-containing protein (Uncharacterized conserved protein) (YegP family protein)	-4.95
ABUW_0734		Uncharacterized protein	-4.13
ABUW_0740		Uncharacterized protein	-5.48
ABUW_0741		Uncharacterized protein	-4.83
ABUW_0742		Uncharacterized protein	-4.68
ABUW_0743		Uncharacterized protein	-5.35
ABUW_0744		Uncharacterized protein	-7.13
ABUW_0985		CSLREA domain-containing protein (Outer membrane protein)	-4.25
ABUW_1004		Uncharacterized protein	-7.63
ABUW_1005	<i>yqfO</i>	GTP cyclohydrolase 1 type 2 (GTP cyclohydrolase 1 type 2-like protein) (NGG1p interacting factor 3 protein, NIF3) (NGG1p interacting factor NIF3) (NIF3 1) (NIF3-like protein 1) (Putative GTP cyclohydrolase 1 type 2) (EC 3.5.4.16) (Uncharacterized protein conserved in bacteria)	-7.63
ABUW_1063		Cellulose biosynthesis cyclic di-GMP-binding regulatory protein BcsB	-8.64
ABUW_1064	<i>icaA</i>	Dolichol-phosphate mannosyltransferase in lipid-linked oligosaccharide synthesis cluster (EC 2.4.1.83) (Glycosyl transferase) (EC 2.4.1.-) (Glycosyltransferase) (Glycosyltransferase family 2 protein) (IcaA)	-8.94
ABUW_1065		Uncharacterized protein	-10.91
ABUW_1066		Membrane protein	-10.33
ABUW_1111	<i>feaB_1</i>	Aldehyde dehydrogenase (Aldehyde dehydrogenase family protein) (NAD-dependent aldehyde dehydrogenase) (EC 1.2.1.39) (Phenylacetaldehyde dehydrogenase(PAD))	-7.26
ABUW_1113	<i>ipdC</i>	Alpha-keto acid decarboxylase family protein (Indole-3-pyruvate decarboxylase) (Indole-3-pyruvate decarboxylase(Indolepyruvatedecarboxylase)) (Pyruvate decarboxylase) (Pyruvate decarboxylase/indolepyruvate decarboxylase) (EC 4.1.1.74) (Thiamine pyrophosphate enzyme, central domain protein)	-8.31

**Table 5. Ontological Grouping of Genes with Decreased Expression in the *uspG::tn* Mutant Strain (Continued)**

ABUW_1114	<i>aroP3</i> <i>aroP_3</i>	Amino acid permease (Aromatic amino acid transport protein) (Aromatic amino acid transport protein <i>aroP</i> (General aromatic aminoacid permease)) (Aromatic amino acid transporter)	-14.02
ABUW_1120		BapA prefix-like domain-containing protein (Subtilisin-like serine protease)	-4.42
ABUW_1206	<i>dtpT</i>	Amino acid/peptide transporter (Peptide:H <sup>+</sup> symporter) family protein (Di-/tripeptide transporter) (Dipeptide/tripeptide permease) (MFS transporter) (Peptide MFS transporter)	-4.79
ABUW_1210		Alpha/beta hydrolase (Hydrolase) (Lysophospholipase) (EC 3.1.1.5)	-5.97
ABUW_1286		Uncharacterized protein	-18.14
ABUW_1287		Uncharacterized protein	-7.33
ABUW_1317		Uncharacterized protein	-6.71
ABUW_1318		Uncharacterized protein	-7.38
ABUW_1332		Alkaline lipase (Alpha/beta fold hydrolase) (Lysophospholipase) (EC 3.1.1.5) (Secretory lipase family protein) (Triacylglycerol lipase)	-5.44
ABUW_1355	<i>hemP</i>	Complement control module protein (Hemin transporter HemP) (Hemin uptake hemP family protein) (Hemin uptake protein HemP)	-6.36
ABUW_1379		Putative signal peptide protein (Signal peptide)	-5.99
ABUW_1416		Uncharacterized protein	-4.42
ABUW_1466		DUF2171 domain-containing protein (Uncharacterized protein conserved in bacteria)	-8.95
ABUW_1467		Acyl-CoA dehydrogenase	-13.75
ABUW_1468		GlcNAc-PI de-N-acetylase family protein (LmbE protein) (LmbE-like protein) (PIG-L family deacetylase)	-14.04
ABUW_1469		Class I SAM-dependent methyltransferase (Methyltransferase) (Methyltransferase domain-containing protein) (Methyltransferase type 12) (Nodulation protein S) (SAM-dependent methyltransferase)	-12.57
ABUW_1470		Glycosyl transferase (Glycosyl transferase 2 family protein) (Glycosyl transferase family 2 family protein) (Glycosyl transferase, family 2) (Glycosyl transferase, group 2 family) (Glycosyltransferase)	-14.4
ABUW_1471		DNA-binding protein (NirD/YgiW/YdeI family stress tolerance protein) (Signal peptide) (Signal peptide protein)	-14.57
ABUW_1499		DMT family transporter (EamA family transporter) (EamA/RhaT family transporter) (Membrane protein putative) (Permease of the drug/metabolite transporter (DMT) superfamily)	-4.38

**Table 5. Ontological Grouping of Genes with Decreased Expression in the *uspG::tn* Mutant Strain (Continued)**

ABUW_1536		Putative signal peptide-containing protein (Signal peptide protein) (Signal peptide-containing protein)	-5.08
ABUW_1541		Alpha-E domain-containing protein (Bacterial domain of uncharacterized function (DUF403))	-6.82
ABUW_1542		Protein containing transglutaminase-like domain (Transglutaminase) (Transglutaminase family protein) (Transglutaminase-like enzyme, putative cysteine protease)	-4.19
ABUW_1561		Cyclohexanone monooxygenase (EC 1.14.13.22) (Flavoprotein)	-5.68
ABUW_1572	<i>fabG_4</i>	2,5-dichloro-2,5-cyclohexadiene-1,4-diol dehydrogenase (EC 1.1.1.35) (3-hydroxy-2-methylbutyryl-CoA dehydrogenase) (3-hydroxyacyl-CoA dehydrogenase) (EC 1.1.1.100) (SDR family NAD(P)-dependent oxidoreductase) (Short chain dehydrogenase family protein) (Short-chain dehydrogenase/reductase)	-26.34
ABUW_1573		Acyl-CoA dehydrogenase (Acyl-CoA dehydrogenase family protein) (Acyl-CoA dehydrogenase protein) (EC 1.3.8.1) (Acyl-CoA dehydrogenase, N-terminal domain protein)	-25.8
ABUW_1601		Uncharacterized protein	-6.63
ABUW_1603		Acetyltransferase (Acetyltransferase (GNAT) family protein) (Acetyltransferase domain protein) (Acetyltransferase, GNAT family) (GNAT family N-acetyltransferase) (N-acetyltransferase) (Putative acetyltransferase)	-6.12
ABUW_1629		Uncharacterized protein	-6.34
ABUW_1631	<i>csuB_2</i> <i>csuB_1</i>	Csu pilus subunit CsuB (Fimbrial major subunit CsuA/B family protein) (Protein U) (Putative biofilm synthesis protein) (SCPU domain-containing protein) (Sigma-fimbriae tip adhesin) (Spore Coat Protein U domain protein) (Spore coat protein SpoU) (Spore coat protein U domain-containing protein)	-12.32
ABUW_1632		CsuC (Fimbria/pilus periplasmic chaperone) (Molecular chaperone) (Pilus assembly protein) (Sigma-fimbriae chaperone protein)	-14.53
ABUW_1633	<i>htrE_1</i>	Fimbria/pilus outer membrane usher protein (Fimbrial biogenesis outer membrane usher protein) (Fimbrial usher protein) (Putative outer membrane usher protein <i>yraJ</i> ) (Sigma-fimbriae usher protein)	-11.26
ABUW_1634		SCPU domain-containing protein	-9.63

**Table 5. Ontological Grouping of Genes with Decreased Expression in the *uspG::tn* Mutant Strain (Continued)**

ABUW_1637		Oxidoreductase (Oxidoreductase short-chain dehydrogenase/reductase family) (Oxidoreductase, short-chain dehydrogenase/reductase family) (SDR family NAD(P)-dependent oxidoreductase) (Short-chain dehydrogenase)	-4.57
ABUW_1649		Uncharacterized protein	-5.41
ABUW_1651		Uncharacterized protein	-89.8
ABUW_1653		Uncharacterized protein	-5.5
ABUW_1657		Uncharacterized protein	-5.22
ABUW_1659	<i>pliG</i>	DNA breaking-rejoining protein (Inhibitor of g-type lysozyme) (Protein ycgK)	-39.81
ABUW_1692	<i>tetC</i>	Bacterial regulatory protein, tetR family protein (Putative transcriptional regulator) (TetR family transcriptional regulator) (TetR/AcrR family transcriptional regulator) (Transcriptional regulator) (Transcriptional regulator, TetR family) (Transposon Tn10 TetC protein)	-4.61
ABUW_1693		Heme oxygenase-like protein	-6.92
ABUW_1723		Uncharacterized protein	-6.91
ABUW_1751		Fels-1 Prophage Protein-like family protein (Putative prophage protein) (Putative signal peptide-containing protein)	-4.66
ABUW_1753		Uncharacterized protein	-6.2
ABUW_1761		Abasic site processing protein (EC 3.4.-.-)	-7.89
ABUW_1775		Membrane protein (Putative membrane protein)	-6.18
ABUW_1787		Uncharacterized protein	-5.4
ABUW_1810		Uncharacterized protein	-4.39
ABUW_1860		Ketosteroid isomerase-like enzyme (Nuclear transport factor 2 family protein) (Polyketide cyclase) (Succinyl-CoA synthetase)	-9.23
ABUW_1861	<i>antA_3</i> <i>antA_1</i>	(2Fe-2S)-binding protein (Aromatic ring-hydroxylating dioxygenase subunit alpha) (Aromatic-ring-hydroxylating dioxygenase large subunit) (EC 1.14.12.1) (Benzoate 1,2-dioxygenase alpha subunit) (EC 1.14.12.10) (Benzoate 1,2-dioxygenase subunit alpha) (Rieske (2Fe-2S) protein) (Rieske 2Fe-2S domain-containing protein) (Ring hydroxylating dioxygenase, Rieske)	-5.42

**Table 5. Ontological Grouping of Genes with Decreased Expression in the *uspG::tn* Mutant Strain (Continued)**

ABUW_1862	<i>cbdB</i>	Anthranilate dioxygenase small subunit (Aromatic-ring-hydroxylating dioxygenase) (Aromatic-ring-hydroxylating dioxygenase beta subunit) (Aromatic-ring-hydroxylating dioxygenase small subunit) (EC 1.14.12.13) (Aromatic-ring-hydroxylating dioxygenase subunit beta) (Putative Aromatic-ring-hydroxylating dioxygenase small subunit) (Ring hydroxylating beta subunit)	-5.06
ABUW_1886	<i>cpo</i>	Alpha/beta fold hydrolase (Alpha/beta hydrolase) (EC 1.11.1.10) (Cpo Non-heme chloroperoxidase) (Non-heme chloroperoxidase)	-4.07
ABUW_1888		Membrane protein (NAD(P)H-binding protein) (Oxidoreductase) (EC 1.3.1.-) (Saccharopine dehydrogenase) (Saccharopine dehydrogenase NADP-binding domain-containing protein) (Saccharopine dehydrogenase family protein)	-4.53
ABUW_1891		ThiJ/Pfpl domain protein (ThiJ/Pfpl domain-containing protein) (Type 1 glutamine amidotransferase domain-containing protein)	-9.16
ABUW_1902	<i>sndH2</i>	L-sorbose dehydrogenase (EC 1.1.1.-) (L-sorbose dehydrogenase(SNDH)) (Sorbose dehydrogenase family protein)	-5.01
ABUW_1903		Predicted membrane protein	-7.33
ABUW_1918		Uncharacterized protein	-33.81
ABUW_1921	<i>ttuB_5</i> <i>rhmT_2</i>	MFS transporter (MFS transporter permease) (Permease of the major facilitator) (Putative tartrate transporter) (Tartrate transporter) (Transporter, anion:cation symporter (ACS) family)	-4.3
ABUW_1958		Type III restriction enzyme, res subunit	-4.79
ABUW_1993		Uncharacterized protein	-5.92
ABUW_2051		Uncharacterized protein	-7.61
ABUW_2058		Phage capsid and scaffold (Phage capsid protein) (Uncharacterized conserved protein)	-9.64
ABUW_2060		Uncharacterized protein	-30.46
ABUW_2061		Uncharacterized protein	-4.41
ABUW_2063		DNA glycosylase (G:T/U mismatch-specific DNA glycosylase) (G:T/U mismatch-specific uracil/thymine DNA-glycosylase) (Uracil-DNA glycosylase family protein)	-6.41
ABUW_2064		Uncharacterized protein	-69.29
ABUW_2065		Uncharacterized protein	-4.01
ABUW_2093		Citrate transporter family protein (D-beta-hydroxybutyrate permease) (GntP family permease) (GntP family transporter)	-8.25
ABUW_2128	<i>lpdA2 lpdA</i>	Dihydrolipoyl dehydrogenase (EC 1.8.1.4)	-66.05

**Table 5. Ontological Grouping of Genes with Decreased Expression in the *uspG::tn* Mutant Strain (Continued)**

ABUW_2130	<i>acoB</i>	Acetoin:2,6-dichlorophenolindophenol oxidoreductase subunit beta	-88.23
ABUW_2131	<i>acoA</i>	ABC transporter substrate-binding protein (Acetoin:2,6-dichlorophenolindophenol oxidoreductase alpha subunit) (Acetoin:2,6-dichlorophenolindophenol oxidoreductase subunit alpha) (EC 1.1.1.-) (Acetoin:DCPIP oxidoreductase alpha subunit) (Pyruvate/2-oxoglutarate dehydrogenase complex, dehydrogenase (E1) component, alpha subunit) (Thiamine pyrophosphate enzyme, C-terminal TPP binding domain protein) (Thiamine pyrophosphate-dependent dehydrogenase E1 component subunit alpha)	-84.13
ABUW_2132	<i>lipA2 lipA lipA_2</i>	Lipoyl synthase (EC 2.8.1.8) (Lip-syn) (LS) (Lipoate synthase) (Lipoic acid synthase) (Sulfur insertion protein LipA)	-42.7
ABUW_2133		Transcriptional regulator (Transcriptional regulatory protein, C terminal family protein)	-5.57
ABUW_2143		Transcriptional regulator	-4.25
ABUW_2156		Uncharacterized protein	-5.78
ABUW_2187	<i>bmr3</i>	DHA2 family efflux MFS transporter permease subunit (Drug resistance MFS transporter, drug:H <sup>+</sup> antiporter-1) (MFS superfamily multidrug resistance protein) (MFS transporter) (Transporter, major facilitator family)	-4.34
ABUW_2188	<i>iucD_2</i>	L-lysine 6-monooxygenase (Lysine/ornithine N-monooxygenase) (EC 1.14.13.59) (NADPH-dependent L-lysine N(6)-monooxygenase) (Ornithine monooxygenase) (SidA/lucD/PvdA family monooxygenase)	-4.32
ABUW_2189	<i>iucA</i>	IucA/IucC-family aerobactin siderophore biosynthesis component (Siderophore biosynthesis protein) (EC 6.3.2.-)	-5.28
ABUW_2215		Nucleoside-diphosphate-sugar epimerase (Semialdehyde dehydrogenase, NAD binding domain protein)	-4.17
ABUW_2219		Uncharacterized protein	-4.4
ABUW_2293	<i>yceI</i>	Polyisoprenoid-binding protein (Protein yceI) (YceI-like domain protein)	-4.53
ABUW_2297		Uncharacterized protein	-5.06
ABUW_2317		Uncharacterized protein	-8.32
ABUW_2321		Uncharacterized protein	-29.9

**Table 5. Ontological Grouping of Genes with Decreased Expression in the *uspG::tn* Mutant Strain (Continued)**

ABUW_2330	<i>artP fbpC_4 fbpC_5 glnQ_2 gltL</i>	ATP-binding cassette domain-containing protein (Amino acid ABC transporter ATP-binding protein) (Arginine transporter ATP-binding subunit) (Glutamate/Aspartate transport ATP-binding protein) (Glutamate/aspartate ABC transporter ATP-binding protein) (Glutamate/aspartate transport system ATP-binding protein) (Glutamine transport ATP-binding protein GlnQ) (Iron(III) ABC transporter, ATP-binding protein) (glutamate/aspartate transport ATP-binding protein GltL)	-6.11
ABUW_2345		Uncharacterized protein	-7.79
ABUW_2372		DUF1427 domain-containing protein (DUF1427 family protein) (XapX domain protein) (XapX domain-containing protein)	-6.47
ABUW_2388		Uncharacterized protein	-8.44
ABUW_2390	<i>cydB cioB cydB1 cydB3 cydB_1</i>	CydB cytochrome d ubiquinol oxidase, subunit II (Cytochrome D Ubiquinol oxidase, subunit II) (Cytochrome bd-I ubiquinol oxidase subunit 2) (Cytochrome d ubiquinol oxidase subunit II) (Putative Cytochrome bd2) (Ubiquinol oxidase subunit II) (Ubiquinol oxidase subunit II, cyanide insensitive) (EC 1.10.3.-)	-6.82
ABUW_2391		DUF2474 domain-containing protein	-4.75
ABUW_2433		KGG domain-containing protein (Putative gene 48 protein) (Stress-induced acidophilic repeat motif-containing protein) (Stress-induced protein)	-12.98
ABUW_2434		Uncharacterized protein	-8.33
ABUW_2435	<i>ydaD entA_10 entA_18 yhxC</i>	2,3-dihydroxybenzoate-2,3-dehydrogenase (3-oxoacyl-[acyl-carrier protein] reductase) (EC 1.1.1.100) (General stress protein 39) (Glucose 1-dehydrogenase) (EC 1.1.1.47) (NAD(P)-dependent oxidoreductase) (Oxidoreductase) (EC 1.-.-.-) (SDR family oxidoreductase) (Short chain dehydrogenase family protein) (Short-chain dehydrogenase)	-15.17
ABUW_2437		Heme oxygenase-like protein (Iron-containing redox enzyme family protein)	-17.33
ABUW_2439		TPR repeat containing protein	-8.43
ABUW_2440		Surface antigen	-15.85
ABUW_2442		Uncharacterized protein	-8.66
ABUW_2443		Uncharacterized protein	-6.39
ABUW_2448		DcaP-like protein (TMF family protein)	-5.81

**Table 5. Ontological Grouping of Genes with Decreased Expression in the *uspG::tn* Mutant Strain (Continued)**

ABUW_2449		Class I SAM-dependent methyltransferase (Methyltransferase domain protein) (Methyltransferase domain-containing protein) (Putative SAM-dependent methyltransferase) (SAM-dependent methyltransferase)	-13.67
ABUW_2450	<i>fadD_1</i>	AMP-binding enzyme family protein (AMP-binding protein) (Acetoacetyl-CoA synthetase/ Long-chain-fatty-acid--CoA ligase) (EC 6.2.1.16) (Acyl-CoA synthetase (AMP-forming)/AMP-acid ligase II) (EC 6.2.1.3) (Fatty acid--CoA ligase) (Long-chain fatty-acid-CoA ligase)	-13.23
ABUW_2451	<i>fadR</i>	Bacterial regulatory protein, tetR family protein (Fatty acid metabolism regulator protein) (TetR family regulatory protein) (TetR family transcriptional regulator) (Transcriptional regulator AcrR family)	-5.99
ABUW_2458		Indolepyruvate ferredoxin oxidoreductase (Indolepyruvate ferredoxin oxidoreductase family protein) (MFS transporter) (Oxidoreductase) (Pyruvate ferredoxin/flavodoxin oxidoreductase family protein)	-9.88
ABUW_2503	<i>yceJ_1</i>	Cytochrome b (Cytochrome b561) (Cytochrome b561 family protein)	-6.45
ABUW_2518		Aminotransferase (Putative aminotransferase)	-19.86
ABUW_2524	<i>paaY yrdA_2</i>	Gamma carbonic anhydrase family protein (PaaY) (Phenylacetic acid degradation acetyltransferase) (Phenylacetic acid degradation protein PaaY)	-4.38
ABUW_2527	<i>paaE paaJ pcaF</i>	3-oxoadipyl-CoA thiolase (EC 2.3.1.174) (Beta-ketoadipyl-CoA thiolase)	-6.26
ABUW_2553		Uncharacterized protein	-9.26
ABUW_2554		DUF333 domain-containing protein (Hemolysin) (Putative hemolysin)	-4.96
ABUW_2594		Glutathione-dependent formaldehyde dehydrogenase	-13.83
ABUW_2604	<i>kipl</i>	5-oxoprolinase/urea amidolyase family protein (Allophanate hydrolase) (Allophanate hydrolase 2 subunit 1 / Allophanate hydrolase 2 subunit 2) (EC 3.5.1.54) (Allophanate hydrolase subunit 1 and 2) (Biotin-dependent carboxylase uncharacterized domain protein)	-30.57
ABUW_2605		Putative hydro-lyase AB71191_03206 (EC 4.2.1.-)	-34.64
ABUW_2606	<i>pxpA</i>	5-oxoprolinase subunit A (5-OPase subunit A) (EC 3.5.2.9) (5-oxoprolinase (ATP-hydrolyzing) subunit A)	-30.86
ABUW_2607	<i>ycsG</i>	Argininosuccinate synthase (Divalent metal cation transporter) (Manganese transporter NRAMP) (Membrane protein) (Mn <sup>2+</sup> /Fe <sup>2+</sup> transporter)	-42.24

**Table 5. Ontological Grouping of Genes with Decreased Expression in the *uspG::tn* Mutant Strain (Continued)**

ABUW_2621		Uncharacterized protein	-10.02
ABUW_2658		Uncharacterized protein	-6.29
ABUW_2672		Uncharacterized protein	-16.53
ABUW_2673		Uncharacterized protein	-20.36
ABUW_2674		Uncharacterized protein	-11.54
ABUW_2678		17 kDa surface antigen (Putative surface antigen)	-30.83
ABUW_2679		DUF4142 domain-containing protein (Putative outer membrane protein)	-33.43
ABUW_2684		Phage putative head morphogenesis protein	-9.68
ABUW_2685		Uncharacterized protein	-15.22
ABUW_2686		Uncharacterized protein	-14.5
ABUW_2700		Uncharacterized protein	-4.69
ABUW_2703	<i>yhjQ</i>	Cysteine-rich helical bundle repeat protein (Ferredoxin) (Four-helix bundle copper-binding protein) (Putative cysteine-rich protein) (Putative cysteine-rich protein YhjQ)	-5.62
ABUW_2723	<i>ahpF ahpF2 ahpF3 ahpF_1 ahpF_2</i>	Alkyl hydroperoxide reductase subunit F	-4.14
ABUW_2730	<i>arfA_2</i>	OmpA family protein (OmpA/MotB) (Outer membrane lipoprotein omp16)	-10.99
ABUW_2744		Membrane protein (Putative membrane protein)	-8.94
ABUW_2799	<i>astA2 astA</i>	Arginine N-succinyltransferase (EC 2.3.1.109) (AstA arginine N-succinyltransferase)	-5.28
ABUW_2887	<i>nlpE cutF</i>	Copper homeostasis protein (Copper homeostasis protein cutF (Lipoprotein nlpE)) (Copper resistance protein NlpE) (Copper resistance protein NlpE N-terminal domain-containing protein) (Lipoprotein) (Lipoprotein NlpE involved in copper resistance) (Lipoprotein involved with copper homeostasis and adhesion) (Putative lipoprotein)	-6.04
ABUW_2901		Activator of HSP90 ATPase (Activator of Hsp90 ATPase homolog 1-like family protein) (SRPBCC domain-containing protein)	-4.67
ABUW_3032	<i>pilT_2 pilT_1 pilU</i>	PilT/PilU family type 4a pilus ATPase (PilU) (Twitching motility protein) (Twitching motility family protein) (Twitching motility protein) (Twitching motility protein PilT) (Twitching motility protein PilU) (Type IV pili twitching motility protein PilT) (Type IV pilus assembly protein, pilus retraction protein PilT) (Type IV pilus twitching motility protein PilT)	-5.48

**Table 5. Ontological Grouping of Genes with Decreased Expression in the *uspG::tn* Mutant Strain (Continued)**

ABUW_3106	<i>lysM ygaU</i>	BON domain protein (LysM domain/BON superfamily protein) (Peptidoglycan-binding LysM) (Peptidoglycan-binding protein LysM) (Phage-like element PBSX protein xkDP)	-4.27
ABUW_3157		Conserved TM helix family protein (Mechanosensitive ion channel) (Small-conductance mechanosensitive channel) (TM helix domain protein) (TM helix protein) (TM helix repeat-containing protein)	-7.46
ABUW_3265	<i>ohrB</i>	Ohr family peroxiredoxin (Ohr-like protein) (Organic hydroperoxide resistance protein)	-4.04
ABUW_3291	<i>alkK</i>	3-methylmercaptopropionyl-CoA ligase (DmdB) (AMP-binding enzyme family protein) (AMP-binding protein) (Acyl-CoA synthase) (Acyl-CoA synthetase) (EC 6.2.1.3)	-5.04
ABUW_3321	<i>copA copA_2</i>	Copper resistance protein A (Copper resistance system multicopper oxidase)	-4.82
ABUW_3322	<i>copB copB_2</i>	Copper resistance protein B	-11.77
ABUW_3325	<i>actP1 actP_3</i>	Copper-translocating P-type ATPase (Copper-transporting P-type ATPase) (EC 3.6.3.4) (Heavy metal translocating P-type ATPase)	-9.05
ABUW_3351		Heme oxygenase-like protein	-9.61
ABUW_3352	<i>nemR_1 nemR_2</i>	HTH-type transcriptional repressor NemR (Putative transcriptional regulator) (TetR family transcriptional regulator) (TetR/AcrR family transcriptional regulator) (Transcriptional regulator) (Transcriptional regulator, AcrR family) (Transposon Tn10 tetC protein (ORFL))	-15.25
ABUW_3524		Uncharacterized protein/domain associated with GTPases	-4.05
ABUW_3575	<i>ydeN</i>	Signal peptide (EC 3.-.-.-)	-7.29
ABUW_3577		Uncharacterized protein	-4.86
ABUW_3582		Putative secreted protein	-5.69
ABUW_3587		DNA transfer protein p32 (Epstein-Barr nuclear antigen 1) (Glycine zipper family protein)	-7.77
ABUW_3622	<i>yjdC</i>	Bacterial regulatory protein, tetR family protein (TetR family transcriptional regulator) (TetR/AcrR family transcriptional regulator) (Transcriptional regulator)	-6.32
ABUW_3702		DUF2726 domain-containing protein (Putative signal peptide-containing protein)	-7.12
ABUW_3777	<i>yhjE_2</i>	MFS transporter (MHS family MFS transporter) (Major facilitator superfamily permease) (Shikimate transporter)	-105.76
ABUW_3778	<i>echA8_7</i>	3-hydroxyisobutyryl-CoA hydrolase (EC 3.1.2.4) (Enoyl-CoA hydratase/isomerase family protein) (EC 4.2.1.17)	-52.74

**Table 5. Ontological Grouping of Genes with Decreased Expression in the *uspG::tn* Mutant Strain (Continued)**

ABUW_3780	<i>mmgC_8</i>	Acyl-CoA dehydrogenase (EC 1.3.8.1) (EC 1.3.99.-) (Acyl-CoA dehydrogenase family protein) (Butyryl-CoA dehydrogenase)	-105.19
ABUW_3794		RNase E inhibitor protein (Ribonuclease E inhibitor RraB)	-4.38
ABUW_3804		Zinc ribbon-containing protein	-5.28
ABUW_3822		Bacterial transferase hexapeptide (Three repeats) family protein	-8.56
ABUW_3823		Putative UDP-galactose phosphate transferase (WeeH)	-11.45
ABUW_3874		Lipoprotein (Lipoprotein, putative) (Putative lipoprotein) (Signal peptide protein)	-7
ABUW_3898		GlsB/YeaQ/YmgE family stress response membrane protein (Transglycosylase) (Transglycosylase associated family protein) (Transglycosylase-associated protein)	-7.01

Annotations and descriptions were assigned using UniProt Retrieve/ID mapping function. Annotations were filed under gene names. Descriptions were under the category of protein names. EC value was used to search KEGG Database. Note: some genes could be classified under multiple categories, here only one was selected per gene. Fold: fold change comparing WT expression / *uspG::tn* expression x -1.

**Table 6. Ontological Grouping of Genes with Increased Expression in the *uspG::tn* Mutant Strain**

ABUW_	Annotation	Description	Fold
<b>Metabolism</b>			
<b>Carbohydrate Metabolism</b>			
ABUW_0203	<i>gabT</i>	4-aminobutyrate aminotransferase (EC 2.6.1.19) (4-aminobutyrate transaminase) (4-aminobutyrate--2-oxoglutarate transaminase) (GabT 4-aminobutyrate transaminase) (Gamma-aminobutyrate:alpha-ketoglutarate aminotransferase)	13.95
ABUW_2973	<i>mgo</i>	Probable malate:quinone oxidoreductase (EC 1.1.5.4) (MQO) (Malate dehydrogenase [quinone])	5.85
<b>Cofactor Metabolism</b>			
ABUW_1195	<i>foIE</i>	GTP cyclohydrolase 1 (EC 3.5.4.16) (GTP cyclohydrolase I) (GTP-CH-I)	4.81
<b>Energy Metabolism</b>			
ABUW_1021	<i>sbp_2 cysP sbp_1</i>	ABC transporter permease (ABC-type sulfate transport system periplasmic protein) (CysP) (Sulfate ABC transporter substrate-binding protein) (Sulfate ABC transporter, sulfate-binding family protein) (Sulfate and thiosulfate binding protein CysP) (Sulfate-binding protein) (Thiosulfate-binding protein)	8.2

**Table 6. Ontological Grouping of Genes with Increased Expression in the *uspG::tn* Mutant Strain (Continued)**

ABUW_1793	<i>cydX ybgT</i>	Cyd operon protein YbgT (Cytochrome bd-I oxidase subunit CydX) (Cytochrome bd-I ubiquinol oxidase subunit X) (EC 1.10.3.10) (Cytochrome d ubiquinol oxidase subunit X) (Membrane protein) (Putative membrane protein)	7.23
ABUW_1794	<i>cydB</i>	CydB cytochrome d ubiquinol oxidase, subunit II (Cytochrome D Ubiquinol oxidase subunit II) (EC 1.10.3.-) (Cytochrome D ubiquinol oxidase, subunit II) (Cytochrome bd-type quinol oxidase, subunit 2) (Cytochrome d ubiquinol oxidase subunit 2)	7.19
ABUW_1795	<i>cydA cydA_1</i>	Cytochrome D Ubiquinol oxidase subunit I (Cytochrome bd-I ubiquinol oxidase subunit CydA) (Cytochrome d terminal oxidase subunit 1) (Cytochrome d terminal oxidase, polypeptide subunit I) (EC 1.10.3.-) (Cytochrome d ubiquinol oxidase subunit 1) (Cytochrome d ubiquinol oxidase subunit I) (Cytochrome d ubiquinol oxidase subunit I)	6.85
ABUW_2379	<i>tauD</i>	Alpha-ketoglutarate-dependent taurine dioxygenase (Taurine dioxygenase) (EC 1.14.11.17)	7.03
ABUW_2380	<i>tauC</i>	Nitrate/sulfonate/bicarbonate ABC transporter permease (Putative aliphatic sulfonates transport permease protein SsuC) (Taurine ABC transporter permease TauC) (Taurine transport system permease protein) (Taurine transport system permease protein TauC) (Taurine transporter subunit)	7.63
ABUW_2382	<i>tauA tauA_2</i>	ABC-type taurine transport system periplasmic protein (Taurine ABC transporter substrate-binding protein) (Taurine ABC transporter, periplasmic binding protein) (Taurine-binding periplasmic protein) (Taurine-binding periplasmic protein TauA)	7.95
<b>Genetic Information Processing</b>			
<b>Translation</b>			
ABUW_0277		#N/A	8.88
ABUW_0405	<i>rpsJ nusE</i>	30S ribosomal protein S10	6.09
ABUW_0406	<i>rplC l3p</i>	50S ribosomal protein L3	5.16
ABUW_0407	<i>rplD</i>	50S ribosomal protein L4	4.83
ABUW_0408	<i>rplW</i>	50S ribosomal protein L23	4.52
ABUW_0410	<i>rpsS</i>	30S ribosomal protein S19	4.1
ABUW_0412	<i>rpsC s3p</i>	30S ribosomal protein S3	4.51
ABUW_0493	<i>rpsI</i>	30S ribosomal protein S9	4.65
ABUW_0494	<i>rplM</i>	50S ribosomal protein L13	4.33

**Table 6. Ontological Grouping of Genes with Increased Expression in the *uspG::tn* Mutant Strain (Continued)**

ABUW_0695		N/A	10.91
ABUW_1547	<i>rpsR</i>	30S ribosomal protein S18	4.41
ABUW_1548	<i>rpsF</i>	30S ribosomal protein S6	4.67
ABUW_2899	<i>lysS</i>	Lysine--tRNA ligase (EC 6.1.1.6) (Lysyl-tRNA synthetase) (LysRS)	4.07
ABUW_3220		N/A	4.7
ABUW_3284	<i>rplT</i>	50S ribosomal protein L20	4.72
ABUW_3285	<i>rplM</i>	50S ribosomal protein L35	4.65
ABUW_3593	<i>rplA</i>	50S ribosomal protein L1	4
<b>Environmental Information Processing</b>			
<b>Signal Transduction</b>			
ABUW_1525	<i>dctA_1</i> <i>dctA_2</i> <i>dctA_3</i>	C4-dicarboxylate transport protein	4.27
ABUW_1581	<i>kdpA</i>	Potassium-transporting ATPase potassium-binding subunit (ATP phosphohydrolase [potassium-transporting] A chain) (Potassium-binding and translocating subunit A) (Potassium-translocating ATPase A chain)	5.51
<b>Unclassified</b>			
ABUW_0201	<i>gabP</i> <i>gabP_1</i>	Amino acid permease (Aromatic amino acid transport protein AroP) (GABA permease) (GABA permease (4-amino butyrate transport carrier)) (GabP)	11.97
ABUW_0275	<i>lysP_1</i> <i>mmuP</i>	Amino acid permease family protein (Amino acid transporter) (Amino-acid permease) (Arginine permease RocE) (Putative S-methylmethionine permease) (Putative amino acid permease, GabP family)	4.15
ABUW_0381	<i>deaD</i>	ATP-dependent RNA helicase (ATP-dependent RNA helicase DeaD) (EC 3.6.4.13) (Cold-shock DEAD box protein A(ATP-dependent RNA helicase deaD)) (DEAD/DEAH box helicase) (Helicase domain protein)	13.23
ABUW_0382		Putative membrane protein	6.21
ABUW_0409	<i>rplB</i>	50S ribosomal protein L2	4.81
ABUW_0603		Putative signal peptide protein (RcnB family protein) (Signal peptide) (Signal peptide protein)	5.75
ABUW_0635		Alpha-beta hydrolase family esterase (Esterase) (Patatin family protein) (Patatin-like phospholipase family protein) (Phospholipase, patatin family)	4.09
ABUW_0691		Uncharacterized protein	13.19

**Table 6. Ontological Grouping of Genes with Increased Expression in the *uspG::tn* Mutant Strain (Continued)**

ABUW_0928	<i>mltF mltF_1 yfhD</i>	ABC transporter substrate-binding protein (Lytic transglycosylase, catalytic) (Membrane-bound lytic murein transglycosylase F) (EC 4.2.2.-) (Periplasmic binding protein of transport/transglycosylase) (Soluble lytic transglycosylase fused to an ABC-type amino acid-binding protein) (Transglycosylase SLT domain protein) (Transglycosylase SLT domain-containing protein) (Transglycosylase, Slt family) (Transporter substrate-binding domain-containing protein)	6.4
ABUW_1020		Alpha/beta hydrolase (Alpha/beta hydrolase fold protein) (Esterase)	6.94
ABUW_1495		Uncharacterized protein	4.22
ABUW_1557	<i>pgaA</i>	Biofilm synthesis protein (Outer membrane protein) (PgaA) (Poly-beta-1,6 N-acetyl-D-glucosamine export porin PgaA)	4.28
ABUW_1599	<i>benM_3 benM_1 metR</i>	HTH-type transcriptional regulator MetR	6.13
ABUW_1763	<i>uspG</i>	Universal stress protein	7.24
ABUW_1764	<i>cdpA_6 gmr gmr_2</i>	Cyclic di-GMP phosphodiesterase (Diguanylate cyclase) (Diguanylate cyclase (GGDEF) domain protein) (Diguanylate cyclase/phosphodiesterase (GGDEF & EAL domains) with PAS/PAC sensor(S)) (EAL domain-containing protein) (GGDEF domain-containing protein) (GGDEF family protein) (Signal transduction protein) (EC 3.1.4.52)	9.97
ABUW_1792	<i>ybgE</i>	Cyd operon YbgE family protein (Cyd operon protein) (Cyd operon protein YbgE (Cyd_oper_YbgE) family protein) (Cytochrome bd biosynthesis protein) (Protein ybgE)	6.81
ABUW_2052	<i>hifA</i>	F17 fimbrial protein (Ferrous iron transporter B) (Fimbrial protein) (Fimbrial subunit) (Type 1 fimbrial protein)	5.63
ABUW_2053	<i>fimC fimC_1 fimC_2 papD-2 yadV_2</i>	Chaperone protein mrkB (Fimbria/pilus periplasmic chaperone) (Molecular chaperone) (P pilus assembly protein) (Pili assembly chaperone) (Pilin chaperone) (Pilus assembly protein) (Putative fimbrial chaperone YadV)	11.33
ABUW_2054	<i>mrkC</i>	Fimbria/pilus outer membrane usher protein (Fimbrial biogenesis outer membrane usher protein) (Outer membrane fimbrial usher protein) (Outer membrane usher protein) (Outer membrane usher protein mrkC)	5.89
ABUW_2102		Uncharacterized protein	5.07

**Table 6. Ontological Grouping of Genes with Increased Expression in the *uspG::tn* Mutant Strain (Continued)**

ABUW_2103		Uncharacterized protein	10.92
ABUW_2169		Probable membrane transporter protein	4.07
ABUW_2270		Uncharacterized protein	9.99
ABUW_2287	<i>putA</i>	Bifunctional protein PutA [Includes: Proline dehydrogenase (EC 1.5.5.2) (Proline oxidase); Delta-1-pyrroline-5-carboxylate dehydrogenase (P5C dehydrogenase) (EC 1.2.1.88) (L-glutamate gamma-semialdehyde dehydrogenase)]	30.39
ABUW_2316	<i>yijE_3</i>	DMT family permease (DMT family transporter) (EamA family transporter) (EamA/RhaT family transporter) (Permease of the drug/metabolite transporter (DMT) superfamily)	4.86
ABUW_2381	<i>tauB ssuB_2</i>	ABC-type taurine transport system, ATPase component (EC 3.6.3.-) (ATP-binding cassette domain-containing protein) (EC 3.6.3.36) (Nitrate transport ATP-binding protein nrtD) (Taurine import ATP-binding protein) (Taurine transport ATP-binding protein TauB) (Taurine transport system ATP-binding protein) (Taurine transporter ATP-binding subunit)	9.02
ABUW_2387		Uncharacterized protein	4.13
ABUW_2513	<i>csp2 cspE_1</i>	Cold shock protein CspE (Cold shock-like protein cspG) (Cold-shock DNA-binding domain protein) (Cold-shock protein)	8.91
ABUW_2516		Uncharacterized protein	5.37
ABUW_2517		Uncharacterized protein	4.82
ABUW_2680		Uncharacterized protein	12.26
ABUW_2690	<i>cspV csp1 cspE cspE_2</i>	'Cold-shock' DNA-binding domain protein (Cold shock domain-containing protein) (Cold shock protein) (Cold shock protein CspG) (Cold shock protein CspV) (Cold shock protein, CSP family) (Cold-shock DNA-binding domain protein)	8.23
ABUW_2696		Transposase	15.19
ABUW_3198		DUF1852 domain-containing protein (DUF1852 family protein) (Domain of uncharacterized function (DUF1852))	7.04
ABUW_3495	<i>trmB_2</i>	Methyltransferase family protein (Methyltransferase superfamily) (Putative methyltransferase) (EC 2.1.1.33) (SAM-dependent methyltransferase)	4.01
ABUW_3706		DUF2938 domain-containing protein (DUF2938 family protein)	5.48

Annotations and descriptions were found using [uniprot.org](http://uniprot.org) Retrieve/ID mapping function. Annotations were filed under gene names. Descriptions were under the category of protein names. EC value was used to search KEGG Pathways. Fold: Fold change calculated by comparing *uspG::tn* expression / AB5075 expression.

**Shifts in the Expression of Energy and Translation Involved Genes Result in Susceptibility of the *uspG::tn* Mutant to Aminoglycosides.** Our transcriptomic studies uncovered a high number of ribosomal proteins with increased expression within the *uspG::tn* strain as compared to the wildtype AB5075 strain (**Table 6**). Specifically, eight genes encoding proteins of the 50S ribosomal subunit, six genes encoding proteins of the 30S subunit, and two genes encoding tRNA synthetases were upregulated by >4-fold in the *uspG::tn* mutant strain. When reviewing the data more closely, including ribosomal protein associated genes that did not fall within the 4-fold analysis group, we determined that 54 out of 55 ribosomal proteins of the 30 or 50S subunits were upregulated in the absence of UspG (**Figure 16**). Further, other genes associated with translation, including initiation and elongation factors and tRNA biosynthesis genes were similarly upregulated in the *uspG::tn* strain, albeit at a level below our 4-fold cutoff. As shown in **Figure 16**, each *rps* gene encoding a member of the 30S ribosomal subunit was upregulated in the *uspG::tn* strain. As aminoglycosides target this component of protein translation, it was of interest to see if susceptibility was altered in the *uspG::tn* mutant strain.

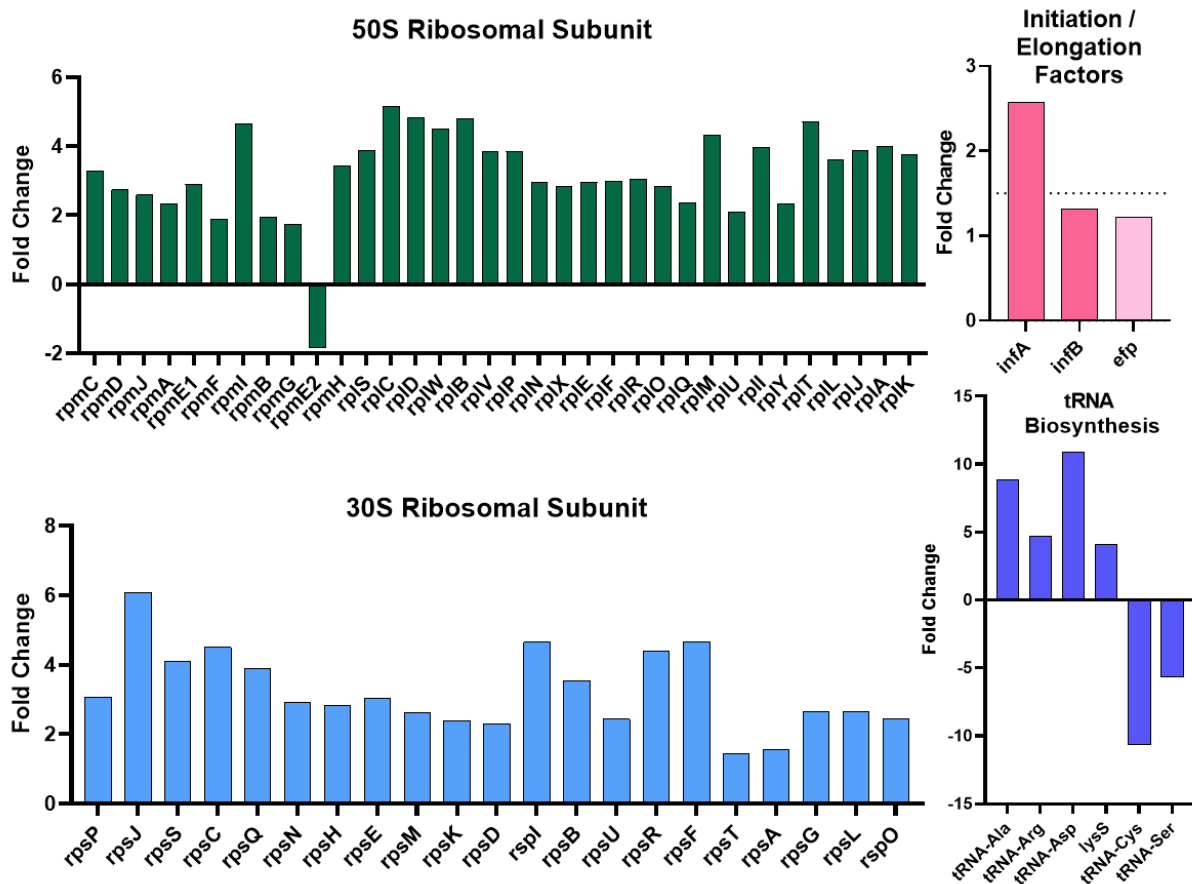


**Figure 16. Translational Machinery Shows Altered Transcription in the *uspG::tn* Strain.** Genes involved in translation are shown based on RNA-sequencing data following 3 hours of growth. Members of the 50S ribosomal subunit are outlined in green, of the 30S subunit are in blue. Initiation factors are in deep pink while the elongation factor is light pink. Amino-acyl tRNA synthesis genes are shown in purple. Fold change was calculated for + values using WT expression / *uspG::tn* expression. If fold change was found to be <1, values were inverted by taking 1 / fold change and then multiplying by -1 (negative fold change).

Further to this, there were significant changes in cofactor production, ubiquinones and other genes associated with electron transport, indicating a shift in energetics of the cell. For example, the NAD(P)<sup>+</sup> transhydrogenases *pntB*, *pntA*, and *pntAA* encoded by ABUW\_3312-ABUW\_3314 were downregulated by greater than -4-fold in the *uspG::tn* strain (**Table 5**). A shift was also evident by the downregulation of cytochrome bd ubiquinol oxidase subunits encoded by ABUW\_2389 and ABUW\_2390 (**Table 5**), and

converse upregulation of cytochrome bd ubiquinol oxidase subunits encoded by ABUW\_1792-ABUW\_1795 in the *uspG::tn* strain (**Table 6**). Further, ABUW\_2973 (*mqo*), a malate:quinone oxidoreductase was upregulated by 5.85-fold, while several other oxidoreductases and putative flavoproteins were downregulated in *uspG::tn*. Again, when considering aminoglycosides, their uptake is influenced by changes in membrane energetics. Specifically, lower levels of uptake are seen in cells with lower levels of ubiquinone present[259]. It is also known that in addition to the difference in membrane potential, the difference in transmembrane H<sup>+</sup> concentration ( $\Delta\text{pH}$ ) also influences the efficiency of aminoglycosides[260]. Further, streptomycin binding to the ribosome has been shown to be dependent on the expression of certain ribosomal proteins, such as RpsL. Several species with *rpsL* mutations, exhibit streptomycin resistance[261-263]. In *uspG::tn*, *rpsL* and many other *rps* genes are upregulated leading us to suggest that the mutant strain would instead be more susceptible to streptomycin.

Therefore, *uspG::tn* and AB5075 were subject to MIC testing against multiple protein synthesis inhibitors, including: aminoglycosides targeting the 30s ribosomal subunit and a macrolide targeting the 50S ribosomal subunit. As expected, *uspG::tn* was found to be more susceptible to the aminoglycosides neomycin, streptomycin, and gentamicin, with MICs 4-fold, 30-fold and greater than 50-fold lower in the *uspG::tn* mutant. Further, *uspG::tn* was 4-fold more susceptible to the atypical aminoglycoside Hygromycin B and 1.5-fold more sensitive to the 50s targeting macrolide Erythromycin (**Figure 17**). This confirms our RNAseq data and associated hypothesis that alterations in ribosomal protein

expression and membrane energetics in our *uspG::tn* mutant is likely causative of the phenotypic changes in response to antimicrobial agents observed herein.

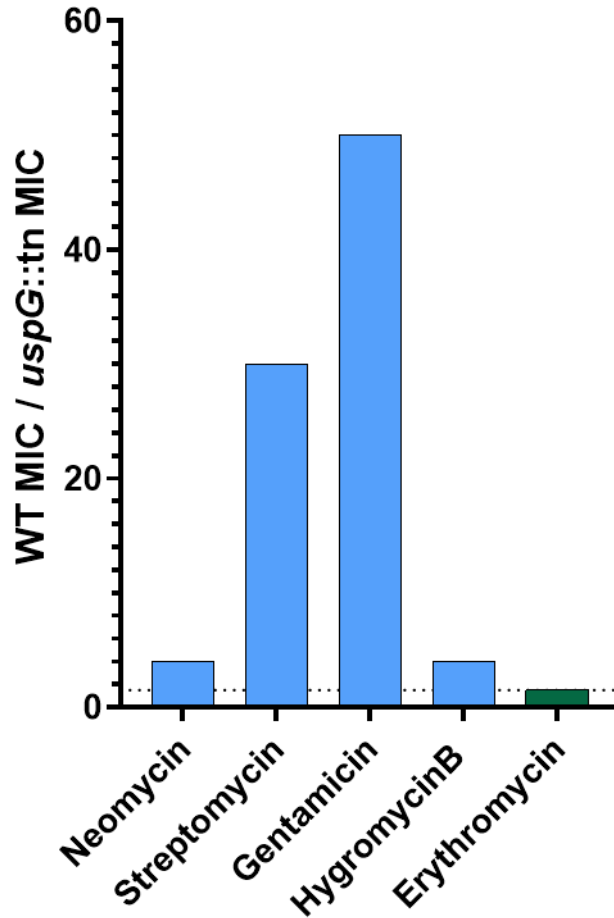


**Figure 17. Aminoglycoside Sensitivity Exhibited by *uspG::tn* Strain.** Fold differences in MIC are shown. Changes were generated comparing MIC of wildtype AB5075 and *uspG::tn* based on in liquid culture inhibition. Studies were performed in biological triplicate and repeated on at least two occasions to verify MIC values. Aminoglycosides: blue, Macrolide: green.

**Increased Susceptibility to Biocides and CCCP Indicates Significant Changes in *uspG::tn* Cell Envelope Structure.** In addition to the changes in membrane energetics, many other membrane-associated genes were differentially expressed in our mutant strain. Specifically, ABUW\_3106 (*lysM*), ABUW\_0921 (*glpQ*), ABUW\_0304 (*pilA1*) and

ABUW\_2730 (*arfA\_2*), which are known to be required for full envelope integrity[264-266], were down regulated in our mutant strain. Therefore, we assessed whether agents that target these processes revealed altered sensitivity in the mutant.

It is known that sodium dodecyl sulfate (SDS) functions as a biocide, targeting lipoproteins as well as other proteins within the membrane[267]. Triclosan acts as a biocide at higher concentrations leading to membrane destabilization[268]. Carbonyl cyanide *m*-chlorophenylhydrazine (CCCP) functions to deplete ATP pools and acts to depolarize the membranes[269]. Therefore, if the mutant does in fact possess an envelope with a disrupted or an altered cell envelope, we would predict that the mutant strain would be more susceptible to exposure to these agents. In order to test this, *uspG::tn* and AB5075 were subject to MIC testing in liquid media using various concentrations of triclosan and SDS. As expected, *uspG::tn* was more susceptible to each treatment. As shown in **Figure 18**, *uspG::tn* was found to have an MIC that was 15-fold lower than AB5075 when challenged with SDS. Further, *uspG::tn* was found to be 2-fold more susceptible to triclosan treatment. These results indeed confirm the prediction that the cell envelope is altered in the *uspG::tn* mutant. Finally, *uspG::tn* was found to be 2-fold more susceptible to CCCP treatment. Since the requirement for an intact proton motive force is necessary for the activity of aminoglycosides and we see increased susceptibility, it is likely that instead the increased susceptibility of *uspG::tn* to CCCP exposure is due to the already depleted ATP pools and not due to a disrupted ETC.

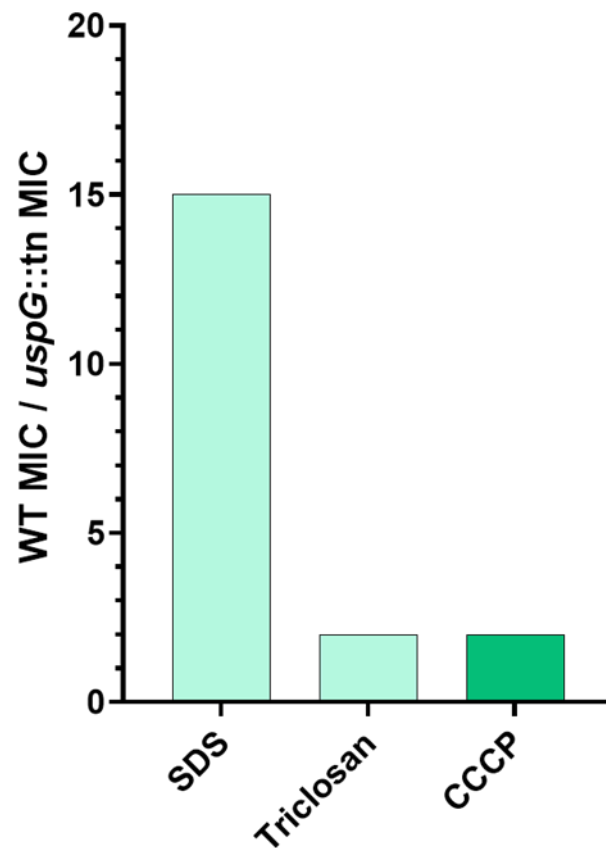


**Figure 18. Cell Envelope Altered in *uspG::tn* Strain Based on Sensitivity to Biocides and CCCP.** Fold differences in MIC are shown. Changes were generated comparing MIC of wildtype AB5075 and *uspG::tn* using liquid culture inhibition. Tests were performed in biological triplicate and repeated at least twice to verify MIC values.

### **Ethanol Susceptibility is Enhanced Due to Downregulation of Ethanol Metabolic**

**Enzymes.** It is known that ethanol exposure at low levels can induce the *uspG* homolog (A1S\_1950) in *A. baumannii* ATCC17978[270]. Within our present study, a large number of genes known to be induced following ethanol exposure were downregulated transcriptionally within our *uspG::tn* strain. For example, ABUW\_2132 encoding *lipA2*, a lipoyl synthase was induced 17-fold by ethanol exposure in ATCC17978, but was downregulated by -42.7-fold in the *uspG::tn* mutant. The same trend was seen for

ABUW\_1624 (*dhaT*), ABUW\_1621 (*ald1*), ABUW\_3582, ABUW\_0468, and ABUW\_0066 (*hppD*).

Based on this, we predicted that the *uspG::tn* mutant would be more susceptible to ethanol exposure as it is unable to transcribe the genes necessary to protect against ethanol toxicity. In order to test this, AB5075 WT and *uspG::tn* strains were tested in liquid culture containing different percentages of ethanol and an MIC was determined. As expected, *uspG::tn* cells were 1.25-fold more sensitive to ethanol treatment than AB5075 (**Figure 19**). The amount of ethanol needed to completely inhibit AB5075 growth was 5% while 4% was enough to inhibit *uspG::tn* cells. Although a subtle change, it is clear and reproducible, and thus represents a legitimate phenotype of *uspG* mutant strains.

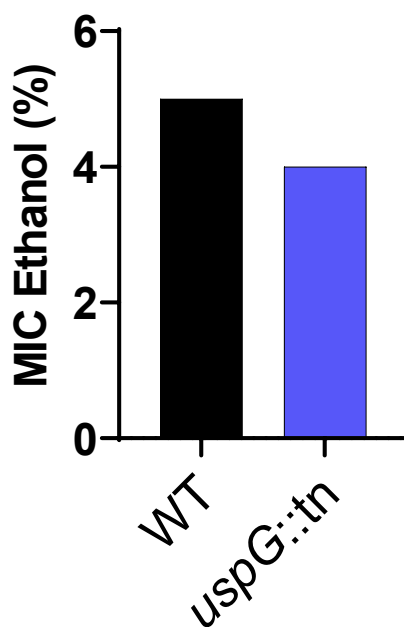


**Figure 19. Ethanol Sensitivity Exhibited by *uspG::tn* Strain.** MIC values are shown for each strain. Studies were performed in biological triplicate and repeated on at least two occasions to verify MIC values.

### **Motility is Hindered in *uspG::tn* Likely Due to Shifts in Pili Expression.**

Transcriptional indications were also present to suggest that motility is influenced by UspG. Specifically, ABUW\_3032 (*pilU*) encodes a type IV pilus ATPase that is associated with twitching motility and was downregulated -5.48-fold. Further, ABUW\_0304 encoding a putative type IV pilin structural subunit, *pilA*, showed -7.58-fold lower transcription in the mutant strain. Another pilus assembly system, the *csu* operon, was also downregulated but has been implicated instead in adhesion and biofilm formation. Since *pilA* and *pilU* are both involved in motility in *A. baumannii*[63], we would expect *uspG::tn* to have a defect in motility. In order to test this assertion, *uspG*<sup>-</sup> (M), *uspG*<sup>+</sup> (C) and wildtype 5075 (WT) were inoculated onto 0.5% LBA containing plasmid selecting antibiotics. Cells were synchronized to ensure the samples contained live cells and cellular debris was limited. Each strain was tested in biological triplicate by placing 10 $\mu$ L on the surface of LBA containing 0.5% agar. Care was taken to ensure spreading did not occur and all strains started at an equal diameter. Agar plates were then wrapped in parafilm and sealed with tape to preserve moisture before being incubated in the dark at 27°C and 37°C.

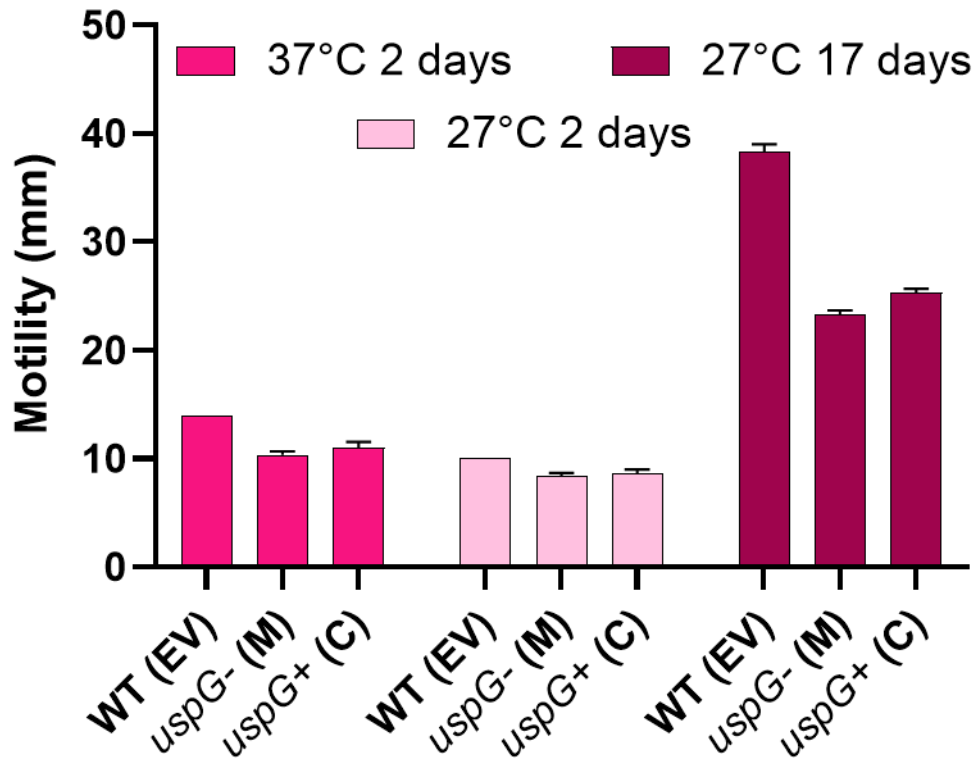


**Figure 20. Motility Defect Observed in *uspG*(M) Strain.** Diameter of cell spread was measured and recorded following 2 and 17 days of growth at the indicated temperatures. WT: AB5075 empty vector control, M: *uspG*<sup>-</sup>, C: *uspG*<sup>+</sup>. Error bars represent the mean  $\pm$  SEM of three biological replicates.

As predicted, following 2 days of growth, it was clear that *uspG*<sup>-</sup> (M) was less motile (Figure 20). This phenotype was observed at both temperatures and time points tested with partial complementation seen under all conditions. Following 17 days of growth, the motility defect was even clearer for *uspG*<sup>-</sup> (M). Each strain was able to grow more quickly at 37°C as compared to 27°C, however, the greatest difference was seen at 27°C following 17 days of growth. Due to evaporation, it was not possible to accurately quantify the diameter of samples grown at 37°C following 17 days of incubation and therefore it is unclear whether differences between *uspG*<sup>-</sup> (M) and AB5075 (WT) would be more

significant at that temperature. Overall, it is clear that UspG is involved in controlling factors associated with motility. This phenotype was also demonstrated by the *uspG::tn* mutant and the wildtype AB5075 strain and is shown in **Figure 21**. These plates were incubated at 27°C for 14 days under the same conditions as the plasmid containing strains (in the dark, wrapped in parafilm and taped to avoid evaporation). Two of the three biological replicates were chosen for visual representation for each strain although all three replicates showed consistent results. These results again indicate that there is a clear role for UspG in influencing motility within AB5075.

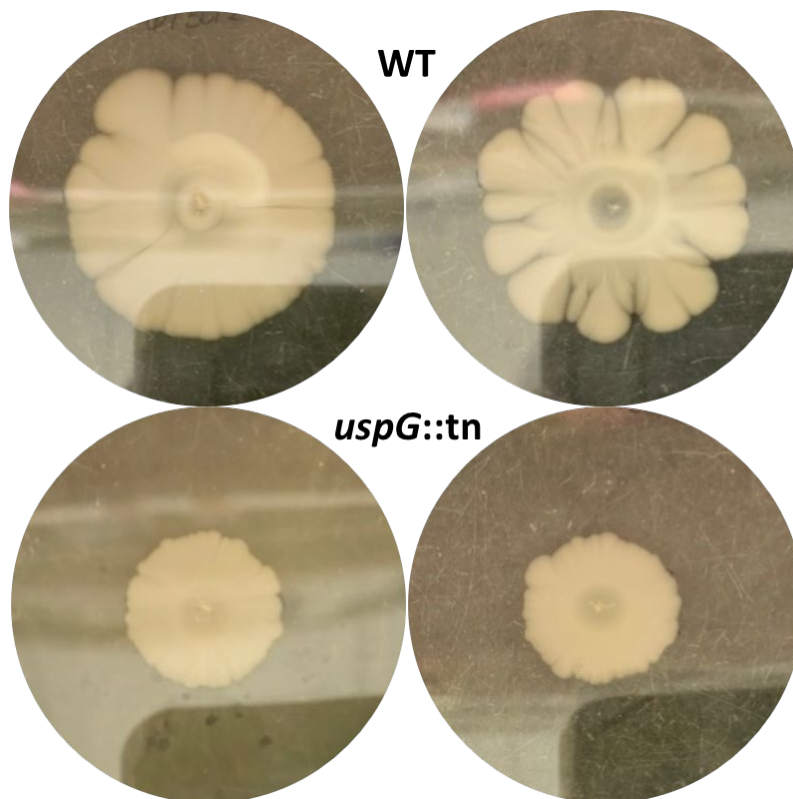


**Figure 21. *uspG::tn* Strain Demonstrates Deficiency in Motility Following 2 Weeks of Incubation at 27°C.** Representative images of strains tested in biological triplicate on 0.5% LBA. Strains standardized prior to inoculation. Top row: wildtype AB5075, bottom row: *uspG::tn*.

**Oxidative Stress Tolerance is Hindered in *uspG::tn*.** Based on the downregulation of various genes associated with oxidative stress and antioxidant defense, including catalase encoding genes, peroxidases and multiple heme-oxygenases (**Figure 22**), it was predicted that *uspG::tn* would be more susceptible to H<sub>2</sub>O<sub>2</sub> exposure. Therefore, an MIC approach was taken to determine the level of hydrogen peroxide that inhibits *uspG::tn* growth. As expected, *uspG::tn* was found to be more sensitive to H<sub>2</sub>O<sub>2</sub> exposure (**Figure 23**). Specifically, *uspG::tn* was four fold more susceptible when tested in MHBII media. This is in agreeance with a variety of other Usp mutants including the paralog, UspA, in *A. baumannii*[209].

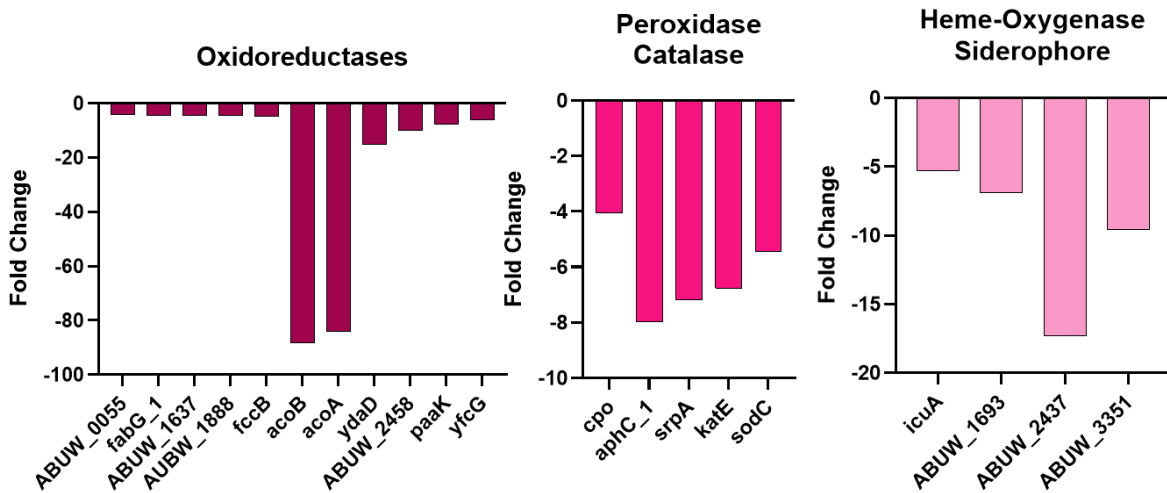


**Figure 22. Various Genes Involved in ROS Mediation are Downregulated in *uspG::tn* Strain.** Fold decrease in expression for *uspG::tn* vs AB5075. Data is equivalent to that listed in Table 5.

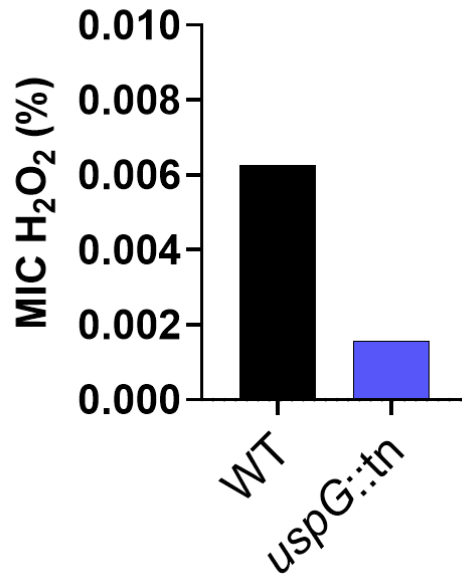


**Figure 23. *uspG::tn* Strain is More Sensitive to H<sub>2</sub>O<sub>2</sub> Exposure.** The MIC was determined for each strain in liquid culture. Tests were performed in biological triplicate and on separate days to confirm activity. The MIC for H<sub>2</sub>O<sub>2</sub> is represented as the percentage of within liquid culture.

**Inhibition of UspG Leads to the Inability to Resist DNA Damaging Agents.** The inability of *uspG::tn* cells to tolerate the same level of oxidative stress as the wildtype strain indicates that a cells are potentially undergoing some level of ROS stress already. In terms of toxicity, oxidative stress is known to cause DNA damage which can have lethal effects; thus, it is reasonable to assume that the *uspG* mutant strain may be more sensitive to challenge by DNA damaging agents. In order to test this, *uspG::tn* and AB5075 were subject to: ethidium bromide, mitomycin C, acridine orange and methyl methanesulfonate (MMS) exposure. As expected, *uspG::tn* was more sensitive to all chemical agents tested (**Figure 24**). This is in line with data from mutants of other Usp proteins[231] and indicates that UspG of *A. baumannii* functions to protect itself from DNA damage.

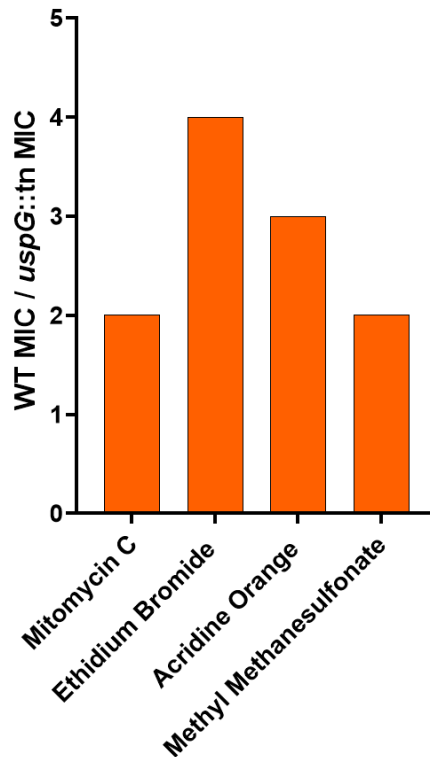


**Figure 24. *uspG::tn* Strain is More Sensitive to DNA Damaging Agents.** MICs were determined in liquid culture for AB5075 and *uspG::tn* strains. Fold change in MIC of each strain is represented. Strains were tested in biological triplicate and on at least two separate days to confirm activity.

**UspG Plays an Essential Role During Survival within Whole Human Blood.** Given the myriad sensitivities displayed by the *uspG* mutant, many of which mimic challenges faced during disease causation, we surmised that the mutant would be less virulent within the host. Additionally, downregulation of the *paa* pathway (**Table 5**) in the mutant indicates the *uspG::tn* population has an accumulation of phenylacetate, which is a chemoattractant for neutrophils and assists in the clearance of bacteria[271]. Therefore, we predicted that survival within whole human blood, containing leukocytes such as neutrophils, would be compromised in the *uspG::tn* mutant. Upon testing, and as expected, *uspG*<sup>-</sup> (M) is displayed a survival defect in human blood (**Figure 25**). Quite

strikingly, exposure to blood appeared to result in a complete loss of viability for the mutant strain within only 30 minutes. To explore this more fully, we examined how quickly such a loss of viability was observed. Accordingly, each strain was diluted in PBS to an equivalent OD<sub>600</sub> and added to blood, with samples immediately removed and plated. As shown in **Figure 25B**, this short amount of time reduced the bacterial load within the *uspG*<sup>-</sup> (M) significantly, although some viability was detectable. This indicates that UspG is indisputably essential for survival within the human host. This is similar to UspA of *A. baumannii* ATCC17978, which was shown to be essential for survival within two different forms of mouse infection[209].

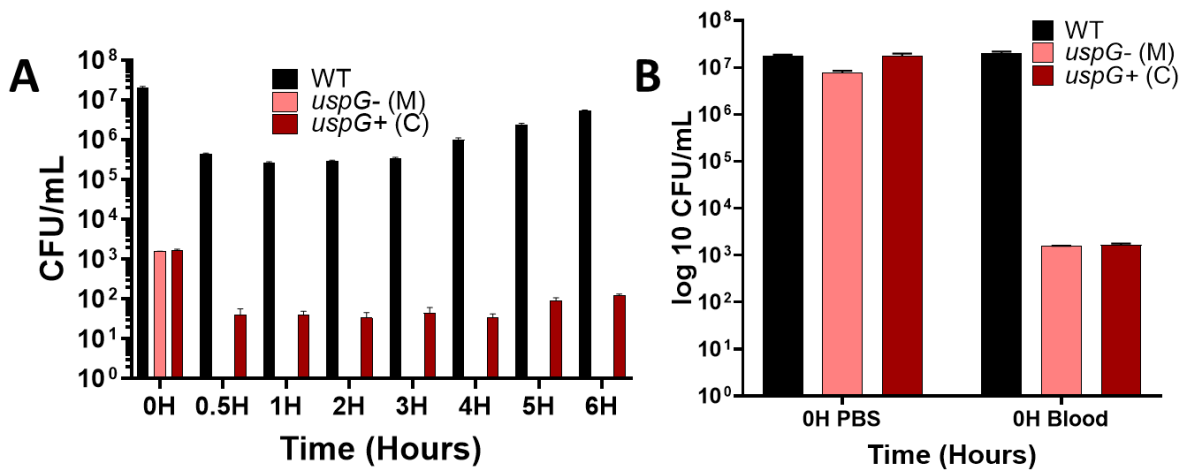


**Figure 25. UspG Plays Critical Role in Human Blood Survival.** Each strain was grown in biological triplicate to exponential phase then normalized to a starting OD<sub>600</sub> of 0.05. CFU/mL was calculated based on plate counts. (A) Log<sub>10</sub> CFU/mL of each strain overtime in blood. (B) Log<sub>10</sub> CFU/mL of initial samples in PBS or blood. Time from inoculation to serial diluting and plating was less than 10 minutes. Error bars represent mean ± SEM of three biological replicates.

## Discussion

Herein we present an analysis of a Universal stress protein produced by *A. baumannii*. Universal stress proteins are produced by a variety of life forms and play a global role in the adaptation of organisms to stress via mechanisms that remain elusive. In *A. baumannii* AB5075 six such proteins exist that have yet to be fully characterized. Prior to our analysis the only studied Usp of *A. baumannii* was A1S\_2692 (ATCC 17978), the homolog of ABUW\_0890. This protein has been annotated as UspA, therefore, to avoid confusion and based on sequence predictions, ABUW\_1763 herein is referred to as UspG.

UspG proteins are class II Usp proteins in *E. coli* and are known to bind ATP. The major functions of UspG in *E. coli* are the ability to protect against DNA damage, to influence motility, and to increase in abundance during starvation. All Usps of *E. coli* are induced during stationary phase when nutrients become limited. Herein, we find that UspG of *A. baumannii* acts in a way that is consistent with other universal stress proteins but also has unique tendencies. For example, we see the accumulation of UspG during exponential growth (**Figure 14**). We also show that *uspG::tn* demonstrates a growth defect in nutrient rich media, a phenotype that is also observed in the absence of *uspA* in *A. baumannii* but is uncommon in other bacterial species. Therefore, it is likely that Usps in *A. baumannii* demonstrate a functional role during exponential phase as well as during stationary growth. This was further highlighted by the significant differences in transcription observed comparing *uspG::tn* and AB5075 strains in early exponential growth. Specifically, following 3 hours of growth over 300 genes were differentially

expressed to a degree greater than 4-fold, indicating that the absence of UspG is detrimental to the population and that *A. baumannii* depends on UspG to function normally during exponential growth.

The *uspG::tn* mutant was also found to be more susceptible to acids (data not shown), alcohol, antibiotics and H<sub>2</sub>O<sub>2</sub> stress, each of which are known stressors Usps generally help protect bacteria from [209, 217, 220, 257, 272, 273]. In addition to the H<sub>2</sub>O<sub>2</sub> phenotype, we also note an inability of the mutant to survive within whole human blood, which could be due to a variety of factors. First, we detect alterations in the electron transport chain (ETC) as well as the proton motive force machinery which generate ROS naturally during electron transfer between quinones, cytochrome complexes, and other ETC machinery. This was demonstrated by the differential expression of cytochrome bd oxidases as well as the downregulation of a variety of genes encoding flavoproteins and NADH/NADPH proton translocating proteins and the upregulation of malate:quinone oxidoreductase. We tentatively suggest that the membrane energetics are altered, but not disrupted, in the *uspG::tn* strain due to the increased sensitivity towards aminoglycosides, which are dependent on a functional ETC and an intact membrane [260, 274, 275]. Further, we predict that UspG is involved in controlling antioxidant production, and, without *uspG*, the production of essential oxidative stress protection proteins is not possible. This would then result in the accumulation of ROS and H<sub>2</sub>O<sub>2</sub> within the cell and would lead to damage to a variety of molecules including DNA, proteins, and lipids. It would also, consequently, explain the defects observed in whole human blood survival.

There are several lines of evidence that support our hypothesis that ROS is accumulating within the *uspG::tn* mutant. First, UspA of *E.coli* is overexpressed in a manner that is directly correlated to the amount of ROS produced within the cell. Specifically, as ROS levels increase within the cell, so does the transcription of *upsA*[276]. It is likely that our cells are in fact producing higher levels of ROS or that ROS is accumulating based on the downregulation of genes associated with detoxifying them, such as *katE*, *sodC*, a variety of peroxidases, and multiple heme oxygenases but also by the 7.24-fold upregulation of *uspG* observed. The upregulation of *uspG* within the *uspG::tn* mutant does not translate into UspG due to the transposon insertion, but instead indicates that the cell is trying to compensate for its absence by attempting to make more albeit unsuccessfully. The increased sensitivity to H<sub>2</sub>O<sub>2</sub> exposure is also in agreement with this notion: ROS is accumulating in the absence of functional UspG. Further, it has been shown in other species such as *Salmonella typhimurium* LT2 that UspA plays a role in protection against H<sub>2</sub>O<sub>2</sub> stress that is more prevalent during exponential growth[224]. Based on our observation that UspG expression is seen during this time (**Figure 14, Table 6**), and antioxidant defense genes are downregulated in *uspG::tn* (**Table 5**), it is tempting to speculate that UspG too functions to protect against ROS production during this phase of growth.

The control of antioxidants has also been shown for other Usps, Specifically the overexpression of MfUSP1 of the plant species *Medicago falcata* leads to the upregulation of antioxidant defense proteins such as catalase and superoxide dismutase[277], the opposite of which is observed for *A. baumannii* in the absence of

UspG. Further, proline accumulation was observed upon upregulation of MfUSP1 due to the downregulation of proline oxidases[277], whereas the most highly upregulated transcript in *uspG::tn* compared to AB5075 was *putA* (>30-fold), which encodes a proline oxidase. Therefore, in *A. baumannii*, the regulation of antioxidant production as well as the regulation of amino acid synthesis and degradation is influenced by UspG.

Another explanation for the presumed accumulation of ROS and proven sensitivity of our *uspG::tn* mutant to H<sub>2</sub>O<sub>2</sub> exposure is based on a likely dysregulation in metal homeostasis. In *E. coli*, sensitivity to H<sub>2</sub>O<sub>2</sub> has been attributed to increased iron uptake within the mutant cells, due to unregulated uptake of siderophores. Iron exacerbates the toxic effects of ROS via hydroxyl radical production in the presence of oxygen[278]. Thus, iron dysregulation can be directly linked to an increase in ROS and therefore the system may be overwhelmed in the presence of blood or H<sub>2</sub>O<sub>2</sub> where more ROS occurs if intracellular levels of iron are present. However, in our mutant, siderophore biosynthesis is downregulated, *icuA* and *icuD* (aerobactin synthesis), by greater than 4-fold. We also see a downregulation in transcription of a multitude of heme oxygenases that are involved in the release of iron from heme[279] in *uspG::tn*, indicating that iron may not be accumulating within the cells nor primarily responsible for death following exposure to blood. Conversely, the downregulation of heme oxygenases strengthens our hypothesis that ROS is accumulated within the *uspG::tn* strain since heme oxygenases are known for their ability to function as antioxidants[279].

Based on our data, instead of iron accumulation leading to ROS and downstream damage through iron transporters, a more likely explanation is the accumulation of copper that can induce ROS production, iron displacement and ultimately DNA and protein damage. Similar to iron, copper can also induce ROS production in the presence of oxygen via a reaction that is similar to Fenton-chemistry[66, 280]. Copper is an essential metal that is necessary for the functionality of a variety of enzymes including cytochromes and superoxide dismutase[281]. However, if levels become too high, copper can become highly toxic. Even in the absence of H<sub>2</sub>O<sub>2</sub> copper can displace iron from Fe-S centers and inhibit the enzymes, many of which are responsible for maintaining the ETC[282]. Further, it is known that copper resistance proteins can function to protect against H<sub>2</sub>O<sub>2</sub> stress via the expulsion of excess Cu I<sup>+</sup> and Cu II<sup>+</sup>. This is important since Cu II<sup>+</sup> reacting with H<sub>2</sub>O<sub>2</sub> can also form Cu III<sup>+</sup> which is a strong oxidant yielding damaged macromolecules such as proteins, lipids and DNA[283]. An example of copper resistance protecting against H<sub>2</sub>O<sub>2</sub> exposure was shown specifically in *Lactobacillus plantarum*, where *copB* mutants were much more susceptible to H<sub>2</sub>O<sub>2</sub> exposure[284]. In *A. baumannii*, both CopA and CopB function to expel copper to ensure the levels are not toxic[66]. In line with the notion that copper homeostasis is compromised in the *uspG::tn* strain, is a downregulation of a variety of copper resistance genes such as *copA*, *copB*, *actP1*, and *nlpE* observed within the *uspG::tn* mutant strain. Further to this, following exposure to copper, *Acinetobacter sp.* have been shown to accumulate both CopA and CopB proteins in addition to a variety of 30S and 50S ribosomal proteins[285]. In *uspG::tn* we see an upregulation of ribosomal proteins and a downregulation of *copA* and *copB*, which makes it tempting to speculate that *copA* and *copB* are indeed under the control of UspG.

Further, in their absence, an accumulation of copper would lead to oxidative stress associated protein damage that would signal the cell to induce translational machinery production in order to overcome the protein damaged caused by copper toxicity. This response would then be exacerbated by the exposure of *uspG::tn* to H<sub>2</sub>O<sub>2</sub> and blood, leading to the increase in sensitivity that is observed. The same deductive reasoning could be extended to the increased sensitivity observed for *uspG::tn* to DNA damaging agents. If copper accumulation and increased levels of ROS has resulted in the oxidation of macromolecules including DNA, exposure to external DNA damaging agents would worsen this response. Within our transcriptional analysis, DNA damage response genes were not differentially expressed to a degree greater than 4-fold. Therefore, DNA damage is likely the result of the presence of excess ROS and further experimentation will be necessary to determine whether UspG plays a direct role in protection against DNA damage.

One of the most substantial conclusions of this work is the essentiality of UspG for survival within the host demonstrated by the rapid killing of *uspG::tn* within 10 minutes of exposure to whole human blood (**Figure 25**). The reasoning behind this phenomenon can be attributed to multiple aspects of whole human blood. For example, blood contains a variety of membrane targeting factors such as the membrane attack complex (MAC) that leads to the lysis of Gram-negative organisms through pore formation[286]. It is highly likely that the cell envelope of our mutant is altered in a way that is weakened. This was demonstrated by the increased susceptibility to protonophores and membrane disrupting agents along with differential expression of genes associated with lipid metabolism,

peptidoglycan synthesis and cell envelope homeostasis. Specifically, surface antigens, lipoproteins, and other lipid biosynthesis genes are downregulated. Some examples include lipoproteins such as ABUW\_2730 (-10.99-fold), encoding an OmpA family lipoprotein, and the putative lipoprotein encoded by ABUW\_3874 (-7.00-fold). In addition, downregulation of lysophospholipases (ABUW\_1332, -5.44-fold and ABUW\_1210, -5.97-fold) charged with maintaining and controlling lipid content within the bacterial membrane was observed. This indicates that the system for maintaining membrane permeability could be altered. Therefore, the MAC complex could be more efficient at targeting and disassembling the membranes of the *uspG::tn* mutant. Further, in *A. baumannii* there is evidence that poly-N-acetyl- $\beta$ -(1,6)-glucosamine (PNAG) produced by the *pga* locus is a target of the MAC complex[287] and *pgaA* is upregulated within the *uspG::tn* mutant. Further, there is evidence that the *uspG::tn* mutant is more likely to be phagocytosed quickly due to the downregulation of the *paa* operon in our mutant strain, a phenotype which leads to the accumulation of the chemoattractant phenylacetate[271]. Therefore, the inability of *uspG::tn* to survive within whole human blood is compounded by the increased expression of MAC targets, a weakened cell envelope, a dysregulation of metal homeostasis that leads to increased ROS damage, and the overproduction of neutrophil chemoattractants leading to rapid killing.

Although there are similarities between UspG of *E. coli* and UspG of AB5057, there are distinct differences, for example, UspG mutant strains are more susceptible to osmotic stress whereas *uspG::tn* of AB5075 was able to resist exposure to 1M NaCl with effects indistinguishable to wildtype AB5075 (data not shown). In addition, a variety of ribosomal

proteins are shown to be downregulated transcriptionally following osmotic pressure in *E. coli* while our *uspG::tn* strain demonstrates an upregulation in the same genes(**Figure 16**)[288]. The same inverse relationship in transcription is observed for *copA*, however with increased expression in *E. coli* following osmotic stress and a downregulation in our *uspG::tn* strain[288]. Therefore, it is unlikely that UspG in *A. baumannii* plays a role in the protection against salt stress. This is in line with the similar lack of differential growth observed for  $\Delta$ *uspA* in *A. baumannii* ATCC17978 following exposure to 500mM of NaCl[209]. In addition, UspG of *E. coli* does not play a role in protection against exposure to H<sub>2</sub>O<sub>2</sub> nor mitomycin C treatment[234], which are indisputably stressors that influence *uspG::tn* survival (**Figures 23 and 24**).

Within the *uspG::tn* strain there were a variety of metabolic changes transcriptionally that implicate UspG in the regulation of carbon flux. This is partially observed with the increased susceptibility observed for *uspG::tn* to ethanol. In another *A. baumannii* strain, ethanol exposure led to the expression of a variety of genes that were downregulated within our *uspG::tn* mutant, while others induced or downregulated upon ethanol exposure were similarly expressed within our mutant[270]. Therefore, it is unlikely that all genes are regulated by UspG, but it is likely that some are. For example, ABUW\_1624, *dhaT* is responsible for the conversion of ethanol to acetaldehyde and was downregulated by -10.71-fold in the *uspG::tn* mutant. Without this gene it is likely that the population is unable to convert ethanol to acetaldehyde and other downstream cellular metabolites. We predict that *dhaT* and *ald1* are under the influence of UspG due to severe transcriptional depression of genes downstream of *dhaT*. Namely, *ald1* is responsible for

converting the acetaldehyde produced by *dhaT* into acetate and is downregulated by -21.75-fold in the *uspG::tn* mutant. Further, ABUW\_3781 encodes *acs*, which acts to then convert the acetate into acetyl-CoA and is downregulated -205.98-fold in the *uspG::tn* mutant. ABUW\_3781 represents only one of three genes with the same function, converting acetate into acetyl-CoA, to be downregulated in the absence of UspG. The role in central carbon metabolism is also observed for other Usp proteins in organisms such as *E. coli*[257], yet the mechanism of regulation is unclear.

Collectively, we have uncovered a global regulator within *A. baumannii* that has a profound impact on the physiology and lifestyle of the organism. Future experimental inquiries will be targeted to defining UspG ligands, interaction partners, and induction patterns. We seek to continue to bring clarity to the complexity of the universal stress response protein network that has remained elusive for almost 30 years[217].

## **Chapter 4: The Discovery of Plant Derived Antimicrobial Peptides Using the “PepSAVI-MS” Pipeline**

### **Introduction**

Plants have been used for centuries for their medicinal properties. Indeed, it is estimated that four billion people around the world still rely on botanical herbs as a primary source of medicine, making them an integral part of community structure[289]. There is, however, very little research that defines the medicinal components of plant-derived remedies, or how they contribute to the treatment of illness. This can be dangerous as many plants contain toxic components that can lead to adverse effects; thus without chemical analysis and standard dosing regimens, those taking such treatments are at risk[290]. With a lack of research in this area and a history of potential as therapeutics, plant products pose as an untapped resource for antimicrobial drug discovery. An underexplored area of study in this regard is the capacity of plants to produce a vast array of antimicrobial peptides (AMPs).

AMPs are small, amphipathic or cationic structures that are produced by almost all forms of life[291]. This includes plants, animals, humans, fungi and bacteria. They function as a form of protection for organisms against invading species and can be either stimulated for production or expressed constitutively[292]. Each organism has a unique set of AMPs

that are unlike that of any other organisms, however, the range of amino acids that make up the peptides and mechanism of action (MOA) is relatively conserved. In general AMPs are known to exhibit broad spectrum antimicrobial activities against bacteria, fungi and viruses[293]. Their amphipathic and cationic nature allows them to integrate into the membrane of target organisms through various methods, including open channel pore formation in a barrel or toroidal conformation, or forming a layer that is dense enough to dissolve the membrane[291, 294]. This is what elicits broad-spectrum activity, as the cationic portions of the peptide are attracted to negatively charged membrane proteins, lipids, and carbohydrates. After a threshold of accumulation is reached due to this attraction, the amphipathic nature of the AMPs allows for a pore to be formed through interaction with membrane lipids[295]. This leads to leaking of internal contents of cells, releasing ions and metabolites that ultimately leads to cell death.

In terms of using AMPs as therapeutics, there are advantages that highlight their potential as antibacterial treatments. Such advantages include their general bactericidal activity with rapid killing, broad-spectrum activity, and anti-inflammatory effects[296, 297]. Towards this latter point, they are able to stimulate the immune system to recruit pathogen clearing immune cells while suppressing tissue damaging inflammation within the host[297]. It is also known that bacteria do not rapidly develop resistance to AMPs, which can likely be explained by their MOA[298]. For example, a common mechanism of resistance to antibacterial agents is the modification of a drug target within the cell. In the case of AMPs, which target cell membranes, alterations to charge and general physicochemical properties of this structure cannot easily be brought about to resist the

attraction of an amphipathic natured AMP. Further, there is mounting evidence that AMPs function to influence cellular processes in addition to pore formation, providing another layer of activity that would need to be overcome by the pathogen[297].

The potential for AMPs as antibacterial agents was considered as early as 1939 with the use of Gramicidin (extracted from a soil bacterium) to treat pneumococcal infections[84]. It was not long after, in 1942, that Purothionin, the first AMP from plants, was discovered to have antimicrobial activity against fungi and bacteria[299]. Since then, numerous AMPs demonstrating antibacterial activity have been extracted from a variety of different plants and plant tissue types[297, 300]. With over 300,000 plant species identified[301], they remain an untapped resource for the discovery of novel AMPs.

There are currently eight classes of plant AMPs, which include: cyclotides, knottins, thionins, snakins, defensins, hevein-like, lipid transfer peptides, and alpha-hairpinins[302]. Commonalities between these peptides are their amphipathic nature, overall positive charge and cysteine-rich modifications to form disulfides, and cyclization to increase stability[303]. All of peptides within these classes have one overarching role, to serve as a part of the innate immune defense for the plant[304, 305]. Some of these classes, such as the cyclotides and lipid transfer peptides, are part of a larger group of peptides called **R**ibosomally-synthesized, **P**ost-translationally modified **P**eptide natural products (RiPPs).

RiPPs are also produced across all three domains of life, and are desirable drug candidates that differ from standard AMPs due to their target specificity[306]. The post-translational modifications of RiPPs lead to conformational restriction of the AMP, which aids in narrowing the target for attachment and integration while also enhancing stability from degradation by chemical or metabolic means[306]. In humans, this reduces the chance of RiPPs inducing off-target effects while increasing the likelihood of the RiPPs reaching the target organism without being degraded. There is also evidence that RiPPs have alternate MOAs, outside of non-specific membrane penetration and content leakage, such as influencing metabolic and structural processes within target cells[303]. Examples of this are seen for Nisin and Bottromycin RiPPs, with the former, a RiPP lanthipeptide, targeting peptidoglycan synthesis by inhibiting lipid II biosynthesis during cell wall formation[307]. Bottromycins differentially target the bacterial 50S ribosome and function to inhibit aminoacyl-tRNA entry into the A site of the ribosome during translation[308].

Herein, we present work using a pipeline for the study of plant AMPs (PepSAVI-MS: statistically-guided bioactive *peptides* prioritized via mass spectrometry) that was developed by our collaborators, the Hicks laboratory at UNC-Chapel Hill. The method was developed to isolate and identify bioactive products from complex natural product sources such as medicinal plant extracts (**Figure 26**). Instead of using the typical approach to natural product discovery through bioassay guided fractionation, PepSAVI-MS provides a more efficient approach that implements a single round of crude extract fractionation before bioassay analysis followed by mass spectrometric and statistical

analysis. This allows one to streamline the process of AMP discovery and identify only active peptides without the bias of size or abundance. Consequently, time and resources are saved by omitting a major screening step and eliminating the possibility for activity loss due to fractionation. Following years of deployment, this process has been further adapted to rapidly evaluate plant species by combining promising fractions into single samples for bioactivity inhibitory screening. Therefore, bioactive plant species are prioritized for further investigation.

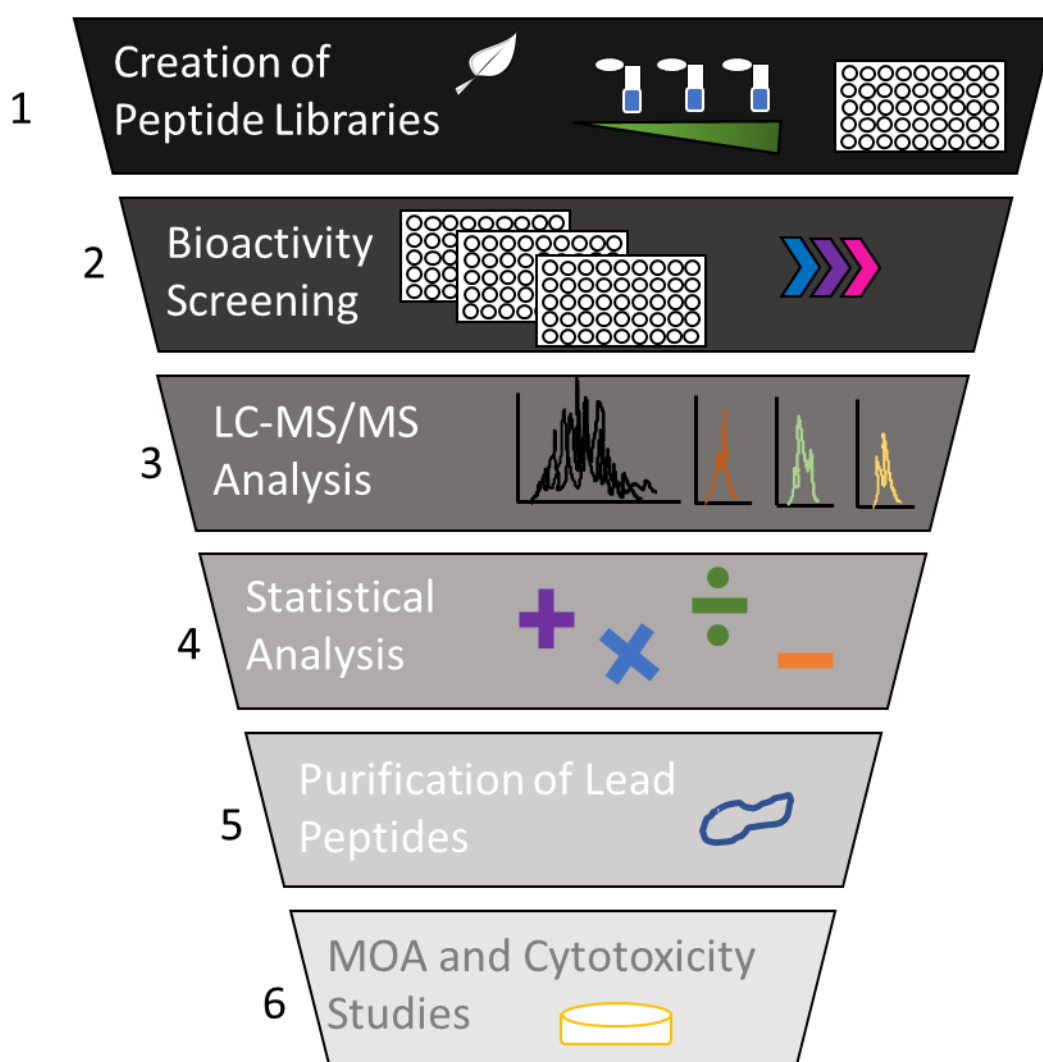


**Figure 26. Workflow for PepSAVI-MS Pipeline and Project Goals.** 1) Creation of peptide libraries through extraction and SCX fractionation of crude samples. 2) Bioactivity screening against ESKAPE pathogens. 3) LC-MS/MS analysis of active peptide libraries.

4) Statistical modeling of MS vs bioactivity regions to identify leads. 5) Purification or synthesis of lead peptides. 6) Determination of mechanism of action and cytotoxicity profiles for lead peptides. Figure adapted from Kirkpatrick et. al. 2017.

The initial deployment of this process was to screen *Viola odorata* (sweet violet, VO) due to the known abundance of cyclotides produced by this species, and previously defined medicinal properties[309-311]. In order to identify peptides of clinical relevance, we employed bioactivity screens of VO against the ESKAPE pathogens (E: *Enterococcus faecium*, S: *Staphylococcus aureus*, K: *Klebsiella pneumoniae*, A: *Acinetobacter baumannii*, P: *Pseudomonas aeruginosa*, E: *Enterobacter cloacae*). Initial exploration showed promising inhibitory activity, uncovering the known RiPP cycloviolacin O2, which had novel activity against *E. coli* and *A. baumannii*, thus validating the PepSAVI-MS approach[95].

Given that the PepSAVI-MS pipeline appears to be highly effective at identifying novel AMPs, we expanded our screen to a panel of additional plant varieties, focusing on the bioactivity of RiPPs. Herein we report the screening of *Linum spp.*, *Solanum spp.*, *Silybum spp.*, *Amaranthus tricolor* (red spinach ATr), and *Capsicum spp.*, among others. The goal of this endeavor is to discover potential therapeutics and generate a greater understanding of herbal medicine overall, with the examples presented herein demonstrating clear and ongoing success in this regard.

## Materials and Methods

**Plant Species.** All plants tested are presented in **Table 7** and were grown as detailed in Kirkpatrick, et. al. 2017[95]. Fractions for antibacterial testing were generated by the Hicks

laboratory as detailed in [95] and shipped to the University of South Florida for testing, as detailed herein.

**Table 7. Plant Genre for Peptide Library Creation and Testing.**

Genus	Strains Tested*	Full	Single
<i>Amaranthus</i>	ESKAPEE		
<i>Anchusa</i>	SA		
<i>Calendula</i>	ESKAPE		
<i>Chelidonium</i>	ESKAPE		
<i>Chichorium</i>	ESKAPE		
<i>Datura</i>	ESKAPE		
<i>Digitalis</i>	ESKAPE		
<i>Dodonaea</i>	ESKAPE		
<i>Echinacea</i>	ESKAPE		
<i>Grindelia</i>	EKA		
<i>Houttuynia</i>	EKA		
<i>Hyoscyamus</i>	ESKAE		
<i>Hyperium</i>	EKA		
<i>Linum</i>	ESKAPE		
<i>Mentha</i>	ESKAPE		
<i>Nasturtium</i>	ESKAPE		
<i>Origanum</i>	EKA		
<i>Salvia</i>	ESKAPE		
<i>Silybum</i>	KA		
<i>Solanum</i>	ESKA		
<i>Trifolium</i>	ESKAPE		
<i>Urtica</i>	ESKAPE		
<i>Viola</i>	ESKAPE		
<i>Withania</i>	ESKA		
<i>Zingiber</i>	ESKAPE		

Strains tested are bacterial species challenged against each botanical fraction set. The acronyms represent the following species in order: E: *Enterococcus faecium*, S: *Staphylococcus aureus*, K: *Klebsiella pneumoniae*, A: *Acinetobacter baumannii*, P: *Pseudomonas aeruginosa*, E: *Enterobacter cloacae* E: *Escherichia coli*. Samples tested against *E. coli* were tested against all 4 strains listed in table 8. Green: full fraction library tested, Light Green: peptide single or pooled library sample tested

**Bacterial Strains and Growth Conditions.** All ESKAPE pathogen and *E. coli* strains are drug resistant clinical isolates detailed in **Table 8**. Bacterial stocks were maintained at -80°C in tryptic soy broth (TSB) and 25% glycerol. Each isolate was struck onto tryptic soy agar (TSA) and grown for 18 hours prior to storage at 4°C for working stocks. Plates were

stored for no longer than 7 days at 4°C. Prior to each assay, a single colony was selected for each species and resuspended in 5mL TSB, followed by incubation at 37°C overnight. For screening, 1mL of overnight cultures were inoculated into 100mL TSB and grown for 3 hours with shaking at 37°C. These were then used in the assays detailed below.

**Table 8. Bacterial Strains Used in This Study.**

Organism	Strain #	Final OD 600nm*	Antibiotic**	Source
<i>Enterococcus faecium</i>	1450	0.1	50µg/mL Tet	[312]
<i>Staphylococcus aureus</i>	635	0.1	50µg/mL Gent	[312]
<i>Klebsiella pneumoniae</i>	1433	0.035	50µg/mL Gent	[312]
<i>Acinetobacter baumannii</i>	5075 or 1403	0.0325	50µg/mL Tet	[143, 312]
<i>Pseudomonas aeruginosa</i>	1423	0.03	50µg/mL Tet	[312]
<i>Enterobacter cloacae</i>	1454	0.03	50µg/mL Gent	[312]
<i>Escherichia coli</i>	MCC62	0.1	50µg/mL Tet	This study
<i>Escherichia coli</i>	MCC67	0.1	50µg/mL Tet	This study
<i>Escherichia coli</i>	MCC70	0.1	50µg/mL Tet	This study
<i>Escherichia coli</i>	TW14359	0.1	50µg/mL Tet	[313]

Antibiotic: Tet: Tetracycline, Gent: Gentamicin. \*Final OD<sub>600</sub> standardized based on OD<sub>600</sub> measurement and is equivalent to 5x10<sup>7</sup> CFU/mL which was diluted 1:5 for a starting inoculation of 1x10<sup>7</sup> CFU/mL per organism per well. TGH: Tampa General Hospital, Tampa, FL. MCC: Moffit Cancer Center, Tampa, FL. \*\*Commercial antibiotic included within each assay to represent 100% inhibition of each organism.

**Antimicrobial Activity Screening using Resazurin.** All assays were performed in standard 96-well polystyrene plates (Thermo Fisher Scientific). A 1:5 ratio of plant fraction to media was achieved by supplementing the reaction with 2x media in equal volume to the water-based fraction. Gram-positive organisms (ES) were cultured in TSB, while the Gram-negative organisms (KAPE) were cultured using MHBI for bioactivity screening with peptide. The addition of 2x media was used to ensure sufficient nutrients since the fractions themselves account for 1/5 of the final volume. TSB was used for the analysis of *E. faecium* and *S. aureus* due to their minimal growth in MHBI. Each well contained 20µL 2x media, 40µL 1x media, 20µL peptide fraction, and 20µL 5x concentrated bacteria (5x10<sup>7</sup> equivalent OD at 600nm (OD<sub>600</sub>)) for a final starting CFU/mL of 1x10<sup>7</sup>. Controls included commercial antibiotics and media only wells in each assay. Tetracycline at

50µg/mL was used as the control for *E. faecium*, *A. baumannii*, and *P. aeruginosa*, while Gentamicin at 50µg/mL was used against *S. aureus*, *K. pneumoniae*, and *E. cloacae*. Standardized cultures were incubated with plant fractions for 1.5 hours with shaking at 37°C, with the exception of *P. aeruginosa*, which was incubated for 3 hours due to slower growth compared to the other organisms. The final turbidity was then recorded at an OD<sub>600</sub> before 10µL Resazurin was added to each well at a final concentration of 1.19mM (30µg/mL). Plates were incubated in the dark under static conditions at 37°C for 30 minutes prior to recording fluorescent measurements. Results were recorded using an excitation frequency of 544nm and emission of 590nm. Plates were then measured consecutively in 15-minute increments until the maximum intensity was reached in untreated (no-treatment) wells. Percent inhibition was calculated after background fluorescence was removed using the following formula:  $(1 - (\text{sample intensity} / \text{average control max intensity})) \times 100$ . Each sample was tested in technical triplicate with at least two biological replicates.

**Antimicrobial Activity Screening using Optical Density.** Bacterial cultures were synchronized by inoculating 50µL of overnight culture into 5mL of TSB and incubating at 37°C for 3 hours. All assays were performed in 96-well flat bottom polypropylene plates (Plate One). Like the Resazurin based screening, each well of the assay plate contained 20µL 2x MHBI broth, 40µL 1x MHBI broth, 20µL peptide and 20µL bacteria. Bacteria were seeded in each well at a final concentration of  $1 \times 10^7$  CFU/mL. Each organism was tested in biological triplicate and each assay included media only controls, solvent only controls, and commercial antibiotic controls. Plates were incubated at 37°C, 275 rpm shaking for

4-7 hours depending on the organism's growth characteristics. Final reads were taken after 4 hours for *S. aureus*, *K. pneumoniae*, and *E. cloacae*. *E. faecium* and *A. baumannii* had final reads taken after 5 hours and *P. aeruginosa* after 7 hours. OD reads were taken using a Citation 5 plate reader (BioTek) at 600nm (OD<sub>600</sub>). Percent inhibition was calculated for each well using the following formula: % inhibition =  $((1 - ((\text{OD}_{600} \text{ of fraction} - \text{OD}_{600} \text{ of positive control}) / (\text{OD}_{600} \text{ of negative control} - \text{OD}_{600} \text{ of positive control}))) \times 100$ .

**Validation of CyO2 Activity from *Viola odorata*.** The minimum inhibitory concentration (MIC) was determined for CyO2 against *E. coli* and *A. baumannii*. Cultures were grown overnight as previously described in TSB before inoculation into MHBI media for a final concentration of  $1 \times 10^5$  CFU/mL. Assays were performed using a broth microdilution method in triplicate starting at 10 $\mu$ M for *E. coli* (Hicks Lab) and 25 $\mu$ M for *A. baumannii*. The peptide was tested at concentrations of 25, 20, 15, 10, and 5 $\mu$ M in biological triplicate and activity was defined by the concentration in which complete clearing was observed in wells following 20 hours of incubation at 37°C.

**Minimum Bactericidal Concentration to Determine Activity of CC-AMP1.** The minimum bactericidal concentration (MBC) was determined for isolate CC-AMP1 against *E. faecium*, *S. aureus*, and *A. baumannii* first by testing bioactivity using the antimicrobial screening by OD<sub>600</sub> method described above, and then by plating the well content of those assays on TSA. The MBC was determined for each concentration of compound tested including no treatment controls in biological triplicate. Following bioassay screening and OD<sub>600</sub> recording, 20 $\mu$ L from each well of the assay plate was extracted and placed into

180µL of PBS. Samples were then serially diluted by intervals of 1:10 and 30µL was plated in technical duplicate onto TSA and incubated overnight at 37°C for 24 hours. Colonies were then counted to determine the CFU/mL for each sample. Percent recovery was then calculated by comparing treated samples to no-drug controls. % recovery = ((CFU/mL test sample)/(CFU/mL negative control)) x 100.

## Results

**Optimization of Resazurin Assay to Assess Antimicrobial Peptide Activity by Quantifying Respiration.** Resazurin is an oxidation-reduction indicator of respiration by bacterial and mammalian cells alike. Resazurin itself is a non-toxic compound that is deep blue in color and does not possess fluorescent properties. When reduced, however, it becomes Resofurin which is pink in color and is highly fluorescent, allowing for detection using a standard monochromatic plate reader. Further, Resofurin itself can be reduced to Hydroresorufin, which is uncolored and non-fluorescent, therefore, if bacteria are allowed to reduce the reagent too far, false inhibitory results can be obtained (**Figure 27**). Based on our preliminary analysis, this occurs when too many bacteria are present per well in a 96-well plate. For this project, two Gram-positive organisms and four Gram-negative organisms were assessed, each with very distinct metabolic profiles and growth rates. Therefore, optimization was necessary to determine the proper incubation times and inocula to obtain the most accurate and consistent results for each organism.

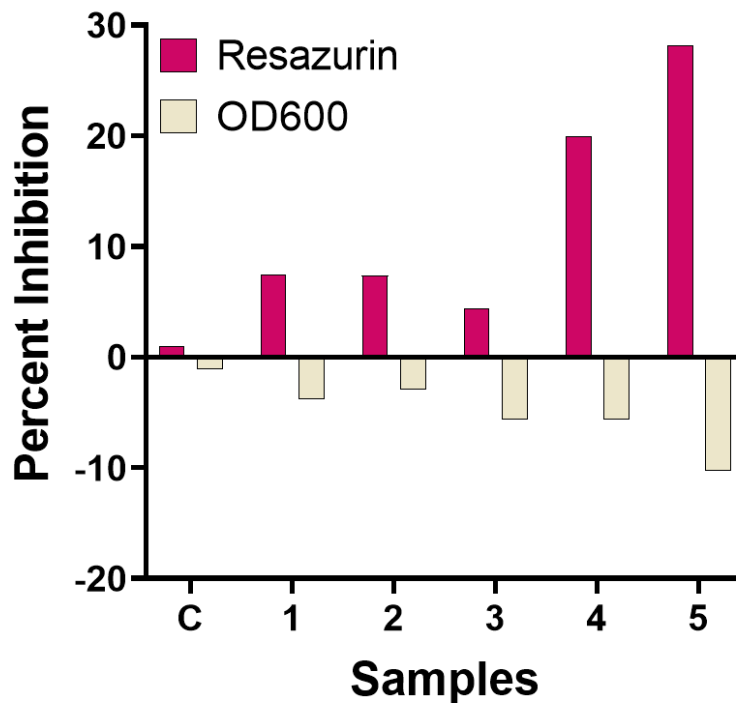


**Figure 27. False Positive Activity Arises with Overexposure of Resazurin.** Each sample was from the same data set with percent inhibition calculated using either resazurin values or the final OD<sub>600</sub> measurements from the same wells. C represents a well where overgrowth and overreduction did not occur and good correlation is seen. Samples 1-5 represent wells where overreduction of resazurin resulted in false positive inhibition.

In order to accomplish this, generation times were determined for each of the organisms by synchronizing and standardizing each bacterial species to a range of OD<sub>600</sub>s and recording the respective OD<sub>600</sub> at various timepoints under conditions that mimic the bioassays to be performed. OD<sub>600</sub>s were then connected to a precise CFU/mL by serial diluting and plating each sample onto TSA (**Figure 28**). Based on this, we were able to fit a linear regression to various OD<sub>600</sub> measurements vs CFU/mL counts to calculate the OD<sub>600</sub> in which each organism produces  $5 \times 10^7$  CFU/mL, the desired starting OD<sub>600</sub> prior to dilution for bioactivity screening (**Table 8**). Each starting OD<sub>600</sub> was generated based on technical replicates of each organism in biological triplicate. For each assay, the OD<sub>600</sub>

equal to  $5 \times 10^7$  CFU/mL was diluted 1:5 to obtain a starting CFU/mL of  $1 \times 10^7$  per well for each organism (Table 8).

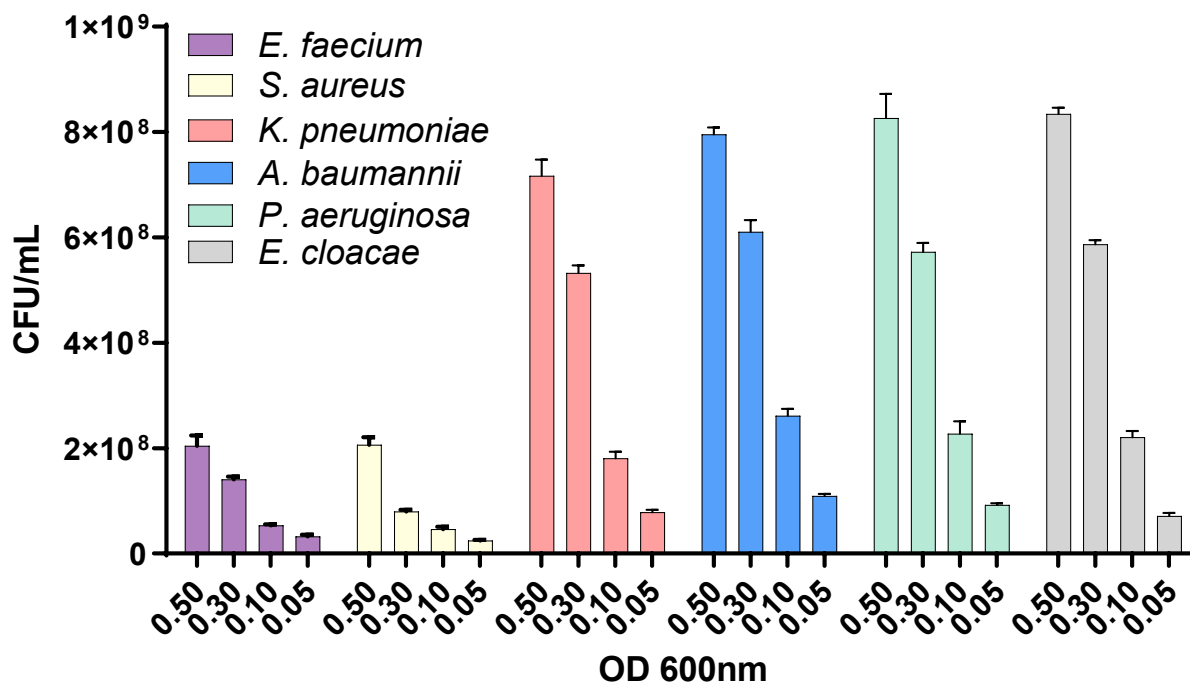


**Figure 28. Determination of Differences in ESKAPE OD<sub>600</sub> vs CFU/mL.** Each ESKAPE pathogen was synchronized and standardized to the shown optical densities to determine the ideal seeding OD<sub>600</sub> for each resazurin bioassay. Error bars represent  $\pm$ SEM of three biological replicates.

**The PepSAVI-MS Approach to Antimicrobial Peptide Discovery.** With the approach for bioactivity screening optimized for each organism to be tested, plant samples were prepared by the Hicks Laboratory at UNC-Chapel Hill following the PepSAVI-MS approach (Figure 26, adapted from Kirkpatrick *et al.* 2017[95]). Our novel approach is implemented, initially by growing specific plant species to a pre-flowering stage and then immediately flash-freezing the aerial plant tissue using liquid nitrogen prior to peptide extraction. Frozen tissue is then ground and treated with protease inhibitors prior to pelleting and centrifugation to fractionate samples using strong cation exchange (SCX)

chromatography. This method of fractionation allows for the isolation of specific AMPs, which are RiPPs. Plant samples containing RiPPs are then separated into 47 fractions, forming libraries to be screened for bioactivity against the ESKAPE pathogens. The crude samples are then tested at a ratio of 1:5 in biological triplicate against the ESKAPE pathogens. Plants tested in this manner are highlighted in **Table 7** in dark green. Under certain circumstances not all ESKAPE pathogens could be tested due to the amount of test material collected and therefore, pathogens were prioritized for testing. These are also highlighted in **Table 7**.

Following the Resazurin based antimicrobial assay to detect inhibition, bioactivity is calculated based on percent inhibition of each crude extract fraction and is converted to a scaled score that directly represents the inhibitory activity. Specifically, if a peptide fraction inhibits 100% of the bacteria within a test well, a scaled score of 10 is given for that sample. Scaled scores are calculated based on the average score of three replicates. Peptide fractions that are found to be most promising based on bioactivity are then analyzed via mass spectrometry (LCMS/MS) to determine which peptides are present and at what concentrations. These peptides are then purified and subjected to further bioactivity screening.

**Assessing the Activity of *Viola odorata* (VO) to Validate the PepSAVI-MS Approach Reveals Novel Antimicrobial Activity.** To implement this approach and prove its potential, a known RiPP AMP producing plant was selected: *Viola odorata* (VO), commonly known as the Sweet Violet plant[310]. As previously described, plants were

grown, and fractionated libraries were created for bioactivity screening against the ESKAPE pathogens (**Figure 29**). From this data, fractions 18-22 represented a peak in bioactivity and therefore underwent LCMS/MS analysis to detect levels of the known RiPP: cycloviolacin O2 (CyO2)[310]. Previous work has shown minimal activity of CyO2 against Gram-positive organisms such as *S. aureus*[311], which is in line with our study that also showed a minimal effect against *E. faecium*.

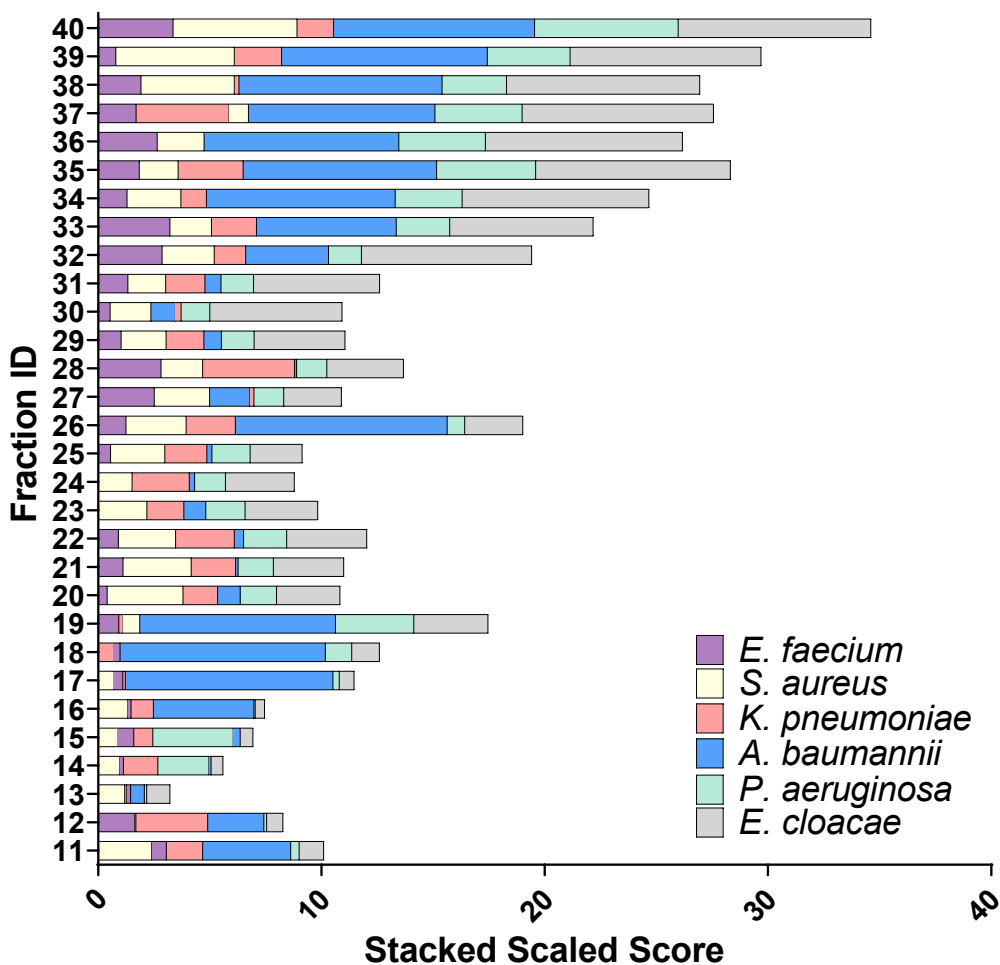


**Figure 29. Bioactivity of *Viola odorata* Fraction Library.** Data is represented as a stacked scaled score (% inhibition/10) for simplicity with all ESKAPE pathogens. Fractions 1-10 and 41-47 were excluded leaving only the samples expected to contain RiPPs. Data points represent the average of 3 biological replicates per species.

To validate the activity of our sample and our approach to AMP discovery using the pipeline, the CyO2 found within fractions 18-22 was purified and subject to bioactivity assessment via screening for its inhibitory potential against two select pathogens: *Escherichia coli* and *A. baumannii*. For this screen, each strain was challenged with pure CyO2 and the MICs were determined. *E. coli* was found to have an MIC of 5 $\mu$ M (conducted by our collaborators) which was expected based on a previous study that demonstrated inhibition of a different strain of *E. coli* by CyO2[311]. *A. baumannii* was inhibited following 15 $\mu$ M of CyO2 treatment. These findings serve as proof of principle for the pipeline and uncovered novel activity for CyO2 against the Gram-negative, multi-drug resistant *A. baumannii* strain. This data was published in[95].

**Bioassay Screening of Fractionated Ethnobotanical Plant Species Against the ESKAPE Pathogens.** Based on the success of our pilot study in VO, multiple species of ethnobotanical plant were subject to the same rigor of testing (**Table 7**). The most active fractions of select samples are shown in **Figures 30-32**. Due to the need to protect intellectual property in our ongoing efforts, only the genera of each plant are revealed herein. Fraction sets of 47 crude samples that contain potentially active RiPPs were tested against the ESKAPE pathogens. Fractions 11-40, most likely to contain the RiPPs were graphed to evaluate their bioactivity. Specifically, fractions 1-10 contain small molecules that could be bioactive and fractions 41-47 contain high levels of salt, which can be toxic to bacteria, therefore, each are omitted from the PepSAVI-MS analysis. Further, high salt concentrations and highly abundant small molecules can lead to instrument contamination during downstream MS/MS peptide quantification. Identifying

fractions containing the most bioactive AMPs is achieved by looking for peaks or small bell curve trends of activity within the data sets since the same AMP is eluted across multiple fractions within a sample at varying concentrations.

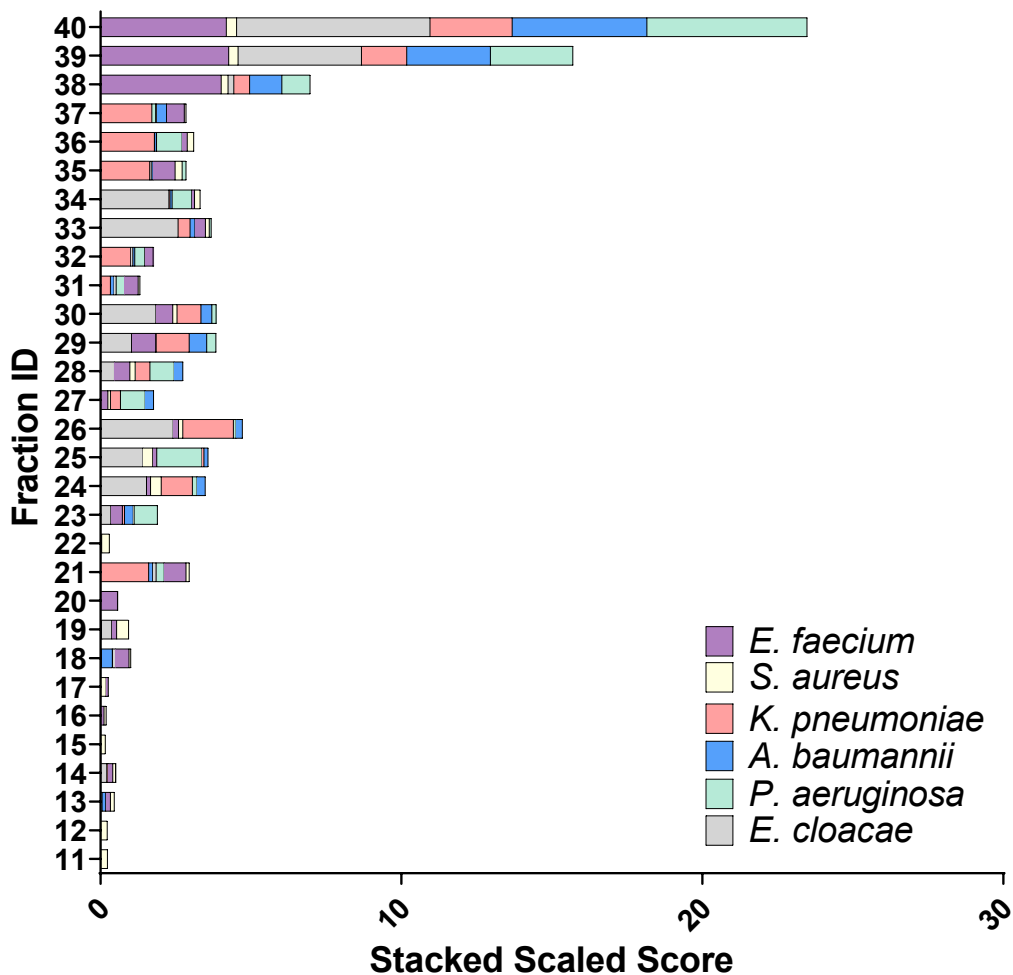


**Figure 30. Bioactivity of *Linum spp.* Fraction Library.** Data is represented as a stacked scaled score (% inhibition/10) for simplicity with all ESKAPE pathogens. Fractions 1-10 and 41-47 were excluded leaving only the samples expected to contain RiPPs. Data points represent the average of 3 biological replicates per species.

**Figure 30** shows the bioactivity of *Linum spp.* where modest peaks of activity are present within fractions 23-26, 28-30, and 32-34. The most abundant activity was seen against *E. cloacae* demonstrating around 20% inhibition when challenged with fractions 26 and 33.

Due to low levels of bioactivity recorded across multiple ESKAPE species, these samples were not pursued further, however, *Linum spp.* would be a candidate to consider investigating to find AMPs specifically targeting *E. cloacae*. Although  $\pm 20\%$  may seem low, it is possible and even likely that the fractions responsible for this activity contain AMPs that are in low abundance and therefore are highly potent themselves against *E. cloacae*. Therefore, isolating and purifying the peptide(s) responsible for the bioactivity observed against *E. cloacae* and re-testing for inhibitory activity would be a viable approach to determine therapeutic potential of AMPs produced by *Linum spp.*

Another example yielding the characteristic peak of activity was found for *Solanum spp.* (**Figure 31**), which was tested against ESKA of the ESKAPE panel. It was clear that fractions 18-25 contained AMP(s) that are effective to inhibit and thus target *K. pneumoniae* and *A. baumannii*. The content of fraction 20 demonstrated the highest amount of inhibition against each species and therefore likely contained the highest concentration of bioactive peptide(s). In addition, this fraction is likely to contain an AMP with broad-spectrum activity. Specifically, this fraction contained a peptide or peptides that inhibited *K. pneumoniae* by an average of 37%, *A. baumannii* by 26.5%, and *E. faecium* by 15.4%. These bioactive fractions (18-25) did not undergo further analyses and therefore it is unclear which peptide(s) led to the inhibitory activity observed, however, the broad-spectrum activity highlights *Solanum spp.* as a candidate for future analysis. Specifically, by investigating the peptides present within fraction 20 and the surrounding elution products would allow us to determine whether a single peptide was responsible for the cross-species activity or if a group of AMPs were responsible.

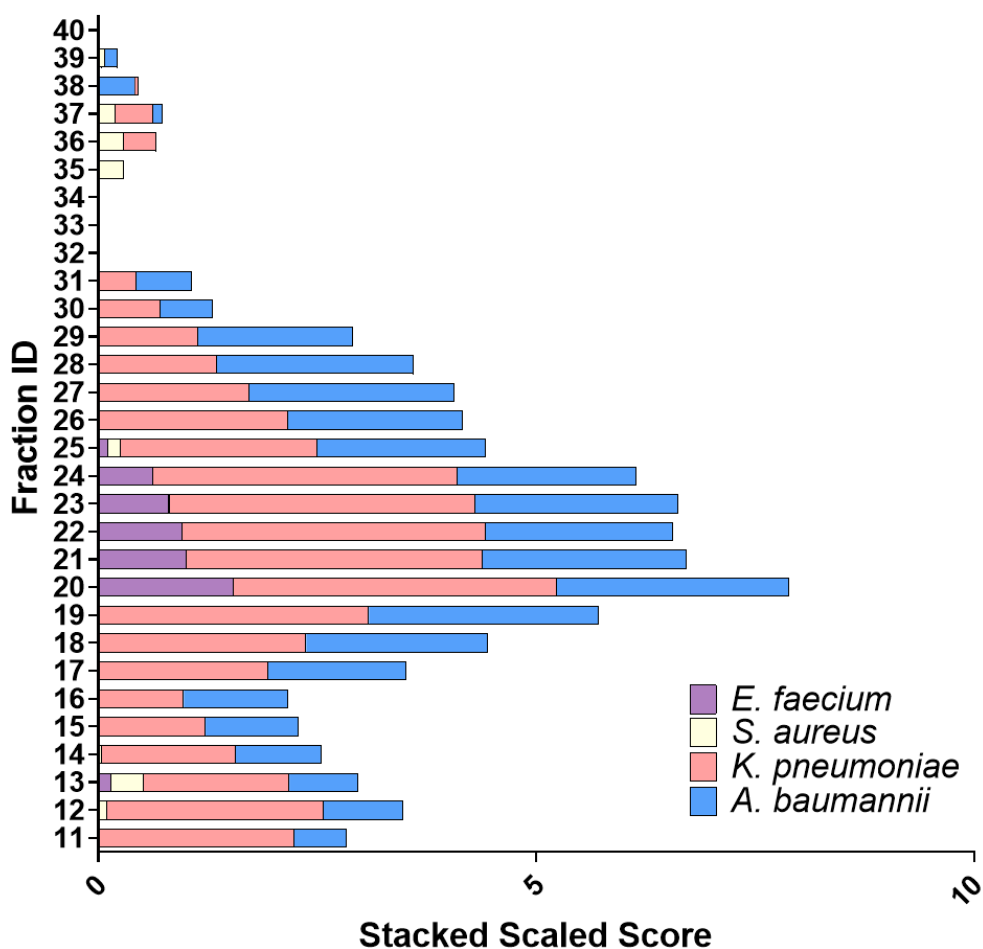


**Figure 31. Bioactivity of *Solanum spp.* Fraction Library.** Data is represented as a stacked scaled score (% inhibition/10) for simplicity with all ESKA pathogens. Fractions 1-10 and 41-47 were excluded leaving only the samples expected to contain RiPPs. Data points represent the average of 3 biological replicates per species.

The next plant that underwent bioactivity assessment comes from the genus *Silybum*. For this sample set, activity was seen against two Gram-negative species as shown in **Figure 32**. Fractions 18-23 show a peak of activity against *K. pneumoniae* and *A. baumannii* suggesting that bioactive AMPs are present within those samples. The activity was found to be Gram-negative specific as *S. aureus* and *E. faecium* were not influenced by treatment with these fractions. However, relatively low levels of inhibition were observed

against *A. baumannii* and *K. pneumoniae*. The maximum level of inhibition was observed for fraction 19, inhibiting *A. baumannii* by 17.5% compared to no-treatment controls. *K. pneumoniae* was inhibited by a maximum of 9% when challenged with fraction 23. Activity, however small, prompted us to investigate this plant species further. Seeing the highest levels of activity against each species in different fractions suggests that different peptides are contributing to the antibacterial activity.

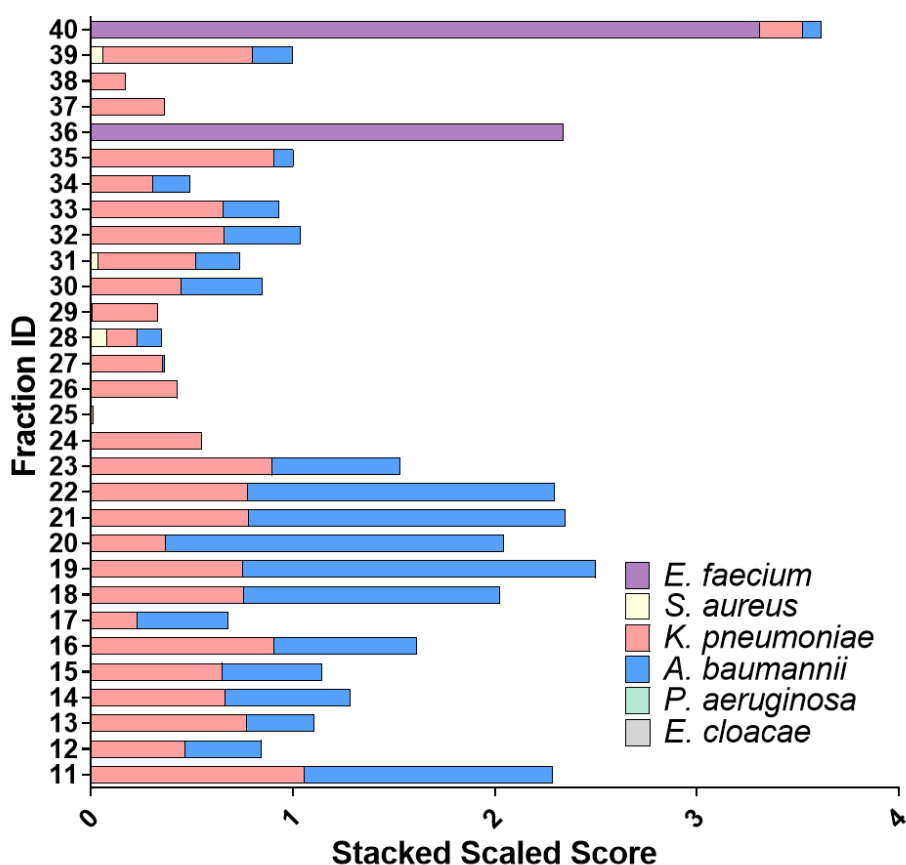


**Figure 32. Bioactivity of *Silybum spp.* Fraction Library.** Data is represented as a stacked scaled score (% inhibition/10) for simplicity with all ESKAPE pathogens. Fractions 1-10 and 41-47 were excluded leaving only the samples expected to contain RiPPs. Data points represent the average of 3 biological replicates per species.

Repeating the assay with more concentrated samples allowed us to confirm this. Thus, to understand which of the fractions were contributing to the bioactivity observed, another

library from *Silybum spp.* containing 3-times the peptide concentration per fraction was generated. *K. pneumoniae* and *A. baumannii* were then subject to bioactivity screening using the concentrated library. As shown in **Figure 33**, activity against *K. pneumoniae* and *A. baumannii* was observed across the same fractions (18-23) highlighting the reliability of our pipeline to aptly replicate our findings across different plant harvests. Despite this, however, the degree of activity was not 3-fold that of the initial library created. Against *A. baumannii*, the second, more concentrated library, yielded similar inhibitory activity while the samples inhibited *K. pneumoniae* to a higher degree albeit less than 3-fold. Therefore, although we are able to confidently isolate the same peptides based on the reflective bioactivity patterns observed, the concentration of bioactive peptides is likely to vary between harvests. Despite this, we have identified fractions containing AMPs capable of targeting two important pathogens and further studies will allow for their identification and structure elucidation. Thus, *Silybum spp.* serves an example plant species, producing multiple bioactive AMPs that are worth isolating and characterizing further utilizing the PepSAVI-MS approach.

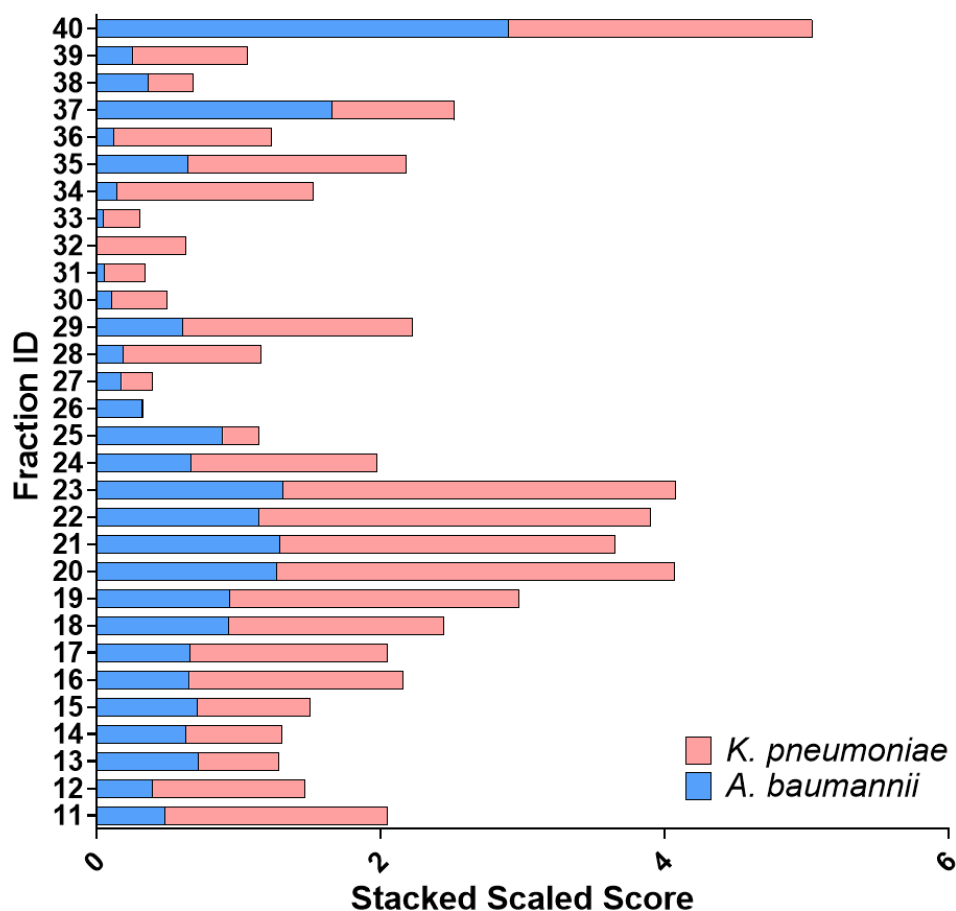


**Figure 33. Bioactivity of *Silybum spp.* 3x Fraction Library.** Data is represented as a stacked scaled score (% inhibition/10) for simplicity with KA pathogens. Fractions 1-10 and 41-47 were excluded leaving only the samples expected to contain RiPPs. Data points represent the average of 3 biological replicates per species.

Throughout this process we were able to screen 19 different ethnobotanical species (Table 7), with the select examples discussed, further demonstrating the validity and power of the PepSAVI-MS approach to AMP discovery. This screening effort has led to the identification of multiple plant species with antimicrobial activity against multi-drug resistant microorganisms. Further, it has allowed for the bioassay guided identification of sample fractions containing AMP pools that likely contain novel AMPs capable of targeting these microorganisms.

**Fast-Tracking Screening Procedure via Assessing Single Fraction Isolates Against the ESKAPE Pathogens.** Although the process for screening fraction libraries proved successful, a majority of libraries did not yield noteworthy results and thus there were no subsequent investigation into the AMPs present. This is not surprising as the panel of bacteria used within these assays are the most clinically relevant based on their isolation locations and ability to resist multiple commercial antibiotics. When considering AMPs of therapeutic relevance, activity against multi-drug resistant organisms will likely translate to activity against other strains of the resistant species. Therefore, hits identified are of high value, however, this means fewer plant species will be identified throughout this process including plants that may produce AMPs with inhibitory activity against less drug-resistant strains of the organisms tested. The high value (smaller) hit identification rate, coupled with the labor and time-intensiveness of screening 47 peptide fractions against six species of bacteria in biological triplicate, led us to modify the initial steps in the screening process to increase efficiency. To do so, the fractionation step for peptide library creation was eliminated creating a single pooled fraction containing all of the plant material and AMPs. This allowed us to save time and resources by rapidly eliminating plant species without bioactivity and identifying bioactive plant species to be assessed fully via fractionated library creation and screening. From this approach we were able to promptly test multiple species of plant simultaneously. These are shown in **Table 7** highlighted in light green. The bioactivity of these concentrated fractions is shown in **Figure 34**.

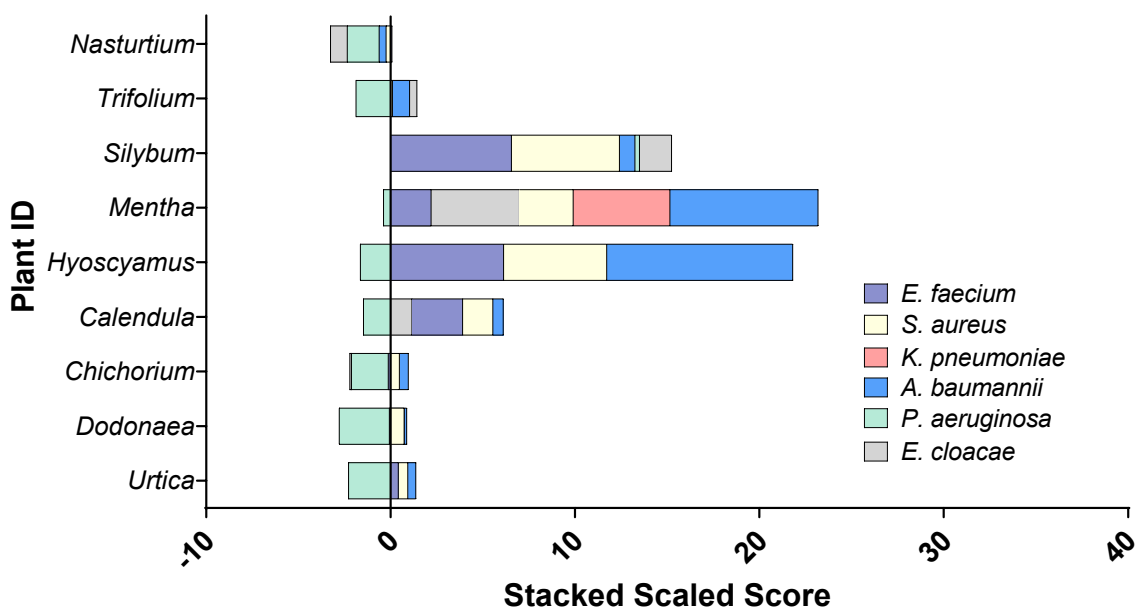


**Figure 34. Bioactivity of Single Fraction Libraries.** Data is represented as a stacked scaled score (% inhibition/10) for simplicity with all ESKAPE pathogens. Data points represent the average of 3 biological replicates per species. Due to issues with ongoing intellectual property, originating plant species names are abbreviated.

The plant sample of the *Mentha* genus demonstrated the highest bioactivity with inhibitory activity against all six ESKAPE pathogens (**Figure 34**). In addition to this, the *Hyoscyamus* sample showed inhibitory activity against Gram-positive (*E. faecium* and *S. aureus*) and Gram-negative species (*A. baumannii*). *Silybum* and *Calendula* genre also demonstrated inhibitory potential albeit to a lesser degree. Based on these results, full fraction libraries of the *Mentha* and *Hyoscyamus* genera are queued for future testing against the ESKAPE panel to identify and isolate fractions containing the peptides contributing to the activity observed in the single fraction screen shown in **Figure 34**. The retesting of *Silybum* using this approach serves as proof of principle for identifying bioactive AMP producing plant varieties even though the activity does not specifically mirror that of the fully fractionated library screen.

**Overcoming Colorimetric Interferences via Turbidity-Based Assessment.** The concentrated fraction approach revealed promising candidates for full fractionation and ESKAPE panel challenge, however, there were still limitations to this approach. Certain plant extracts possess components with visible color, which is not ideal for a colorimetric based assay such as Resazurin screening. Specifically, the color of the samples was found to interfere with the spectrometer readings of Resazurin and resulted in measurements that could not reliably be used to calculate the inhibitory effect of the peptide samples. In the fractionated library screens, the colorimetric components of the plants were eluted into fractions collected early and were not considered in the inhibitory data (within fractions 1-10). To overcome this in the pooled single fractions, an OD<sub>600</sub>-based approach was employed using the same parameters and seeding concentrations as previously used but modifying the amount of time each bacterial species within the ESKAPE panel was grown in the presence of peptide samples. To find the optimal time to allow for growth and detect statistically significant inhibitory data solely utilizing OD<sub>600</sub>, growth curves were performed using no-treatment controls and antibiotic-treated controls as the baseline for inhibitory activity (**Figures 35-40**).

As shown in **Figure 35**, it was found that an optimal time for assaying activity was between 4 and 7 hours for *E. faecium*. An optimal time is defined as the condition(s) in which the difference in OD<sub>600</sub> of the treated sample and the OD<sub>600</sub> of the non-treated sample are most significantly separated. For example, it is known that our control antibiotic (treated sample) is able to inhibit the population and represents 100% inhibition. However, the OD<sub>600</sub> does not change throughout the timepoints since the organism is

inhibited throughout all tested timepoints. So, if percent inhibition is calculated at each point, the highest level of inhibition is seen for the timepoints at which the highest level of separation is present between the treated and non-treated samples. Specifically, for *E. faecium*, using raw OD<sub>600</sub> values without subtracting background, percent inhibition at hour 2 is 34%, whereas nearly 70% inhibition is calculable at hour 7.

Using this logic, the ideal time ranges were determined for the remainder of the ESKAPE pathogens. The ideal time for *S. aureus* was found to be between 3 and 8 hours (**Figure 36**), while for *K. pneumoniae* the ideal range was between 4-8 hours (**Figure 37**). The ideal time range was found to be between 5-8 hours and 7-11 hours for *A. baumannii* (**Figure 38**) and *P. aeruginosa* (**Figure 39**) respectively. Finally, the ideal range of time for incubation of *E. cloacae* was determined to be between 4-9 hours (**Figure 40**). Following this analysis, it was determined that the ideal time of inhibitory quantification was after 5 hours of incubation with peptides for *E. faecium* and *A. baumannii*, 4 hours for *S. aureus*, *K. pneumoniae*, and *E. cloacae*, and 7 hours for *P. aeruginosa*. These time points were chosen to represent a time within the established ideal range that also allowed for an efficient high-throughput screening approach. By assessing multiple organisms at the same timepoint, data of statistical significance could be generated more quickly and efficiently. For example, *E. faecium* and *A. baumannii* could be seeded within the same assay plate and measured together instead of the alternative combination of *E. faecium* and *S. aureus*. Incubating *E. faecium* and *S. aureus* together would result in a disruption in incubation time for *E. faecium* when *S. aureus* samples needed to be measured whereas *E. faecium* and *A. baumannii* could be incubated for 5 hours without

interruption. Thus, more consistent results could be generated. Keeping these timepoints consistent also established a baseline to serve as a control and ensured that peptide samples across different plant species and preparations could be reliably compared.

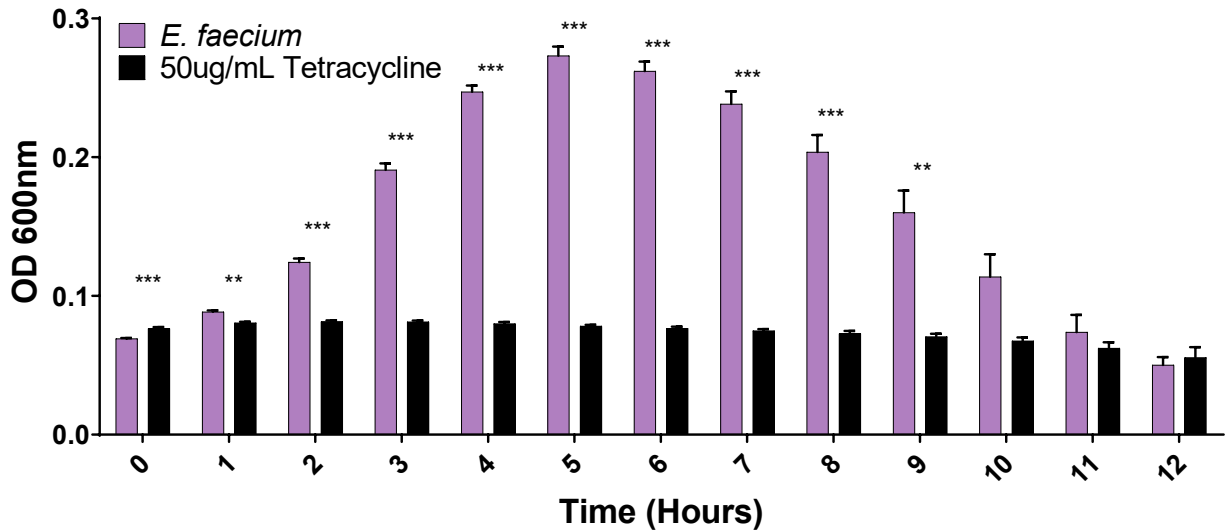


**Figure 35. Growth of *E. faecium* Reveals 5 Hours to be Optimal Assay Point.** Data was collected using a BioTek Plate reader following synchronizing and standardizing to a starting OD<sub>600</sub> of 0.1. Each data point represents the OD<sub>600</sub> of three biological replicates of the organism in MHBI with or without antibiotic treatment. Error bars represent the mean ± SEM of the three replicates. P-values for each time point were determined for the antibiotic treated and non-treated samples. Asterisks represent P values using Student's t-test : 0.05<\*, 0.01<\*\* , 0.001<\*\*\* relative to controls.

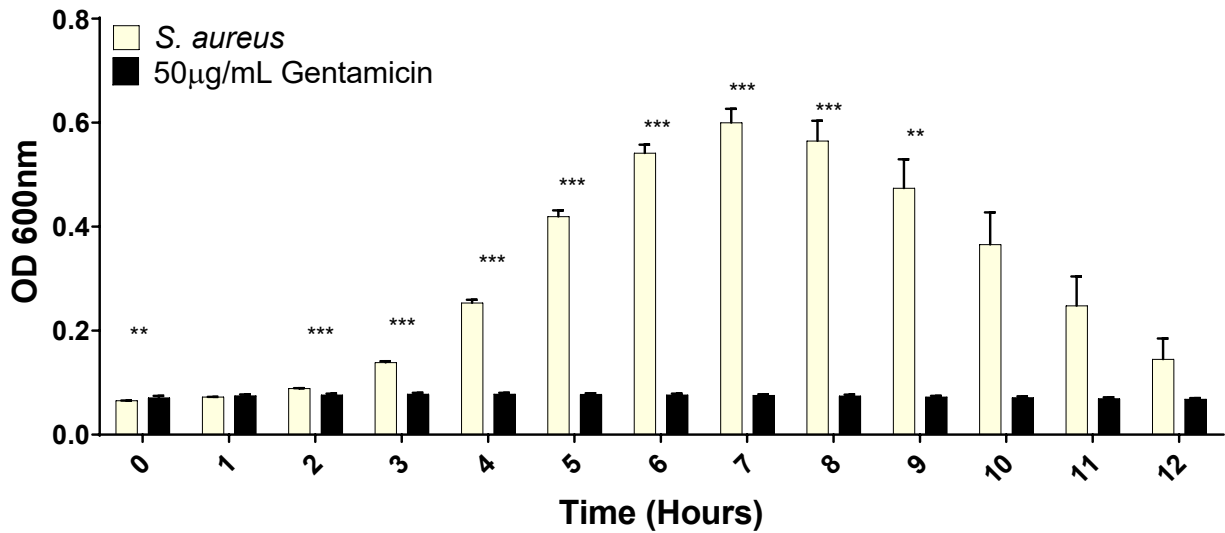


**Figure 36. Growth of *S. aureus* Reveals 4 Hours to be Optimal Assay Point.** Data was collected using a BioTek Plate reader following synchronizing and standardizing to a starting OD<sub>600</sub> of 0.1. Each data point represents the OD<sub>600</sub> of three biological replicates of the organism in MHBI with or without antibiotic treatment. Error bars represent the mean ± SEM of the three replicates. P-values for each time point were determined for the antibiotic treated and non-treated samples. Asterisks represent P values using Student's t-test : 0.05<\*, 0.01<\*\* , 0.001<\*\*\* relative to controls.

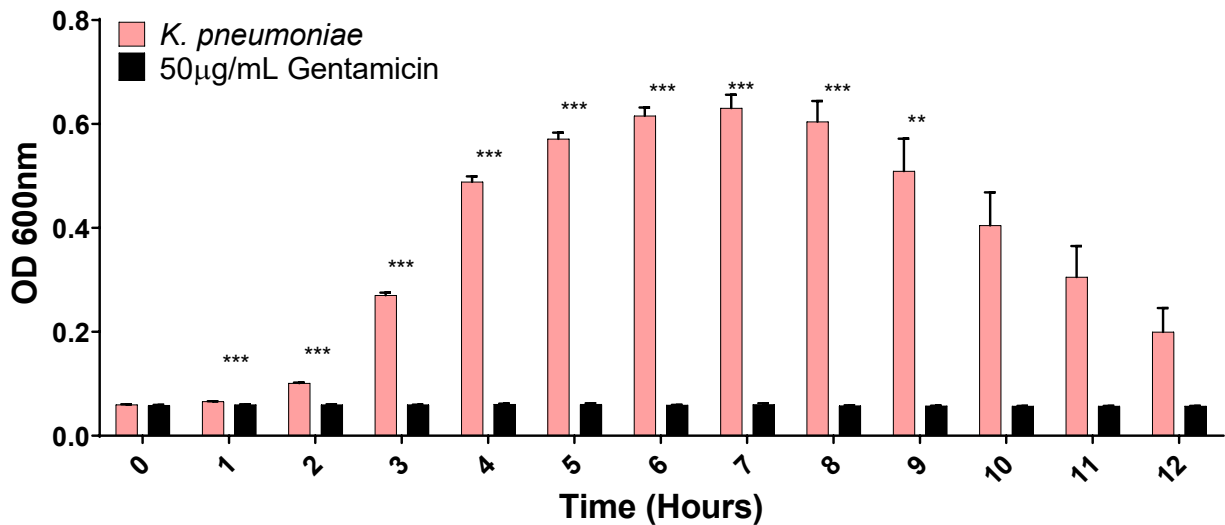


**Figure 37. Growth of *K. pneumoniae* Reveals 4 Hours to be Optimal Assay Point.** Data was collected using a BioTek Plate reader following synchronizing and standardizing to a starting OD<sub>600</sub> of 0.035. Each data point represents the OD<sub>600</sub> of three biological replicates of the organism in MHBI with or without antibiotic treatment. Error bars represent the mean ± SEM of the three replicates. P-values for each time point were determined for the antibiotic treated and non-treated samples. Asterisks represent P values using Student's t-test : 0.05<\*, 0.01<\*\* , 0.001<\*\*\* relative to controls.

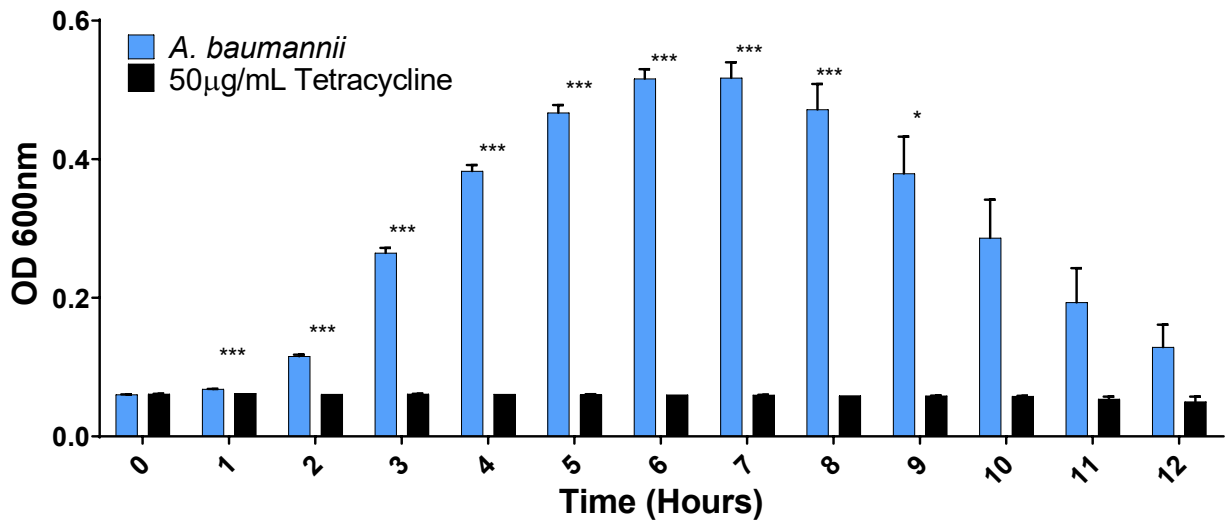


**Figure 38. Growth of *A. baumannii* Reveals 5 Hours to be Optimal Assay Point.** Data was collected using a BioTek Plate reader following synchronizing and standardizing to a starting OD<sub>600</sub> of 0.0325. Each data point represents the OD<sub>600</sub> of three biological replicates of the organism in MHBI with or without antibiotic treatment. Error bars represent the mean ± SEM of the three replicates. P-values for each time point were determined for the antibiotic treated and non-treated samples. Asterisks represent P values using Student's t-test : 0.05<\*, 0.01<\*\*, 0.001<\*\*\* relative to controls.

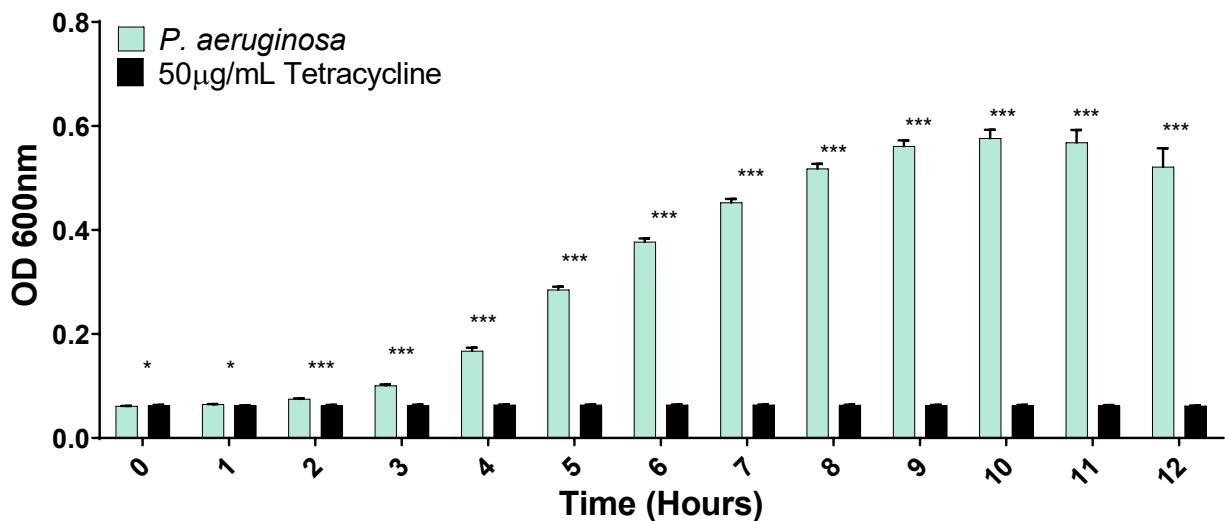


**Figure 39. Growth of *P. aeruginosa* Reveals 7 Hours to be Optimal Assay Point.** Data was collected using a BioTek Plate reader following synchronizing and standardizing to a starting OD<sub>600</sub> of 0.03. Each data point represents the OD<sub>600</sub> of three biological replicates of the organism in MHBI with or without antibiotic treatment. Error bars represent the mean ± SEM of the three replicates. P-values for each time point were determined for the antibiotic treated and non-treated samples. Asterisks represent P values using Student's t-test : 0.05<\*, 0.01<\*\*, 0.001<\*\*\* relative to controls.

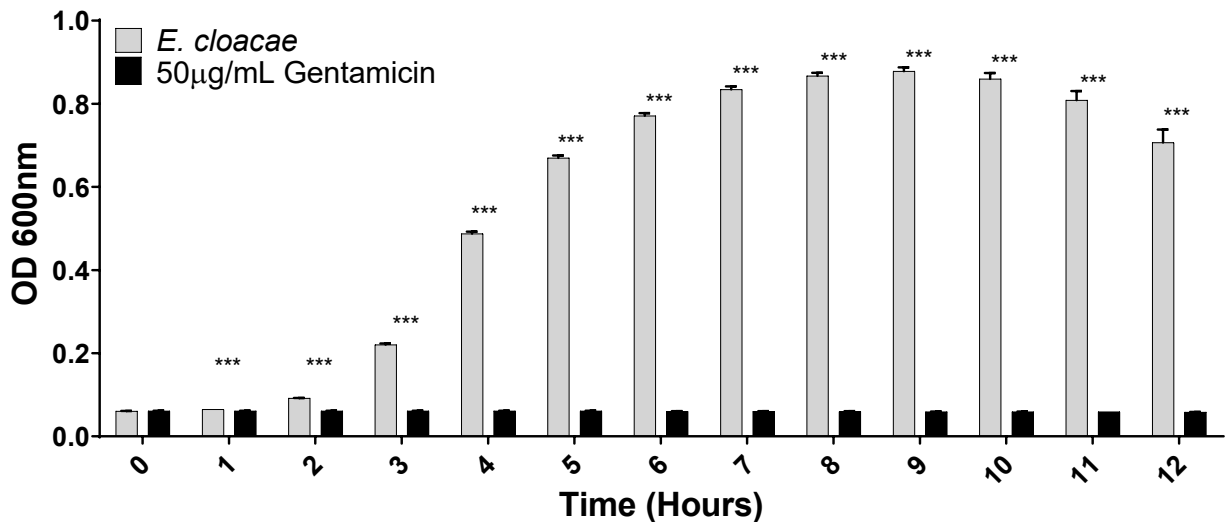


**Figure 40. Growth of *E. cloacae* Reveals 4 Hours to be Optimal Assay Point.** Data was collected using a BioTek Plate reader following synchronizing and standardizing to a starting OD<sub>600</sub> of 0.03. Each data point represents the OD<sub>600</sub> of three biological replicates of the organism in MHBI with or without antibiotic treatment. Error bars represent the mean ± SEM of the three replicates. P-values for each time point were determined for the antibiotic treated and non-treated samples. Asterisks represent P values using Student's t-test: 0.05 < \*, 0.01 < \*\*, 0.001 < \*\*\* relative to controls.

***Amaranthus tricolor* (ATr) has Limited Activity Against ESKAPE Pathogens but Shows Enhanced Activity Against *Escherichia coli*.** Initially, *A. tricolor* (ATr) was tested against 3 of the 6 ESKAPE pathogens (*S. aureus*, *K. pneumoniae*, and *A. baumannii*) using the fully fractionated library PepSAVI-MS approach, but little activity was observed (**Figure 41**). The highest level of activity was found against *A. baumannii* with around 15% inhibition recorded when treated with ATr fraction 21. Alternatively, preliminary activity was generated against a laboratory strain of *E. coli* and inhibition was observed (Hick's lab, data not shown). Based on this data, the PepSAVI-MS approach was implemented and revealed a novel short chain proline-rich AMP (ATr-AMP1) that has been previously described as possessing activity against laboratory strains of *E. coli* and *S. aureus*[314].

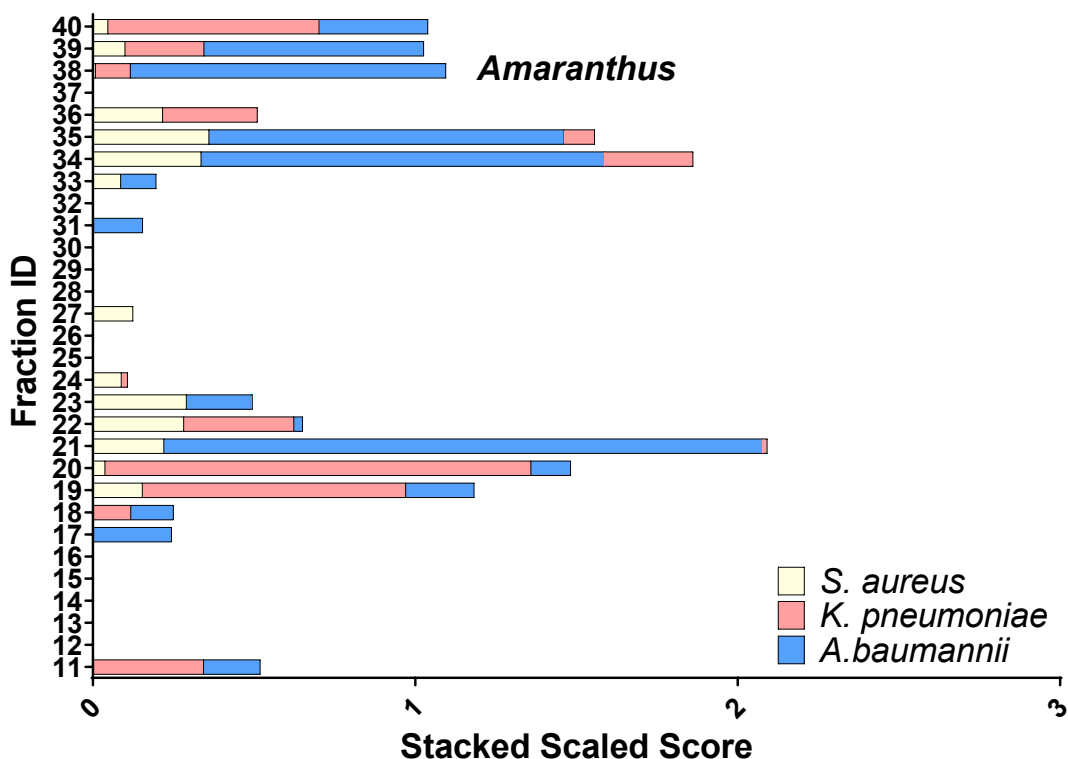


**Figure 41. Bioactivity of *Amaranthus tricolor* Fraction Library.** Data is represented as a stacked scaled score (% inhibition/10) for simplicity with SKA pathogens. Fractions 1-10 and 41-47 were excluded leaving only the samples expected to contain RiPPs. Data points represent the average of 3 biological replicates per species.

This success led us to reevaluate the potential of ATr against the ESKAPE pathogens and therefore a concentrated single fraction of ATr was tested against the ESKAPE panel as well as multiple strains of *E. coli* (**Figure 42**). The *E. coli* isolates used for this screen came from a spinach outbreak (TW14359) or were collected from infected patients at the Moffit Cancer Center (MCC) (Tampa, FL), giving clinical relevance to the findings. Specifically, over 50% inhibition was observed against all three clinical isolates of *E. coli* (MCC62, MCC67, and MCC70) as well as the TW14359 isolate. This finding is in line with the previous inhibitory activity observed by our collaborators when testing a laboratory strain of *E. coli* and highlights this species of plant as a valuable source of AMPs capable

of targeting multiple strains of *E. coli*. This data also revealed inhibitory activity of AMPs produced by *A. tricolor* that target other Gram-negative organisms. The pooled single fraction was most active against *P. aeruginosa* and resulted in over 70% inhibition. Further, *A. baumannii* was inhibited by over 60% and *E. cloacae* by over 45% (**Figure 42**). *K. pneumoniae* was the least susceptible Gram-negative isolate tested and exhibited inhibition by close to 20% when challenged with ATr. It should be noted that the concentrated fraction again showed activity against *K. pneumoniae* and *A. baumannii* at levels higher than any specific fraction. This indicates that there are potentially multiple AMPs to isolate that are effective against these pathogens and harnessing the products produced by this plant would require a different approach to identify them. These findings also indicate that the AMPs produced by *A. tricolor* are specific to Gram-negative microorganisms as no activity was observed against *E. faecium* nor *S. aureus* (**Figure 42**).

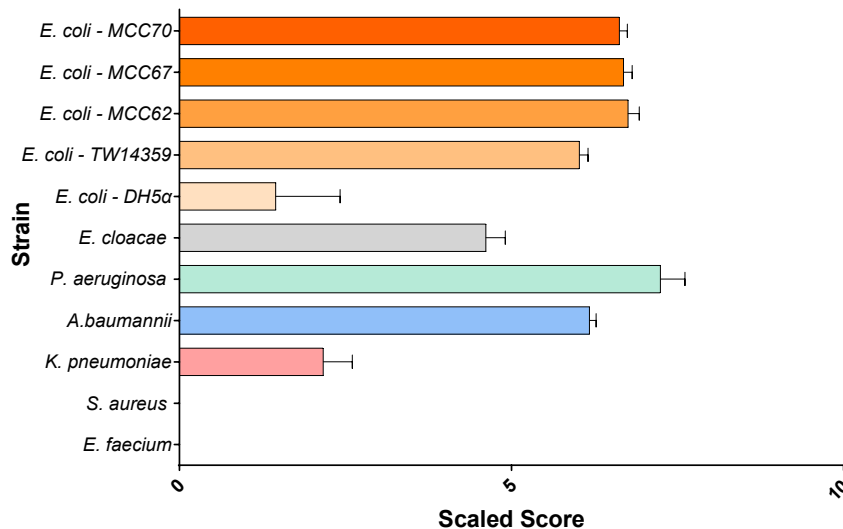


**Figure 42. Bioactivity of *Amaranthus tricolor* Concentrated Fraction Against ESKAPE and *E. coli* Isolates.** Data is represented as a stacked scaled score (% inhibition/10) for simplicity. Data points represent the average of 3 biological replicates per species. Error bars represent the mean  $\pm$ SEM of the three replicates.

**Transcriptome Mining Reveals Potential Antimicrobial Peptide Candidates Effective Against Select ESKAPE Pathogens.** The absence of substantial inhibition observed against *S. aureus*, *K. pneumoniae* and *A. baumannii* when challenged with the fully fractionated peptide library of ATr, coupled with Gram-negative specific inhibition observed for the ATr single pooled fraction, prompted us to take an alternate approach to peptide identification for this plant species. Instead of identifying the AMPs responsible for the bioactivity seen for the pooled sample of ATr using the PepSAVI-MS approach, translated transcriptome mining through *in silico* analysis was performed. Specifically, 181 AMPs have been predicted to be present within this plant species based on *in silico* analyses leaving much room for discovery[314, 315]. Using a top-down and bottom-up mass spectrometry approach, our collaborators were able to identify 127 proteins within ATr, seven of which were predicted AMPs[316]. Amongst those seven was a lipopeptide (ATr-LTP1) which was partially purified and tested against the ESKAPE panel as shown in **Figure 43**. Specifically, this peptide demonstrated activity against both Gram-positive organisms; *S. aureus* was inhibited by nearly 35% while *E. faecium* was inhibited by over 20%. However, the highest activity was seen for *K. pneumoniae*, where partially purified ATr-LTP1 inhibited the population by over 40%. Conversely, the remaining Gram-negative organisms (*A. baumannii*, *P. aeruginosa*, and *E. cloacae*) were less impacted by ATr-LTP1 and demonstrated inhibition values of less than 20% when challenged with the peptide sample.

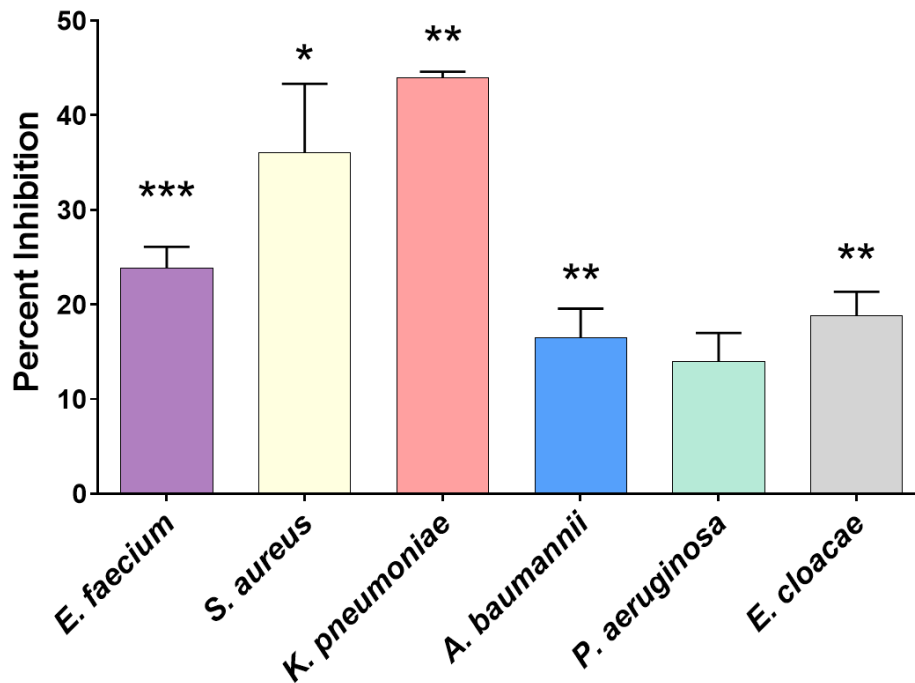


**Figure 43. Bioactivity of *Amaranthus tricolor* Partially Purified Lipopeptide ATr-LTP1 Against ESKAPE.** Data is represented as percent inhibition compared to no drug controls following treatment with 50 $\mu$ M LTP1. Data points represent the average of 3 biological replicates per species. Error bars represent the mean  $\pm$ SEM of the three replicates. Asterisks represent P-value using Student's t-test. P-value <0.05 \*, <0.01 \*\*, <0.001 \*\*\*.

Based on the promising activity against *K. pneumoniae*, the peptide was further purified and retested against *K. pneumoniae* at 50 $\mu$ M and 25 $\mu$ M as shown in **Figure 44**. At 50 $\mu$ M, the peptide was able to inhibit growth by greater than 40% while 25 $\mu$ M challenge resulted in 32% inhibition. Therefore, the MIC was found to be higher than the tested range. Due to the difficulty in isolating this peptide, testing at higher concentrations could not be performed and an MIC could not be determined.

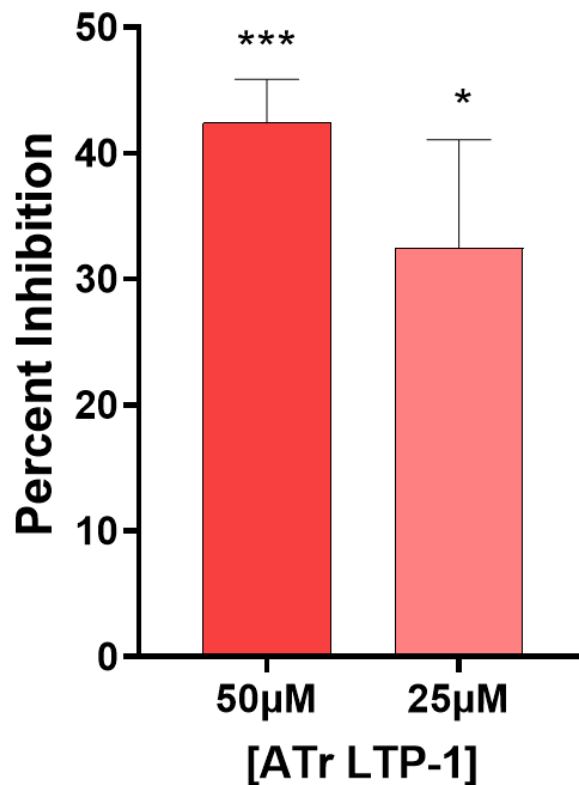


**Figure 44. Bioactivity of *Amaranthus tricolor* Purified Lipopeptide ATr-LTP1 Against *K. pneumoniae*.** Data is represented as percent inhibition compared to no drug controls following treatment with 50µM and 25µM ATr-LTP1. Data points represent the average of 3 biological replicates per species. Error bars represent the mean ±SEM of the three replicates. Asterisks represent P-value using Student's t-test. P-value <0.05 \*, <0.01 \*\*, <0.001 \*\*\*.

When looking further within the transcriptome of *A. tricolor*, a defensin (ATr-Def1) was identified[316] and a truncated version was synthesized for bioactivity screening. This truncated peptide showed activity against the ESKAPE pathogens as depicted in **Figure 45**. Against *S. aureus*, ATr-Def1 led to over 50% inhibition at 50µM. The inhibition was not considered Gram-positive specific, but *S. aureus* specific, as *E. faecium* was inhibited by less than 10%. Further, the next highest amount of inhibition was observed against *P. aeruginosa* where nearly 20% inhibition was reported. ATr-Def1 challenge resulted in less

than 15% inhibition of *K. pneumoniae* and *E. cloacae*, while *A. baumannii* was completely resistant to treatment at the concentration tested. This targeted approach led to a host of AMPs being identified some of which showed antimicrobial activity against members of the ESKAPE panel. Specifically, we observed *K. pneumoniae* specific activity for AMP-LTP1 and *S. aureus* specific activity for ATr-Def1. This highlights the value of combining the PepSAVI-MS pipeline with bioinformatics-based approaches to find promising AMP candidates for therapeutic characterization.

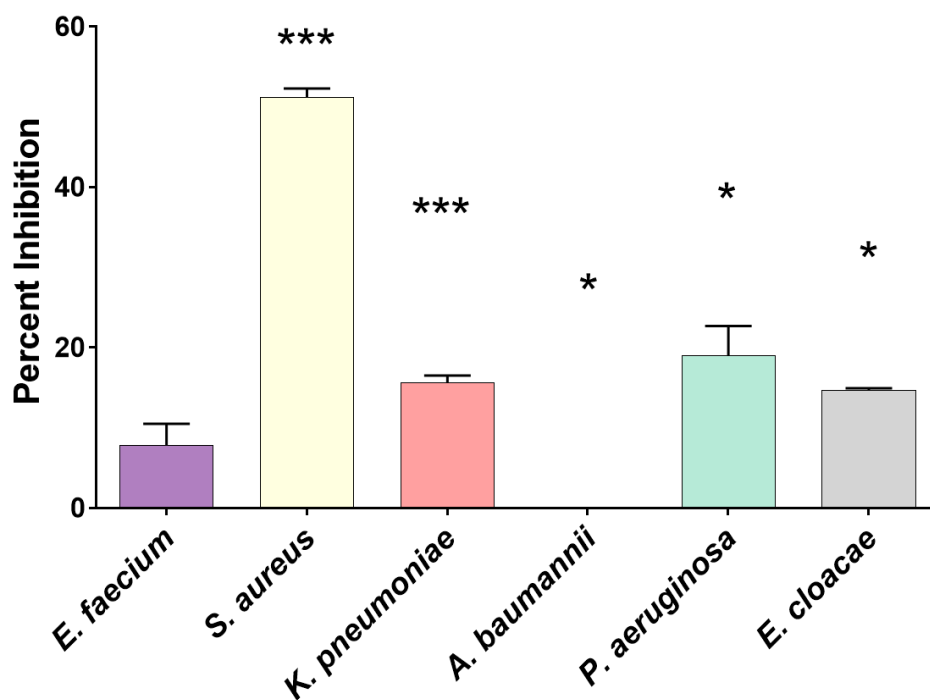


**Figure 45. Bioactivity of *Amaranthus tricolor* ATr-Def1 Against ESKAPE.** Data is represented as percent inhibition compared to no drug controls following treatment with 50 $\mu$ M ATr-Def1. Data points represent the average of 3 biological replicates per species. Error bars represent the mean  $\pm$ SEM of the three replicates. Asterisks represent P-value using Student's t-test. P-value <0.05 \*, <0.01 \*\*, <0.001 \*\*\*.

***Capsicum chinense x frutescens* (CC) a Hybrid Ghost Pepper Plant Displays Gram-Negative Specific Activity.** Another plant, *C. chinense x frutescens* (CC), was evaluated

using the same approach to AMP discovery as ATr, combining top-down and bottom-up proteomics coupled with *in silico* predictions to identify potential AMPs for testing. Through this, 14 potential AMPs with characterized sequences were identified in the aerial tissue of CC out of the 115 predicted from the closely related *C. chinense* proteome[317]. Through this, two AMPs termed CC-AMP1 and CC-AMP2 were identified. CC-AMP1 was partially purified and was found to have activity against laboratory strains of *E. coli* and *K. pneumoniae* based on testing by our collaborators. Because of this, CC-AMP1 was suspected to have anti-Gram-negative activity and was therefore tested against three of the multi-drug resistant pathogens (*A. baumannii*, *P. aeruginosa*, and *E. cloacae*). There were high levels of inhibitory activity found for each pathogen as shown in **Figure 46**. Specifically, when challenged with 70.16 $\mu$ M of CC-AMP1, *E. cloacae* was inhibited by 75%. This was the lowest amount of inhibitory activity recorded, with CC-AMP1 inhibiting *A. baumannii* and *P. aeruginosa* populations by 92% and 97% respectively.

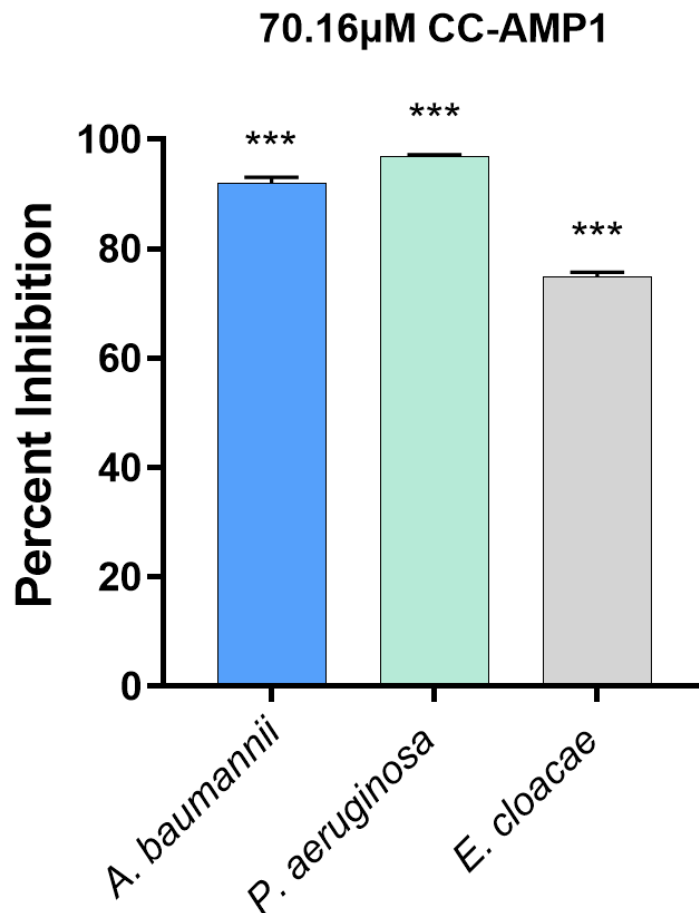


**Figure 46. Bioactivity of *Capsicum chinense x frutescens* CC-AMP1 Against APE.** Data is represented as percent inhibition compared to no drug controls following treatment with 70.16 $\mu$ M CC-AMP. Data points represent the average of 3 biological replicates per species. Error bars represent the mean  $\pm$ SEM of the three replicates. Asterisks represent P-value using Student's t-test. P-value <0.05 \*, <0.01 \*\*, <0.001 \*\*\*. Based on the substantial activity against *A. baumannii* and *P. aeruginosa*, the peptide

was then tested in a dose dependent manner against ESKAP isolates (**Figure 47**). It was clear that the Gram-negative isolates were inhibited in a dose dependent manner, however, for the Gram-positive isolates challenged, a similar level of activity was observed at all concentrations tested. This further solidified our prediction that CC-AMP1 was specifically targeting Gram-negative organisms. The highest level of activity was observed against *A. baumannii* and *P. aeruginosa* with over 90% inhibition recorded at

the highest concentration tested (71 μM). *K. pneumoniae* was also significantly influenced by CC-AMP1 at the highest concentration tested with 83.7% inhibition observed. CC-AMP1 was able to inhibit *A. baumannii* by greater than 90% at concentrations as low as 8.875 μM.

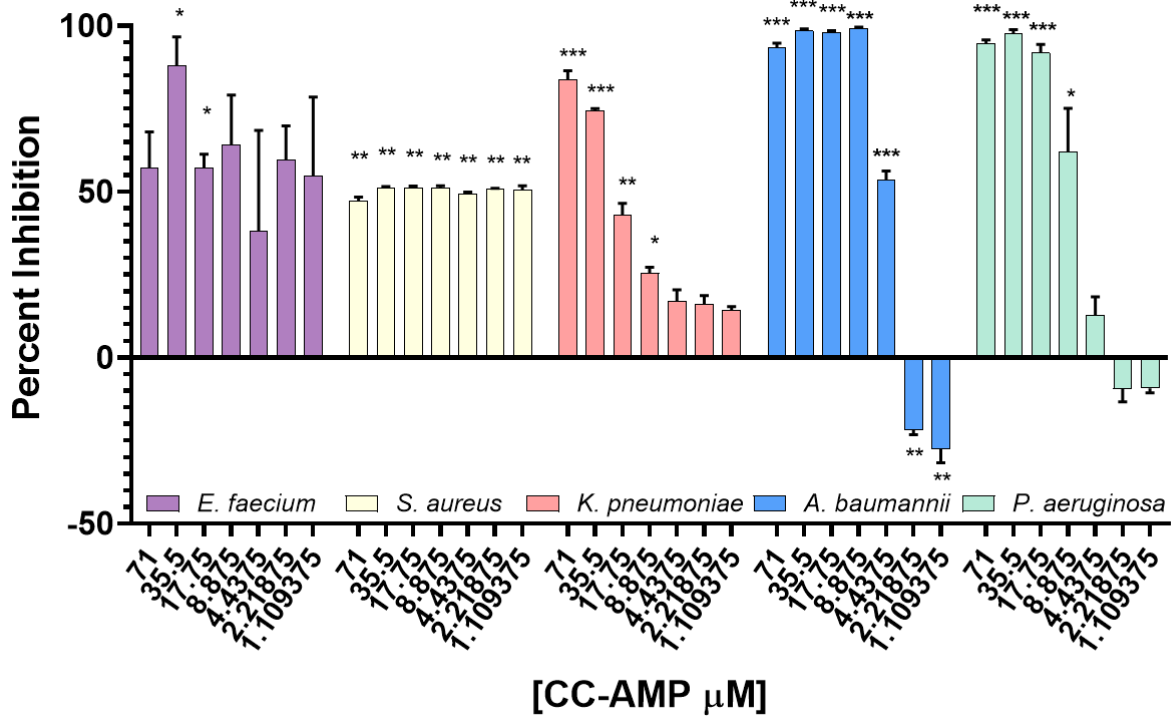


**Figure 47. Bioactivity of *Capsicum chinense x frutescens* CC-AMP1 Peptide Against ESKAP.** Data is represented as percent inhibition compared to no drug controls following treatment with CC-AMP at various concentrations. Data points represent the average of 3 biological replicates per species. Error bars represent the mean ±SEM of the three replicates. Asterisks represent P-value using Student’s t-test. P-value <0.05 \*, <0.01 \*\*, <0.001 \*\*\*.

This led us to perform an MBC against *A. baumannii* to gain an understanding of the MOA of the peptide, distinguishing if it functions as a bactericidal or bacteriostatic peptide. From this data it was determined that the peptide was acting as a bactericidal agent against the Gram-negative isolates as demonstrated by *A. baumannii* in **Figure 48**. From the dose

dependent testing shown in **Figure 47**, the MIC against *A. baumannii* was defined as 8.875 $\mu$ M. As shown in **Figure 48**, at this concentration (between 17.2 $\mu$ M and 8.6 $\mu$ M), 0% recovery is observed and therefore at the MIC, CC-AMP1 is acting as a bactericidal peptide and killing the bacterial population. The peptide was able to eradicate over 90% of the bacterial cells at concentrations ranging from 68.8 $\mu$ M-4.3  $\mu$ M, further validating this bactericidal MOA. Based on the similar levels of inhibition observed for *K. pneumoniae*, *P. aeruginosa* and *E. cloacae* when compared to *A. baumannii*, it is reasonable to predict that CC-AMP1 is also acting as a bactericidal peptide against the remaining Gram-negative ESKAPE pathogens. Within the CC plant, using the PepSAVI-MS approach, we have identified an AMP that specifically targets Gram-negative microorganisms and acts bactericidally at low concentrations. This provides another example of the power of using bioinformatics and the PepSAVI-MS approach to discover AMPs from ethnobotanical plant species and demonstrates how downstream biological testing can help define the MOA of those peptides.

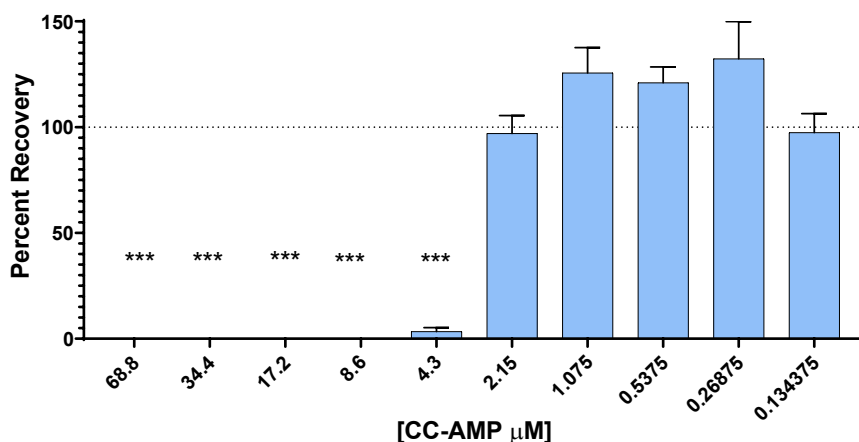


**Figure 48. Bactericidal Activity of CC-AMP1 Against *A. baumannii*.** Data is represented as percent recovery following treatment with CC-AMP at various concentrations. Data points represent the average of 3 biological replicates. Error bars represent the mean  $\pm$ SEM of the three replicates. Asterisks represent P-value using Student's t-test comparing CFU/mL of treated samples to no-drug controls. P-value <0.05 \*, <0.01 \*\*, <0.001 \*\*\*.

## Discussion

Plants have been used since ancient times to treat human ailments, some of which are still used today, such as garlic and honey. For example, in the fifth century B.C. Hippocrates documented nearly 400 medicinal plants in detail[318]. Further, it is estimated that there are between 250,000-500,000 species of plant on earth[301] leaving many/most to be explored for medicinal purposes. Although there are currently no plant-derived commercially available antibiotics, there are various plant-based compounds used to treat human disease. Arguably, the most widely known is aspirin, isolated from willow bark.

Antimicrobial peptides (AMPs) are small polymers consisting of amino acids that are produced by all forms of life and possess antimicrobial activity. AMPs have served therapeutically as a defense against invading bacterial pathogens since the introduction of Gramicidin in 1939. Since then, various antimicrobial agents have been sourced from natural materials including soil bacteria, plants, humans, and all forms of multicellular life. For this study, we have attempted to harness the medicinal properties from plant species in the form of AMPs in an attempt to combat the high levels of drug resistance seen for the ESKAPE pathogens in the post-antibiotic era[319, 320].

Herein we have investigated the antibacterial potential of over 20 species of plant using a novel PepSAVI-MS approach that has evolved over the past five years. The approach, validated in 2017, has revealed multiple species of plant that contain novel RiPPs. The

advantage to using this approach is highlighted when it is compared to other approaches to natural product drug discovery. For example, bioassay guided fractionation is considered a gold standard for natural products drug discovery. This approach initially involves the isolation of material followed by bioactivity testing[321]. The bioactive samples are then scaled up and re-tested for bioactivity. If still active, the sample is subject to numerous rounds of chromatographic fractionation and subsequent bioactivity testing until a single compound is deemed responsible for the activity[321]. The structure of this compound is then deciphered, and the compound is further characterized for an MOA. In theory, this is an excellent approach, however, multiple rounds of fractionation are time consuming and result in the loss of sample each round. Further, many times the activity of the compound is lost following fractionation due to the necessity of certain compounds to interact with others to become toxic to the target organism, or the effects of two compounds are additive and lead to the activity observed. Finally, the tedious effort often results in the isolation of a compound that has already been discovered. The PepSAVI-MS approach differs in that the initial isolation and testing step is eliminated. Samples are initially fractionated and therefore bioactivity can be assigned to a smaller pool of peptides very rapidly. There is also a lesser chance for false positive results due to interacting or codependent peptides.

Over time our approach has evolved to become more efficient in identifying plant species containing novel AMPs. This came in the form of screening pooled single fractions against the ESKAPE pathogens and led to rapidly identifying plant species of interest prior to implementing the full power of the PepSAVI-MS system. For example, during our

investigation, the samples from the *Mentha*, *Hyoscyamus*, *Silybum*, and *Calendula* genre demonstrated broad-spectrum antibacterial properties and are considered plants of interest for the PepSAVI-MS pipeline. Conversely, samples from the genre *Nasturtium*, *Trifolium*, *Chichorium*, *Dodonaea*, and *Urtica* yielded negligible bioactivity and could be eliminated from further investigation. The categorization of nine plant species based on bioactivity was therefore possible within one day. This can be compared to the minimum of two weeks necessary to screen all nine species of plant against all six ESKAPE pathogens if libraries of 47 fractions were initially tested.

The validated PepSAVI-MS pipeline was used to identify a novel peptide of the *Amaranthus tricolor* (ATr) plant species which was published in 2019[314]. This peptide is a proline rich RiPP AMP that exists in multiple peptidoforms in ATr. Proline-rich AMPs are unique in that many are able to inhibit microorganisms without membrane disruption and instead have targets within the cell that ultimately lead to cell death[89, 322]. The identification of proline-rich AMPs within plants is relatively new, as the first one was identified in *Brassica napus* in 2015[323]. The proline-rich AMP of ATr, ATr-AMP1, was found to exist as heterogeneous population with multiple isoforms that were partially purified and demonstrated inhibitory activity against *E. coli* and *S. aureus*[314]. ATr-AMP1 is the second known AMP of ATr to be isolated and to demonstrate antimicrobial activity. The PepSAVI-MS approach allowed for an unbiased look at this species that confirmed the therapeutic potential of this plant. The MOA of ATr-AMP1 has yet to be characterized, although this is a point of interest in our ongoing efforts. We will investigate whether the

peptide indeed acts as other proline-rich AMPs to influence bacterial cells internally without inducing membrane lysis.

The investigation that led to the identification of ATr-AMP1 then led us to consider this species in more depth via transcriptome mining and proteomic validation. This resulted in the identification of seven AMPs[315] and included one unclassified AMP, two snakins, a defensin, and three lipid transfer proteins[316]. These were identified via bottom-up and top-down proteomics. Bottom-up proteomics works to enumerate all peptides within the plant sample, which are then compared to *in silico* predicted AMPs of ATr. Following this, top-down proteomics enables the visualization of post-translational modifications (PTMs) and full-length peptides in various isoforms. Two of the AMPs identified through these studies were evaluated for bioactivity against the ESKAPE pathogens. Specifically, ATr-LTP1, a lipopeptide, was determined to have activity against *K. pneumoniae*, however, an MIC was not able to be established. This level of activity was not surprising, however, based on previous studies investigating homologs of this lipopeptide reporting similarly low levels of bioactivity[324, 325].

The other peptide identified via top-down proteomics was a defensin (ATr-Def1) however the concentration of peptide was too low to isolate and purify in its native form. Therefore, a truncated version containing the gamma core region of the peptide was synthesized and assessed for bioactivity. It has been shown that the gamma core of defensins alone are less effective at inhibiting target organisms than their full-length parent peptides, but they do function as a predictor of antimicrobial activity[326]. Thus, screening the gamma-

core region alone would allow us to determine whether the full-length peptide was worth pursuing further without the difficulty of extracting the lowly expressed peptide possessing PTMs. Screening of ATr-Def1 revealed activity against *S. aureus* which prompted us to attempt to determine whether the peptide would be stable in human serum and therefore a good candidate for *in vivo* applications. In order to do this, purified peptide was added directly to human serum and evaluated via mass spectrometry at various timepoints. Although purified peptide in buffer could be detected on the mass spectrometer, there was no detection within the serum/peptide mixture indicating that either that peptide itself is degraded very rapidly in serum (within 10 minutes) or it is aggregating with other peptides or proteins within the human serum (data not shown). Therefore, although we see Gram-positive activity, ATr-Def1 in its truncated form is not an ideal candidate and further testing with the native peptide is necessary to fully understand the potential of this AMP as a therapeutic.

A similar approach to peptide identification was implemented in *C. chinense x frutescens* (CC) and revealed yet another AMP candidate with potential. Transcriptome mining of the translated proteome of the closest relative, *C. chinense*, *in silico* led to the validation of 15 AMPs present within CC via bottom-up proteomics[317]. In addition to this, two novel AMPs were identified with little homology to known AMPs. One of those, CC-AMP1 was tested and found to be Gram-negative specific and to function as a bactericidal agent. Based on these results, our collaborators further characterized the MOA of CC-AMP1 by performing membrane permeability assays and determined that the bactericidal activity was due to a membrane permeabilizing event of both the outer and inner

membranes[317]. Future studies to characterize this AMP will be aimed at determining whether this AMP is effective at inhibiting fungal isolates as well. Members of the *Capsicum* genus have been described as having medicinal properties most widely due to the production of capsaicin. It is not a peptide itself, but has been shown to have antibacterial activity against *Bacillus subtilis* functioning through membrane disruption[327] similar to CC-AMP1. The *Capsicum chinense* x *frutescens* species specifically is able to relieve pain associated with arthritis, gastritis, indigestion, and many other disorders[327]. Further, although most treatments involve the use of the fruit or the entire plant, where capsaicins are produced, leaves of the *C. frutescens* species have been used to treat boils, abscesses and wounds in the Fijian culture[328]. This antibacterial activity is in line with the antibacterial activity we observe from the CC-AMP1 peptide isolated from the aerial tissue of the pre-fruiting plant. Thus, the healing properties within the leaves of *C. frutescens* used by the Fijians could be due to the presence of bioactive AMPs.

Over the years our collaboration with the Hicks Laboratory at UNC-Chapel Hill has provided the data necessary to prove the usefulness and versatility of the PepSAVI-MS pipeline to identify RiPP AMPs effective against multi-drug resistant bacteria. Consequently, this contributes to the knowledge and diversity in which this pipeline can be applied. We have also worked to troubleshoot and enhance the efficiency of the pipeline through more targeted approaches which implement bioinformatics and full coverage forms of mass spectrometry to identify leads. Allowing for this system to evolve has led to the identification of novel bioactive peptides that are now ready for full

characterization as potential therapeutics. Throughout this process we have identified various plant species with a plethora of unclassified AMPs that simply need investigating. This project serves as a foundation for future studies, generating leads for the next phase of success using PepSAVI-MS. Ongoing investigations will continue to unveil novel peptide products that will contribute to the ongoing fight against multi-drug resistant bacteria while contributing legitimizing knowledge to our understanding of medicinal plants.

## **Chapter 5: Concluding Remarks and Future Directions**

### **Final Discussion**

**Chapter 2.** *Acinetobacter baumannii* is a multi-drug resistant pathogen responsible for a variety of diseases, but it is most known for its ability to resist carbapenem and its high transmissibility in hospitals. This organism is responsible for thousands of deaths yearly within the United States alone. The difficulty in treating *A. baumannii* infections of multi-drug resistant strains is exacerbated when the infection manifests in the form of a biofilm. Bacterial biofilms are known to be 1000x more resistant than their planktonically growing counterparts due to innate tolerance. This is in the form of an extracellular matrix (ECM) produced during biofilm formation that consists of polysaccharides, eDNA and proteins, all creating a seemingly impenetrable barrier of protection for the bacterial population dwelling within.

In order to identify factors important for biofilm formation in *A. baumannii*, a variety of transposon mutants were screened for their ability to form biofilms. We were able to randomly select 2,648 mutants out of a pool of 10,000 and categorize them phenotypically. Categories consisted of putative positive effectors of biofilm with mutants exhibiting decreased biofilm formation and putative negative effectors of biofilm formation that were unable to produce biofilms with substantial biomass. This analysis

led to the identification of over 100 strains, nearly 50 of which were verified to generate a biofilm biomass that was either 2-fold greater or 2-fold lesser than the biofilm formed by the wildtype AB5075 strain. From this group, 16 were pursued for ECM characterization.

Of these mutant strains, eight are presumed negative effectors and eight were presumed positive effectors of biofilm formation. Specifically, each was assessed for their adherence capacity through real-time tracking of impedance. In addition to this, eDNA composition of mature biofilms was quantified and protein and polysaccharide content was assessed at late and early-stage biofilm formation. Each mutant exhibited a unique ECM profile based on these results that was then used to implicate their roles in the biofilm formation process of *A. baumannii*.

Our approach was validated in part by the observation that four different *tn* insertion mutants of the biofilm associated protein Bap, were deficient in biofilm formation. Further, we observed a decrease in eDNA within the *bap::tn* mutant strain. Due to the essentiality of Bap in stabilizing mature biofilms formed by *A. baumannii*, we predict that Bap could serve as a scaffold for eDNA binding within mature biofilms and contribute to biofilm stability, in part, through this mechanism.

We have also identified an uncharacterized lysogenic phage within AB5075 that contributes to biofilms formation likely through cell lysis as a means of contributing ECM components to strengthen the biofilm as has been shown in other organisms[182-184]. Further, we show that peptidoglycan editing as well as amino acid transport contribute to

the formation and maintenance of *A. baumannii* biofilms. We also reveal a variety of metabolic enzymes that positively and negatively influence biofilms produced by AB5075. Specifically, it was found that *gapN::tn*, typically expressed when levels of free phosphate ions are low, formed a weakened biofilm. Therefore, it is probable that phosphate limitation and resulting metabolic shifts induce biofilm formation. Alternatively, the gene adjacent to *gapN*, *gntK*, is involved in producing intermediates of the Entner-Doudoroff pathway of carbon metabolism and negatively influences biofilm formation likely through the indirect downregulation of polysaccharide production.

This work has also implicated a necessity for an intact SOS response system for proper biofilm formation. Conversely, we have shown that a member of the DNA damage response negatively impacts biofilm formation, likely through the repression of another biofilm effector (*ddrR*) that positively regulates biofilm associated genes. A similar mechanism is proposed for an uncharacterized transcription factor that is adjacent to a gene that is upregulated in *A. baumannii* biofilms. We were also able to demonstrate that the over initiation of translation and dysregulation of replication lead to increases in biofilm biomass. Finally, we have begun to characterize a component of a putative type IV secretion system that when disrupted, alters the biofilm architecture, and likely leads to bacterial aggregation instead of adherence.

Out of over 2,600 mutants investigated, the biofilm formed by the *uspG::tn* mutant (referred to as *usp::tn* in Chapter 2) was the most substantial. Specifically, this strain was able to form a biofilm with over 8-fold more biomass than the wildtype AB5075 strain. This

prompted a full investigation into the functionality of this newly discovered universal stress protein of *A. baumannii* and served as the topic of Chapter 3. In doing so, we have uncovered links between UspG and some of the tn mutants characterized in this chapter that may help to better explain the biofilm phenotypes demonstrated and will be discussed in brief in the following section.

There are still many questions that remain concerning the mechanism behind biofilm formation and maintenance in *A. baumannii* due to the complexity, however, this work has uncovered key proteins that influence this system. It is the hope that these findings will contribute to our ability to fight these infections through our contribution of new molecular targets for biofilm eradication.

**Chapter 3.** Universal stress proteins are as the name suggests, universally expressed following exposure to a variety of different stresses. Our initial investigation into biofilm effectors of *A. baumannii* led to the identification of an uncharacterized member of the Usp (UspA) family (Pfam PF00582). Our results indicated the role of UspG as a negative effector of biofilm formation based on the increase in biofilm formation of over 8-fold in the tn mutant strain. This was surprising due to the demonstration of other organisms such as *P. aeruginosa* showing an increase in Usp expression in biofilms[210, 211]. Arguably, the most drastic phenotype observed was the defect in growth accompanied by a large spike in adhesion. Within the *uspG::tn* mutant, we see the upregulation of *pgaA*, which is involved in polysaccharide formation and is an important structural component of biofilms, particularly during the earlier stages of adherence[44]. In addition, we see an

upregulation in a variety of ribosomal genes, which is also observed in biofilms formed by *A. baumannii*[44]. However, genes shown to be upregulated in biofilms of *A. baumannii* were conversely downregulated in our *uspG::tn* strain following 3-hours of growth. For example, the *paa* operon as well as the *csu* operon are upregulated in biofilms but were downregulated in our study[44]. Therefore, UspG may be influencing certain components within the cell that lead to the dysregulated production of biofilm products without necessarily directly influencing the system overall. However, the *csu* operon is upregulated nearly 200-fold in the biofilm population of some *A. baumannii* strains compared to their planktonic counterparts[44] indicating that their downregulation in our planktonic population may be a result of the growth arrested state instead of UspG specific influence.

Another important phenotype observed was the inability of *uspG::tn* strain to survive in the presence of blood. This indicates that survival within the host is dependent in some part to this regulator. In an assessment of *A. baumannii* virulence and survival within *Galleria mellonella*, a *tn* mutant of ABUW\_1763 (UspG herein, annotated as UspA in the cited work) was unable to survive[150], which supports this prediction.

**Chapter 4.** Plants serve as a valuable source for the discovery of novel AMPs with antibacterial properties due to their diversity, abundance, and previously described medicinal properties. RiPPs in particular are advantageous due to their target specificity, novel MOAs and natural origin[303, 329]. There are currently 41 classes of RiPPs across

the three domains of life and these numbers are projected to continue to rise[306] as more investigations such as ours are conducted.

In this study, we were able to identify a variety of plant species that conferred antibacterial activity against both Gram-positive and Gram-negative multi-drug resistant organisms. Further, the PepSAVI-MS approach allowed us to narrow in on specific peptide fractions containing RiPPs that are likely novel. It will be important to continue our investigation into these fractions.

Through the use of a rapid single fraction screening approach we were able to identify plant species from the genre *Mentha*, *Hyoscyamus*, *Silybum*, and *Calendula* as AMP producing plants of interest. The *Mentha* genus was found to be the most bioactive with inhibition observed against all members of the ESKAPE panel. There are nearly 30 species within this genre, many of which are known to possess medicinal qualities. Members of the *Mentha* genus have been tested for antibacterial activity following essential oil extraction. The major components within the essential oils were found to be phenolic compounds. To our knowledge, this is the first instance for AMP screening within this genus.

## **Future Directions**

**Chapter 2.** The investigation into the biofilm forming mechanics of *A. baumannii* has revealed nearly 50 genes that influence biofilm formation in a statistically substantial way. Of these, only 16 underwent ECM and attachment profiling and one was subject to

classical molecular function assessment. This highlights the endless opportunities for future exploration based on the findings of this chapter. However, there are experiments that will validate a few of the presumed influences of the top genes that will further our understanding of biofilm formation.

We were able to uncover genes involved in the regulation of carbon metabolism and demonstrated that gluconate kinase *gntK* is a negative effector of biofilm formation in *A. baumannii* and its involvement leads to a decrease in polysaccharide production, perhaps through the accumulation of D-gluconate. Therefore, measuring levels of this metabolite will be implemented.

Alternatively, *gapN*, a non-phosphorylating NADP<sup>+</sup> dependent glyceraldehyde-3-phosphate dehydrogenase positively influences biofilm formation. Specifically, GapN leads to the production of 3-phosphoglycerate through a modified Entner-Doudoroff pathway that can produce NADH when levels of inorganic phosphate are low. Therefore, levels of free phosphate within *A. baumannii* biofilms will be evaluated.

Additionally, *mmsA1*, encoding methylmalonate semialdehyde dehydrogenase that is involved in the citrate cycle as well as other metabolic pathways was found to be a positive regulator of surface-liquid interface biofilm formation but also a negative regulator of pellicle formation, in effect, acting as a metabolic switch to induce changes in population behavior based on changes to metabolism. This was exhibited within the *mmsA1::tn* mutant in which a hypermucoviscous pellicle was formed at the expense of surface

attachment. We predict that the pellicle is composed of polysaccharides due to the consistency of the culture pellicle and previous literature on the subject, but this is yet to be verified experimentally. However, in Chapter 3, when investigating the influence of *uspG::tn* on exponential growth, we observed a substantial decrease in *mmsA1* transcription (downregulation of over 100-fold) as well as an upregulation of *pgaA*, responsible for polysaccharide production in the *uspG::tn* mutant strain. This is accompanied by the observation of increased biofilm formation by the *uspG::tn* mutant that was found to be in part due to the overproduction of polysaccharides, particularly in the initial stages of biofilm formation.

**Chapter 3.** First, it will be important to understand and address the lack of full complementation in the *uspG+* (C) strain. This inability to complement wildtype phenotypes fully is observed for other Usp genes in *A. baumannii* such as UspA in ATCC17978 but was also demonstrated in a study of virulence within AB5075[150]. This inability to complement the same gene (ABUW\_1763) in the same background (AB5075) using an alternate vector highlights a universal problem. However, ways to combat this will be to explore other vectors, for example multi-copy plasmids or a plasmid with an inducible promoter that can be overexpressed. Further, the construct designed in this study contains a histidine tag that could be interfering with the ability of the protein to form dimers or interact with other proteins that elicit its function. To investigate this, different techniques for tag attachment will be explored. For example, adding the histidine marker to the other end of the protein. A tag is important because of our next set of future

directions that include the investigation of interaction partners, ligands, and dimerization activity.

Specifically, it will be of great interest to determine interaction partners of UspG through *in silico* predictions followed by protein purification and pull-down experiment to determine the interaction partners using LCMS/MS. The *in silico* analysis will identify proteins within the translated genome of AB5075 that contain a Usp domain. It will also be important to determine whether, like Usps of *E. coli*, heterodimerization occurs between different Usp paralogs of *A. baumannii*. Further, although it is highly likely, it will be necessary to confirm the interaction of UspG with itself. These interaction studies can be performed using a bacterial two-hybrid (BATCH) approach. Following the pull-down experiments to identify interaction partners, the BATCH approach can be implemented to confirm these interactions. Further, specific residues of UspG responsible for the interactions will be assessed through the use of site-directed mutagenesis on both UspG and the defined interaction partner.

Purified UspG will also be used to assess ligand partners, in particular whether phosphorylation occurs and if ATP or AMP binding is possible. Further, identifying the exact conditions of stress that induce transcription will be determined. This can be achieved through qPCR analysis following exposure to a variety of stressors. In particular, oxidative stress, aminoglycoside exposure, biocide exposure, and heat exposure.

It will be of interest to investigate the role of UspG in desiccation survival, which is a major contributor of *A. baumannii* infection rates and transmission. We predict that UspG is upregulated under these conditions and likely under the control of BfmR. This is partly due to evidence that BfmR, a response regulator that mediates desiccation tolerance, also regulates stress responses such as nutrient starvation and oxidative stress[74], each of which are influenced by UspG.

Long-term studies would be aimed at investigating the regulators of UspG. Based on our findings, these are likely linked to other regulators of oxidative stress. This includes investigating the implication of Zur and zinc limitation in controlling the expression of *uspG*. This hypothesis is based on the observation that  $\Delta zur$  is unable to resist oxidative stress and has higher levels of ROS produced[330]. Levels of glutathione were also increased along with ratios of NAD<sup>+</sup>/NADH and ADP/ATP, which could be similar to our *uspG::tn* strain.

Finally, evaluating the protein composition of the *uspG::tn* mutant strain as compared to AB5075 using proteomics during early and late exponential phase will uncover insights into the influence of UspG. In particular we will further understand the unique role UspG plays during exponential phase, which is unique to this species. Evaluating the metabolome of *uspG::tn* and AB5075 will also validate some of our questions concerning the metabolic and energetic state of the cell in the absence of UspG. We can evaluate if ATP pools or cofactor ratios are skewed to reflect a state of oxidative stress in the mutant strain. We will also be able to detect whether acetate is accumulated. ROS levels, which

we predict to be upregulated will also be quantified using the 2',7'-dichlorofluorescein diacetate or hydroxylphenyl fluorescein dyes[331]. Antioxidant tracking kits are also available and could be used to validate the lower levels of catalase and superoxide dismutase observed transcriptionally in the *uspG::tn* mutant. By evaluating the transcription and production of these factors in the *uspG::tn* mutant following exposure to a variety of stresses that induce *uspG* expression we will determine whether these components of the oxidative stress response are under the control of UspG.

To understand the role of UspG in biofilm regulation and the increase in biofilm formation observed in the *uspG::tn* strain, levels of glutamate should will be assessed, as this could hold the key to better biofilm formation. Glutamate is necessary for the formation of peptidoglycan and may influence the cell envelope as a whole. We predict that glutamate is accumulated within our *uspG*- (M) based on the upregulation of *putA*, which converts proline to L-glutamate in addition to the upregulation of *pgaA*.

Diguanylate cyclase is also a contributor to biofilm formation through the formation of cyclic di-GMP which accumulates to signal biofilm formation in a variety of bacteria. A gene encoding diguanylate cyclase is located directly adjacent to *uspG*, and was upregulated nearly 10-fold in the *uspG::tn* mutant following 3 hours of growth. Therefore, it is probably that expression is translated to cyclic di-GMP production and thus the increased biofilm phenotype observed. Specifically, diguanylate cyclase is accumulated within biofilms and acts as a secondary messenger to induce a variety of biofilm promoting factors that promote motility, adhesins and capsule production[23]. Based on the

upregulation of this gene, we will investigate the cyclic di-GMP levels within the *uspG*-(M) strain with the prediction that levels will be elevated.

**Chapter 4.** Investigating the components of species of plant that exhibited bioactivity will be important to continue our efforts of AMP discovery. In particular, investigating the *Mentha*, *Hyoscyamus*, and *Calenula* genre samples for antibacterial activity through generating and screening fully fractionated libraries against the ESKAPE panel. From this, we will be able to isolate and purify leads similar to the approach taken for ATr and CC samples. Identifying the bioavailability of the lead AMPs identified within this work will also be a goal of this project. Through determining the stability within serum as well as their toxicity towards human cell lines and hemolytic properties we will have a better understanding of their therapeutic potential.

We have also uncovered fractions within the fractionated libraries that require follow up screening to identify the RiPPs contributing to the antibacterial activity observed. For example, antibacterial activity against *A. baumannii* and *K. pneumoniae* was isolated to fractions 18-23 of the *Silybum* spp. library. Further, fractions 26 and 33 of the *Linum* spp. library contain RiPPs with activity against *E. cloacae*. These samples should be integrated back into the pipeline for statistical analysis to quantify abundance via LCMS/MS. This should then be followed up with purification of the bioactive peptide or peptides and finally sequence and structure elucidation. Throughout this process, peptides will be screened for their inhibitory activity.

Long term goals of this project include upscaling the scope of ethnobotanical species to enter the pipeline. By increasing the number of plant species tested using the pooled, single fraction screening approach, we will have more opportunities to uncover novel AMPs more quickly. For example, up to 18 species of plant can be tested in biological triplicate against a single species of bacteria using a 96-well plate format that includes anti-evaporation measures and the proper controls. Another approach could be the generation of single fraction plant libraries containing 56 different AMP samples to be screened in a high-throughput manner against the EKSAPe pathogens. In essence, a 96-well plate-based library of plant species could further fast-track the bioactive plant identification process and would reveal which are effective against which of the ESKAPE pathogens. Without screening in biological triplicate, material would be saved, however variations in bioactivity due to bio replicate variability would need to be considered when analyzing results. This variability could be calculated using the average variation of a single species across biological replicates using all previous screens. Therefore, the PepSAVI-MS approach would be employed more efficiently, only generating fully fractionated libraries for the plant species with the most potential based on the target organism of interest.

## References

1. Hall-Stoodley, L., J.W. Costerton, and P. Stoodley, *Bacterial biofilms: from the Natural environment to infectious diseases*. Nature Reviews Microbiology, 2004. **2**(2): p. 95-108.
2. Vestby, L.K., et al., *Bacterial Biofilm and its Role in the Pathogenesis of Disease*. Antibiotics (Basel), 2020. **9**(2).
3. Li, X.H. and J.H. Lee, *Antibiofilm agents: A new perspective for antimicrobial strategy*. J Microbiol, 2017. **55**(10): p. 753-766.
4. Moser, C., et al., *Biofilms and host response - helpful or harmful*. APMIS, 2017. **125**(4): p. 320-338.
5. Donlan, R.M., *Biofilm formation: a clinically relevant microbiological process*. Clin Infect Dis, 2001. **33**(8): p. 1387-92.
6. Ruhai, R. and R. Kataria, *Biofilm patterns in gram-positive and gram-negative bacteria*. Microbiol Res, 2021. **251**: p. 126829.
7. Lopes, S.P., N.F. Azevedo, and M.O. Pereira, *Quantitative assessment of individual populations within polymicrobial biofilms*. Sci Rep, 2018. **8**(1): p. 9494.
8. Peters, B.M., et al., *Polymicrobial interactions: impact on pathogenesis and human disease*. Clin Microbiol Rev, 2012. **25**(1): p. 193-213.
9. Hauser, A.R., et al., *Clinical significance of microbial infection and adaptation in cystic fibrosis*. Clin Microbiol Rev, 2011. **24**(1): p. 29-70.

10. Alves, P.M., et al., *Interaction between Staphylococcus aureus and Pseudomonas aeruginosa is beneficial for colonisation and pathogenicity in a mixed biofilm*. Pathog Dis, 2018. **76**(1).
11. Korgaonkar, A., et al., *Community surveillance enhances Pseudomonas aeruginosa virulence during polymicrobial infection*. Proc Natl Acad Sci U S A, 2013. **110**(3): p. 1059-64.
12. Wang, R., *Biofilms and Meat Safety: A Mini-Review*. J Food Prot, 2019. **82**(1): p. 120-127.
13. Abebe, G.M., *The Role of Bacterial Biofilm in Antibiotic Resistance and Food Contamination*. Int J Microbiol, 2020. **2020**: p. 1705814.
14. Yaron, S. and U. Romling, *Biofilm formation by enteric pathogens and its role in plant colonization and persistence*. Microb Biotechnol, 2014. **7**(6): p. 496-516.
15. Teschler, J.K., et al., *Living in the matrix: assembly and control of Vibrio cholerae biofilms*. Nat Rev Microbiol, 2015. **13**(5): p. 255-68.
16. Rago, L., et al., *Bioelectrochemical Nitrogen fixation (e-BNF): Electro-stimulation of enriched biofilm communities drives autotrophic nitrogen and carbon fixation*. Bioelectrochemistry, 2019. **125**: p. 105-115.
17. Chen, S., et al., *Bioelectrochemical Fixation of Nitrogen to Extracellular Ammonium by Pseudomonas stutzeri*. Appl Environ Microbiol, 2021. **87**(5): p. e0199820.
18. Maunders, E. and M. Welch, *Matrix exopolysaccharides; the sticky side of biofilm formation*. FEMS Microbiol Lett, 2017. **364**(13).

19. Monds, R.D. and G.A. O'Toole, *The developmental model of microbial biofilms: ten years of a paradigm up for review*. Trends Microbiol, 2009. **17**(2): p. 73-87.
20. Gupta, P., et al., *Biofilm, pathogenesis and prevention--a journey to break the wall: a review*. Arch Microbiol, 2016. **198**(1): p. 1-15.
21. Greene, C., et al., *Evaluation of the ability of Acinetobacter baumannii to form biofilms on six different biomedical relevant surfaces*. Lett Appl Microbiol, 2016. **63**(4): p. 233-9.
22. Cerca, N., et al., *Quantitative analysis of adhesion and biofilm formation on hydrophilic and hydrophobic surfaces of clinical isolates of Staphylococcus epidermidis*. Res Microbiol, 2005. **156**(4): p. 506-14.
23. Cho, K.H., R.G. Tryon, and J.H. Kim, *Screening for Diguanylate Cyclase (DGC) Inhibitors Mitigating Bacterial Biofilm Formation*. Front Chem, 2020. **8**: p. 264.
24. Bordi, C. and S. de Bentzmann, *Hacking into bacterial biofilms: a new therapeutic challenge*. Ann Intensive Care, 2011. **1**(1): p. 19.
25. Fournier, P.E. and H. Richet, *The epidemiology and control of Acinetobacter baumannii in health care facilities*. Clin Infect Dis, 2006. **42**(5): p. 692-9.
26. Wong, D., et al., *Clinical and Pathophysiological Overview of Acinetobacter Infections: a Century of Challenges*. Clin Microbiol Rev, 2017. **30**(1): p. 409-447.
27. Dijkshoorn, L., A. Nemec, and H. Seifert, *An increasing threat in hospitals: multidrug-resistant Acinetobacter baumannii*. Nat Rev Microbiol, 2007. **5**(12): p. 939-51.

28. Ayoub Moubareck, C. and D. Hammoudi Halat, *Insights into Acinetobacter baumannii: A Review of Microbiological, Virulence, and Resistance Traits in a Threatening Nosocomial Pathogen*. *Antibiotics*, 2020. **9**(3): p. 119.
29. Camp, C. and O.L. Tatum, *A Review of Acinetobacter baumannii as a Highly Successful Pathogen in Times of War*. *Laboratory Medicine*, 2010. **41**(11): p. 649-657.
30. Scott, P., et al., *An outbreak of multidrug-resistant Acinetobacter baumannii-calcoaceticus complex infection in the US military health care system associated with military operations in Iraq*. *Clin Infect Dis*, 2007. **44**(12): p. 1577-84.
31. Berlau, J., et al., *Isolation of Acinetobacter spp. including A. baumannii from vegetables: implications for hospital-acquired infections*. *J Hosp Infect*, 1999. **42**(3): p. 201-4.
32. La Scola, B. and D. Raoult, *Acinetobacter baumannii in human body louse*. *Emerg Infect Dis*, 2004. **10**(9): p. 1671-3.
33. Corbella, X., et al., *Relevance of digestive tract colonization in the epidemiology of nosocomial infections due to multiresistant Acinetobacter baumannii*. *Clin Infect Dis*, 1996. **23**(2): p. 329-34.
34. Berlau, J., et al., *Distribution of Acinetobacter species on skin of healthy humans*. *Eur J Clin Microbiol Infect Dis*, 1999. **18**(3): p. 179-83.
35. Yavankar, S.P., K.R. Pardesi, and B.A. Chopade, *Species distribution and physiological characterization of Acinetobacter genospecies from healthy human skin of tribal population in India*. *Indian J Med Microbiol*, 2007. **25**(4): p. 336-45.

36. Sievert, D.M., et al., *Antimicrobial-resistant pathogens associated with healthcare-associated infections: summary of data reported to the National Healthcare Safety Network at the Centers for Disease Control and Prevention, 2009-2010*. *Infect Control Hosp Epidemiol*, 2013. **34**(1): p. 1-14.
37. Spellberg, B. and J.H. Rex, *The value of single-pathogen antibacterial agents*. *Nat Rev Drug Discov*, 2013. **12**(12): p. 963.
38. Weiner-Lastinger, L.M., et al., *Antimicrobial-resistant pathogens associated with adult healthcare-associated infections: Summary of data reported to the National Healthcare Safety Network, 2015-2017*. *Infect Control Hosp Epidemiol*, 2020. **41**(1): p. 1-18.
39. McDonald, L.C., S.N. Banerjee, and W.R. Jarvis, *Seasonal variation of Acinetobacter infections: 1987-1996*. *Nosocomial Infections Surveillance System*. *Clin Infect Dis*, 1999. **29**(5): p. 1133-7.
40. Maragakis, L.L. and T.M. Perl, *Acinetobacter baumannii: epidemiology, antimicrobial resistance, and treatment options*. *Clin Infect Dis*, 2008. **46**(8): p. 1254-63.
41. Mousa, M., et al., *Droplet aerosol dissemination of carbapenem-resistant Acinetobacter baumannii surrounding ventilated patients*. *Infect Control Hosp Epidemiol*, 2019. **40**(3): p. 365-367.
42. Blot, S., K. Vandewoude, and F. Colardyn, *Nosocomial bacteremia involving Acinetobacter baumannii in critically ill patients: a matched cohort study*. *Intensive Care Med*, 2003. **29**(3): p. 471-5.

43. Garnacho, J., et al., *Clinical impact of pneumonia caused by Acinetobacter baumannii in intubated patients: a matched cohort study*. Crit Care Med, 2003. **31**(10): p. 2478-82.
44. Colquhoun, J.M. and P.N. Rather, *Insights Into Mechanisms of Biofilm Formation in Acinetobacter baumannii and Implications for Uropathogenesis*. Frontiers in Cellular and Infection Microbiology, 2020. **10**(253).
45. Pelletier, M.R., et al., *Unique structural modifications are present in the lipopolysaccharide from colistin-resistant strains of Acinetobacter baumannii*. Antimicrob Agents Chemother, 2013. **57**(10): p. 4831-40.
46. Beceiro, A., et al., *Phosphoethanolamine modification of lipid A in colistin-resistant variants of Acinetobacter baumannii mediated by the pmrAB two-component regulatory system*. Antimicrob Agents Chemother, 2011. **55**(7): p. 3370-9.
47. Arroyo, L.A., et al., *The pmrCAB operon mediates polymyxin resistance in Acinetobacter baumannii ATCC 17978 and clinical isolates through phosphoethanolamine modification of lipid A*. Antimicrob Agents Chemother, 2011. **55**(8): p. 3743-51.
48. Adams, M.D., et al., *Resistance to colistin in Acinetobacter baumannii associated with mutations in the PmrAB two-component system*. Antimicrob Agents Chemother, 2009. **53**(9): p. 3628-34.
49. Moffatt, J.H., et al., *Colistin resistance in Acinetobacter baumannii is mediated by complete loss of lipopolysaccharide production*. Antimicrob Agents Chemother, 2010. **54**(12): p. 4971-7.

50. Abdi, S.N., et al., *Acinetobacter baumannii Efflux Pumps and Antibiotic Resistance*. Infect Drug Resist, 2020. **13**: p. 423-434.
51. Kroger, C., et al., *Genetic Regulation of Virulence and Antibiotic Resistance in Acinetobacter baumannii*. Genes (Basel), 2016. **8**(1).
52. Hassan, K.A., et al., *Transcriptomic and biochemical analyses identify a family of chlorhexidine efflux proteins*. Proc Natl Acad Sci U S A, 2013. **110**(50): p. 20254-9.
53. Jimenez-Mejias, M.E., et al., *Cerebrospinal fluid penetration and pharmacokinetic/pharmacodynamic parameters of intravenously administered colistin in a case of multidrug-resistant Acinetobacter baumannii meningitis*. Eur J Clin Microbiol Infect Dis, 2002. **21**(3): p. 212-4.
54. Garnacho-Montero, J., et al., *Treatment of multidrug-resistant Acinetobacter baumannii ventilator-associated pneumonia (VAP) with intravenous colistin: a comparison with imipenem-susceptible VAP*. Clin Infect Dis, 2003. **36**(9): p. 1111-8.
55. Kalin, G., et al., *Comparison of colistin and colistin/sulbactam for the treatment of multidrug resistant Acinetobacter baumannii ventilator-associated pneumonia*. Infection, 2014. **42**(1): p. 37-42.
56. Bassetti, M., et al., *Therapeutic options for difficult-to-treat Acinetobacter baumannii infections: a 2020 perspective*. Expert Opin Pharmacother, 2021. **22**(2): p. 167-177.

57. Cerqueira, G.M., et al., *A global virulence regulator in Acinetobacter baumannii and its control of the phenylacetic acid catabolic pathway*. J Infect Dis, 2014. **210**(1): p. 46-55.
58. Mortensen, B.L., et al., *Acinetobacter baumannii response to host-mediated zinc limitation requires the transcriptional regulator Zur*. J Bacteriol, 2014. **196**(14): p. 2616-26.
59. Tuttobene, M.R., P. Cribb, and M.A. Mussi, *BlsA integrates light and temperature signals into iron metabolism through Fur in the human pathogen Acinetobacter baumannii*. Sci Rep, 2018. **8**(1): p. 7728.
60. Johnson, T.L., et al., *Acinetobacter baumannii Is Dependent on the Type II Secretion System and Its Substrate LipA for Lipid Utilization and *In Vivo* Fitness*. Journal of Bacteriology, 2016. **198**(4): p. 711-719.
61. Harding, C.M., et al., *Medically Relevant Acinetobacter Species Require a Type II Secretion System and Specific Membrane-Associated Chaperones for the Export of Multiple Substrates and Full Virulence*. PLoS Pathog, 2016. **12**(1): p. e1005391.
62. Mea, H.J., P.V.C. Yong, and E.H. Wong, *An overview of Acinetobacter baumannii pathogenesis: Motility, adherence and biofilm formation*. Microbiol Res, 2021. **247**: p. 126722.
63. Clemmer, K.M., R.A. Bonomo, and P.N. Rather, *Genetic analysis of surface motility in Acinetobacter baumannii*. Microbiology (Reading), 2011. **157**(Pt 9): p. 2534-2544.

64. Hood, M.I., et al., *Identification of an Acinetobacter baumannii zinc acquisition system that facilitates resistance to calprotectin-mediated zinc sequestration*. PLoS Pathog, 2012. **8**(12): p. e1003068.
65. Nairn, B.L., et al., *The Response of Acinetobacter baumannii to Zinc Starvation*. Cell Host Microbe, 2016. **19**(6): p. 826-36.
66. Williams, C.L., et al., *Characterization of Acinetobacter baumannii Copper Resistance Reveals a Role in Virulence*. Front Microbiol, 2020. **11**: p. 16.
67. Tiwari, V., M.R. Rajeswari, and M. Tiwari, *Proteomic analysis of iron-regulated membrane proteins identify FhuE receptor as a target to inhibit siderophore-mediated iron acquisition in Acinetobacter baumannii*. Int J Biol Macromol, 2019. **125**: p. 1156-1167.
68. Catel-Ferreira, M., et al., *The outer membrane porin OmpW of Acinetobacter baumannii is involved in iron uptake and colistin binding*. FEBS Lett, 2016. **590**(2): p. 224-31.
69. Russo, T.A., et al., *The K1 capsular polysaccharide of Acinetobacter baumannii strain 307-0294 is a major virulence factor*. Infect Immun, 2010. **78**(9): p. 3993-4000.
70. Harding, C.M., S.W. Hennon, and M.F. Feldman, *Uncovering the mechanisms of Acinetobacter baumannii virulence*. Nat Rev Microbiol, 2018. **16**(2): p. 91-102.
71. Wendt, C., et al., *Survival of Acinetobacter baumannii on dry surfaces*. J Clin Microbiol, 1997. **35**(6): p. 1394-7.
72. Catalano, M., et al., *Survival of Acinetobacter baumannii on bed rails during an outbreak and during sporadic cases*. J Hosp Infect, 1999. **42**(1): p. 27-35.

73. Denton, M., et al., *Role of environmental cleaning in controlling an outbreak of Acinetobacter baumannii on a neurosurgical intensive care unit*. J Hosp Infect, 2004. **56**(2): p. 106-10.
74. Farrow, J.M., 3rd, G. Wells, and E.C. Pesci, *Desiccation tolerance in Acinetobacter baumannii is mediated by the two-component response regulator BfmR*. PLoS One, 2018. **13**(10): p. e0205638.
75. Houang, E.T., et al., *Effect of desiccation on the ultrastructural appearances of Acinetobacter baumannii and Acinetobacter lwoffii*. J Clin Pathol, 1998. **51**(10): p. 786-8.
76. Feng, S.H., A. Stojadinovic, and M. Izadjoo, *Distinctive stages and strain variations of A. baumannii biofilm development under shear flow*. J Wound Care, 2013. **22**(4): p. 173-4, 176-8, 180-1.
77. Tomaras, A.P., et al., *Characterization of a two-component regulatory system from Acinetobacter baumannii that controls biofilm formation and cellular morphology*. Microbiology (Reading), 2008. **154**(Pt 11): p. 3398-3409.
78. Loehfelm, T.W., N.R. Luke, and A.A. Campagnari, *Identification and characterization of an Acinetobacter baumannii biofilm-associated protein*. J Bacteriol, 2008. **190**(3): p. 1036-44.
79. Harding, C.M., et al., *Pathogenic Acinetobacter species have a functional type I secretion system and contact-dependent inhibition systems*. Journal of Biological Chemistry, 2017. **292**(22): p. 9075-9087.

80. Bentancor, L.V., et al., *Identification of Ata, a multifunctional trimeric autotransporter of Acinetobacter baumannii*. J Bacteriol, 2012. **194**(15): p. 3950-60.
81. Choi, A.H., et al., *The pgaABCD locus of Acinetobacter baumannii encodes the production of poly-beta-1-6-N-acetylglucosamine, which is critical for biofilm formation*. J Bacteriol, 2009. **191**(19): p. 5953-63.
82. Iwashkiw, J.A., et al., *Identification of a general O-linked protein glycosylation system in Acinetobacter baumannii and its role in virulence and biofilm formation*. PLoS Pathog, 2012. **8**(6): p. e1002758.
83. Mangas, E.L., et al., *Pangenome of Acinetobacter baumannii uncovers two groups of genomes, one of them with genes involved in CRISPR/Cas defence systems associated with the absence of plasmids and exclusive genes for biofilm formation*. Microb Genom, 2019. **5**(11).
84. Dubos, R.J., *Studies on a Bactericidal Agent Extracted from a Soil Bacillus : li. Protective Effect of the Bactericidal Agent against Experimental Pneumococcus Infections in Mice*. J Exp Med, 1939. **70**(1): p. 11-7.
85. Dubos, R.J., *Studies on a Bactericidal Agent Extracted from a Soil Bacillus : I. Preparation of the Agent. Its Activity in Vitro*. J Exp Med, 1939. **70**(1): p. 1-10.
86. Bucki, R., et al., *Cathelicidin LL-37: a multitask antimicrobial peptide*. Arch Immunol Ther Exp (Warsz), 2010. **58**(1): p. 15-25.
87. Ilić, N., et al., *Selective antimicrobial activity and mode of action of adepantins, glycine-rich peptide antibiotics based on anuran antimicrobial peptide sequences*.

- Biochimica et Biophysica Acta (BBA)-Biomembranes, 2013. **1828**(3): p. 1004-1012.
88. Seefeldt, A.C., et al., *The proline-rich antimicrobial peptide Onc112 inhibits translation by blocking and destabilizing the initiation complex*. Nat Struct Mol Biol, 2015. **22**(6): p. 470-5.
89. Scocchi, M., A. Tossi, and R. Gennaro, *Proline-rich antimicrobial peptides: converging to a non-lytic mechanism of action*. Cell Mol Life Sci, 2011. **68**(13): p. 2317-30.
90. Wang, G., *Improved methods for classification, prediction, and design of antimicrobial peptides*. Methods Mol Biol, 2015. **1268**: p. 43-66.
91. Shen, B., *A New Golden Age of Natural Products Drug Discovery*. Cell, 2015. **163**(6): p. 1297-300.
92. Bernardini, S., et al., *Natural products for human health: an historical overview of the drug discovery approaches*. Nat Prod Res, 2018. **32**(16): p. 1926-1950.
93. Spradlin, J.N., E. Zhang, and D.K. Nomura, *Reimagining Druggability Using Chemoproteomic Platforms*. Accounts of Chemical Research, 2021. **54**(7): p. 1801-1813.
94. Nothias, L.F., et al., *Bioactivity-Based Molecular Networking for the Discovery of Drug Leads in Natural Product Bioassay-Guided Fractionation*. J Nat Prod, 2018. **81**(4): p. 758-767.
95. Kirkpatrick, C.L., et al., *The "PepSAVI-MS" Pipeline for Natural Product Bioactive Peptide Discovery*. Anal Chem, 2017. **89**(2): p. 1194-1201.

96. Kristensen, K., J.R. Henriksen, and T.L. Andresen, *Adsorption of Cationic Peptides to Solid Surfaces of Glass and Plastic*. PLOS ONE, 2015. **10**(5): p. e0122419.
97. Chico, D.E., R.L. Given, and B.T. Miller, *Binding of cationic cell-permeable peptides to plastic and glass*. Peptides, 2003. **24**(1): p. 3-9.
98. Kumar, P., J.N. Kizhakkedathu, and S.K. Straus, *Antimicrobial Peptides: Diversity, Mechanism of Action and Strategies to Improve the Activity and Biocompatibility In Vivo*. Biomolecules, 2018. **8**(1).
99. Tam, J.P., et al., *Antimicrobial Peptides from Plants*. Pharmaceuticals (Basel), 2015. **8**(4): p. 711-57.
100. Reffuveille, F., et al., *A broad-spectrum antibiofilm peptide enhances antibiotic action against bacterial biofilms*. Antimicrob Agents Chemother, 2014. **58**(9): p. 5363-71.
101. Shanmugaraj, B., et al., *Biotechnological Insights on the Expression and Production of Antimicrobial Peptides in Plants*. Molecules, 2021. **26**(13).
102. Hotchkiss, R.D. and R.J. Dubos, *Fractionation of the bactericidal agent from cultures of a soil Bacillus*. Journal of Biological Chemistry, 1940. **132**(2): p. 791-792.
103. Divyashree, M., et al., *Clinical Applications of Antimicrobial Peptides (AMPs): Where do we Stand Now?* Protein Pept Lett, 2020. **27**(2): p. 120-134.
104. Shai, Y., *Mode of action of membrane active antimicrobial peptides*. Biopolymers, 2002. **66**(4): p. 236-48.

105. Sani, M.-A. and F. Separovic, *How Membrane-Active Peptides Get into Lipid Membranes*. Accounts of Chemical Research, 2016. **49**(6): p. 1130-1138.
106. Park, C.B., H.S. Kim, and S.C. Kim, *Mechanism of action of the antimicrobial peptide buforin II: buforin II kills microorganisms by penetrating the cell membrane and inhibiting cellular functions*. Biochem Biophys Res Commun, 1998. **244**(1): p. 253-7.
107. Bergogne-Berezin, E. and K.J. Towner, *Acinetobacter spp. as nosocomial pathogens: microbiological, clinical, and epidemiological features*. Clin Microbiol Rev, 1996. **9**(2): p. 148-65.
108. Tuan Anh, N., et al., *Molecular epidemiology and antimicrobial resistance phenotypes of Acinetobacter baumannii isolated from patients in three hospitals in southern Vietnam*. J Med Microbiol, 2017. **66**(1): p. 46-53.
109. Lebeaux, D., J.M. Ghigo, and C. Beloin, *Biofilm-related infections: bridging the gap between clinical management and fundamental aspects of recalcitrance toward antibiotics*. Microbiol Mol Biol Rev, 2014. **78**(3): p. 510-43.
110. Abdar, M.H., et al., *Prevalence of extended-spectrum beta-lactamase genes in Acinetobacter baumannii strains isolated from nosocomial infections in Tehran, Iran*. GMS Hyg Infect Control, 2019. **14**: p. Doc02.
111. Pfeifer, Y., A. Cullik, and W. Witte, *Resistance to cephalosporins and carbapenems in Gram-negative bacterial pathogens*. Int J Med Microbiol, 2010. **300**(6): p. 371-9.
112. Peleg, A.Y., H. Seifert, and D.L. Paterson, *Acinetobacter baumannii: emergence of a successful pathogen*. Clin Microbiol Rev, 2008. **21**(3): p. 538-82.

113. Jamal, M., et al., *Bacterial biofilm and associated infections*. J Chin Med Assoc, 2018. **81**(1): p. 7-11.
114. Giannouli, M., et al., *Virulence-related traits of epidemic Acinetobacter baumannii strains belonging to the international clonal lineages I-III and to the emerging genotypes ST25 and ST78*. BMC Infect Dis, 2013. **13**: p. 282.
115. Marti, S., et al., *Biofilm formation at the solid-liquid and air-liquid interfaces by Acinetobacter species*. BMC Res Notes, 2011. **4**: p. 5.
116. Espinal, P., S. Marti, and J. Vila, *Effect of biofilm formation on the survival of Acinetobacter baumannii on dry surfaces*. J Hosp Infect, 2012. **80**(1): p. 56-60.
117. Gaddy, J.A. and L.A. Actis, *Regulation of Acinetobacter baumannii biofilm formation*. Future Microbiol, 2009. **4**(3): p. 273-8.
118. Goh, H.M., et al., *Molecular analysis of the Acinetobacter baumannii biofilm-associated protein*. Appl Environ Microbiol, 2013. **79**(21): p. 6535-43.
119. Tiwari, V., et al., *Effect of secondary metabolite of Actinidia deliciosa on the biofilm and extra-cellular matrix components of Acinetobacter baumannii*. Microb Pathog, 2017. **110**: p. 345-351.
120. Tiwari, V., V. Patel, and M. Tiwari, *In-silico screening and experimental validation reveal L-Adrenaline as anti-biofilm molecule against biofilm-associated protein (Bap) producing Acinetobacter baumannii*. Int J Biol Macromol, 2018. **107**(Pt A): p. 1242-1252.
121. Brossard, K.A. and A.A. Campagnari, *The Acinetobacter baumannii biofilm-associated protein plays a role in adherence to human epithelial cells*. Infect Immun, 2012. **80**(1): p. 228-33.

122. Azizi, O., et al., *Molecular Analysis and Expression of bap Gene in Biofilm-Forming Multi-Drug-Resistant Acinetobacter baumannii*. Rep Biochem Mol Biol, 2016. **5**(1): p. 62-72.
123. De Gregorio, E., et al., *Biofilm-associated proteins: news from Acinetobacter*. BMC Genomics, 2015. **16**: p. 933.
124. Skerniskyte, J., et al., *Blp1 protein shows virulence-associated features and elicits protective immunity to Acinetobacter baumannii infection*. BMC Microbiol, 2019. **19**(1): p. 259.
125. Choi, C.H., et al., *Acinetobacter baumannii invades epithelial cells and outer membrane protein A mediates interactions with epithelial cells*. BMC Microbiol, 2008. **8**: p. 216.
126. Gaddy, J.A., A.P. Tomaras, and L.A. Actis, *The Acinetobacter baumannii 19606 OmpA protein plays a role in biofilm formation on abiotic surfaces and in the interaction of this pathogen with eukaryotic cells*. Infect Immun, 2009. **77**(8): p. 3150-60.
127. Weidensdorfer, M., et al., *Analysis of Endothelial Adherence of Bartonella henselae and Acinetobacter baumannii Using a Dynamic Human Ex Vivo Infection Model*. Infect Immun, 2015. **84**(3): p. 711-22.
128. Eijkelkamp, B.A., et al., *Comparative analysis of surface-exposed virulence factors of Acinetobacter baumannii*. BMC Genomics, 2014. **15**: p. 1020.
129. Weidensdorfer, M., et al., *The Acinetobacter trimeric autotransporter adhesin Ata controls key virulence traits of Acinetobacter baumannii*. Virulence, 2019. **10**(1): p. 68-81.

130. Tomaras, A.P., et al., *Attachment to and biofilm formation on abiotic surfaces by Acinetobacter baumannii: involvement of a novel chaperone-usher pili assembly system*. Microbiology, 2003. **149**(Pt 12): p. 3473-3484.
131. Valle, J., M. Echeverez, and I. Lasa, *sigma(B) Inhibits Poly-N-Acetylglucosamine Exopolysaccharide Synthesis and Biofilm Formation in Staphylococcus aureus*. J Bacteriol, 2019. **201**(11).
132. Eddenden, A., et al., *An Inactive Dispersin B Probe for Monitoring PNAG Production in Biofilm Formation*. ACS Chem Biol, 2020.
133. Kentache, T., et al., *Global Dynamic Proteome Study of a Pellicle-forming Acinetobacter baumannii Strain*. Mol Cell Proteomics, 2017. **16**(1): p. 100-112.
134. Lees-Miller, R.G., et al., *A common pathway for O-linked protein-glycosylation and synthesis of capsule in Acinetobacter baumannii*. Mol Microbiol, 2013. **89**(5): p. 816-30.
135. Sahu, P.K., et al., *Characterization of eDNA from the clinical strain Acinetobacter baumannii AIIMS 7 and its role in biofilm formation*. ScientificWorldJournal, 2012. **2012**: p. 973436.
136. Tomaras, A.P., et al., *Characterization of a two-component regulatory system from Acinetobacter baumannii that controls biofilm formation and cellular morphology*. Microbiology, 2008. **154**(Pt 11): p. 3398-409.
137. Tomaras, A.P., et al., *Attachment to and biofilm formation on abiotic surfaces by Acinetobacter baumannii: involvement of a novel chaperone-usher pili assembly system*. Microbiology, 2003. **149**(Pt 12): p. 3473-84.

138. Geisinger, E., et al., *A global regulatory system links virulence and antibiotic resistance to envelope homeostasis in Acinetobacter baumannii*. PLoS Pathog, 2018. **14**(5): p. e1007030.
139. Anbazhagan, D., et al., *Detection of quorum sensing signal molecules and identification of an autoinducer synthase gene among biofilm forming clinical isolates of Acinetobacter spp*. PLoS One, 2012. **7**(7): p. e36696.
140. Rumbo-Feal, S., et al., *Whole transcriptome analysis of Acinetobacter baumannii assessed by RNA-sequencing reveals different mRNA expression profiles in biofilm compared to planktonic cells*. PLoS One, 2013. **8**(8): p. e72968.
141. Niu, C., et al., *Isolation and characterization of an autoinducer synthase from Acinetobacter baumannii*. J Bacteriol, 2008. **190**(9): p. 3386-92.
142. Stacy, D.M., et al., *Attenuation of quorum sensing in the pathogen Acinetobacter baumannii using non-native N-Acyl homoserine lactones*. ACS Chem Biol, 2012. **7**(10): p. 1719-28.
143. Jacobs, A.C., et al., *AB5075, a Highly Virulent Isolate of Acinetobacter baumannii, as a Model Strain for the Evaluation of Pathogenesis and Antimicrobial Treatments*. mBio, 2014. **5**(3): p. e01076-14.
144. Gallagher, L.A., et al., *Resources for Genetic and Genomic Analysis of Emerging Pathogen Acinetobacter baumannii*. J Bacteriol, 2015. **197**(12): p. 2027-35.
145. Sager, M., et al., *Characterization of Biofilm Formation in [Pasteurella] pneumotropica and [Actinobacillus] muris Isolates of Mouse Origin*. PLoS One, 2015. **10**(10): p. e0138778.

146. Yang, C.H., et al., *Biofilm Formation in Acinetobacter Baumannii: Genotype-Phenotype Correlation*. *Molecules*, 2019. **24**(10).
147. Zimmermann, L., et al., *A Completely Reimplemented MPI Bioinformatics Toolkit with a New HHpred Server at its Core*. *J Mol Biol*, 2018. **430**(15): p. 2237-2243.
148. Casella, L.G., et al., *Towards the complete proteinaceous regulome of Acinetobacter baumannii*. *Microb Genom*, 2017. **3**(3): p. mgen000107.
149. van der Ploeg, J.R., et al., *Involvement of CysB and Cbl regulatory proteins in expression of the tauABCD operon and other sulfate starvation-inducible genes in Escherichia coli*. *J Bacteriol*, 1997. **179**(24): p. 7671-8.
150. Gebhardt, M.J., et al., *Joint Transcriptional Control of Virulence and Resistance to Antibiotic and Environmental Stress in Acinetobacter baumannii*. *mBio*, 2015. **6**(6): p. e01660-15.
151. Aranda, J., et al., *Role of Acinetobacter baumannii UmuD homologs in antibiotic resistance acquired through DNA damage-induced mutagenesis*. *Antimicrob Agents Chemother*, 2014. **58**(3): p. 1771-3.
152. Junka, A.F., et al., *Use of the Real Time xCelligence System for Purposes of Medical Microbiology*. *Pol J Microbiol*, 2012. **61**(3): p. 191-197.
153. Cihalova, K., et al., *Staphylococcus aureus and MRSA Growth and Biofilm Formation after Treatment with Antibiotics and SeNPs*. *Int J Mol Sci*, 2015. **16**(10): p. 24656-72.
154. Gutierrez, D., et al., *Monitoring in Real Time the Formation and Removal of Biofilms from Clinical Related Pathogens Using an Impedance-Based Technology*. *PLoS One*, 2016. **11**(10): p. e0163966.

155. Ferrer, M.D., et al., *Effect of antibiotics on biofilm inhibition and induction measured by real-time cell analysis*. J Appl Microbiol, 2017. **122**(3): p. 640-650.
156. Mira, A., et al., *Development of an in vitro system to study oral biofilms in real time through impedance technology: validation and potential applications*. J Oral Microbiol, 2019. **11**(1): p. 1609838.
157. Kaplan, J.B., et al., *Genes involved in the synthesis and degradation of matrix polysaccharide in Actinobacillus actinomycetemcomitans and Actinobacillus pleuropneumoniae biofilms*. J Bacteriol, 2004. **186**(24): p. 8213-20.
158. Dagorn, A., et al., *Effect of GABA, a bacterial metabolite, on Pseudomonas fluorescens surface properties and cytotoxicity*. Int J Mol Sci, 2013. **14**(6): p. 12186-204.
159. Dagorn, A., et al., *Gamma-aminobutyric acid acts as a specific virulence regulator in Pseudomonas aeruginosa*. Microbiology, 2013. **159**(Pt 2): p. 339-51.
160. Li, S., et al., *Comparative transcriptomics analyses of the different growth states of multidrug-resistant Acinetobacter baumannii*. Biomed Pharmacother, 2017. **85**: p. 564-574.
161. Zapras, A., et al., *The gamma-aminobutyrate permease GabP serves as the third proline transporter of Bacillus subtilis*. J Bacteriol, 2014. **196**(3): p. 515-26.
162. Rinaldo, S., et al., *Beyond nitrogen metabolism: nitric oxide, cyclic-di-GMP and bacterial biofilms*. FEMS Microbiol Lett, 2018. **365**(6).
163. Scribano, D., et al., *Insights into the Periplasmic Proteins of Acinetobacter baumannii AB5075 and the Impact of Imipenem Exposure: A Proteomic Approach*. Int J Mol Sci, 2019. **20**(14).

164. Kang, K.N., et al., *Septal Class A Penicillin-Binding Protein Activity and Id-Transpeptidases Mediate Selection of Colistin-Resistant Lipooligosaccharide-Deficient Acinetobacter baumannii*. mBio, 2021. **12**(1).
165. Szklarczyk, D., et al., *STRING v11: protein-protein association networks with increased coverage, supporting functional discovery in genome-wide experimental datasets*. Nucleic Acids Res, 2019. **47**(D1): p. D607-D613.
166. Magnet, S., et al., *Identification of the L,D-transpeptidases for peptidoglycan cross-linking in Escherichia coli*. J Bacteriol, 2008. **190**(13): p. 4782-5.
167. Le, N.H., et al., *Peptidoglycan editing provides immunity to Acinetobacter baumannii during bacterial warfare*. Sci Adv, 2020. **6**(30): p. eabb5614.
168. Piattoni, C.V., et al., *Nonphosphorylating glyceraldehyde-3-phosphate dehydrogenase is phosphorylated in wheat endosperm at serine-404 by an SNF1-related protein kinase allosterically inhibited by ribose-5-phosphate*. Plant Physiol, 2011. **156**(3): p. 1337-50.
169. Iddar, A., et al., *Widespread occurrence of non-phosphorylating glyceraldehyde-3-phosphate dehydrogenase among gram-positive bacteria*. Int Microbiol, 2005. **8**(4): p. 251-8.
170. Asanuma, N. and T. Hino, *Presence of NAD<sup>+</sup>-specific glyceraldehyde-3-phosphate dehydrogenase and CcpA-dependent transcription of its gene in the ruminal bacterium Streptococcus bovis*. FEMS Microbiol Lett, 2006. **257**(1): p. 17-23.
171. Spaans, S.K., et al., *NADPH-generating systems in bacteria and archaea*. Front Microbiol, 2015. **6**: p. 742.

172. Liu, D., et al., *Comparative transcriptomic analysis of Clostridium acetobutylicum biofilm and planktonic cells*. J Biotechnol, 2016. **218**: p. 1-12.
173. Shon, A.S., R.P. Bajwa, and T.A. Russo, *Hypervirulent (hypermucoviscous) Klebsiella pneumoniae: a new and dangerous breed*. Virulence, 2013. **4**(2): p. 107-18.
174. Nait Chabane, Y., et al., *Characterisation of pellicles formed by Acinetobacter baumannii at the air-liquid interface*. PLoS One, 2014. **9**(10): p. e111660.
175. Krystynowicz, A., et al., *Factors affecting the yield and properties of bacterial cellulose*. J Ind Microbiol Biotechnol, 2002. **29**(4): p. 189-95.
176. Myllykallio, H., et al., *Life without dihydrofolate reductase FoaA*. Trends Microbiol, 2003. **11**(5): p. 220-3.
177. Penesyan, A., et al., *Rapid microevolution of biofilm cells in response to antibiotics*. NPJ Biofilms Microbiomes, 2019. **5**: p. 34.
178. Moon, K.H., B.S. Weber, and M.F. Feldman, *Subinhibitory Concentrations of Trimethoprim and Sulfamethoxazole Prevent Biofilm Formation by Acinetobacter baumannii through Inhibition of Csu Pilus Expression*. Antimicrob Agents Chemother, 2017. **61**(9).
179. Hare, J.M., et al., *Prophage induction and differential RecA and UmuDAb transcriptome regulation in the DNA damage responses of Acinetobacter baumannii and Acinetobacter baylyi*. PLoS One, 2014. **9**(4): p. e93861.
180. Devaraj, A., et al., *The extracellular DNA lattice of bacterial biofilms is structurally related to Holliday junction recombination intermediates*. Proc Natl Acad Sci U S A, 2019. **116**(50): p. 25068-25077.

181. Arndt, D., et al., *PHASTER: a better, faster version of the PHAST phage search tool*. Nucleic Acids Res, 2016. **44**(W1): p. W16-21.
182. Resch, A., et al., *Phage release from biofilm and planktonic Staphylococcus aureus cells*. FEMS Microbiol Lett, 2005. **252**(1): p. 89-96.
183. Whiteley, M., et al., *Gene expression in Pseudomonas aeruginosa biofilms*. Nature, 2001. **413**(6858): p. 860-4.
184. Godeke, J., et al., *Phage-induced lysis enhances biofilm formation in Shewanella oneidensis MR-1*. ISME J, 2011. **5**(4): p. 613-26.
185. Carrolo, M., et al., *Prophage spontaneous activation promotes DNA release enhancing biofilm formation in Streptococcus pneumoniae*. PLoS One, 2010. **5**(12): p. e15678.
186. Hare, J.M., et al., *The Acinetobacter regulatory UmuDAb protein cleaves in response to DNA damage with chimeric LexA/UmuD characteristics*. FEMS Microbiol Lett, 2012. **334**(1): p. 57-65.
187. Aranda, J., et al., *Identification of a DNA-damage-inducible regulon in Acinetobacter baumannii*. J Bacteriol, 2013. **195**(24): p. 5577-82.
188. Peterson, M.A., A.N. Grice, and J.M. Hare, *A corepressor participates in LexA-independent regulation of error-prone polymerases in Acinetobacter*. Microbiology (Reading), 2020. **166**(2): p. 212-226.
189. Peterson, M.A., A.N. Grice, and J.M. Hare, *A corepressor participates in LexA-independent regulation of error-prone polymerases in Acinetobacter*. Microbiology, 2020. **166**(2): p. 212-226.

190. Kato, J. and T. Katayama, *Hda, a novel DnaA-related protein, regulates the replication cycle in Escherichia coli*. EMBO J, 2001. **20**(15): p. 4253-62.
191. Robinson, A., et al., *Essential biological processes of an emerging pathogen: DNA replication, transcription, and cell division in Acinetobacter spp*. Microbiol Mol Biol Rev, 2010. **74**(2): p. 273-97.
192. Garcia Garcia, T., et al., *Phosphorylation of the Bacillus subtilis Replication Controller YabA Plays a Role in Regulation of Sporulation and Biofilm Formation*. Front Microbiol, 2018. **9**: p. 486.
193. Feeney, M.A., N. Ke, and J. Beckwith, *Mutations at several loci cause increased expression of ribonucleotide reductase in Escherichia coli*. J Bacteriol, 2012. **194**(6): p. 1515-22.
194. Cendra Mdel, M., A. Juarez, and E. Torrents, *Biofilm modifies expression of ribonucleotide reductase genes in Escherichia coli*. PLoS One, 2012. **7**(9): p. e46350.
195. Mitchell, A.L., et al., *InterPro in 2019: improving coverage, classification and access to protein sequence annotations*. Nucleic Acids Res, 2019. **47**(D1): p. D351-D360.
196. El-Gebali, S., et al., *The Pfam protein families database in 2019*. Nucleic Acids Res, 2019. **47**(D1): p. D427-D432.
197. Gohara, D.W. and M.F. Yap, *Survival of the drowsiest: the hibernating 100S ribosome in bacterial stress management*. Curr Genet, 2018. **64**(4): p. 753-760.

198. Colquhoun, J.M. and P.N. Rather, *Insights Into Mechanisms of Biofilm Formation in Acinetobacter baumannii and Implications for Uropathogenesis*. Front Cell Infect Microbiol, 2020. **10**: p. 253.
199. Vijayashree Priyadharsini, J., A.S. Smiline Girija, and A. Paramasivam, *In silico analysis of virulence genes in an emerging dental pathogen A. baumannii and related species*. Arch Oral Biol, 2018. **94**: p. 93-98.
200. Hu, F.Z., et al., *Deletion of genes involved in the ketogluconate metabolism, Entner-Doudoroff pathway, and glucose dehydrogenase increase local and invasive virulence phenotypes in Streptococcus pneumoniae*. PLoS One, 2019. **14**(1): p. e0209688.
201. Rossi, E., et al., *Glucose availability enhances lipopolysaccharide production and immunogenicity in the opportunistic pathogen Acinetobacter baumannii*. Future Microbiol, 2016. **11**(3): p. 335-49.
202. Huang, T.P., E.B. Somers, and A.C. Wong, *Differential biofilm formation and motility associated with lipopolysaccharide/exopolysaccharide-coupled biosynthetic genes in Stenotrophomonas maltophilia*. J Bacteriol, 2006. **188**(8): p. 3116-20.
203. Genevaux, P., et al., *Identification of Tn10 insertions in the rfaG, rfaP, and galU genes involved in lipopolysaccharide core biosynthesis that affect Escherichia coli adhesion*. Arch Microbiol, 1999. **172**(1): p. 1-8.
204. Carretero-Ledesma, M., et al., *Phenotypic changes associated with Colistin resistance due to Lipopolysaccharide loss in Acinetobacter baumannii*. Virulence, 2018. **9**(1): p. 930-942.

205. Molin, S. and T. Tolker-Nielsen, *Gene transfer occurs with enhanced efficiency in biofilms and induces enhanced stabilisation of the biofilm structure*. Curr Opin Biotechnol, 2003. **14**(3): p. 255-61.
206. Folkesson, A., et al., *Biofilm induced tolerance towards antimicrobial peptides*. PLoS One, 2008. **3**(4): p. e1891.
207. Arutyunov, D., et al., *F plasmid TraF and TraH are components of an outer membrane complex involved in conjugation*. J Bacteriol, 2010. **192**(6): p. 1730-4.
208. Maneewannakul, S., P. Kathir, and K. Ippenihler, *Characterization of the F-Plasmid Mating Aggregation Gene Tran and of a New F-Transfer Region Locus Trbe*. Journal of Molecular Biology, 1992. **225**(2): p. 299-311.
209. Elhosseiny, N.M., et al., *Acinetobacter baumannii universal stress protein A plays a pivotal role in stress response and is essential for pneumonia and sepsis pathogenesis*. Int J Med Microbiol, 2015. **305**(1): p. 114-23.
210. Yoon, S.S., et al., *Pseudomonas aeruginosa anaerobic respiration in biofilms: relationships to cystic fibrosis pathogenesis*. Dev Cell, 2002. **3**(4): p. 593-603.
211. Schreiber, K., et al., *Anaerobic survival of Pseudomonas aeruginosa by pyruvate fermentation requires an Usp-type stress protein*. J Bacteriol, 2006. **188**(2): p. 659-68.
212. Kuramitsu, H.K., W. Chen, and A. Ikegami, *Biofilm formation by the periodontopathic bacteria Treponema denticola and Porphyromonas gingivalis*. J Periodontol, 2005. **76**(11 Suppl): p. 2047-51.

213. Chen, W., et al., *A universal stress protein of Porphyromonas gingivalis is involved in stress responses and biofilm formation*. FEMS Microbiol Lett, 2006. **264**(1): p. 15-21.
214. Nystrom, T. and F.C. Neidhardt, *Cloning, mapping and nucleotide sequencing of a gene encoding a universal stress protein in Escherichia coli*. Mol Microbiol, 1992. **6**(21): p. 3187-98.
215. Siegele, D.A., *Universal stress proteins in Escherichia coli*. J Bacteriol, 2005. **187**(18): p. 6253-4.
216. O'Toole, R. and H.D. Williams, *Universal stress proteins and Mycobacterium tuberculosis*. Res Microbiol, 2003. **154**(6): p. 387-92.
217. Vollmer, A.C. and S.J. Bark, *Twenty-Five Years of Investigating the Universal Stress Protein: Function, Structure, and Applications*. Adv Appl Microbiol, 2018. **102**: p. 1-36.
218. Nystrom, T. and F.C. Neidhardt, *Expression and role of the universal stress protein, UspA, of Escherichia coli during growth arrest*. Mol Microbiol, 1994. **11**(3): p. 537-44.
219. Yang, Q., et al., *The impact of pH and nutrient stress on the growth and survival of Streptococcus agalactiae*. Antonie Van Leeuwenhoek, 2012. **102**(2): p. 277-87.
220. Kvint, K., et al., *The bacterial universal stress protein: function and regulation*. Curr Opin Microbiol, 2003. **6**(2): p. 140-5.

221. Seifart Gomes, C., et al., *Universal stress proteins are important for oxidative and acid stress resistance and growth of Listeria monocytogenes EGD-e in vitro and in vivo*. PLoS One, 2011. **6**(9): p. e24965.
222. Nachin, L., U. Nannmark, and T. Nystrom, *Differential roles of the universal stress proteins of Escherichia coli in oxidative stress resistance, adhesion, and motility*. J Bacteriol, 2005. **187**(18): p. 6265-72.
223. Yohannes, E., D.M. Barnhart, and J.L. Slonczewski, *pH-dependent catabolic protein expression during anaerobic growth of Escherichia coli K-12*. J Bacteriol, 2004. **186**(1): p. 192-9.
224. Liu, W.T., et al., *Role of the universal stress protein UspA of Salmonella in growth arrest, stress and virulence*. Microb Pathog, 2007. **42**(1): p. 2-10.
225. Mangalappalli-Illathu, A.K. and D.R. Korber, *Adaptive resistance and differential protein expression of Salmonella enterica serovar Enteritidis biofilms exposed to benzalkonium chloride*. Antimicrob Agents Chemother, 2006. **50**(11): p. 3588-96.
226. Galindo Blaha, C.A. and I.S. Schrank, *An Azospirillum brasilense Tn5 mutant with modified stress response and impaired in flocculation*. Antonie Van Leeuwenhoek, 2003. **83**(1): p. 35-43.
227. Mistry, J., et al., *Pfam: The protein families database in 2021*. Nucleic Acids Res, 2021. **49**(D1): p. D412-D419.
228. Gustavsson, N., A. Diez, and T. Nystrom, *The universal stress protein paralogues of Escherichia coli are co-ordinately regulated and co-operate in the defence against DNA damage*. Mol Microbiol, 2002. **43**(1): p. 107-17.

229. Havis, S., et al., *A Universal Stress Protein That Controls Bacterial Stress Survival in Micrococcus luteus*. J Bacteriol, 2019. **201**(24).
230. Farewell, A., et al., *Role of the Escherichia coli FadR regulator in stasis survival and growth phase-dependent expression of the uspA, fad, and fab genes*. J Bacteriol, 1996. **178**(22): p. 6443-50.
231. Diez, A., N. Gustavsson, and T. Nystrom, *The universal stress protein A of Escherichia coli is required for resistance to DNA damaging agents and is regulated by a RecA/FtsK-dependent regulatory pathway*. Mol Microbiol, 2000. **36**(6): p. 1494-503.
232. Kvint, K., et al., *Emergency derepression: stringency allows RNA polymerase to override negative control by an active repressor*. Mol Microbiol, 2000. **35**(2): p. 435-43.
233. Oshima, T., et al., *Transcriptome analysis of all two-component regulatory system mutants of Escherichia coli K-12*. Mol Microbiol, 2002. **46**(1): p. 281-91.
234. Bochkareva, E.S., A.S. Girshovich, and E. Bibi, *Identification and characterization of the Escherichia coli stress protein UP12, a putative in vivo substrate of GroEL*. Eur J Biochem, 2002. **269**(12): p. 3032-40.
235. O'Toole, R., et al., *A two-component regulator of universal stress protein expression and adaptation to oxygen starvation in Mycobacterium smegmatis*. J Bacteriol, 2003. **185**(5): p. 1543-54.
236. Kim, H., et al., *Regulation of universal stress protein genes by quorum sensing and RpoS in Burkholderia glumae*. J Bacteriol, 2012. **194**(5): p. 982-92.

237. Rezuchova, B., et al., *New members of the Escherichia coli sigmaE regulon identified by a two-plasmid system*. FEMS Microbiol Lett, 2003. **225**(1): p. 1-7.
238. Freestone, P., et al., *The universal stress protein, UspA, of Escherichia coli is phosphorylated in response to stasis*. J Mol Biol, 1997. **274**(3): p. 318-24.
239. Saveanu, C., et al., *Structural and nucleotide-binding properties of YajQ and YnaF, two Escherichia coli proteins of unknown function*. Protein Sci, 2002. **11**(11): p. 2551-60.
240. Weber, A. and K. Jung, *Biochemical properties of UspG, a universal stress protein of Escherichia coli*. Biochemistry, 2006. **45**(6): p. 1620-8.
241. Zarembinski, T.I., et al., *Structure-based assignment of the biochemical function of a hypothetical protein: a test case of structural genomics*. Proc Natl Acad Sci U S A, 1998. **95**(26): p. 15189-93.
242. Nachin, L., et al., *Heterodimer formation within universal stress protein classes revealed by an in silico and experimental approach*. J Mol Biol, 2008. **380**(2): p. 340-50.
243. Glass, L.N., et al., *Mycobacterium tuberculosis universal stress protein Rv2623 interacts with the putative ATP binding cassette (ABC) transporter Rv1747 to regulate mycobacterial growth*. PLoS Pathog, 2017. **13**(7): p. e1006515.
244. Heermann, R., et al., *The universal stress protein UspC scaffolds the KdpD/KdpE signaling cascade of Escherichia coli under salt stress*. J Mol Biol, 2009. **386**(1): p. 134-48.
245. Carroll, R.K., A. Weiss, and L.N. Shaw, *RNA-Sequencing of Staphylococcus aureus Messenger RNA*. Methods Mol Biol, 2016. **1373**: p. 131-41.

246. Kanehisa, M. and S. Goto, *KEGG: kyoto encyclopedia of genes and genomes*. Nucleic Acids Res, 2000. **28**(1): p. 27-30.
247. Kanehisa, M., *Toward understanding the origin and evolution of cellular organisms*. Protein Sci, 2019. **28**(11): p. 1947-1951.
248. Kanehisa, M., et al., *KEGG: integrating viruses and cellular organisms*. Nucleic Acids Res, 2021. **49**(D1): p. D545-D551.
249. CLSI, *Methods for Dilution Antimicrobial Susceptibility Tests for Bacteria That Grow Aerobically*. 11th ed. ed. CLSI standard M07. 2018, Wayne, PA: 2018 Clinical and Laboratory Standards Institute
250. Kolar, S.L., et al., *NsaRS is a cell-envelope-stress-sensing two-component system of Staphylococcus aureus*. Microbiology (Reading), 2011. **157**(Pt 8): p. 2206-2219.
251. Xu, Y., et al., *Crystal structure and functional implications of the tandem-type universal stress protein UspE from Escherichia coli*. BMC Struct Biol, 2016. **16**: p. 3.
252. Omasits, U., et al., *Protter: interactive protein feature visualization and integration with experimental proteomic data*. Bioinformatics, 2014. **30**(6): p. 884-6.
253. Yang, J. and Y. Zhang, *I-TASSER server: new development for protein structure and function predictions*. Nucleic Acids Res, 2015. **43**(W1): p. W174-81.
254. Kelley, L.A., et al., *The Phyre2 web portal for protein modeling, prediction and analysis*. Nat Protoc, 2015. **10**(6): p. 845-58.
255. Tkaczuk, K.L., et al., *Structural and functional insight into the universal stress protein family*. Evol Appl, 2013. **6**(3): p. 434-49.

256. Wang, N., et al., *Genome-wide identification of Acinetobacter baumannii genes necessary for persistence in the lung*. mBio, 2014. **5**(3): p. e01163-14.
257. Nystrom, T. and F.C. Neidhardt, *Isolation and properties of a mutant of Escherichia coli with an insertional inactivation of the uspA gene, which encodes a universal stress protein*. J Bacteriol, 1993. **175**(13): p. 3949-56.
258. UniProt, C., *UniProt: the universal protein knowledgebase in 2021*. Nucleic Acids Res, 2021. **49**(D1): p. D480-D489.
259. Bryan, L.E. and S. Kwan, *Roles of ribosomal binding, membrane potential, and electron transport in bacterial uptake of streptomycin and gentamicin*. Antimicrob Agents Chemother, 1983. **23**(6): p. 835-45.
260. Taber, H.W., et al., *Bacterial uptake of aminoglycoside antibiotics*. Microbiol Rev, 1987. **51**(4): p. 439-57.
261. Nair, J., et al., *The rpsL gene and streptomycin resistance in single and multiple drug-resistant strains of Mycobacterium tuberculosis*. Mol Microbiol, 1993. **10**(3): p. 521-7.
262. Olkkola, S., et al., *Mutations in the rpsL gene are involved in streptomycin resistance in Campylobacter coli*. Microb Drug Resist, 2010. **16**(2): p. 105-10.
263. Dai, R., et al., *A novel mechanism of streptomycin resistance in Yersinia pestis: Mutation in the rpsL gene*. PLoS Negl Trop Dis, 2021. **15**(4): p. e0009324.
264. Grinter, R., et al., *BonA from Acinetobacter baumannii Forms a Divisome-Localized Decamer That Supports Outer Envelope Function*. mBio, 2021: p. e0148021.

265. Yeo, K.J., et al., *d-Stereoisomer preference of the OmpA-like domain of Pal in peptidoglycan of Acinetobacter baumannii*. *Process Biochemistry*, 2017. **55**: p. 110-115.
266. Mlynarcik, P. and M. Kolar, *Molecular mechanisms of polymyxin resistance and detection of mcr genes*. *Biomed Pap Med Fac Univ Palacky Olomouc Czech Repub*, 2019. **163**(1): p. 28-38.
267. Nakamura, H., *Genetic determination of resistance to acriflavine, phenethyl alcohol, and sodium dodecyl sulfate in Escherichia coli*. *J Bacteriol*, 1968. **96**(4): p. 987-96.
268. Villalain, J., et al., *Membranotropic effects of the antibacterial agent Triclosan*. *Arch Biochem Biophys*, 2001. **390**(1): p. 128-36.
269. Osei Sekyere, J. and D.G. Amoako, *Carbonyl Cyanide m-Chlorophenylhydrazine (CCCP) Reverses Resistance to Colistin, but Not to Carbapenems and Tigecycline in Multidrug-Resistant Enterobacteriaceae*. *Front Microbiol*, 2017. **8**: p. 228.
270. Camarena, L., et al., *Molecular mechanisms of ethanol-induced pathogenesis revealed by RNA-sequencing*. *PLoS Pathog*, 2010. **6**(4): p. e1000834.
271. Bhuiyan, M.S., et al., *Acinetobacter baumannii phenylacetic acid metabolism influences infection outcome through a direct effect on neutrophil chemotaxis*. *Proc Natl Acad Sci U S A*, 2016. **113**(34): p. 9599-604.
272. Gury, J., et al., *Inactivation of PadR, the repressor of the phenolic acid stress response, by molecular interaction with Usp1, a universal stress protein from*

- Lactobacillus plantarum*, in *Escherichia coli*. Appl Environ Microbiol, 2009. **75**(16): p. 5273-83.
273. Farewell, A., K. Kvint, and T. Nystrom, *uspB*, a new *sigmaS*-regulated gene in *Escherichia coli* which is required for stationary-phase resistance to ethanol. J Bacteriol, 1998. **180**(23): p. 6140-7.
274. Maiden, M.M. and C.M. Waters, *Triclosan depletes the membrane potential in Pseudomonas aeruginosa biofilms inhibiting aminoglycoside induced adaptive resistance*. PLoS Pathog, 2020. **16**(10): p. e1008529.
275. Bruni, G.N. and J.M. Kralj, *Membrane voltage dysregulation driven by metabolic dysfunction underlies bactericidal activity of aminoglycosides*. Elife, 2020. **9**.
276. Bandyopadhyay, D. and M. Mukherjee, *Reactive oxygen species and uspA overexpression: an alternative bacterial response toward selection and maintenance of multidrug resistance in clinical isolates of uropathogenic E. coli*. Eur J Clin Microbiol Infect Dis, 2020. **39**(9): p. 1753-1760.
277. Gou, L., et al., *A Universal Stress Protein from Medicago falcata (MfUSP1) confers multiple stress tolerance by regulating antioxidant defense and proline accumulation*. Environmental and Experimental Botany, 2020. **178**: p. 104168.
278. Imlay, J.A., *Pathways of oxidative damage*. Annu Rev Microbiol, 2003. **57**: p. 395-418.
279. Frankenberg-Dinkel, N., *Bacterial heme oxygenases*. Antioxid Redox Signal, 2004. **6**(5): p. 825-34.

280. Macomber, L. and J.A. Imlay, *The iron-sulfur clusters of dehydratases are primary intracellular targets of copper toxicity*. Proc Natl Acad Sci U S A, 2009. **106**(20): p. 8344-9.
281. Besold, A.N., E.M. Culbertson, and V.C. Culotta, *The Yin and Yang of copper during infection*. J Biol Inorg Chem, 2016. **21**(2): p. 137-44.
282. Macomber, L. and J.A. Imlay, *The iron-sulfur clusters of dehydratases are primary intracellular targets of copper toxicity*. Proceedings of the National Academy of Sciences, 2009. **106**(20): p. 8344.
283. Pham, A.N., et al., *Fenton-like copper redox chemistry revisited: Hydrogen peroxide and superoxide mediation of copper-catalyzed oxidant production*. Journal of Catalysis, 2013. **301**: p. 54-64.
284. Yang, Y., et al., *The Copper Homeostasis Transcription Factor CopR Is Involved in H<sub>2</sub>O<sub>2</sub> Stress in Lactobacillus plantarum CAUH2*. Front Microbiol, 2017. **8**: p. 2015.
285. Gracioso, L.H., et al., *Analysis of copper response in Acinetobacter sp. by comparative proteomics*. Metallomics, 2019. **11**(5): p. 949-958.
286. Joiner, K.A., E.J. Brown, and M.M. Frank, *Complement and bacteria: chemistry and biology in host defense*. Annu Rev Immunol, 1984. **2**: p. 461-91.
287. Bentancor Leticia, V., et al., *Poly-N-Acetyl- $\beta$ -(1-6)-Glucosamine Is a Target for Protective Immunity against Acinetobacter baumannii Infections*. Infection and Immunity, 2012. **80**(2): p. 651-656.
288. Weber, A. and K. Jung, *Profiling early osmostress-dependent gene expression in Escherichia coli using DNA microarrays*. J Bacteriol, 2002. **184**(19): p. 5502-7.

289. Ekor, M., *The growing use of herbal medicines: issues relating to adverse reactions and challenges in monitoring safety*. Front Pharmacol, 2014. **4**: p. 177.
290. Cowan, M.M., *Plant products as antimicrobial agents*. Clin Microbiol Rev, 1999. **12**(4): p. 564-82.
291. Tavares, L.S., et al., *Strategies and molecular tools to fight antimicrobial resistance: resistome, transcriptome, and antimicrobial peptides*. Front Microbiol, 2013. **4**: p. 412.
292. Sachetto-Martins, G., L.O. Franco, and D.E. de Oliveira, *Plant glycine-rich proteins: a family or just proteins with a common motif?* Biochim Biophys Acta, 2000. **1492**(1): p. 1-14.
293. Zasloff, M., *Antimicrobial peptides of multicellular organisms*. Nature, 2002. **415**(6870): p. 389-95.
294. Guralp, S.A., et al., *From design to screening: a new antimicrobial peptide discovery pipeline*. PLoS One, 2013. **8**(3): p. e59305.
295. Nawrot, R., et al., *Plant antimicrobial peptides*. Folia Microbiol (Praha), 2014. **59**(3): p. 181-96.
296. Gordon, Y.J., E.G. Romanowski, and A.M. McDermott, *A review of antimicrobial peptides and their therapeutic potential as anti-infective drugs*. Curr Eye Res, 2005. **30**(7): p. 505-15.
297. Srivastava, S., et al., *Cysteine-rich antimicrobial peptides from plants: The future of antimicrobial therapy*. Phytother Res, 2021. **35**(1): p. 256-277.
298. Seo, M.D., et al., *Antimicrobial peptides for therapeutic applications: a review*. Molecules, 2012. **17**(10): p. 12276-86.

299. Ohtani, S., et al., *Complete primary structures of two subunits of purothionin A, a lethal protein for brewer's yeast from wheat flour*. J Biochem, 1977. **82**(3): p. 753-67.
300. Barbosa Pelegrini, P., et al., *Antibacterial peptides from plants: what they are and how they probably work*. Biochem Res Int, 2011. **2011**: p. 250349.
301. Borris, R.P., *Natural products research: perspectives from a major pharmaceutical company*. J Ethnopharmacol, 1996. **51**(1-3): p. 29-38.
302. Dos Santos-Silva, C.A., et al., *Plant Antimicrobial Peptides: State of the Art, In Silico Prediction and Perspectives in the Omics Era*. Bioinform Biol Insights, 2020. **14**: p. 1177932220952739.
303. Arnison, P.G., et al., *Ribosomally synthesized and post-translationally modified peptide natural products: overview and recommendations for a universal nomenclature*. Nat Prod Rep, 2013. **30**(1): p. 108-60.
304. Goransson, U., et al., *Circular proteins from plants and fungi*. J Biol Chem, 2012. **287**(32): p. 27001-6.
305. Hammami, R., et al., *PhytAMP: a database dedicated to antimicrobial plant peptides*. Nucleic Acids Res, 2009. **37**(Database issue): p. D963-8.
306. Rowe, S.M. and D.R. Spring, *The role of chemical synthesis in developing RiPP antibiotics*. Chem Soc Rev, 2021. **50**(7): p. 4245-4258.
307. Lubelski, J., et al., *Biosynthesis, immunity, regulation, mode of action and engineering of the model lantibiotic nisin*. Cell Mol Life Sci, 2008. **65**(3): p. 455-76.

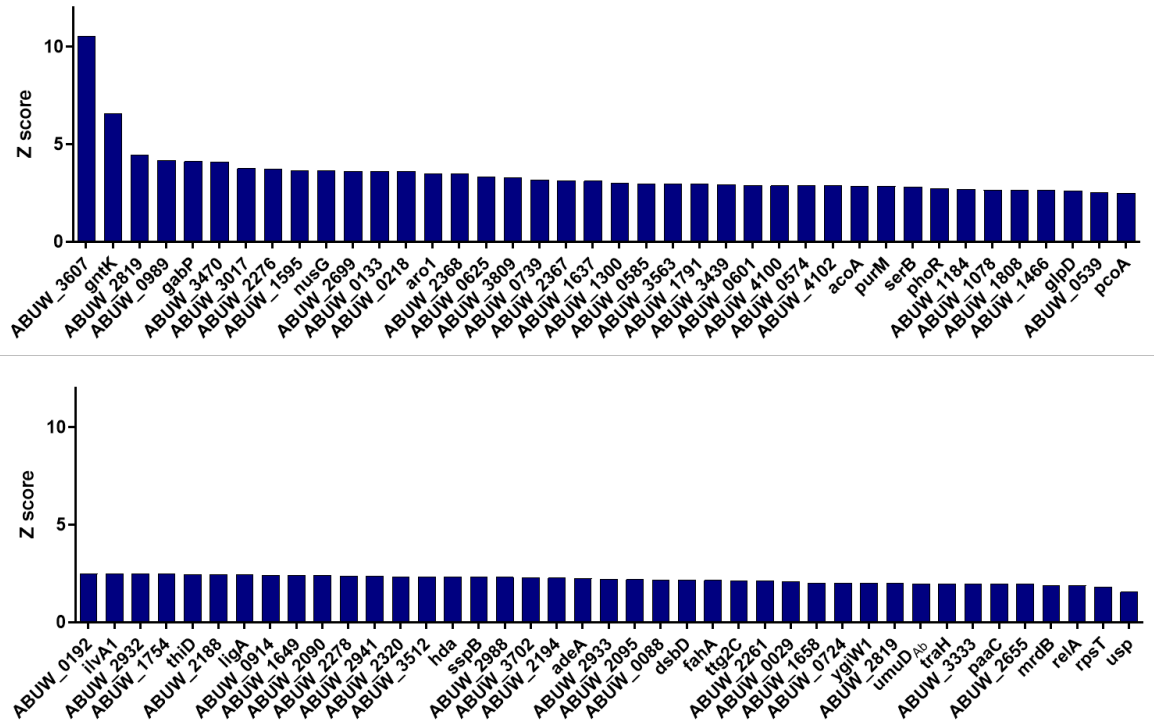
308. Otaka, T. and A. Kaji, *Mode of action of bottromycin A2. Release of aminoacyl- or peptidyl-tRNA from ribosomes.* J Biol Chem, 1976. **251**(8): p. 2299-306.
309. Narayani, M., A. Chadha, and S. Srivastava, *Cyclotides from the Indian Medicinal Plant Viola odorata (Banafsha): Identification and Characterization.* J Nat Prod, 2017. **80**(7): p. 1972-1980.
310. Ireland, D.C., M.L. Colgrave, and D.J. Craik, *A novel suite of cyclotides from Viola odorata: sequence variation and the implications for structure, function and stability.* Biochem J, 2006. **400**(1): p. 1-12.
311. Pranting, M., et al., *The cyclotide cycloviolacin O2 from Viola odorata has potent bactericidal activity against Gram-negative bacteria.* J Antimicrob Chemother, 2010. **65**(9): p. 1964-71.
312. Fleeman, R., et al., *Combinatorial Libraries As a Tool for the Discovery of Novel, Broad-Spectrum Antibacterial Agents Targeting the ESKAPE Pathogens.* J Med Chem, 2015. **58**(8): p. 3340-55.
313. Manning, S.D., et al., *Variation in virulence among clades of Escherichia coli O157:H7 associated with disease outbreaks.* Proc Natl Acad Sci U S A, 2008. **105**(12): p. 4868-73.
314. Moyer, T.B., et al., *PepSAVI-MS Reveals a Proline-rich Antimicrobial Peptide in Amaranthus tricolor.* J Nat Prod, 2019. **82**(10): p. 2744-2753.
315. Shelenkov, A., A. Slavokhotova, and T. Odintsova, *Predicting Antimicrobial and Other Cysteine-Rich Peptides in 1267 Plant Transcriptomes.* Antibiotics (Basel), 2020. **9**(2).

316. Moyer, T.B., et al., *Multiple Classes of Antimicrobial Peptides in Amaranthus tricolor Revealed by Prediction, Proteomics, and Mass Spectrometric Characterization*. J Nat Prod, 2021. **84**(2): p. 444-452.
317. Culver, K.D., et al., *Too Hot to Handle: Antibacterial Peptides Identified in Ghost Pepper*. J Nat Prod, 2021. **84**(8): p. 2200-2208.
318. Thomson, W.A.R., *Medicines from the earth : a guide to healing plants*. 1978, New York: McGraw-Hill. 208 p.
319. Rice, L.B., *Federal funding for the study of antimicrobial resistance in nosocomial pathogens: no ESKAPE*. J Infect Dis, 2008. **197**(8): p. 1079-81.
320. Mulani, M.S., et al., *Emerging Strategies to Combat ESKAPE Pathogens in the Era of Antimicrobial Resistance: A Review*. Front Microbiol, 2019. **10**: p. 539.
321. Sarker, S.D. and L. Nahar, *An introduction to natural products isolation*. Methods Mol Biol, 2012. **864**: p. 1-25.
322. Welch, N.G., et al., *(Re)Defining the Proline-Rich Antimicrobial Peptide Family and the Identification of Putative New Members*. Front Chem, 2020. **8**: p. 607769.
323. Cao, H., et al., *Identification of a Novel Proline-Rich Antimicrobial Peptide from Brassica napus*. PLoS One, 2015. **10**(9): p. e0137414.
324. Yokoyama, S., et al., *Purification, characterization, and sequencing of antimicrobial peptides, Cy-AMP1, Cy-AMP2, and Cy-AMP3, from the Cycad (Cycas revoluta) seeds*. Peptides, 2008. **29**(12): p. 2110-7.
325. Ge, X., et al., *Resistance function of rice lipid transfer protein LTP110*. J Biochem Mol Biol, 2003. **36**(6): p. 603-7.

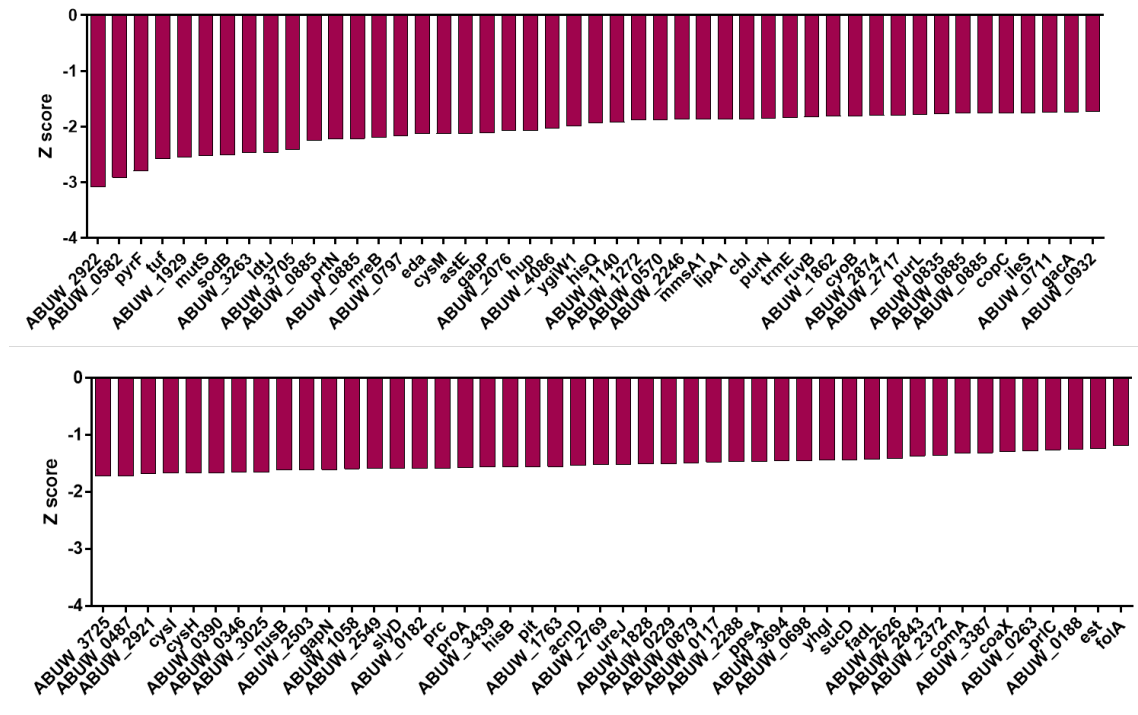
326. Sathoff, A.E., et al., *Plant Defensin Peptides have Antifungal and Antibacterial Activity Against Human and Plant Pathogens*. *Phytopathology*, 2019. **109**(3): p. 402-408.
327. Baruah, J. and M. Lal, *Capsicum chinense Jacq.: Ethnobotany, Bioactivity and Future Prospects*, in *Botanical Leads for Drug Discovery*, B. Singh, Editor. 2020, Springer Singapore: Singapore. p. 349-362.
328. Meghvansi, M.K., et al., *Naga chilli: a potential source of capsaicinoids with broad-spectrum ethnopharmacological applications*. *J Ethnopharmacol*, 2010. **132**(1): p. 1-14.
329. Essig, A., et al., *Copsin, a novel peptide-based fungal antibiotic interfering with the peptidoglycan synthesis*. *J Biol Chem*, 2014. **289**(50): p. 34953-64.
330. Ajiboye, T.O., E. Skiebe, and G. Wilharm, *Impact of zinc uptake regulator Zur on the susceptibility and oxidative stress response of Acinetobacter baumannii to antibiotics*. *Int J Antimicrob Agents*, 2019. **53**(4): p. 467-473.
331. Van Acker, H., et al., *The Role of Reactive Oxygen Species in Antibiotic-Induced Cell Death in Burkholderia cepacia Complex Bacteria*. *PLoS One*, 2016. **11**(7): p. e0159837.

## **Appendices**

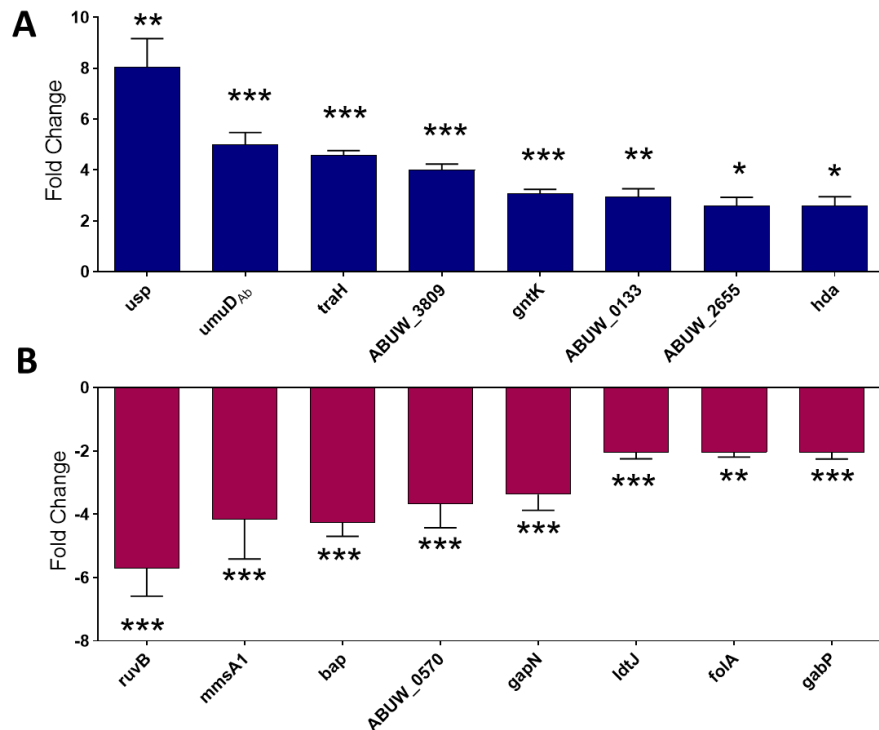
## Appendix I: Supplemental Figures for Chapter 2



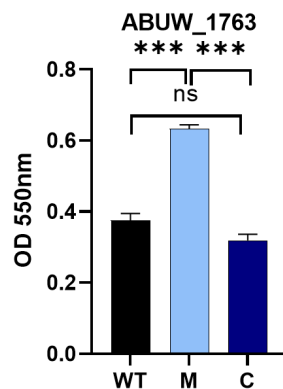
**Supplementary Figure A1. Transposon Mutants of *A. baumannii* Demonstrating Increased Biofilm Formation.** Shown are the Z-scores (see methods) for each mutant demonstrating an increase in biofilm formation with a cutoff of  $\geq 12.5^{\text{th}}$  percentile for each plate assayed.



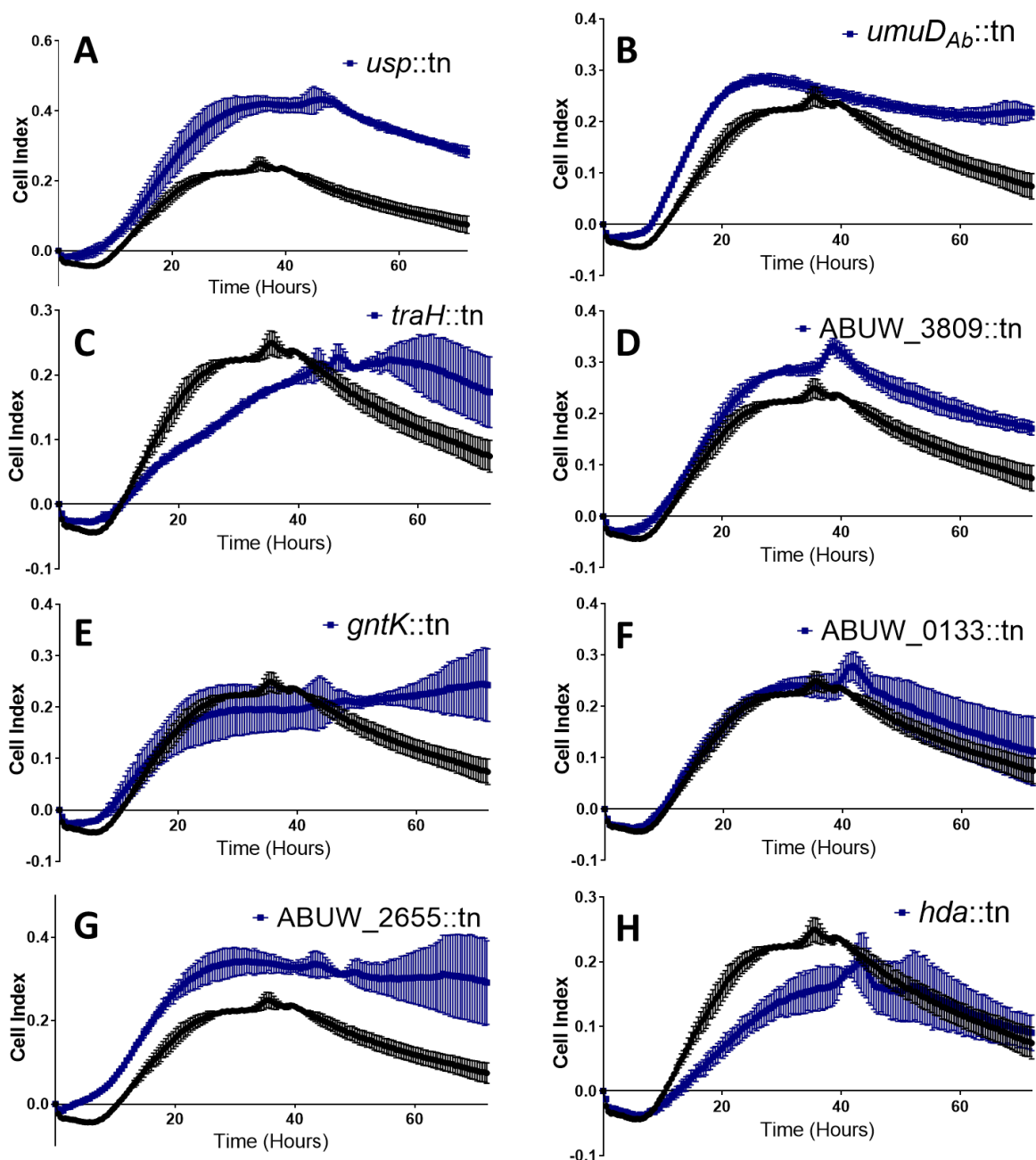
**Supplemental Figure A2. Transposon Mutants of *A. baumannii* Demonstrating Decreased Biofilm Formation.** Shown are the Z-scores (see methods) for each mutant demonstrating an increase in biofilm formation with a cutoff of  $\leq 12.5^{\text{th}}$  percentile for each assay plate.



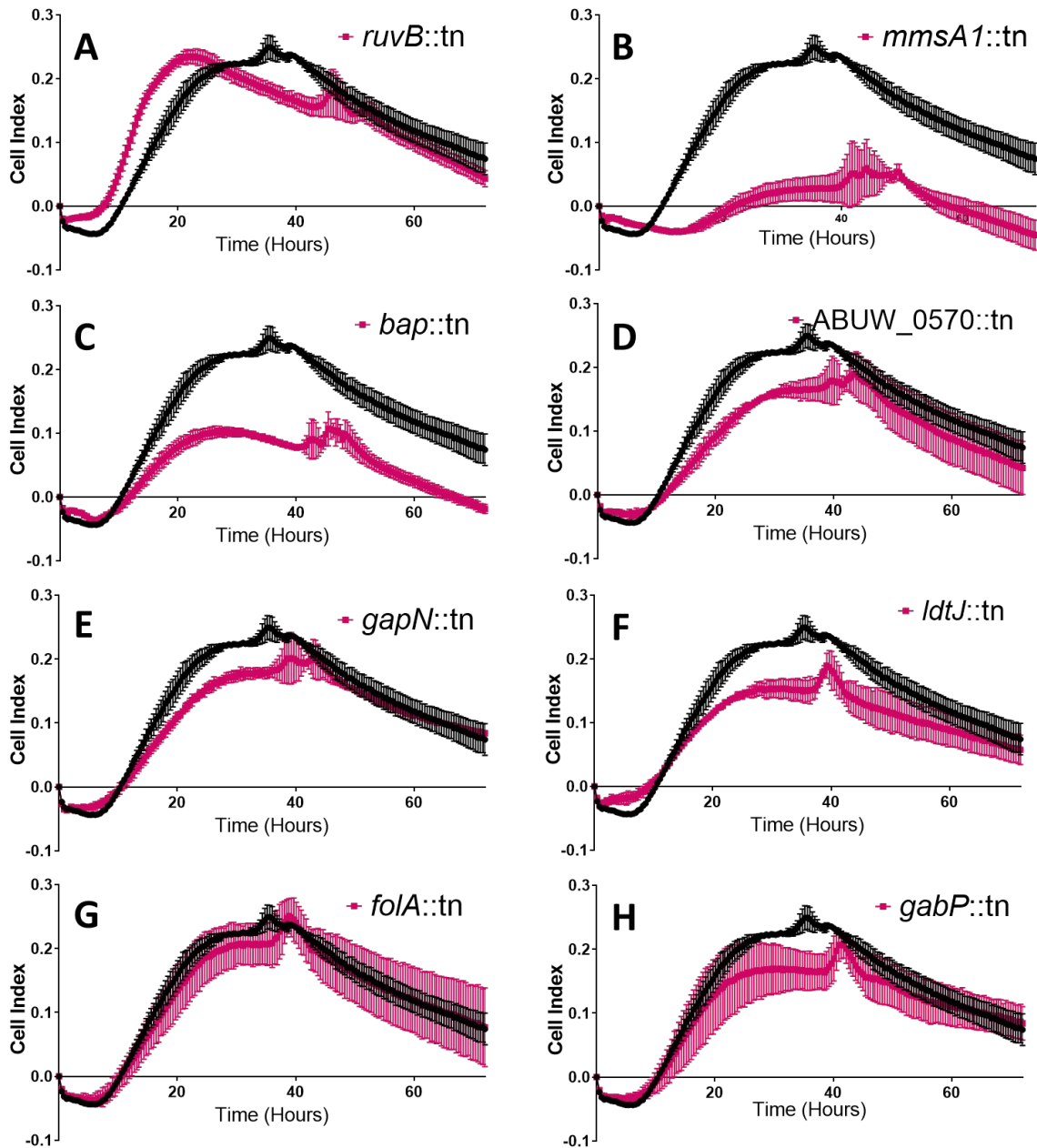
**Supplemental Figure A3. Lead Mutants Demonstrate Significant Changes in Biofilm Biomass.** Each mutant was seeded in sextuplicate with biofilms assessed after 24 hours of growth. **(A)** Blue indicates samples that had an increase in biofilm formation, **(B)** pink indicates mutants that had a decrease in biofilm formation; both as compared to wildtype using CV assays. Error bars are shown  $\pm$ SEM. Statistical significance was assessed using Student's t-test, P-value: \* =0.01 ; \*\* =0.001 ; \*\*\* = 0.0001.



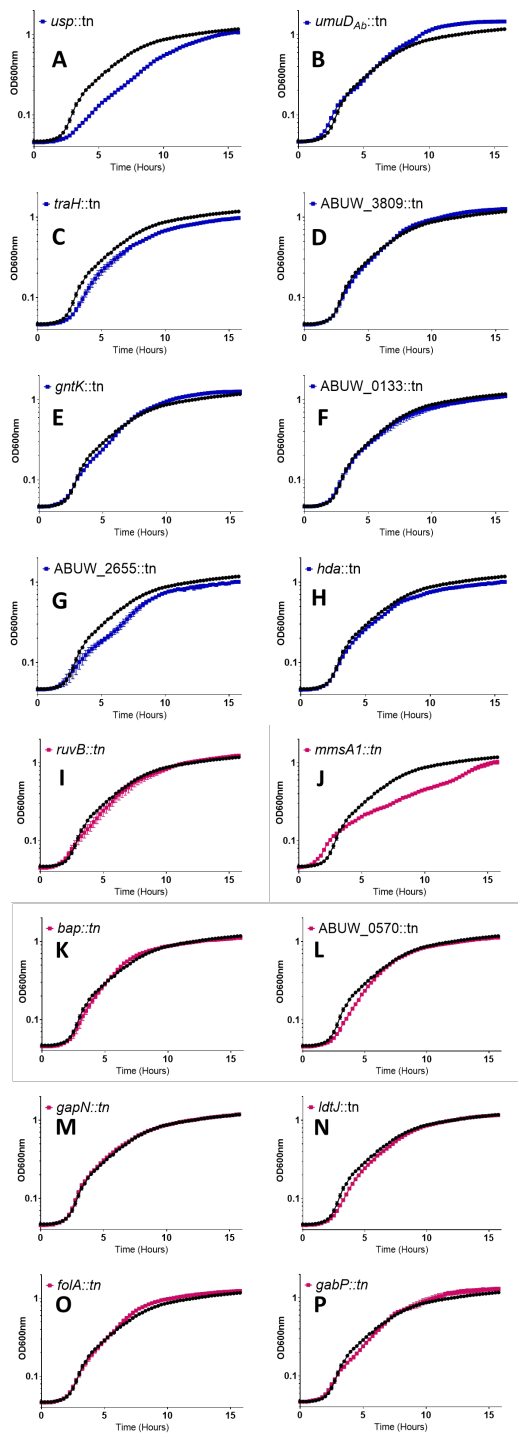
**Supplemental Figure A4. Verification of Screen Integrity by Complementation Analysis.** Each strain was seeded in sextuplicate into 96-well plates, with biofilms assessed after 24 hours of growth via CV staining. Empty vector: pMQ557 in tn strain background. Error bars are shown  $\pm$ SEM. Statistical significance was assessed using Student's t-test, P-value: \* =0.01 ; \*\* =0.001 ; \*\*\* = 0.0001. WT = Wild-Type, M = Mutant, C = Complemented strain. The wild-type and mutant strains all contained an empty copy of the pMQ557 complementing vector.



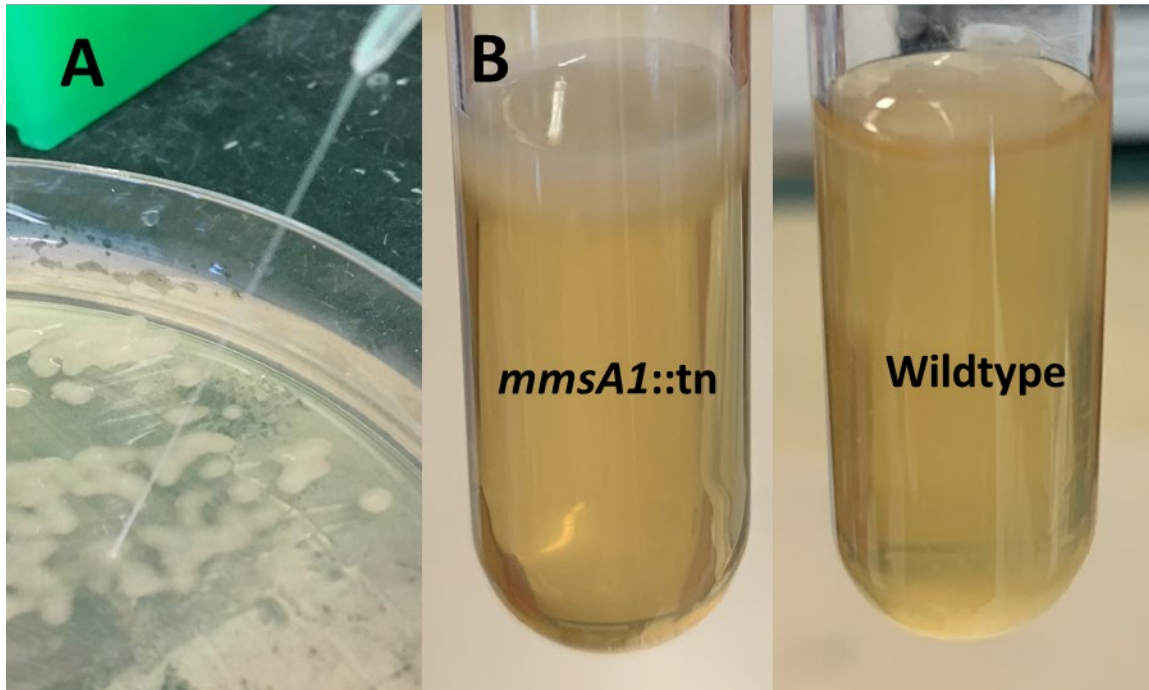
**Supplemental Figure A5. Real-Time Profiling of Biofilm Formation for Mutants Exhibiting Enhanced Biomass in CV Screens.** Each mutant was seeded into the wells of gold-plated 96-well plates in biological triplicate and technical duplicate at an OD<sub>600</sub> of 0.05. Reads were taken every five minutes over a 72h growth period. Blue indicates mutants with increased biofilm formation during CV staining, whilst the wildtype is shown in black in each case. Error bars are shown  $\pm$ SEM.



**Supplemental Figure A6. Real-Time Profiling of Biofilm Formation for Mutants Exhibiting Diminished Biomass in CV Screens.** Each mutant was seeded into the wells of gold-plated 96-well plates in biological triplicate and technical duplicate at an OD<sub>600</sub> of 0.05. Reads were taken every five minutes over a 72h growth period. Pink indicates mutants with decreased biofilm formation during CV staining, whilst the wildtype is shown in black in each case. Error bars are shown  $\pm$ SEM.



**Supplemental Figure A7. Growth Assessment of All Mutants.** Each mutant was seeded into the wells of a 96-well plates in biological triplicate at an OD<sub>600</sub> of 0.05. Reads (OD<sub>600</sub>) were taken every fifteen minutes over 15h. Blue indicates strains with increased biofilm formation during CV staining, whilst pink indicates strains that had a defect in biofilm formation. Wildtype is shown in black in each case. Error bars are shown  $\pm$ SEM.



**Supplemental Figure A8. Pellicle Formation and Hypermucoviscosity of *mmsA1::tn*.** (A) Viscosity test for the mutant using a sterile tip. (B) Samples were inoculated with a single colony prior to incubation under static conditions at 37°C for 24 hours.

## Appendix II: Supplemental Tables for Chapter 2

**Supplemental Table A1. Bacterial Strains and Plasmids.**

Strain Name	Gene	ID/Description	Source
tnab1_kr130917p01q113	ABUW_0133	-	[144]
tnab1_kr121119p01q189	ABUW_0201	<i>gabP</i>	[144]
tnab1_kr121119p04q148	ABUW_0570	-	[144]
tnab1_kr130913p07q112	ABUW_0885	<i>bap</i>	[144]
tnab1_kr130913p04q101	ABUW_0983	<i>hda</i>	[144]
tnab1_kr121210p04q115	ABUW_0999	<i>ruvB</i>	[144]
tnab1_kr121204p05q144	ABUW_1189	<i>ldtJ</i>	[144]
tnab1_kr121213p03q109	ABUW_1763	<i>uspA</i>	[144]
tnab1_jr130919p01q142	ABUW_2431	<i>umuD<sub>Ab</sub></i>	[144]
tnab1_kr130916p04q169	ABUW_2655	-	[144]
tnab1_kr121119p04q136	ABUW_3390	<i>gapN</i>	[144]
tnab1_kr130917p09q181	ABUW_3391	<i>gntK</i>	[144]
tnab1_kr121203p04q142	ABUW_3421	<i>foIA</i>	[144]
tnab1_kr121119p04q144	ABUW_3783	<i>mmsA1</i>	[144]
tnab1_kr121203p04q151	ABUW_3809	-	[144]
tnab1_kr130913p04q147	ABUW_4114	<i>traH</i>	[144]
AB5075		Wildtype Strain	[143]
JLA2878	ABUW_1763	ABUW_1763::tn with pMQ557 EV	This study
JLA2879	ABUW_1763	ABUW_1763::tn with complement pMQ557::ABUW_1763	This study
JLA2887		AB075 with pMQ557 EV	This study
<b>Plasmid</b>			
pMQ557 cloning vector for complementation		Gift: Dr. R. Shanks, University of Pittsburg	

EV: empty vector

**Supplemental Table A2. Primers Used in This Study.**

Primer	Sequence	Enzyme	Ref.
OL5750 ABUW_1763 F	ATGTCTCGAGTGGCGATAATATAACCATA ACGATAACAAG	XhoI	This study
OL5751 ABUW_1763 R	ATGTGGTACCTTAGTGGTGGTGGTGGTG GTGTTTCAGTTACGACCAATACTGGCAC	KpnI	This study
OL4163 pMQ557 F	ATCTTCTCTCATCCGCCAAA		This study
OL4164 pMQ557 R	CTGTTTCTCCATACCCGTAG		This study
T261	CAAATCCTATTGTATGGATTAGTCGAGC		This study

**Supplemental Table A2. Primers Used in This Study. (Continued)**

T262	GTATGCTATACGAAGTTATGGCGC		This study
T263	TGAGCTTTT TAGCTCGACTAATCCAT		[144]

Enzyme: Restriction enzyme used. Ref.: reference. Restriction sites are underlined. His-6 tag is bold and italicized.

**Supplemental Table A3. Mutant Strains Identified as Producing Significantly Greater Biofilm Biomass from Crystal Violet Screens.**

ID	Gene	Description	Z-Score
ABUW_3607	-	putative general secretion pathway protein	10.54
ABUW_3391	<i>gntK</i>	shikimate kinase	6.58
ABUW_2819	-	hypothetical protein	4.46
ABUW_0989	-	tRNA/rRNA methyltransferase	4.17
ABUW_3470	-	N-acyl-phosphatidylethanolamine -hydrolysing phospholipase D	4.11
ABUW_3017	-	integrase	3.76
ABUW_2276	-	transcriptional regulator, ArsR family	3.75
ABUW_1595	-	ion transport protein	3.65
ABUW_3595	<i>nusG</i>	transcription termination/antitermination factor NusG	3.64
ABUW_2699	-	hypothetical protein	3.63
ABUW_0133	-	ribosomal protein S30EA/sigma 54 modulation protein	3.61
ABUW_0218	-	aldo-keto reductase	3.61
ABUW_1816	<i>aro1</i>	3-deoxy-7-phosphoheptulonate synthase	3.50
ABUW_2368	-	transcriptional regulator, LysR family	3.50
ABUW_0625	-	sporulation related domain-containing protein	3.33
ABUW_3809	-	transcriptional regulator, GntR family	3.31
ABUW_0739	-	hypothetical protein	3.16
ABUW_2367	-	chromate transporter	3.14
ABUW_1637	-	oxidoreductase short-chain dehydrogenase/reductase family	3.12
ABUW_1300	-	stress-responsive protein Ish1	3.01
ABUW_0585	-	two-component system histidine kinase sensor component	2.98
ABUW_3563	-	transcriptional regulator, IclR family	2.96
ABUW_1791	-	hypothetical protein	2.96
ABUW_3439	-	hypothetical protein	2.92
ABUW_0601	-	hypothetical protein	2.89
ABUW_4100	-	conjugative transfer system protein TraK	2.88
ABUW_0574	-	phage-related tail completion protein (GPR-like)	2.88

**Supplemental Table A3. Mutant Strains Identified as Producing Significantly Greater Biofilm Biomass from Crystal Violet Screens. (Continued)**

ABUW_4102	-	protein-disulfide isomerase	2.87
ABUW_2131	<i>acoA</i>	acetoin:2,6-dichlorophenolindophenol oxidoreductase alpha subunit	2.87
ABUW_0981	<i>purM</i>	phosphoribosylformylglycinamidine cyclo-ligase	2.85
ABUW_0097	<i>serB</i>	phosphoserine phosphatase	2.81
ABUW_0105	<i>phoR</i>	phosphate regulon sensor kinase PhoR	2.74
ABUW_1184	-	ABC transporter, ATP-binding protein	2.70
ABUW_1078	-	major facilitator family transporter	2.65
ABUW_1808	-	hypothetical protein	2.65
ABUW_1466	-	hypothetical protein	2.64
ABUW_0912	<i>glpD</i>	glycerol-3-phosphate dehydrogenase	2.61
ABUW_0539	-	hypothetical protein	2.51
ABUW_3228	<i>pcoA</i>	copper resistance protein A	2.50
ABUW_0192	-	hypothetical protein	2.50
ABUW_1806	<i>ilvA1</i>	threonine dehydratase	2.49
ABUW_2932	-	hypothetical protein	2.48
ABUW_1754	-	acetyltransferase gnat family	2.47
ABUW_3105	<i>thiD</i>	putative phosphomethylpyrimidine kinase	2.46
ABUW_2188	-	L-lysine 6-monooxygenase/L-ornithine 5-monooxygenase	2.45
ABUW_3127	<i>ligA</i>	DNA ligase, NAD-dependent	2.44
ABUW_0914	-	diacylglycerol kinase catalytic domain-containing protein	2.42
ABUW_1649	-	hypothetical protein	2.41
ABUW_2090	-	4-hydroxybenzoate transporter	2.41
ABUW_2278	-	permease	2.36
ABUW_2941	-	thiamine pyrophosphate enzyme domain protein TPP-binding	2.36
ABUW_2320	-	transcriptional Regulator, LysR family	2.35
ABUW_3512	-	glutathione-regulated potassium-efflux system protein KefB	2.34
ABUW_0983	<i>hda</i>	DnaA family protein	2.33
ABUW_0491	<i>sspB</i>	stringent starvation protein B	2.32
ABUW_2988	-	transcriptional regulator, LysR family	2.31
ABUW_3702	-	hypothetical protein	2.28
ABUW_2194	-	acyl-CoA dehydrogenase, middle domain protein	2.27
ABUW_1974	<i>adeA</i>	multidrug efflux protein AdeA	2.26
ABUW_2933	-	aldose 1-epimerase	2.21
ABUW_2095	-	transcriptional regulator, LysR family	2.20
ABUW_0088	-	hypothetical protein	2.16
ABUW_0136	<i>dsbD</i>	thiol:disulfide interchange protein	2.16

**Supplemental Table A3. Mutant Strains Identified as Producing Significantly Greater Biofilm Biomass from Crystal Violet Screens. (Continued)**

ABUW_0070	<i>fahA</i>	fumarylacetoacetase	2.15
ABUW_0385	<i>ttg2C</i>	toluene tolerance efflux transporter	2.14
ABUW_2261	-	MotA/TolQ/ExbB proton channel	2.13
ABUW_0029	-	transcriptional regulator, LysR family	2.10
ABUW_1658	-	hypothetical protein	2.01
ABUW_0724	-	membrane protein involved in aromatic hydrocarbon degradation	2.01
ABUW_2819	-	hypothetical protein	1.99
ABUW_2431	<i>umuDAb</i>	DNA damage response transcriptional regulator	1.99
ABUW_4114	<i>traH</i>	TraH family protein	1.98
ABUW_3333	-	DnaJ/SEA domain-containing protein	1.97
ABUW_2528	<i>paaC</i>	3-hydroxyacyl-CoA dehydrogenase	1.97
ABUW_2655	-	hypothetical protein	1.96
ABUW_1244	<i>mrdB</i>	rod shape-determining protein RodA (EsvE3)	1.91
ABUW_3302	<i>relA</i>	GTP pyrophosphokinase (ppGpp synthetase I)	1.90
ABUW_2216	<i>rpsT</i>	ribosomal protein S20	1.81
ABUW_1763	<i>usp</i>	Universal stress protein A domain	1.56

**Supplemental Table A4. Mutant Strains Identified as Producing Significantly Less Biofilm Biomass from Crystal Violet Screens.**

ID	Gene	Description	Z-Score
ABUW_3421	<i>folA</i>	dihydrofolate reductase	-1.19
ABUW_0138	<i>est</i>	esterase	-1.24
ABUW_0188	-	GGDEF family protein	-1.25
ABUW_0443	<i>prlC</i>	oligopeptidase A	-1.26
ABUW_0263	-	hypothetical protein	-1.27
ABUW_3133	<i>coaX</i>	pantothenate kinase, type III	-1.29
ABUW_3387	-	leucine carboxyl methyltransferase	-1.31
ABUW_0976	<i>comA</i>	competence factor involved in DNA uptake	-1.32
ABUW_2372	-	hypothetical protein	-1.36
ABUW_2843	-	NADH pyrophosphatase	-1.37
ABUW_2626	-	neuraminidase domain-containing protein	-1.41
ABUW_3242	<i>fadL</i>	FiID	-1.43
ABUW_0876	<i>sucD</i>	succinyl-CoA synthetase, alpha subunit	-1.43
ABUW_2917	<i>yhgl</i>	IscR-regulated protein Yhgl	-1.44
ABUW_0698	-	flavodoxin/nitric oxide synthase	-1.45
ABUW_3694	-	protein YegH	-1.45
ABUW_1555	<i>ppsA</i>	phosphoenolpyruvate synthase	-1.46
ABUW_2288	-	hypothetical protein	-1.47
ABUW_0117	-	hypothetical protein	-1.47

**Supplementary Table A4. Mutant Strains Identified as Producing Significantly Less Biofilm Biomass From Crystal Violet Screens.(Continued)**

ABUW_0879	-	hypothetical protein	-1.49
ABUW_1828	-	hypothetical protein	-1.50
ABUW_0229	-	transcriptional regulator, AraC family	-1.50
ABUW_2769	-	acetyl-hydrolase	-1.52
ABUW_2878	<i>ureJ</i>	urease accessory protein J	-1.52
ABUW_3806	<i>acnD</i>	2-methylisocitrate dehydratase, Fe/S-dependent	-1.53
ABUW_2925	<i>pit</i>	phosphate transporter	-1.56
ABUW_0250	<i>hisB</i>	imidazoleglycerol-phosphate dehydratase	-1.56
ABUW_3439	-	hypothetical protein	-1.56
ABUW_3389	<i>proA</i>	glutamate-5-semialdehyde dehydrogenase	-1.57
ABUW_3385	<i>prc</i>	carboxy- protease	-1.58
ABUW_0182	-	two-component system hybrid histidine kinase/response regulator	-1.58
ABUW_1068	<i>slyD</i>	peptidyl-prolyl cis-trans isomerase, FKBP-type	-1.59
ABUW_2549	-	GntR-type transcription regulator HTH	-1.59
ABUW_1058	-	2-nitropropane dioxygenase	-1.59
ABUW_3390	<i>gapN</i>	aldehyde dehydrogenase	-1.61
ABUW_0093	<i>nusB</i>	transcription antitermination factor NusB	-1.62
ABUW_2503	-	cytochrome B561	-1.62
ABUW_3025	-	hypothetical protein	-1.65
ABUW_0346	-	hypothetical protein	-1.66
ABUW_0390	-	hydrolase, NUDIX family protein	-1.66
ABUW_0722	<i>cysH</i>	phosphoadenosine phosphosulfate reductase	-1.66
ABUW_0643	<i>cysI</i>	sulfite reductase	-1.67
ABUW_2921	-	formylglycine-generating sulfatase enzyme domain-containing protein	-1.67
ABUW_0487	-	acyl-CoA dehydrogenase	-1.72
ABUW_3725	-	transporter, drug/metabolite exporter family	-1.72
ABUW_0932	-	non-ribosomal peptide synthetase	-1.74
ABUW_3639	<i>gacA</i>	response regulator	-1.74
ABUW_0711	-	intracellular protease, Pfpl family	-1.75
ABUW_3862	<i>ileS</i>	isoleucyl-tRNA synthetase	-1.76
ABUW_3326	<i>copC</i>	copper resistance protein CopC	-1.76
ABUW_0885	-	biofilm-associated protein	-1.76
ABUW_0885	-	biofilm-associated protein	-1.77
ABUW_0835	-	hypothetical protein	-1.77
ABUW_1002	<i>purL</i>	phosphoribosylformylglycinamide synthase	-1.79
ABUW_2717	-	3-oxoacyl-(acyl carrier protein) synthase	-1.80
ABUW_2874	-	hypothetical protein	-1.80
ABUW_1552	<i>cyoB</i>	cytochrome O ubiquinol oxidase, subunit I	-1.81

**Supplementary Table A4. Mutant Strains Identified as Producing Significantly Less Biofilm Biomass From Crystal Violet Screens.(Continued)**

ABUW_1862	-	aromatic-ring-hydroxylating dioxygenase beta subunit	-1.81
ABUW_0999	<i>ruvB</i>	Holliday junction DNA helicase RuvB	-1.83
ABUW_3902	<i>trmE</i>	tRNA modification GTPase TrmE	-1.84
ABUW_0980	<i>purN</i>	phosphoribosylglycinamide formyltransferase	-1.86
ABUW_1016	<i>cbl</i>	transcriptional regulator, LysR family	-1.87
ABUW_1228	<i>lipA1</i>	lipoic acid synthetase	-1.87
ABUW_3783	<i>mmsA1</i>	methylmalonate-semialdehyde dehydrogenase	-1.87
ABUW_2246	-	putative enoyl-CoA hydratase/isomerase	-1.87
ABUW_0570	-	phage-related baseplate assembly protein (GPJ-like)	-1.88
ABUW_1272	-	hypothetical protein	-1.89
ABUW_1140	-	lysine 2,3-aminomutase family protein	-1.93
ABUW_1340	<i>hisQ</i>	histidine transport system permease protein HisQ	-1.94
ABUW_1352	<i>ygiW1</i>	bacterial OB fold domain-containing protein YgiW	-1.99
ABUW_4086	-	Transposase	-2.03
ABUW_2198	<i>hup</i>	DNA-binding protein HU	-2.07
ABUW_2076	-	2,3-dihydro-2,3-dihydroxybenzoate dehydrogenase	-2.07
ABUW_0201	<i>gabP</i>	GABA permease	-2.11
ABUW_0355	<i>astE</i>	succinylglutamate desuccinylase	-2.13
ABUW_3305	<i>cysM</i>	cysteine synthase B	-2.13
ABUW_3393	<i>eda</i>	khg/kdpg aldolase	-2.13
ABUW_0797	-	lipoprotein, putative	-2.17
ABUW_0715	<i>mreB</i>	rod shape-determining protein MreB	-2.20
ABUW_0885	-	biofilm-associated protein	-2.22
ABUW_3340	<i>prtN</i>	transcriptional regulator PrtN	-2.22
ABUW_0885	-	biofilm-associated protein	-2.25
ABUW_3705	-	transcriptional regulator SoxR-family	-2.41
ABUW_1189	<i>ldtJ</i>	ErfK/YbiS/YcfS/YnhG family	-2.47
ABUW_3263	-	hypothetical protein	-2.47
ABUW_1216	<i>sodB</i>	superoxide dismutase (Fe)	-2.51
ABUW_2634	<i>mutS</i>	DNA mismatch repair protein MutS	-2.53
ABUW_1929	-	hypothetical protein	-2.56
ABUW_3060	<i>tuf</i>	translation elongation factor Tu	-2.58
ABUW_2239	<i>pyrF</i>	orotidine 5'-phosphate decarboxylase	-2.80
ABUW_0582	-	phage-related capsid scaffolding protein (GPO-like)	-2.92
ABUW_2922	-	hypothetical protein	-3.09